**DOCTORAL (PhD) DISSERTATION**

**University of Sopron**

**Roth Gyula Doctoral School of Forestry and Wildlife Management Sciences**

# Understanding and Predicting the Potential Impacts of Climate Change and Anthropogenic Drivers on Savanna Ecosystems

By:
Emad Hassan Elawad Yasin

Supervisor:

Prof. Dr. Kornel Czimber

Sopron
2026

**Understanding and Predicting the Potential Impacts of Climate Change and Anthropogenic Drivers on Savanna Ecosystems**

Written in order to obtain Doctoral (PhD) degree:

By:
**Emad Hassan Elawad Yasin**

---

Prepared in the frame
of the Roth Gyula Doctoral School of Forestry and Wildlfie Management Sciences of the University of Sopron

Supervisor:

Dr. Kornél Czimber
Acceptance recommended ( yes / no) ……
(signature)

The candidate achieved ……% in the doctoral examination.

Sopron, …… day …… month …… year ……
Chairman of the Examination Committee

I propose to accept the dissertation as a reviewer ( yes / no )

1st Reviewer (Dr ……) yes / no ……
(signature)

2nd Reviewer (Dr ……) yes / no ……
(signature)

(Opt. 3rd Reviewer (Dr ……) yes / no) ……
(signature)

The candidate achieved ……% in the public defence of the dissertation.

Sopron, …… day …… month …… year ……
Chairman of the Public Defence Committee

Qualification of the doctoral (PhD) diploma ……

……
Chairman of the UDHC

## DECLARATION

I, the undersigned Emad Hassan Elawad Yasin, by signing this declaration declare that my PhD thesis entitled "**Understanding and Predicting the Potential Impacts of Climate Change and Anthropogenic Drivers on Savanna Ecosystems"** was my own work; during the dissertation I complied with the regulations of Act LXXVI of 1999 on Copyright and the rules of the doctoral dissertation prescribed by the Roth Gyula Doctoral School, especially regarding references and citations.[1]

Furthermore, I declare that during the preparation of the dissertation I did not mislead my supervisor(s) or the programme leader with regard to the independent research work.

By signing this declaration, I acknowledge that if it can be proved that the dissertation is not self-made or the author of a copyright infringement is related to the dissertation, the University of Sopron is entitled to refuse the acceptance of the dissertation.

Refusing to accept a dissertation does not affect any other legal (civil law, misdemeanour law, criminal law) consequences of copyright infringement.

Sopron, April 2026

Emad Hassan Elawad Yasin
PhD candidate

[1] **Act LXXVI of 1999** Article 34 (1) Anyone is entitled to quote details of the work, to the extent justified by the nature and purpose of the recipient work, by designating the source and the author specified therein.

Article 36 (1) Details of publicly lectures and other similar works, as well as political speeches, may be freely used for the purpose of information to the extent justified by the purpose. For such use, the source, along with the name of the author, shall be indicated, unless this is impossible.

**TABLE OF CONTENTS**

## List of Tables

**List of Figures**

## Abstract

Understanding the long-term impacts of climatic variability and anthropogenic pressures on Sudan's savanna ecosystems is essential for sustainable management, biodiversity conservation, and climate adaptation planning. This study investigates the climate–land–vegetation dynamics of savanna woodlands in southeastern Sudan using an integrated, multi-scale framework that combines geospatial analysis, field-based ecological assessment, machine learning, and species distribution modeling. The research addresses five interrelated objectives: (1) analyzing climatic variability and drought dynamics; (2) assessing land use/land cover (LULC) changes and their interactions with climate; (3) evaluating woody species composition, diversity, and regeneration status; (4) mapping dominant tree species using multi-source remote sensing and machine learning; and (5) modeling the current and future distribution of *Acacia seyal* (Delile) under climate change scenarios.

Climate variability and drought patterns were analyzed using long-term temperature and precipitation datasets (1950–2024) processed within Google Earth Engine (GEE). Non-parametric trend detection methods (Mann–Kendall test and Sen's slope estimator), standardized anomalies, and coefficients of variation were applied, with validation conducted in R and Statistica. Drought conditions were quantified using the Standardized Precipitation Evapotranspiration Index (SPEI) across multiple time scales. LULC dynamics in the Elnour Natural Forest Reserve (ENFR) were mapped using Landsat imagery (1995, 2008, and 2021) and Random Forest classification. Vegetation structure and regeneration were assessed using field data from 229 permanent sample plots surveyed in 2008 and revisited in 2013, 2018, and 2021. Dominant tree species were mapped using multi-temporal Landsat 5 TM (2008), Landsat 8 OLI (2013), and Sentinel-2 MSI (2018 and 2021) imagery combined with NDVI and DEM-derived variables, applying Random Forest (RF), Support Vector Machine (SVM), Classification and Regression Trees (CART), and ensemble classifiers. The potential distribution of *Acacia seyal* was modeled using MaxEnt with spatially filtered occurrence records and bioclimatic predictors, and model performance was evaluated using AUC and TSS metrics.

The results demonstrate significant warming trends since the late 1970s, particularly during the dry season, leading to increased evaporative demand. Rainfall exhibited high interannual variability, with a modest increasing trend (+3.48 mm $yr^{-1}$, $R^2 = 0.181$) that is insufficient to offset increasing drought stress. SPEI analysis revealed a marked increase in drought frequency, severity, and persistence, especially at longer time scales (12–48 months). LULC analysis indicates substantial forest degradation, with dense forest declining from 26.7%

to 15.7%, while semi-bareland expanded from 23.1% to 40.0% between 1995 and 2021. Field-based assessments revealed pronounced declines in species richness (35 to 19 species), tree density (741.44 to 65.41 trees $ha^{-1}$), and basal area (53.07 to 10.8 $m^2$ $ha^{-1}$), accompanied by reduced regeneration capacity and increased dominance of disturbance-tolerant species. Classification results show that RF and SVM achieved high accuracy (OA = 85–92%, $\kappa$ = 0.81–0.89), outperforming CART and ensemble approaches. MaxEnt projections indicate a decline in *Acacia seyal* habitat under SSP2–4.5 in the near future, followed by partial recovery by the late century, whereas SSP5–8.5 predicts substantial long-term habitat loss, with southeastern regions identified as potential climate refugia.

Overall, the findings demonstrate that Sudan's savanna ecosystems are undergoing rapid structural and compositional changes driven by the combined effects of climatic warming, increasing drought stress, and persistent anthropogenic pressures. The integrated methodological framework developed in this study provides a robust and scalable approach for monitoring ecosystem dynamics, improving predictive modeling, and supporting evidence-based conservation and climate adaptation strategies in dryland environments.

**List of acronyms and abbreviations**

| | |
|---|---|
| IPCC | Intergovernmental Panel on Climate Change |
| LULC | Land Use/Land Cover |
| SDMs | Species Distribution Models |
| MODIS | Moderate Resolution Imaging Spectroradiometer |
| FAO | Food and Agriculture Organization |
| UNEP | United Nations Environment Programme |
| CA–ANN | Cellular Automata–Artificial Neural Network |
| SAR | Synthetic Aperture Radar |
| MSI | MultiSpectral Instrument |
| RF | Random Forest |
| SVM | Support Vector Machine |
| CART | Classification and Regression Trees |
| NDVI | Normalized Difference Vegetation Index |
| SAVI | Soil-Adjusted Vegetation Index |
| GEE | Google Earth Engine |
| CNNs | Convolutional Neural Networks |
| GAMs | Generalized Additive Models |
| GLMs | Generalized Linear Models |
| GCMs | Global Climate Models |
| RCPs | Representative Concentration Pathways |
| ENM | Ecological Niche Modeling |
| ENFR | Elnour Natural Forest Reserve |
| CRU | Climatic Research Unit |
| CV | Coefficient of Variation |
| MK | Mann–Kendall Test |
| PET | Potential Evapotranspiration |
| SPEI | Standardized Precipitation Evapotranspiration Index |
| SPI | Standardized Precipitation Index |

| | |
|---|---|
| R | R Programming Language |
| TM | Thematic Mapper |
| OLI | Operational Land Imager |
| SWIR1 | Shortwave Infrared Band 1 |
| SWIR2 | Shortwave Infrared Band 2 |
| NIR | Near Infrared |
| DEM | Digital Elevation Model |
| PA | Producer's Accuracy |
| UA | User's Accuracy |
| OA | Overall Accuracy |
| QD | Quantity Disagreement |
| AD | Allocation Disagreement |
| DBH | Diameter at Breast Height |
| RDe | Relative Density |
| RDo | Relative Dominance |
| IVI | Importance Value Index |
| RA | Relative Abundance |
| QA | Quality Assurance |
| SRTM | Shuttle Radar Topography Mission |
| Kappa | Kappa Coefficient |
| NFI | National Forest Inventory |
| IUCN | International Union for Conservation of Nature |
| GBIF | Global Biodiversity Information Facility |
| FNC | Forest National Corporation |
| WorldClim | Global Climate Data Database |
| WISE | World Inventory of Soil Emission Potentials |
| ISRIC | International Soil Reference and Information Centre |
| ESRI | Environmental Systems Research Institute |
| VIF | Variance Inflation Factor |

| | |
|---|---|
| CMIP6 | Coupled Model Intercomparison Project Phase 6 |
| SSP | Shared Socioeconomic Pathway |
| SSP2-4.5 | Intermediate Emissions Scenario |
| SSP5-8.5 | High Emissions Scenario |
| AUC | Area Under the Curve |
| TSS | True Skill Statistic |
| AMO | Atlantic Multidecadal Oscillation |
| CDDmax | Maximum Consecutive Dry Days |
| HI | Heat Index |
| Tmin | Minimum Temperature |
| Tmax | Maximum Temperature |
| SD | Standard Deviation |
| BA | Basal Area |
| ha | Hectare |
| Mha | Million Hectares |
| kha | Thousand Hectares |
| MaxEnt | Maximum Entropy Model |

# 1. INTRODUCTION

## 1.1. Background

Climate change poses a major global threat to biodiversity, driving widespread shifts in species distributions, ecosystem structure, and ecological processes (IPCC, 2022; Yasin et al., 2024; Musa et al., 2024). Over the past century, global temperatures have increased by approximately 0.74 °C, with accelerated warming since the mid-1970s exceeding that of any comparable period in the last millennium (IPCC, 2022; Zohrabi et al., 2014; Babatolu & Akinnubi, 2013). In many regions, minimum temperatures are rising more rapidly than maximum temperatures, intensifying stress on species with narrow thermal tolerances (Hughes et al., 2003; Guan et al., 2015; Yasin et al., 2025). Concurrently, atmospheric $CO_2$ concentrations have increased by nearly 100 ppm above pre-industrial levels, altering plant physiology, productivity, and ecosystem functioning (IPCC, 2014; IPCC, 2022; Coleine et al., 2024).

Beyond climatic drivers, ecosystems are increasingly exposed to anthropogenic pressures, including agricultural expansion, deforestation, overgrazing, wildfires, habitat fragmentation, and resource overexploitation, which collectively reduce ecosystem resilience and adaptive capacity (Jump & Peñuelas, 2005; Musa & Sahoo, 2023; Abuelbashar et al., 2022). The interaction between climatic and human-induced stressors amplifies ecological vulnerability, with projections suggesting that up to 30% of global species may face elevated extinction risk under combined climate and land-use pressures (Maclean & Wilson, 2011; Musa et al., 2024; Yasin & Mulyana, 2022).

Tropical and dryland ecosystems, including African savannas, are particularly sensitive to these interacting drivers due to high biodiversity, narrow ecological tolerances, and limited dispersal capacity (Colwell et al., 2008; Deutsch et al., 2008; Yasin et al., 2024). Despite their ecological importance, Sudanese savannas remain underrepresented in climate impact assessments, particularly in studies integrating both climatic and anthropogenic drivers (Musa et al., 2024; Coleine et al., 2024). Human activities further exacerbate climate-induced stress by modifying fire regimes, reducing canopy cover, degrading soils, and fragmenting habitats (Musa & Sahoo, 2023; Abuelbashar et al., 2022; Glover & Elsiddig, 2012). These combined pressures accelerate biodiversity loss and reduce ecosystem service provision, including forage production, carbon sequestration, and soil stabilization (Yasin et al., 2024; Wang et al., 2020; Musa et al., 2024).

Savanna ecosystems are ecologically and socio-economically critical across Africa, forming transitional landscapes between deserts and tropical forests (Harrison & Jackson, 1958; Fahmi, 2017). In Sudan, they occupy extensive areas and support rural livelihoods while maintaining key ecological functions such as biodiversity conservation, nutrient cycling, and climate regulation (Siddig et al., 2018; Musa & Sahoo, 2023; Yasin & Mulyana, 2022). Their structure is characterized by a mosaic of grasses and woody vegetation shaped by rainfall gradients, soil properties, fire regimes, and human activities (Fahmi, 2017; Musa et al., 2024; Gurashi et al., 2024a). Latitudinal rainfall gradients strongly influence species composition, with drought-tolerant shrubs dominating arid northern zones, while mesic southern regions support key tree species such as *Acacia seyal*, *Combretum hartmannianum*, and *Anogeissus leiocarpus* (Ibrahim & Osman, 2014; Yasin et al., 2024; Musa et al., 2024).

Savannas provide essential ecosystem services that underpin both ecological stability and human well-being. These include habitat provision, carbon storage, soil stabilization, nutrient cycling, and the supply of fuelwood and forage (Abuelbashar et al., 2022; Coleine et al., 2024; Yasin et al., 2022; Agustino et al., 2011). Structural heterogeneity regulates microclimate, light availability, and nutrient turnover, thereby influencing ecosystem productivity and resilience (Fahmi, 2017; Gurashi et al., 2024a; Yasin et al., 2024).

Sudanese savannas are highly sensitive to hydroclimatic variability. Rising temperatures, erratic rainfall, and prolonged droughts directly affect tree growth, mortality, and regeneration, particularly for drought-sensitive species such as *Acacia seyal* (Fahmi, 2017; D'Odorico & Bhattachan, 2012; Yasin et al., 2025). When combined with land-use pressures, these stressors lead to reduced woody cover, altered species composition, and declining ecosystem functionality (Smith et al., 2019; Musa et al., 2024; Coleine et al., 2024). However, spatially explicit and integrated assessments that jointly evaluate climatic variability, land-use change, and species-level responses remain limited.

Recent advances in remote sensing and machine learning provide powerful tools for addressing these challenges. Multi-temporal satellite data from Landsat, Sentinel, MODIS, and radar systems enable large-scale monitoring of vegetation dynamics and land-cover changes (Gorelick et al., 2017; Huete et al., 2002; Persson et al., 2018). At the same time, species-level classification in dryland environments remains challenging because sparse canopy cover, spectral similarity among woody species, and moderate spatial resolution can reduce class separability. In this context, machine learning algorithms such as Random Forest (RF), Support Vector Machine (SVM), and Classification and Regression Trees (CART) are particularly useful for modeling complex, non-linear relationships between environmental variables and

vegetation patterns (Pal, 2005; Belgiu & Drăguţ, 2016; Raczko & Zagajewski, 2017). Cloud-based platforms such as Google Earth Engine further enhance the capacity to integrate multi-source datasets and conduct large-scale analyses efficiently (Wang et al., 2020; Zhou et al., 2020; Stromann et al., 2019).

Species distribution models (SDMs) and ecological niche models (ENMs) extend these capabilities by predicting species responses to future climate scenarios. By linking occurrence data with environmental variables, these models enable projections of range shifts, identification of climate refugia, and support for conservation planning (Fahmi, 2017; Yasin et al., 2024; Coleine et al., 2024; Moss et al., 2010; Ludwig et al., 2013). Such approaches are particularly important for dominant savanna species such as *Acacia seyal*, whose ecological and socio-economic importance necessitates understanding of its vulnerability under changing climatic conditions (Price et al., 2013; Rajasugunasekar et al., 2023; Yasin et al., 2024).

Despite these advances, significant gaps remain, particularly in long-term, integrated assessments of climate variability, land-use change, and vegetation dynamics in dryland ecosystems such as those in Sudan (Abuelbashar et al., 2022; Fahmi, 2017; Lu et al., 2023; Musa et al., 2024). Furthermore, limited integration of ecological, socio-economic, and policy perspectives constrains the development of effective adaptation strategies (Hemida et al., 2023).

This study addresses these gaps by integrating climate analysis, remote sensing, field-based ecological data, machine learning, and species distribution modeling to assess the combined impacts of climatic variability and anthropogenic pressures on Sudanese savanna ecosystems. The findings provide a scientifically robust basis for conservation planning, adaptive management, and policy development aimed at enhancing ecosystem resilience under current and future climate scenarios.

### 1.2. Problem statement and research rationale

Sudan’s savanna ecosystems are increasingly threatened by the combined effects of climate variability and anthropogenic land-use pressures. These dryland forests and woodlands provide essential ecological, social, and economic services, including carbon sequestration, soil stabilization, livestock forage, and biodiversity conservation (Musa et al., 2024; Yasin et al., 2024; Glover & Elsiddig, 2012). However, rising temperatures, erratic rainfall, prolonged droughts, and increasing frequency of extreme climatic events are altering vegetation structure, species composition, and regeneration processes. Climate-sensitive species, such as *Acacia seyal*, are particularly vulnerable to these changes (IPCC, 2007a; Fahmi, 2017; Yasin et al., 2025).

These climatic stressors are further intensified by human-induced pressures, including deforestation, agricultural expansion, overgrazing, and uncontrolled fires, leading to habitat fragmentation, soil degradation, and declining ecosystem functionality (Musa & Sahoo, 2023; Abuelbashar et al., 2022; Glover & Elsiddig, 2012).

Despite the increasing severity of these threats, biodiversity monitoring and management systems in Sudan remain limited. There is a lack of systematic long-term ecological monitoring, insufficient understanding of species regeneration dynamics, and limited capacity to assess the vulnerability of dominant savanna species under current and future climate scenarios (IPCC, 2007b; IPCC, 2013; Musiyiwa et al., 2014; Simba et al., 2012). Consequently, conservation strategies often lack a strong scientific basis for prioritizing intervention areas and designing adaptive management approaches that simultaneously address climatic and anthropogenic pressures.

Advances in remote sensing and machine learning offer significant opportunities to address these challenges. However, their application in Sudan remains limited and fragmented. Few studies have integrated long-term climate analysis, land use/land cover (LULC) assessment, field-based ecological data, species distribution modeling, and predictive mapping within a unified analytical framework. As a result, critical information on spatial vulnerability patterns, climate-sensitive species, and priority areas for conservation and restoration remains limited.

A major knowledge gap also exists in understanding the regeneration dynamics and climate sensitivity of dominant savanna species. Limited insight into how species respond to temperature increases, altered precipitation regimes, and anthropogenic disturbances constrains the development of effective adaptation strategies (Jensen, 2009; Coleine et al., 2024; Musa et al., 2024; Yasin et al., 2025). Furthermore, predictive modeling of species distributions under future climate scenarios remains scarce in Sudan, despite its importance for identifying vulnerable populations, potential climate refugia, and suitable areas for restoration (Kim & Kaluarachchi, 2009; Ludwig et al., 2013; Taye et al., 2011).

The absence of comprehensive and integrative studies that simultaneously address climate variability, land-use change, vegetation dynamics, and predictive modeling represents a critical limitation for evidence-based conservation in Sudan. To address this gap, this study develops an integrated, multi-scale framework that combines long-term climate analysis, land use/land cover assessment, field-based vegetation studies, species mapping, and predictive modeling of future habitat suitability. This approach provides a robust scientific foundation for adaptive management, informed policy development, and community-based conservation

strategies aimed at enhancing ecosystem resilience, conserving biodiversity, and sustaining ecosystem services under ongoing and future climate change (Yasin et al., 2024; Musa et al., 2024; Rajasugunasekar et al., 2023).

### 1.3. General Objective

The general objective of this study is to understand and predict the combined impacts of climatic variability and anthropogenic pressures on savanna ecosystems in Sudan by integrating climate analysis, land use/land cover dynamics, field-based ecological assessment, and geospatial machine learning approaches.

### 1.4. Specific Objectives

1. To analyze the long-term climatic variability, trends, and drought patterns in savanna woodlands of southeastern Sudan.
2. To assess the spatio-temporal land use/land cover (LULC) changes and their interactions with climatic variability.
3. To evaluate the changes in woody species composition, diversity, and regeneration in response to climatic variability and anthropogenic pressures.
4. To map the dominant tree species using multi-source remote sensing data and machine learning approaches.
5. To model and predict the current and future potential distribution of *Acacia seyal* (Delile) under different climate change scenarios.

### 1.5. Research Questions

1. How have climatic variability, long-term trends, and drought dynamics evolved in Sudanese savanna ecosystems?
2. What are the spatio-temporal patterns of land use/land cover (LULC) change, and how are they influenced by climatic variability?
3. How do climatic variability and anthropogenic pressures influence woody species composition, diversity, and regeneration?
4. How accurately can machine learning and multi-source remote sensing data map dominant tree species?
5. How will climate change affect the future distribution of *Acacia seyal* (Delile)?

### 1.6. Research Hypotheses

1. Sudanese savanna ecosystems have experienced significant warming, increased rainfall variability, and intensified drought conditions over recent decades.

2. Land use/land cover (LULC) changes in savanna ecosystems are primarily driven by the interaction between climatic variability and anthropogenic pressures.
3. Woody species composition, diversity, and regeneration decline significantly under increasing climatic stress and human disturbance.
4. Machine learning approaches can achieve high classification accuracy in mapping dominant tree species using multi-source remote sensing data.
5. Climate change will reduce the extent of suitable habitats for *Acacia seyal* in arid regions while shifting suitability toward relatively more mesic areas.

### 1.7. Dissertation structure

This dissertation is organized into five interrelated chapters, each contributing to a comprehensive assessment of climate variability, drought dynamics, land-use change, and savanna ecosystem responses in Sudan.

**1. Introduction**: This chapter provides the background on climate variability, land-use dynamics, and savanna ecosystem processes in Sudan. It defines the research problem, objectives, research questions, hypotheses, and overall study rationale.

**2. Literature Review**: This chapter presents a critical review of existing literature on climate change, drought assessment, land use/land cover (LULC) dynamics, savanna ecology, remote sensing applications, and species distribution modeling. It identifies key knowledge gaps that justify the study.

**3. Research Methodology**: This chapter describes the research design, data sources, and analytical methods used in the study. It includes approaches for climate variability analysis, drought assessment, LULC classification, mapping of dominant tree species, and species distribution modeling using geospatial and Machine Learning techniques.

**4. Results and Discussion**: This chapter presents and interprets the results of the study, including climate variability and drought trends, land-use dynamics, woody species composition and regeneration, mapping of dominant tree species, and the current and future distribution of *Acacia seyal*.

**5. Conclusion and Recommendations**: This chapter synthesizes the key findings of the study and provides recommendations for sustainable savanna management, biodiversity conservation, and climate change adaptation strategies in Sudan.

# 2. LITERATURE REVIEW

This chapter synthesizes current scientific knowledge on Sudanese savanna ecosystems, with a particular focus on the interactions among climate variability, land use/land cover (LULC) change, vegetation dynamics, and advanced monitoring and modeling approaches. It integrates ecological, climatic, and geospatial perspectives to provide a coherent understanding of the processes driving ecosystem transformation.

Particular emphasis is placed on recent advances in remote sensing, machine learning, and species distribution modeling, as well as their application in assessing vegetation change and predicting future habitat dynamics. The chapter also examines sustainable management and climate adaptation strategies within a socio-ecological context.

Importantly, this review identifies critical gaps in existing research, particularly the lack of integrated, spatially explicit frameworks that simultaneously link climate variability, LULC dynamics, and species-level responses. Addressing this gap constitutes the central focus and scientific contribution of the present study.

## 2.1. Ecology, Structure, and Functional Dynamics of Sudanese Savanna Ecosystems

Sudan's savanna ecosystems are among the country's most ecologically and socio-economically significant biomes, forming a transitional zone between the arid northern deserts and the humid southern tropical forests (Harrison & Jackson, 1958; Fahmi, 2017). These landscapes consist of heterogeneous mosaics of grasses interspersed with scattered woody species, shaped by interactions among rainfall gradients, soil fertility, fire regimes, and long-term human land use (Siddig et al., 2018; Musa & Sahoo, 2023; Yasin & Mulyana, 2022). Species distributions closely follow precipitation patterns: northern savannas are dominated by drought-tolerant grasses and shrubs, whereas southern mesic zones support taller woody canopies characterized by key species such as *Acacia seyal*, *Combretum hartmannianum*, and *Anogeissus leiocarpus* (Gurashi et al., 2024b; Ibrahim & Osman, 2014; Musa et al., 2024).

Ecologically, Sudanese savannas provide a wide range of essential ecosystem services, including biodiversity conservation, grazing resources, non-wood forest products, fuelwood, soil stabilization, hydrological regulation, and carbon sequestration (Abuelbashar et al., 2022; Agustino et al., 2011; Yasin et al., 2022). Unlike closed-canopy tropical forests, savanna ecosystems are characterized by a discontinuous tree layer interspersed with dense herbaceous vegetation (Harrison & Jackson, 1958; Yasin et al., 2024). Structural attributes such as tree density, canopy height, and crown architecture vary along precipitation gradients, influencing

microclimate regulation, light availability, nutrient cycling, and understory composition (Ibrahim et al., 2014; Gurashi et al., 2024a; Fahmi, 2017).

Woody species composition in Sudanese savannas reflects interactions among soil properties, disturbance regimes, and water availability (Mohammed et al., 2021a; Mohammed et al., 2021b; Musa et al., 2024). Dry savannas are typically dominated by drought- and fire-tolerant leguminous species, particularly *Acacia* spp., whereas mesic savannas support a more diverse assemblage of deciduous broad-leaved species. This compositional variation enhances structural and functional heterogeneity, contributing to ecosystem resilience (Siddig et al., 2018; Gurashi et al., 2024a). Key adaptive traits, including deciduousness, thick bark, and strong resprouting capacity, enable woody species to persist under recurrent fire, herbivory, and drought stress (Mohammed et al., 2021a; Abuelbashar et al., 2022).

Regeneration processes in Sudanese savannas are episodic and strongly dependent on rainfall variability, with seedling recruitment occurring primarily during favorable wet periods (Musa et al., 2024; Fahmi, 2017). Fire and grazing may either constrain or facilitate regeneration by modifying competitive interactions, soil conditions, and seedling survival (Yasin et al., 2025; Musa & Sahoo, 2023). Dominant tree species exhibit high regenerative plasticity, supporting long-term population persistence and contributing to ecosystem resilience under combined climatic and anthropogenic pressures (Gurashi et al., 2024b; Abuelbashar et al., 2022).

Biodiversity patterns across Sudanese savannas are spatially heterogeneous and closely aligned with environmental gradients and land-use intensity (Siddig et al., 2018; Musa et al., 2024). Species richness generally increases from arid to mesic zones, corresponding to higher primary productivity and greater habitat complexity (Mohammed et al., 2021a; Yasin & Mulyana, 2022). Nevertheless, even species-poor dry savannas support specialized flora and fauna that perform essential ecological functions and contribute to ecosystem stability (Abuelbashar et al., 2022; Coleine et al., 2024). The characteristic grass–woody mosaic sustains trophic interactions, nutrient cycling, and resilience to climatic variability, thereby maintaining key ecosystem services (Fahmi, 2017; Musa & Sahoo, 2023).

Although the ecological structure and functional importance of Sudanese savannas are well established, quantitative and spatially explicit assessments of vegetation structure, species composition, and regeneration dynamics across environmental gradients remain limited. This limitation constrains the ability to accurately evaluate ecosystem responses to combined climatic variability and anthropogenic pressures. Improving understanding of these dynamics is therefore critical for biodiversity conservation, sustainable land management, and climate

change adaptation. Effective management strategies require the integration of field-based observations with remote sensing, advanced analytical techniques, and socio-ecological knowledge to inform restoration planning, sustainable grazing management, and climate-resilient forestry practices (Yasin et al., 2024; Musa et al., 2024; Abuelbashar et al., 2022). Given their multifunctional role, savanna ecosystems lie at the nexus of ecological stability, rural livelihoods, and climate resilience, underscoring the need for coordinated, adaptive, and evidence-based management approaches.

### 2.2. Historical and Projected Climate Impacts on Savanna Ecosystems

Savanna woodlands of Sudan are highly sensitive to climate variability and long-term changes in temperature and precipitation, which strongly influence ecosystem structure, species composition, and productivity (Fahmi, 2017; D'Odorico & Bhattachan, 2012; Yasin et al., 2024). Historical climate records indicate substantial interannual and decadal fluctuations in rainfall, characterized by recurrent droughts interspersed with episodic wet years that have long shaped vegetation dynamics and resource availability (Fahmi, 2017; Musa & Sahoo, 2023). Over recent decades, rising temperatures, particularly in semi-arid and dryland zones, have increased evapotranspiration rates, soil moisture deficits, and water stress on both herbaceous and woody species (Price et al., 2013; Coleine et al., 2024). These changes directly affect tree growth, recruitment, and mortality, with pronounced impacts on drought-sensitive species such as *Acacia seyal* (Yasin et al., 2025; Lu et al., 2023).

Quantitative assessments using drought and hydroclimatic indices, including the Standardized Precipitation Index (SPI), Standardized Precipitation Evapotranspiration Index (SPEI), Palmer Drought Severity Index (PDSI), and soil moisture anomalies, reveal an increasing frequency and intensity of dry periods over the past 50–75 years (D'Odorico & Bhattachan, 2012; Fahmi, 2017). These hydroclimatic extremes drive shifts in species dominance, reductions in woody cover, and changes in understory composition (Smith et al., 2019; Coleine et al., 2024). Prolonged droughts constrain seedling establishment, increase mortality of shallow-rooted species, and favor resprouting and drought-adapted taxa, thereby reinforcing selective pressures that shape community composition (Abuelbashar et al., 2022; Musa et al., 2024). The combined effects of warming and increasingly irregular rainfall highlight the need for adaptive management strategies in dryland ecosystems.

Observed impacts of climate change across Sudanese savannas include altered phenological patterns, shifts in species distributions, and increased susceptibility to invasive or opportunistic species (Coleine et al., 2024; Lu et al., 2023; Rajasugunasekar et al., 2023). For

example, *Acacia seyal* is projected to experience range contraction under future warming scenarios, whereas some *Combretum* species exhibit greater tolerance to temperature extremes (Yasin & Mulyana, 2022; Yasin et al., 2024). Multi-temporal remote sensing analyses have documented declines in tree cover in regions experiencing severe hydroclimatic stress, particularly where land-use pressures amplify climatic impacts, illustrating the synergistic effects of climate variability and anthropogenic disturbance (Wang et al., 2020; Wang et al., 2024).

Climate–vegetation modeling approaches, including statistical methods (e.g., Generalized Linear Models and Generalized Additive Models) and machine learning–based species distribution models (SDMs), provide robust frameworks for quantifying and projecting ecosystem responses to climate change (Bishop & Nasrabadi, 2006; Cortes & Vapnik, 1995; Praticò et al., 2021; Smith et al., 2019; Yasin et al., 2025). By integrating temperature, precipitation, soil moisture, and other bioclimatic variables, these models identify key drivers of species distributions, project future habitat suitability under different climate scenarios, and support evidence-based adaptive management (Yasin et al., 2024; Coleine et al., 2024; Price et al., 2013).

Vulnerability assessments reveal substantial variation in species sensitivity, adaptive capacity, and exposure to climate stress across savanna types (D'Odorico & Bhattachan, 2012; Yasin et al., 2025; Wang et al., 2024). Dryland and semi-arid savannas are particularly vulnerable due to limited water availability, shallow soils, and the strong dependence of local communities on ecosystem services (Fahmi, 2017; Musa & Sahoo, 2023; Osewe et al., 2024). In contrast, mesic savannas exhibit comparatively higher resilience, supported by greater species richness, structural complexity, diverse regeneration strategies, and fire-adapted traits (Abuelbashar et al., 2022; Mohammed et al., 2021a; Musa et al., 2024). These differences are critical for identifying climate refugia and prioritizing conservation and management interventions.

Advances in remote sensing and cloud-based platforms, such as Google Earth Engine, have transformed the monitoring of vegetation responses across spatial and temporal scales (Gorelick et al., 2017; Zhou et al., 2020). Multi-temporal datasets from Landsat, Sentinel, and MODIS enable the tracking of canopy cover changes, phenological shifts, and drought-induced vegetation stress (Huete et al., 2002; Tucker, 1979; Smith et al., 2019). Machine learning algorithms, including Random Forest and Support Vector Machine, have proven effective in classifying vegetation types, mapping degradation patterns, and predicting species vulnerability under future climate scenarios (Pal, 2005; Belgiu & Drăguţ, 2016; Cortes & Vapnik, 1995;

Halldorsson et al., 2003; Praticò et al., 2021; Raczko & Zagajewski, 2017; Sabat-Tomala et al., 2020).

Despite these advances, integrated and spatially explicit assessments that simultaneously link long-term climate variability, vegetation dynamics, species-level responses, and predictive modeling remain limited in Sudanese savanna ecosystems. This gap constrains the ability to accurately assess ecosystem vulnerability and to design targeted, climate-informed management strategies. Addressing this limitation requires the integration of long-term climatic datasets, remote sensing observations, field-based ecological data, and predictive modeling approaches within a unified analytical framework.

Overall, climate variability and long-term climatic changes pose substantial challenges to Sudanese savanna ecosystems by altering species distributions, forest structure, and the provision of ecosystem services (Fahmi, 2017; Yasin et al., 2025; Coleine et al., 2024). Integrating long-term climate observations, remote sensing, and predictive modeling offers a comprehensive framework for understanding ecosystem responses and anticipating future change. Enhancing savanna resilience will require adaptive land-use planning, strengthened community engagement, and targeted conservation interventions to mitigate the impacts of drought, temperature extremes, and land degradation, thereby ensuring the long-term sustainability of these ecologically and socio-economically vital ecosystems (Musa & Sahoo, 2023; Wang et al., 2024; Osewe et al., 2024; Rajasugunasekar et al., 2023).

### 2.3. Drivers, Impacts, and Modeling of Land Use/Land Cover Dynamics in Savannas

Land use/land cover (LULC) change represents one of the most influential drivers of ecological transformation in Sudanese savanna ecosystems, with profound implications for forest structure, biodiversity, and ecosystem service provision (Musa & Sahoo, 2023; Yasin & Mulyana, 2022; Abuelbashar et al., 2022). Anthropogenic pressures, particularly agricultural expansion, overgrazing, urbanization, and unsustainable logging, have historically fragmented dryland forests, accelerated the degradation of key woody taxa such as *Acacia seyal* and *Combretum* spp., and altered vegetation composition and stand structure (Glover & Elsiddig, 2012; Musa et al., 2024). These land-use pressures are increasingly compounded by climatic stressors, as recurrent drought events reduce regeneration capacity and increase mortality rates, thereby heightening ecosystem vulnerability to further degradation and land conversion (Fahmi, 2017; Smith et al., 2019; Coleine et al., 2024).

Socio-economic drivers play a central role in shaping LULC dynamics across Sudanese savannas. Rapid population growth, strong dependence on forests for fuelwood and non-wood

forest products, and the intensification of agricultural activities exert sustained pressure on natural landscapes (Osman et al., 2023; Yasin et al., 2022; Yasin et al., 2025). Selective harvesting practices disproportionately target commercially valuable or easily accessible species, resulting in reduced forest carbon stocks and disrupted ecosystem functioning (Yasin et al., 2022; Musa & Sahoo, 2023). The expansion of mechanized and rainfed agriculture preferentially affects fertile lowland areas, while extensive pastoral systems alter herbaceous cover and suppress seedling recruitment, further constraining forest recovery processes (Arfat, 2010; Glover & Elsiddig, 2012; Tolessa et al., 2017). Collectively, these pressures drive biodiversity loss, reduce habitat connectivity, and threaten the persistence of endemic and specialist species adapted to savanna ecosystems (Siddig et al., 2018; Musa et al., 2024).

Advances in remote sensing technologies have substantially improved the capacity to map LULC dynamics and assess their ecological consequences across multiple spatial and temporal scales (Gorelick et al., 2017; Wang et al., 2020; Yasin et al., 2024). Multi-temporal satellite datasets from Landsat, Sentinel, and MODIS platforms enable robust detection of deforestation, forest degradation, and vegetation regrowth across heterogeneous savanna landscapes (Lu & Weng, 2007; Tesfaye et al., 2024). The integration of optical and radar imagery further enhances classification accuracy, particularly for spectrally similar land-cover classes such as shrublands and sparse woodlands (Stromann et al., 2019; Torres et al., 2012). In parallel, machine learning algorithms, including Random Forest and Support Vector Machine, consistently outperform traditional pixel-based and unsupervised approaches, providing more reliable and precise LULC classifications (Belgiu & Drăguţ, 2016; Cortes & Vapnik, 1995; Halldorsson et al., 2003; Pal, 2005; Raczko & Zagajewski, 2017; Sabat-Tomala et al., 2020).

The conversion of forested savannas into croplands or degraded shrublands has far-reaching ecological consequences. These transitions reduce canopy cover and litter inputs, increase soil compaction, impair seedling establishment, and facilitate the spread of invasive species, ultimately undermining ecosystem productivity and resilience (FAO, 2010; MacDicken, 2015; Zewdie & Csaplovics, 2016; Lin et al., 2020; Yasin et al., 2022). Changes in herbaceous biomass and fuel loads also modify fire regimes, often increasing fire frequency and intensity, which further reshapes species composition and ecological feedback processes within savanna systems (Smith et al., 2019; Coleine et al., 2024). Long-term LULC changes documented in central Sudanese savannas reveal declines in biodiversity indices and pronounced shifts in woody species dominance, characterized by the retreat of mesic species and the persistence of drought-tolerant taxa (Musa et al., 2024; Yasin et al., 2024).

To anticipate future trajectories of land transformation, LULC modeling increasingly employs hybrid approaches such as Cellular Automata–Artificial Neural Networks (CA–ANN), which integrate spatial dynamics with predictive modeling under varying socio-economic and climatic scenarios (Tesfaye et al., 2024; Tripathi & Verma, 2024). These models explicitly incorporate spatial autocorrelation, neighborhood effects, and policy-driven constraints, enabling realistic simulations of transitions among land-cover classes (Guo et al., 2023; Abbasnezhad et al., 2023; Zhang et al., 2017). By combining satellite-derived LULC data with field inventories and socio-economic drivers, CA–ANN frameworks generate robust projections of forest loss, potential regeneration zones, and vulnerability hotspots, thereby supporting evidence-based land management and conservation planning (Abuelbashar et al., 2022; Haq et al., 2024; Musa et al., 2024).

Beyond structural changes, deforestation and land conversion exert cascading effects on ecosystem processes, including pollination, seed dispersal, and trophic interactions (Musa et al., 2024; Osewe et al., 2024; Siddig et al., 2018). Habitat fragmentation reduces connectivity among forest patches, constraining gene flow and increasing extinction risk for specialist species (Siddig et al., 2018; Guiller et al., 2023; Peacock, 2025). Concurrently, canopy loss exacerbates soil moisture depletion, intensifying the impacts of rising temperatures and increasingly erratic rainfall patterns (Fahmi, 2017; Smith et al., 2019).

Integrating remote sensing, machine learning, and predictive modeling provides a comprehensive framework for monitoring LULC dynamics and disentangling their drivers, ecological impacts, and future trajectories (Gorelick et al., 2017; Praticò et al., 2021; Wang et al., 2020; Yasin et al., 2024). This integrative approach supports conservation prioritization, sustainable land-use planning, and adaptive management strategies that balance ecosystem resilience with livelihood security (Musa & Sahoo, 2023; Osewe et al., 2024; Rajasugunasekar et al., 2023). Incorporating socio-ecological data alongside remote sensing outputs ensures that both ecological integrity and human well-being are addressed under accelerating environmental change (Abuelbashar et al., 2022; Wang et al., 2024).

Despite these advances, integrated and spatially explicit assessments that simultaneously quantify the relative contributions of climatic variability and anthropogenic drivers to LULC dynamics, and explicitly link these changes to species-level responses and ecosystem degradation pathways, remain limited in Sudanese savannas. This gap constrains the ability to identify dominant degradation processes, evaluate ecosystem resilience, and develop targeted, climate-informed land management strategies.

LULC change therefore represents a critical determinant of savanna sustainability in Sudan. A comprehensive understanding of its underlying drivers, ecological consequences, and projected trajectories is essential for mitigating biodiversity loss, maintaining forest structure, and enhancing ecosystem resilience under ongoing climatic and anthropogenic pressures (Musa & Sahoo, 2023; Yasin et al., 2024; Coleine et al., 2024; Yasin et al., 2025).

### 2.4. Advances in Remote Sensing and Machine Learning for Vegetation and Species Monitoring

Remote sensing combined with machine learning has substantially improved vegetation and species-level monitoring, particularly in heterogeneous savanna ecosystems where pronounced seasonality and structural complexity limit the effectiveness of conventional field-based assessments (Gorelick et al., 2017; Yasin et al., 2024; Coleine et al., 2024). Multi-temporal and multi-source satellite observations enable consistent, large-scale quantification of vegetation structure, canopy dynamics, and species distributions, providing critical information for conservation planning and sustainable forest management (Drusch et al., 2012; Huete et al., 2002; Persson et al., 2018). In savanna environments, the integration of optical, radar, and high-resolution imagery has proven particularly effective for detecting subtle variations in canopy density, understory structure, and species composition that are otherwise difficult to capture (Axelsson et al., 2021; Torres et al., 2012; Wan et al., 2021; Du et al., 2015).

Satellite platforms such as Sentinel-1 SAR, Sentinel-2 MSI, Landsat, MODIS, and WorldView provide complementary capabilities for vegetation monitoring across a range of spatial and temporal scales (Lu & Weng, 2007; Stromann et al., 2019; Axelsson et al., 2021). Optical sensors offer detailed spectral information related to chlorophyll content, leaf area, and canopy condition, whereas radar sensors capture vegetation structure and biomass and are largely unaffected by cloud cover, making them particularly valuable in data-scarce or persistently cloudy regions (Torres et al., 2012; Drusch et al., 2012; Wan et al., 2021). High-resolution imagery further supports individual tree crown delineation and fine-scale species discrimination, enabling accurate mapping of dominant savanna taxa such as *Acacia seyal* and *Combretum* spp. (Ferreira et al., 2019; Karlson et al., 2014).

Despite these advances, species-level classification using medium-resolution sensors such as Landsat (30 m) and Sentinel-2 (10–20 m) remains a major challenge, particularly in heterogeneous dryland ecosystems. The presence of mixed pixels and strong spectral similarity among coexisting savanna species significantly reduces class separability (Fassnacht et al., 2016; Immitzer et al., 2012; Axelsson et al., 2021). These limitations are further exacerbated in

sparsely vegetated environments, where discontinuous canopy cover and background soil reflectance introduce additional spectral noise.

Recent studies further highlight that, although Sentinel-2 improves classification performance through higher spatial resolution and the inclusion of red-edge bands sensitive to vegetation structure and chlorophyll content, its ability to fully discriminate species with similar phenological and structural characteristics remains limited (Drusch et al., 2012; Immitzer et al., 2012; Axelsson et al., 2021). Even with these improvements, classification accuracy declines in heterogeneous dryland environments where spectral similarity and sparse canopy cover persist (Fassnacht et al., 2016; Zhong et al., 2024).

To address these limitations, machine learning approaches, particularly Random Forest (RF) and Support Vector Machine (SVM), have been widely applied due to their ability to capture non-linear relationships between spectral, temporal, and environmental variables (Belgiu & Drăguţ, 2016; Raczko & Zagajewski, 2017). However, challenges remain related to class imbalance, mixed pixels, and intra-class variability, which reduce classification reliability for rare or less dominant species (Persson et al., 2018; Liu et al., 2021). In addition, most existing studies rely on single-date or single-sensor datasets, whereas multi-temporal and multi-source approaches remain underutilized, particularly in African dryland ecosystems.

This limitation reveals a critical research gap in developing integrated and scalable frameworks that combine multi-temporal satellite data, field observations, and advanced machine learning methods to improve species-level mapping accuracy under complex environmental conditions.

Within this context, machine learning algorithms play a central role due to their capacity to model complex, non-linear relationships and handle high-dimensional datasets (Belgiu & Drăguţ, 2016; Pal, 2005; De'ath & Fabricius, 2000). Random Forest (RF) is widely applied because of its robustness to noise, resistance to overfitting, and strong performance with imbalanced ecological datasets (Fassnacht et al., 2016; Raczko & Zagajewski, 2017; Fathizad et al., 2020). Support Vector Machine (SVM) is particularly effective when training data are limited, enabling accurate separation of spectrally similar classes through non-linear decision boundaries (Cortes & Vapnik, 1995; Halldorsson et al., 2003; Sabat-Tomala et al., 2020). Classification and Regression Trees (CART), while generally less accurate than ensemble-based approaches, provide interpretable rule-based structures that facilitate understanding of species–environment relationships (Breiman et al., 1984; De'ath & Fabricius, 2000; Sesnie et al., 2008).

The use of multi-temporal datasets substantially enhances species discrimination by capturing phenological variability and seasonal dynamics. Time series of vegetation indices, such as Normalized Difference Vegetation Index (NDVI) and Soil-Adjusted Vegetation Index (SAVI), allow differentiation of species based on growth cycles, leaf flushing, and senescence patterns, particularly in environments where spectral overlap is high during peak growing seasons (Tucker, 1979; Qi et al., 1994; Huete et al., 2002; Persson et al., 2018). Texture metrics derived from high-resolution imagery further improve the delineation of individual trees and heterogeneous stands, increasing classification accuracy in structurally complex savannas (Ferreira et al., 2019; Karlson et al., 2014). Multi-year analyses also reduce misclassification associated with episodic disturbances such as fire and grazing by identifying stable temporal signatures (Liu et al., 2021; Praticò et al., 2021).

Cloud-based platforms, particularly Google Earth Engine (GEE), have significantly advanced large-scale vegetation and species monitoring in data-limited regions such as Sudan (Gorelick et al., 2017; Wang et al., 2020; Zhou et al., 2020). GEE enables scalable access to multi-source datasets, automated preprocessing, and rapid implementation of classification workflows, supporting reproducible and transparent analysis of large spatiotemporal datasets (Chung et al., 2021; Lee et al., 2016; Stromann et al., 2019). However, field-based observations remain essential for training, calibration, and validation, ensuring that remotely sensed classifications accurately represent ecological conditions on the ground (Abuelbashar et al., 2022; Mohammed et al., 2021a; Gurashi et al., 2024a).

Reliable accuracy assessment and uncertainty evaluation are critical components of species-level mapping. Standard metrics, including confusion matrices, producer's accuracy, user's accuracy, and F1-score, are widely used to quantify classification performance (Congalton & Green, 2019; Sabins & Ellis, 2020; Du et al., 2015). Empirical evidence indicates that RF and SVM consistently outperform CART and unweighted ensemble approaches, particularly for dominant species, whereas ensemble methods may introduce bias under class imbalance conditions (Yasin et al., 2025; Axelsson et al., 2021; Raczko & Zagajewski, 2017). Persistent challenges, including spectral similarity, seasonal variability, cloud contamination, and class imbalance, can be mitigated through multi-temporal data fusion, feature selection, and stratified sampling strategies (Fassnacht et al., 2016; Ließ et al., 2012; Hu et al., 2021).

Recent developments in deep learning, particularly Convolutional Neural Networks (CNNs) and hybrid architectures, enable automated feature extraction and improved representation of spatial and temporal patterns, enhancing species discrimination in heterogeneous landscapes (Zhong et al., 2024; Liu et al., 2021; Xu et al., 2020). However, their

application in savanna ecosystems remains constrained by the need for large training datasets, high computational requirements, and limited availability of labeled data (Ali et al., 2023; Bishop & Nasrabadi, 2006).

Overall, the integration of multi-temporal, multi-source remote sensing data with machine learning algorithms and cloud-based platforms has substantially advanced vegetation and species monitoring in savanna ecosystems (Yasin & Mulyana, 2022; Persson et al., 2018; Coleine et al., 2024). In this context, the present study addresses key limitations of medium-resolution imagery by integrating monthly NDVI time series, topographic variables, and multiple machine learning classifiers within a Google Earth Engine framework. This approach enhances species discrimination, reduces classification uncertainty, and enables robust mapping of dominant woody species in Sudanese savanna ecosystems under complex environmental conditions. Continued improvements in data availability, algorithm development, and computational infrastructure are expected to further enhance species-level monitoring and support evidence-based decision-making under accelerating environmental change (Gorelick et al., 2017; Wang et al., 2024; Yasin et al., 2025).

### 2.5. Modeling Climate–Vegetation Interactions and Species Habitat under Changing Climates

Understanding climate–vegetation interactions is fundamental for predicting species distributions, assessing ecosystem resilience, and informing adaptive management in savanna ecosystems characterized by strong climatic gradients and pronounced seasonal variability (Fahmi, 2017; Yasin et al., 2024; Coleine et al., 2024). Climate–vegetation modeling integrates long-term climate records, satellite-derived vegetation metrics, and field-based observations to quantify how variations in temperature, precipitation, and hydroclimatic extremes regulate plant growth, phenology, and community composition (Hulme et al., 2001; Conway, 2000; D'Odorico & Bhattachan, 2012). In Sudanese savannas, where spatial heterogeneity and sharp rainfall gradients prevail, such integrative approaches are particularly important for capturing non-linear and spatially variable vegetation responses (Harrison & Jackson, 1958; Musa et al., 2024; Yasin et al., 2025).

Statistical modeling frameworks, including generalized linear models (GLMs), generalized additive models (GAMs), and regression tree-based approaches, have been widely used to characterize species–environment relationships and generate spatially explicit predictions of habitat suitability (De'ath & Fabricius, 2000; Vorpahl et al., 2012; Fahmi, 2017). These approaches are effective for identifying key climatic drivers and threshold responses, particularly where ecological processes follow gradual environmental gradients. However, their

ability to capture complex interactions, feedback mechanisms, and non-stationary responses is often limited in highly heterogeneous savanna landscapes.

Machine learning–based species distribution models (SDMs) have therefore emerged as powerful alternatives for modeling the distributions of dominant savanna tree species, including *Acacia seyal* and *Combretum hartmannianum* (Gadalla et al., 2025; Belgiu & Drăguţ, 2016; Cortes & Vapnik, 1995). Algorithms such as Random Forest (RF) and Support Vector Machine (SVM) effectively capture non-linear relationships and interactions between species occurrence and environmental predictors, frequently outperforming conventional statistical approaches in predictive accuracy and robustness (Pal, 2005; Raczko & Zagajewski, 2017; Sabat-Tomala et al., 2020). Ensemble modeling frameworks, which integrate outputs from multiple algorithms, can further improve model stability by reducing algorithm-specific biases and uncertainty (Ali et al., 2023; Ramezan et al., 2019; Yasin et al., 2025). Predictor variables typically include climate metrics (temperature, precipitation, drought indices), topography, soil properties, and remotely sensed vegetation indicators, providing a multidimensional representation of species' realized ecological niches (D'Odorico & Bhattachan, 2012; Haddeland et al., 2012; Fahmi, 2017).

Projecting current and future habitat suitability under climate change scenarios is essential for anticipating range shifts, identifying vulnerable populations, and prioritizing conservation interventions (Solomon, 2007; Moss et al., 2010; Beyene et al., 2010). Coupling SDMs with outputs from global climate models (GCMs) under Representative Concentration Pathways (RCPs) enables the simulation of species distribution trajectories under alternative warming and precipitation regimes (Kim & Kaluarachchi, 2009; Ludwig et al., 2013; Taye et al., 2011). Empirical evidence indicates that increasing temperatures and prolonged dry periods are likely to reduce suitable habitat for *Acacia seyal* in northern and central Sudan, while more humid southern and eastern regions may retain or expand climatically suitable conditions due to higher rainfall and soil moisture availability (Fahmi, 2017; Yasin et al., 2024; Coleine et al., 2024). Incorporating climate variability, extreme events, and land-use dynamics into predictive frameworks improves model realism and enables assessment of cumulative stressors affecting savanna ecosystems (Conway, 2000; Nicholson, 2009; Atique et al., 2014).

Ecological niche modeling (ENM) complements SDMs by distinguishing between fundamental and realized niches, identifying climate refugia, and delineating areas of high vulnerability under projected climate change (Price et al., 2013; Yasin et al., 2024; Rajasugunasekar et al., 2023). For *Acacia seyal*, ENM studies consistently highlight strong sensitivity to rainfall seasonality, soil moisture availability, and drought frequency,

underscoring the vulnerability of northern populations to prolonged dry conditions and land degradation (Abuelbashar et al., 2022; Mohammed et al., 2021a; Yasin et al., 2025). Integrating ENMs with remote sensing–derived indices such as NDVI, SAVI, and canopy cover enhances spatial precision and facilitates the identification of priority conservation and restoration areas (Tucker, 1979; Huete et al., 2002; Persson et al., 2018).

Uncertainty remains a central challenge in climate–vegetation modeling, arising from data limitations, model structure, parameterization choices, and assumptions regarding species' ecological tolerances and dispersal capacities (Hulme et al., 2001; Haddeland et al., 2012; Moss et al., 2010). The use of ensemble SDMs, cross-validation techniques, and independent field-based validation datasets is widely recommended to quantify and reduce predictive uncertainty (Ali et al., 2023; Ramezan et al., 2019; Sabat-Tomala et al., 2020). In addition, multi-temporal satellite observations improve model performance by capturing intra-annual phenological variability, which is particularly pronounced in seasonally dynamic savanna ecosystems (Axelsson et al., 2021; Persson et al., 2018; Coleine et al., 2024).

Climate–vegetation modeling provides actionable insights for ecosystem management by identifying vulnerable zones, potential climate refugia, and areas suitable for restoration, reforestation, or adaptive grazing management (Yasin et al., 2024; Musa et al., 2023; Rajasugunasekar et al., 2023). Integrating model outputs with socio-ecological datasets, including land-use patterns and population distribution, further enhances their relevance for land-use planning and policy formulation (Wang et al., 2024; Musa et al., 2024; Yasin et al., 2024). Such integrative frameworks support proactive conservation strategies aimed at maintaining biodiversity, ecosystem services, and climate resilience under intensifying climatic and anthropogenic pressures.

Despite these advances, integrated modeling frameworks that explicitly couple climate variability, land-use dynamics, and species-level responses within a unified and spatially explicit approach remain limited in Sudanese savannas. In particular, few studies simultaneously quantify climate-driven habitat shifts, identify climate refugia, and link these projections to observed ecological degradation and species dynamics.

Addressing this gap requires the integration of long-term climate analysis, remote sensing–derived indicators, machine learning–based species distribution models, and ecological field data within a coherent framework. Such an approach enables more robust prediction of ecosystem trajectories and supports evidence-based conservation and climate adaptation planning.

Climate–vegetation modeling and species distribution analysis therefore provide critical insights into the functioning and future trajectories of Sudanese savanna ecosystems (Fahmi, 2017; Yasin et al., 2024, Yasin et al., 2025; Coleine et al., 2024). The combined application of statistical approaches, machine learning–based SDMs, remote sensing data, and ecological niche modeling enables a comprehensive assessment of habitat dynamics, vulnerability, and adaptive capacity, particularly for keystone species such as *Acacia seyal*, whose ecological roles in nitrogen fixation, forage provision, and landscape stabilization are central to savanna resilience (Yasin & Mulyana, 2022; Musa et al., 2024).

### 2.6. Sustainable Management and Climate Adaptation Strategies for Sudanese Savannas

Sudanese savanna ecosystems are highly sensitive to the combined influences of climate variability and land-use dynamics, making sustainable forest management and climate adaptation strategies essential for maintaining ecosystem functions and services (Fahmi, 2017; Musa et al., 2023; Yasin et al., 2024). Alterations in precipitation regimes, rising temperatures, and increasing drought frequency strongly regulate species composition, regeneration processes, and forest structure across savanna gradients (D'Odorico & Bhattachan, 2012; Price et al., 2013; Smith et al., 2019). These climatic pressures are further intensified by anthropogenic drivers, including agricultural expansion, overgrazing, and deforestation, which accelerate habitat fragmentation, biodiversity loss, and degradation of ecosystem services (Abuelbashar et al., 2022; Gibreel et al., 2013; Musa & Sahoo, 2023). The convergence of climatic and human-induced stressors highlights the need for adaptive management approaches that integrate ecological processes with socio-economic and institutional dimensions to enhance savanna resilience (Osewe et al., 2024; Rajasugunasekar et al., 2023; Wang et al., 2024).

Climate change affects savanna ecosystems through both direct and indirect pathways. Direct impacts include changes in tree physiology, phenology, and mortality driven by water stress and temperature extremes, while indirect effects arise through altered species interactions, fire regimes, and broader ecosystem processes (D'Odorico & Bhattachan, 2012; Smith et al., 2019). Dominant species such as *Acacia seyal* are particularly sensitive to prolonged dry periods and soil moisture deficits, which constrain growth, seedling recruitment, and long-term population viability (Coleine et al., 2024; Lu et al., 2023; Yasin et al., 2025). Shifts toward drought-tolerant or opportunistic species under warming and irregular rainfall regimes have been widely reported, often at the expense of less resilient native taxa (Fahmi, 2017; Musa et al., 2024; Rajasugunasekar et al., 2023). Concurrently, land-use conversion to croplands or grazing areas accelerates soil erosion, reduces canopy cover, and disrupts habitat

connectivity, compounding climatic stress and amplifying ecosystem degradation (Abuelbashar et al., 2022; Glover & Elsiddig, 2012; Musa & Sahoo, 2023). Remote sensing–based assessments further indicate declines in carbon stocks and shifts in species composition, with cascading effects on key ecosystem services such as nitrogen fixation, forage provision, and soil stabilization (Musa et al., 2024; Wang et al., 2020; Yasin & Mulyana, 2022).

Adaptive forest management strategies are widely recognized as essential for enhancing the resilience of Sudanese savannas under increasing climatic and anthropogenic pressures. Restoration initiatives, sustainable harvesting practices, and assisted regeneration have been shown to maintain structural complexity, biodiversity, and ecosystem functionality when appropriately implemented (Hemida et al., 2023; Musa et al., 2024; Yasin et al., 2024). Agroforestry systems, including Taungya and intercropping approaches, contribute to soil fertility improvement, erosion control, and carbon sequestration while maintaining tree cover and supporting livelihood diversification (Hemida et al., 2023; Musa & Sahoo, 2023). Assisted natural regeneration, often through enrichment planting of keystone species, facilitates recovery of degraded landscapes and enhances ecological resilience, particularly in areas where natural recruitment is limited by grazing or drought (Abuelbashar et al., 2022; Mohammed et al., 2021a; Yasin et al., 2025). Additional measures, such as controlled grazing, protection of riparian forests, and the establishment of ecological corridors, help maintain landscape connectivity, supporting gene flow and long-term species persistence (Yasin & Mulyana, 2022; Gurashi et al., 2024a; Musa et al., 2024; Yasin et al., 2024). Climate-smart management increasingly emphasizes the selection of drought- and heat-tolerant species and the integration of remote sensing and machine learning–based monitoring systems to support anticipatory and flexible adaptation planning (Coleine et al., 2024; Stromann et al., 2019; Wang et al., 2024).

Effective implementation of sustainable management strategies depends strongly on supportive policy frameworks, institutional capacity, and community participation. In Sudan, weak regulatory enforcement, limited monitoring infrastructure, and competing land-use demands have historically constrained sustainable forest governance (Siddig et al., 2018; Musa & Sahoo, 2023). Participatory management approaches that actively involve local communities in planning, conservation, and monitoring have been shown to promote sustainable resource use and improve compliance with management regulations (Huber et al., 2023; Gusman & Supriyadi, 2024; Djosetro & Behagel, 2024). Community-based forest management programs, supported by extension services and climate-risk awareness, enhance local adaptive capacity while ensuring more equitable distribution of forest-derived benefits (Hemida et al., 2023; Musa et al., 2024; Osewe et al., 2024). Integrating traditional ecological knowledge with modern

geospatial monitoring and modeling tools further strengthens the effectiveness and contextual relevance of management interventions in heterogeneous savanna landscapes (Naidoo & Hill, 2006; Yasin & Mulyana, 2022).

Despite advances in remote sensing, machine learning, and climate–vegetation modeling, substantial knowledge gaps remain regarding the coupled effects of climate change and land-use dynamics on species responses in Sudanese savannas (Coleine et al., 2024; Smith et al., 2019; Yasin et al., 2025). Long-term monitoring data are scarce, particularly for dryland species and regeneration processes, limiting the ability to detect gradual or non-linear ecological changes (Abuelbashar et al., 2022; Musa et al., 2024). Moreover, the impacts of extreme climatic events, including heatwaves, prolonged droughts, and episodic flooding, on tree physiology, mortality, and recruitment remain insufficiently quantified (Fahmi, 2017; Lu et al., 2023; Price et al., 2013).

In addition, integrated frameworks that explicitly link climate variability, land-use change, species-level responses, and management interventions remain limited in Sudanese savannas. This gap constrains the development of targeted, evidence-based adaptation strategies and limits the capacity to translate scientific insights into operational forest management and policy implementation.

Addressing these challenges requires integrative research approaches that combine socio-ecological systems analysis, climate projections, and spatially explicit modeling to support actionable management decisions (Rajasugunasekar et al., 2023; Wang et al., 2024; Yasin et al., 2024). Cloud-based platforms such as Google Earth Engine, coupled with machine learning techniques, provide scalable solutions for long-term monitoring and predictive assessment, enabling adaptive forest management that can respond dynamically to evolving climatic and land-use pressures (Gorelick et al., 2017; Stromann et al., 2019; Yasin et al., 2025).

Overall, the sustainability of Sudanese savanna ecosystems depends on integrative strategies that combine climate-smart forest management, community engagement, policy support, and science-based monitoring (Hemida et al., 2023; Musa et al., 2023; Yasin et al., 2024). Strengthening adaptive management, addressing persistent knowledge gaps, and leveraging emerging geospatial and modeling technologies are critical for mitigating climate and land-use impacts, conserving biodiversity, sustaining ecosystem services, and supporting local livelihoods in these vulnerable dryland environments (Musa et al., 2024; Rajasugunasekar et al., 2023; Yasin & Mulyana, 2022).

# 3. RESEARCH METHODOLOGY

## 3.1 Study Area

This thesis integrates analyses across three nested spatial scales to comprehensively assess climatic variability, forest dynamics, and species distribution within Sudan's savanna ecosystems. Objective 1 focuses on Blue Nile State in southeastern Sudan. Objectives 2–4 are conducted within the Elnour Natural Forest Reserve (ENFR) in Blue Nile State, while Objective 5 is addressed at the national scale across Sudan. The locations of the study areas are presented in Fig. 3.1.

### 3.1.1 Sudan (Objective 5)

Sudan, one of the largest countries in Africa, exhibits substantial ecological heterogeneity (Fig. 3.4; Appendix A), largely attributable to its broad latitudinal extent and pronounced climatic gradients (Berry, 2015). The northern regions are dominated by hyper-arid conditions associated with the Nubian and Libyan Deserts, where annual precipitation is minimal and summer temperatures frequently exceed 45 °C. In contrast, the southern regions experience relatively moderate temperatures and higher annual rainfall (Osman & Ali, 2021). These gradients strongly influence savanna ecosystems, tree-species biogeography, and the distribution of ecologically important species such as *Acacia seyal* (Delile).

The spatial and temporal distribution of rainfall in Sudan is governed primarily by two major monsoonal systems. The southwest monsoon, active from May to October, transports moist air masses from the Atlantic Ocean and the Congo Basin and generates most of the annual rainfall in southern and central Sudan (Alriah et al., 2021). This system is fundamental to the productivity and ecological functioning of Sudan's savanna and agro-ecological zones (Osman & Ali, 2021). In contrast, the northeast monsoon, prevailing from November to March, brings cool and dry northeasterly winds from the Arabian Peninsula, contributing to arid conditions, limited precipitation, and frequent dust storms in northern Sudan (Elagib & Mansell, 2000).

Superimposed on these seasonal climatic controls, ongoing climate change and increased climatic variability, including more frequent ENSO-related anomalies, have intensified drought occurrence and wildfire activity (Hamadalnel et al., 2022). These processes exert cascading effects on vegetation structure, mortality, regeneration capacity, and species distribution patterns.

Sudan's environmental heterogeneity is further reflected in a pronounced pedological gradient. Sandy soils dominate the northern and west-central regions, clay-rich Vertisols characterize much of the central belt, lateritic soils predominate in the south, and fertile alluvial

soils occur along the White Nile, Blue Nile, and Main Nile systems, as well as in the Qash, Arrahad, and Atbara deltas (SUSIS-ARC, 2016; UNEP, 2020). This transition from hyper-arid desert to semi-humid savanna strongly influences vegetation assemblages, biodiversity patterns, and species niche boundaries. For example, climate-related stress has been associated with increased mortality and reduced regeneration in baobab populations (Osman & Ali, 2021).

*Acacia seyal* (Delile) is an ecologically and economically important savanna tree species native to Sudan's dryland woodlands (Darbyshire et al., 2015; Mohamed et al., 2016; Siddig et al., 2018). A clear understanding of Sudan's ecological zonation and climatic variability is therefore essential for calibrating and validating species distribution models. This biogeographic context strengthens the predictive capacity of the modelling framework used to estimate the current and future distribution of *Acacia seyal* under climate-change scenarios, thereby supporting evidence-based conservation and land management.

### 3.1.2 Blue Nile State (Objective 1)

Blue Nile State is located in southeastern Sudan within a transitional zone between the arid northern regions and the more humid southern savannas. The region is characterized by a tropical savanna climate, with a distinct wet season extending from April to November and a dry season from December to March. Annual rainfall is highly variable, generally ranging between 300 and 700 mm, with peak rainfall occurring between July and September. Temperatures are high during the dry season and often exceed 40 °C, whereas they are relatively lower during the rainy season due to increased cloud cover and atmospheric humidity. These climatic conditions strongly influence vegetation dynamics, drought occurrence, and ecosystem processes across the region.

### 3.1.3 Elnour Natural Forest Reserve (ENFR) (Objectives 2–4)

Objectives 2–4 were conducted in the Elnour Natural Forest Reserve (ENFR), located in Blue Nile State, southeastern Sudan, approximately 6 km southeast of El Damazin and about 3 km east of El Roseires (Fig. 3.1). The reserve lies between 11°48′19″ N and 11°53′30″ N latitude and 34°28′47″ E and 34°32′35″ E longitude.

ENFR was declared a reserved forest on 15 June 1959 and covers approximately 4,667.17 ha. The reserve was established to protect biodiversity and reduce unsustainable resource exploitation, including tree cutting, poaching, and excessive grazing pressure.

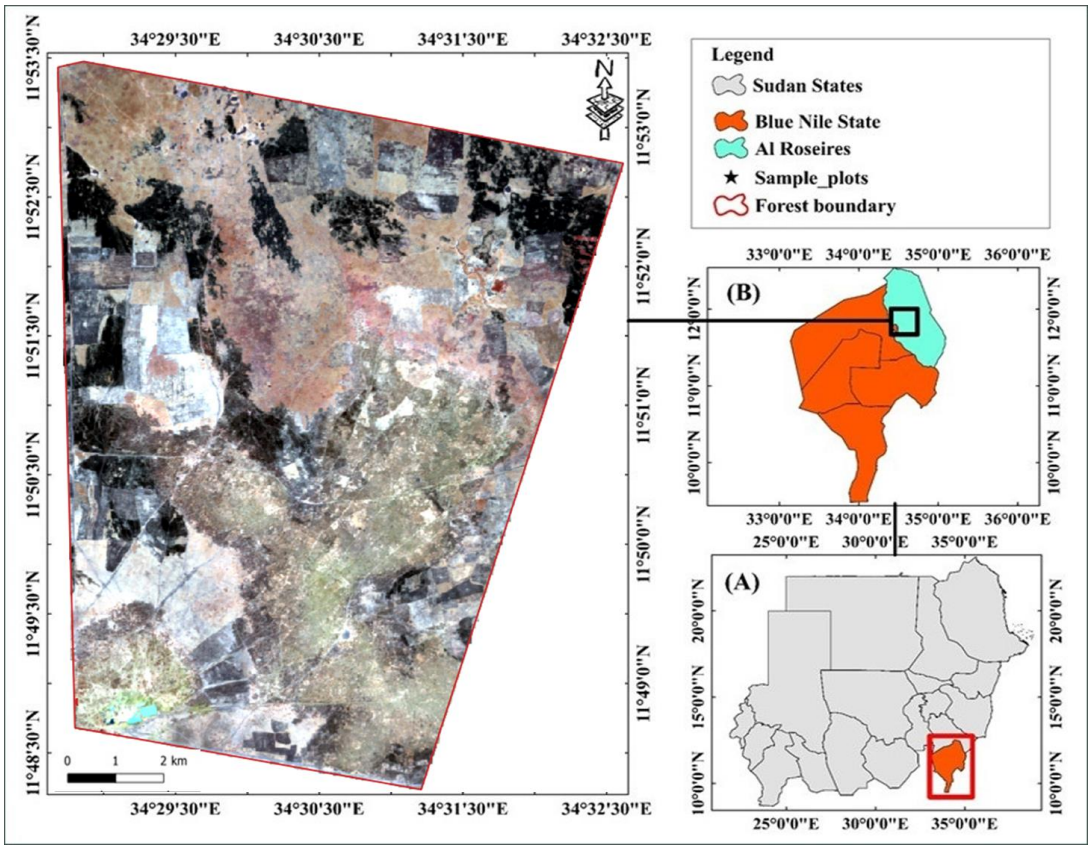


Fig. 3.1. Maps for the location of Blue Nile State in southeastern Sudan (A) and the location of Elnour Natural Forest Reserve (study area) in Blue Nile State (B), as well as the overview of Elnour Natural Forest Reserve (C).

The climate of ENFR is tropical and subcontinental, characterized by humid rainy summers and dry winters. Mean temperatures during the coolest months range from approximately 15.62 °C in January to 16.41 °C in December, whereas the hottest months, April and May, reach mean temperatures of approximately 39.91 °C and 41.48 °C, respectively. Rainfall is strongly influenced by moist air masses originating from the South Atlantic and the Congo Basin, with limited influence from the Indian Ocean. Annual rainfall ranges between 300 and 700 mm and is concentrated between April and November, peaking from July to September.

According to Harrison and Jackson (1958), ENFR belongs to the low-rainfall woodland savanna zone. The reserve supports diverse woody vegetation, comprising 55 woody plant species belonging to 36 genera and 18 families (Ibrahim et al., 2014). Dominant species include *Sterculia setigera* Delile, *Combretum hartmannianum* Schweinf., *Acacia seyal* (Delile), *Terminalia brownii* Fresen., *Terminalia laxiflora* Engl., *Anogeissus leiocarpus* (DC.) Guill. & Perr., *Balanites aegyptiaca* (L.) Delile, *Combretum micranthum* G. Don, and *Lannea fruticosa* (Hochst. ex A. Rich.) Engl. (Ibrahim and Osman, 2014; Fig. 3.2).

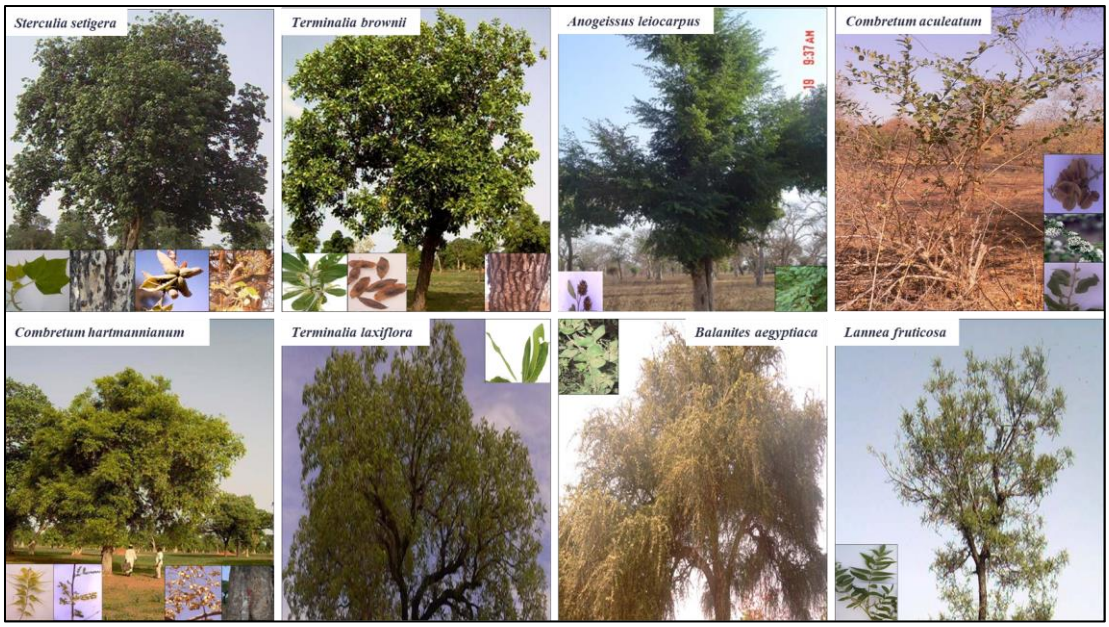


Fig. 3.2. Representative dominant woody species of the savanna woodland ecosystem in Elnour Natural Forest Reserve (ENFR), Sudan, illustrating key species composition and structural diversity.

The reserve also contains ecologically important and threatened species such as *Adansonia digitata* L., *Boswellia papyrifera* (Delile) Hochst., *Dalbergia melanoxylon* Guill. & Perr., *Grewia* spp., *Lonchocarpus laxiflorus* Guill. & Perr., *Piliostigma reticulatum* (DC.) Hochst., and *Xeromphis nilotica* (Stapf) Keay (Gibreel et al., 2013; Fig. 3.3).

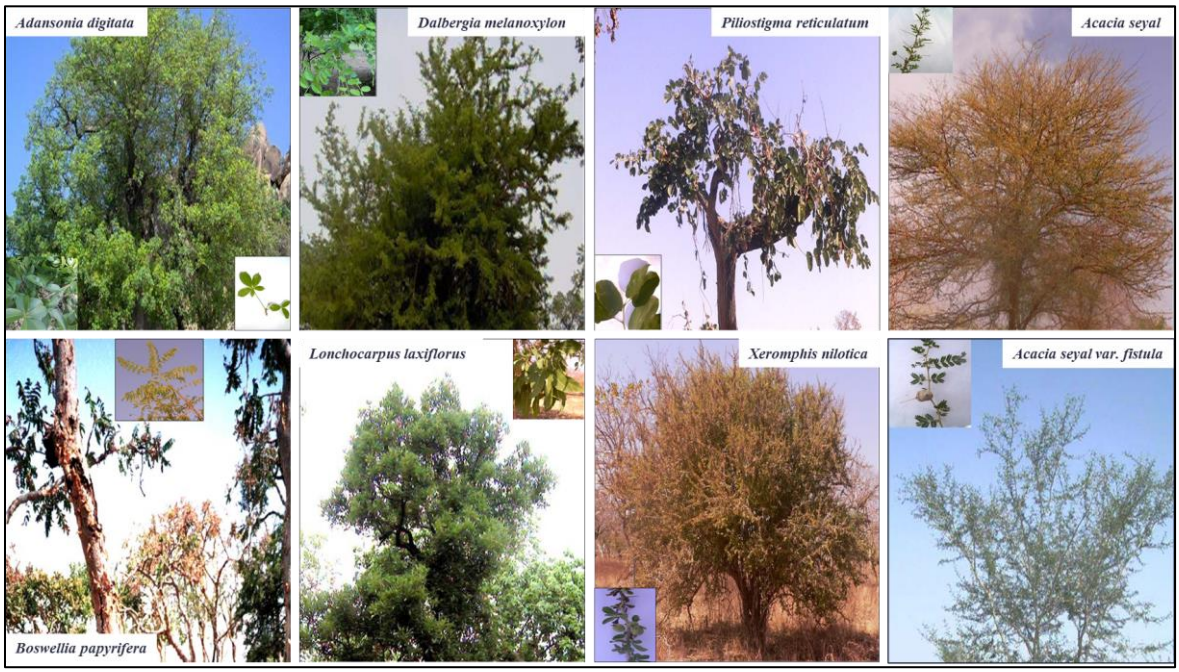


Fig. 3.3. Representative ecologically important and threatened woody species in the Elnour Natural Forest Reserve (ENFR), Sudan, highlighting species of conservation significance and their structural characteristics.

In addition, the vegetation includes a range of shrub and secondary species, including *Dichrostachys cinerea*, *Combretum molle*, Ziziphus abyssinica, *Acacia mellifera*, *Acacia senegal*, Ziziphus spina-christi, and *Acacia nubica*, which contribute to structural diversity and regeneration dynamics within the ecosystem (Fig. 3.4).

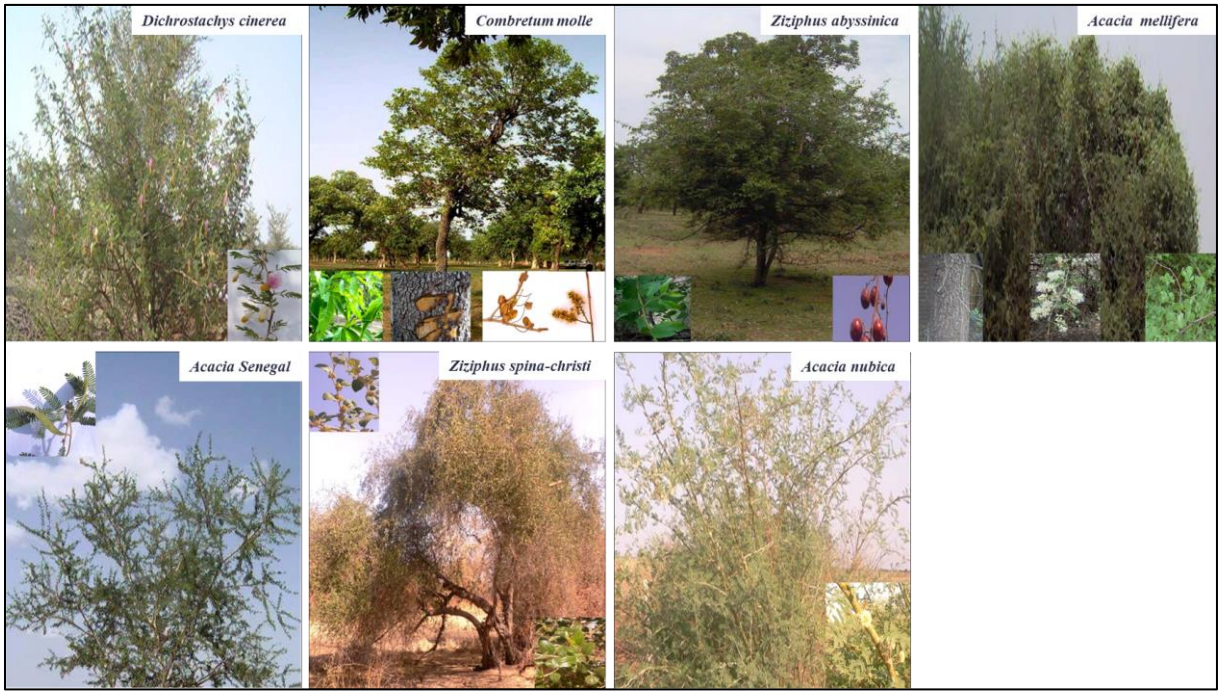


Fig. 3.4. Representative ecologically important and threatened woody species in the Elnour Natural Forest Reserve (ENFR), Sudan, highlighting species of conservation significance and their structural characteristics.

Topographically, ENFR is generally flat to gently undulating, with shallow depressions in the central and northern clay-rich sectors (Fahmi, 2017). The reserve contains two major soil groups: dark cracking clay soils, covering approximately 64.2% of the area (2,994.31 ha), and sandy loam to gravelly soils, covering the remaining 35.8% (1,672.86 ha).

ENFR is surrounded by rural communities, including Azaza village, whose inhabitants depend on forest resources for firewood, medicinal plants, fruits, fodder, and construction materials. The reserve is also used seasonally for livestock grazing, particularly during the dry season (March–May), except in areas undergoing active regeneration. These anthropogenic pressures represent key drivers of vegetation change and degradation processes within the reserve.

### 3.2. Analysis of Long-Term Climatic Variability, Trends, and Drought Patterns in Savanna Woodlands of Southeastern Sudan (Objective 1)

This section describes the procedures used to quantify long-term variability in rainfall and temperature, detect climatic trends, and characterize drought dynamics in Blue Nile State.

The methodological framework includes data acquisition, climatic variability analysis, trend detection, drought assessment, and statistical analysis.

### 3.2.1. Data collection

#### 3.2.1.1. Historical Climate Data (1950–2024)

The analysis period for Objective 1 spans 1950–2024. Monthly rainfall and temperature data for the period 1950–2020 were obtained from the Climatic Research Unit Time Series dataset (CRU TS v4.x) at a spatial resolution of 0.5°. The dataset was accessed and pre-processed in Google Earth Engine (GEE), which enables efficient cloud-based management and analysis of long-term climate data (Gorelick et al., 2017). CRU TS is widely used in hydroclimatic and drought studies due to its long temporal coverage, internal consistency, and suitability for trend analysis (Harris et al., 2020).

To extend the dataset to 2024 and provide recent local context, station observations from the Sudan Meteorological Authority were incorporated. These data were used for temporal consistency checks, validation of observed trends, and extension of the most recent portion of the time series (Pradhan et al., 2024; Xu et al., 2025). This integration ensures both long-term consistency and improved reliability of recent climate signals.

#### 3.2.1.2. Climate Variability and Anomaly Analysis

Annual and seasonal rainfall and temperature series were derived from the monthly records. Climatic anomalies were calculated as deviations from the long-term mean, following standard climatological practice (IPCC, 2022; Harris et al., 2020):

$$A_i = X_i - \bar{X} \qquad (1)$$

where $A_i$is the anomaly in year $i$, $X_i$is the observed value of the climatic variable, and $\bar{X}$is the long-term mean.

Interannual variability was quantified using the coefficient of variation (CV), which is widely applied in rainfall variability studies in Africa (Wilks, 2011; Asaye et al., 2025; Adane & Asmeron, 2025):

$$CV = \frac{\sigma}{\bar{X}} \times 100 \qquad (2)$$

where $\sigma$ is the standard deviation of the climatic variable.

#### 3.2.1.3. Trend Detection and Magnitude Estimation

Long-term trends in rainfall and temperature were evaluated using the non-parametric Mann–Kendall (MK) trend test (Mann, 1945; Kendall, 1975). The MK test was selected

because it does not require normally distributed data, is robust to outliers and missing values, and is widely recommended for hydroclimatic time series in semi-arid and data-scarce environments (Tegos et al., 2023; Lee et al., 2024). Compared with parametric approaches such as linear regression, the MK test provides more reliable detection of monotonic trends in non-normally distributed environmental datasets.

To quantify the magnitude of detected trends, Sen's slope estimator was applied (Sen, 1968):

$$\beta = \text{median}\left(\frac{X_j - X_i}{j - i}\right), for\ j > i \qquad (3)$$

Trend significance was evaluated at the 0.05 and 0.01 confidence levels.

Because the Mann–Kendall test may be influenced by serial autocorrelation, the analysis was conducted using aggregated annual, seasonal, and decadal time series to reduce the effect of short-term dependence. This limitation is acknowledged but does not affect the interpretation of long-term climatic trends.

**3.2.1.4. Drought Indices and Characterization**

Meteorological drought conditions were quantified using the Standardized Precipitation Evapotranspiration Index (SPEI) at multiple time scales (1-, 3-, 6-, 9-, 12-, 24-, 36-, and 48 months). SPEI was selected because it is multi-scalar and incorporates both precipitation deficits and temperature-driven evaporative demand, making it particularly suitable for drought assessment under climate warming (Vicente-Serrano et al., 2010; Beguería et al., 2014).

In contrast to indices such as the Standardized Precipitation Index (SPI), which considers only precipitation, SPEI includes the effect of temperature through potential evapotranspiration (PET), thereby providing a more comprehensive representation of drought conditions.

The climatic water balance used for SPEI calculation is defined as (Thornthwaite, 1948):

$$D_i = P_i - PET_i \qquad (4)$$

where $P_i$is precipitation and $PET_i$is potential evapotranspiration.

PET was estimated using the Thornthwaite method, which requires only temperature data and is therefore suitable for data-scarce regions. Despite its simplicity, this method has been widely applied in large-scale drought studies across Africa and provides reliable estimates for climatic water balance analysis (Tegos et al., 2023).

Drought severity was classified into moderate, severe, and extreme categories based on standard SPEI thresholds recommended by the World Meteorological Organization (WMO, 2023).

### 3.2.2. Data analysis

Initial data extraction and preprocessing were performed in Google Earth Engine (GEE). Subsequent statistical analyses were conducted using R (version 4.5.2), Statistica (version 13.0), and Microsoft Excel. GEE was primarily used for data access, filtering, and spatial preprocessing, whereas R and Statistica were used for statistical analysis, trend detection, drought characterization, and graphical visualization.

## 3.3. Assessment of Spatio-Temporal Land Use/Land Cover (LULC) Changes and Their Interaction with Climatic Variability (Objective 2)

This section describes the methods used to map land use/land cover (LULC), evaluate classification accuracy, and quantify spatio-temporal LULC transitions within the Elnour Natural Forest Reserve (ENFR). The methodological framework integrates multi-source satellite data, field observations, machine learning classification, and change detection analysis to ensure a robust and reproducible assessment of landscape dynamics (Fig. 3.5).

### 3.3.1. Data collection and Preprocessing

The methodological workflow adopted in this study is illustrated in Fig. 3.5. Landsat imagery provides a consistent long-term archive suitable for historical LULC analysis, whereas Sentinel-2 imagery offers higher spatial resolution that improves the detection of fine-scale vegetation patterns in recent years (Qu et al., 2021). In this study, multi-temporal datasets from Landsat 5 Thematic Mapper (TM) and Sentinel-2 MultiSpectral Instrument (MSI) were obtained from the Google Earth Engine (GEE) open-access data catalogue. Landsat 5 TM imagery was used for the years 1995 and 2008, while Sentinel-2 MSI imagery was used for 2021.

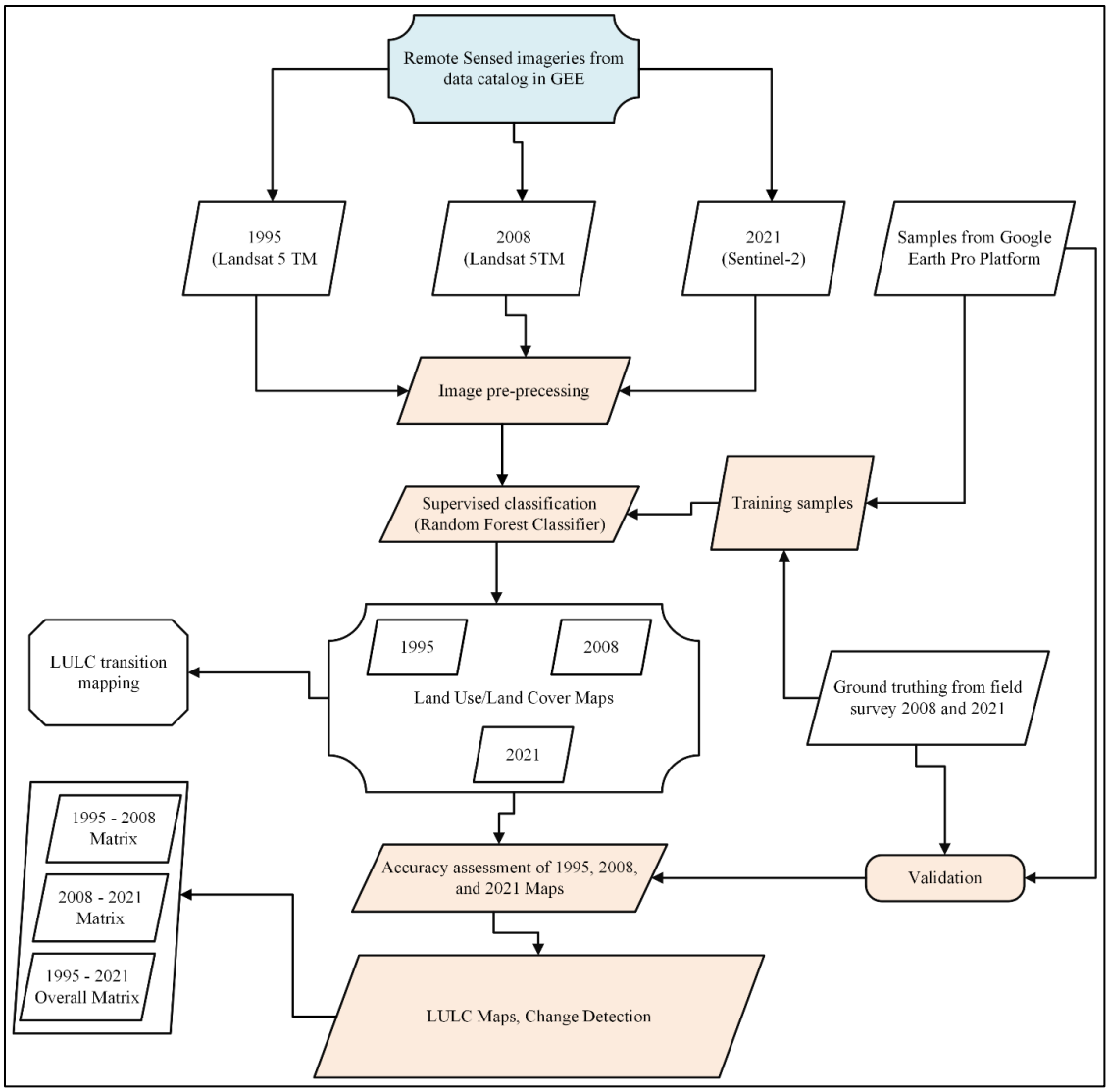


Fig. 3.5. Workflow of data collection, preprocessing, classification, accuracy assessment, and LULC change detection in Elnour Natural Forest Reserve (ENFR).

The use of Sentinel-2 for 2021 was justified by its higher spatial resolution (10 m), which enhances the discrimination of heterogeneous vegetation structures and improves classification accuracy in dryland ecosystems. In contrast, Landsat data (30 m) were used for earlier years due to their long historical record and consistency, ensuring temporal comparability across the study period. Surface reflectance products were used for all sensors to ensure atmospheric correction and radiometric consistency, including Landsat Collection 2 Level-2 and Sentinel-2 Level-2A datasets. All preprocessing was conducted within the GEE environment to maintain methodological consistency across sensors and years. Preprocessing steps included cloud and cloud-shadow masking using quality-assurance bands, image filtering based on cloud cover thresholds (<20%), geometric correction, and spectral band stacking.

To ensure spatial compatibility between datasets, Landsat imagery was resampled to 10 m to match Sentinel-2 spatial resolution. Although resampling does not increase the intrinsic spatial detail of Landsat data, it ensures pixel-level alignment and facilitates integration within a unified classification framework.

The number of cloud-free images retained after filtering varied across reference years due to differences in sensor characteristics, revisit frequency, and atmospheric conditions. Landsat sensors (TM and OLI) have a revisit interval of 16 days, whereas Sentinel-2 MSI provides a higher revisit frequency (5–10 days), resulting in a greater number of available observations in recent years. In addition, interannual variability in cloud cover and atmospheric conditions influenced the number of usable images after quality filtering. Consequently, approximately 21 images were used for 1995, 23 images for 2008, and 45 images for 2021.

For each reference year, annual median composites were generated using all available cloud-free images acquired between 1 January and 31 December. This compositing approach reduces noise, minimizes the influence of residual clouds and atmospheric variability, and ensures a robust and consistent representation of vegetation conditions for multi-temporal comparison (Griffiths et al., 2013; Hermosilla et al., 2015).

### 3.3.2. Training and Testing Data for the Classification Algorithm

Accurate LULC mapping depends on the quality of training data, the representativeness of classes, and the reliability of reference information (Griffiths et al., 2013; Idreas, 2015; Gorelick et al., 2017). In this study, four LULC classes were defined consistently across all years: Bareland, Semi-bareland, Light Forest, and Dense Forest (Table 3.1).

Table 3.1. Definitions of land use classes used in this study

| No. | Land Use Classes | Class description |
|---|---|---|
| 1 | Bareland | Areas with no vegetation cover and exposed soil surfaces |
| 2 | Semi-bareland | Areas with less than 10% tree-canopy cover |
| 3 | Light Forest | Areas with at least 10% but less than 40% tree-canopy cover |
| 4 | Dense Forest | Areas with more than 40% tree-canopy cover |

These classes were established based on canopy cover thresholds and ecological characteristics derived from previous studies (Potapov et al., 2022), supported by field observations, expert knowledge, and interpretation of high-resolution imagery in Google Earth Pro. Representative field photographs illustrating the structural characteristics of each class are provided in Fig. 3.6 to support class interpretation.

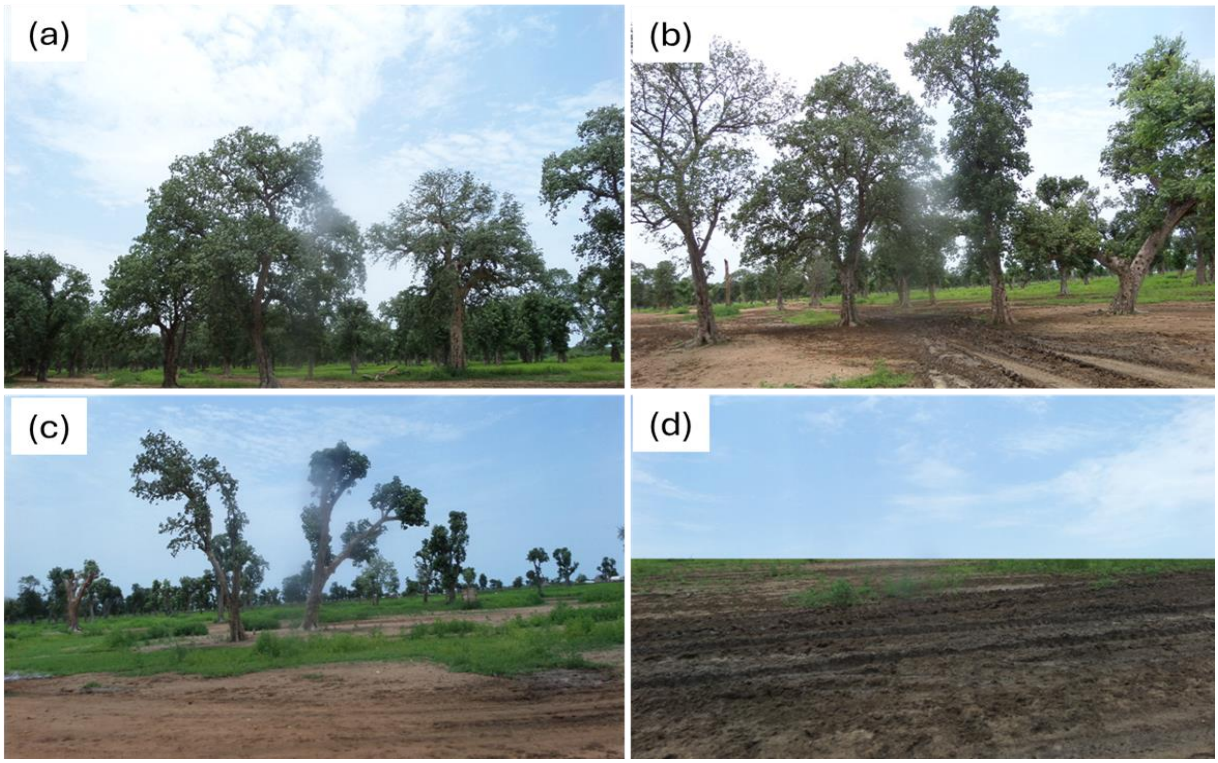


Fig. 3.6. Representative field photographs of land cover classes in the Elnour Natural Forest Reserve (ENFR): (a) Dense Forest, (b) Light Forest, (c) Semi-bareland, and (d) Bareland.

Two field campaigns were conducted in 2008 and 2021, each providing 229 georeferenced ground reference samples. These were complemented by 687 samples derived from onscreen digitization of high-resolution imagery in Google Earth Pro, a method widely recognized for generating reliable training and validation datasets in remote sensing studies (Hansen et al., 2008; Phan et al., 2020; de Sousa et al., 2020). This resulted in a total of 916 samples per reference year. All samples were carefully cross-checked against the corresponding satellite imagery and high-resolution reference data to ensure correct class labeling, spectral consistency, and internal homogeneity, thereby reducing classification uncertainty.

Training polygons were deliberately selected to be small, compact, and internally homogeneous to minimize spectral mixing and spatial autocorrelation while capturing intra-class variability. Although LULC classes were partly defined based on canopy cover thresholds, homogeneous sampling units were ensured by selecting spectrally uniform patches that clearly represent each class. The sampling strategy was aligned with the spatial resolution of the imagery after resampling to 10 m, enabling improved discrimination between spectrally similar classes such as Bareland and Semi-bareland. All reference samples were visually verified against the corresponding year-specific satellite imagery and high-resolution Google Earth imagery prior to classification to ensure spatial accuracy and class consistency.

For each reference year (1995, 2008, and 2021), independent datasets were prepared to avoid temporal bias. Each dataset was split into 70% (641 samples) for training and 30% (275 samples) for independent validation (Appendix B). To further reduce spatial dependence and overfitting, validation samples were randomly distributed and located at least 100 m away from training samples, following best-practice recommendations (Hansen et al., 2008). This approach ensured robust, independent, and representative datasets for each reference year. Consequently, each year was classified using fully independent training and validation datasets, ensuring temporal consistency and preventing data leakage between years.

### 3.3.3. Classification of Landsat and Sentinel-2 Images

Supervised classification was performed using the Random Forest (RF) algorithm implemented in Google Earth Engine (GEE), which provides advanced non-parametric machine-learning approaches for remote sensing applications, including RF, Support Vector Machines (SVM), and Classification and Regression Trees (CART) (Lin et al., 2020). RF is widely applied in land-use/land-cover (LULC) mapping due to its high predictive accuracy, robustness to noise and outliers, and strong resistance to overfitting (Breiman, 2001; Tamiminia et al., 2020; Pelletier et al., 2016; Zurqani et al., 2018; Tong et al., 2020). Its effectiveness has been demonstrated in multi-source and multi-temporal remote sensing studies, particularly in heterogeneous dryland environments.

The RF algorithm constructs an ensemble of decision trees, where each tree contributes a vote to determine the final class label (Breiman, 2001; Fonseka et al., 2019). It requires optimization of a limited number of parameters and performs efficiently on large and noisy datasets. Its ability to handle high-dimensional data and reduce overfitting enhances its reliability for LULC classification tasks (Phan et al., 2020; de Sousa et al., 2020; Ge et al., 2019). A meta-analysis of more than 300 studies confirmed that RF is the most widely used classifier for satellite-based LULC mapping in GEE (Tamiminia et al., 2020).

To ensure consistency across sensors with different spectral configurations, only spectrally comparable bands were selected. For Landsat 5 TM, the selected bands were Blue, Green, Red, Near-Infrared (NIR), Shortwave Infrared 1 (SWIR1), and Shortwave Infrared 2 (SWIR2). For Sentinel-2 MSI, the corresponding bands were B2 (Blue), B3 (Green), B4 (Red), B8 (NIR), B11 (SWIR1), and B12 (SWIR2). In total, six spectrally comparable bands were used for each sensor, ensuring cross-sensor consistency while effectively capturing vegetation structure, chlorophyll content, and moisture conditions.

The Normalized Difference Vegetation Index (NDVI) was used as the sole vegetation index due to its robustness, simplicity, and proven effectiveness in characterizing vegetation dynamics in dryland ecosystems. Additional vegetation indices were not included to avoid redundancy and multicollinearity, as NDVI sufficiently captures vegetation greenness and productivity for the purposes of this study.

The RF model was implemented using 100 trees (ntree = 100), while the number of variables considered at each split followed the default square-root rule (mtry). These parameter settings are widely recommended and provide stable and reliable classification performance across different environmental conditions (Ghimire et al., 2012; Fonseka et al., 2019).

### 3.3.4. Accuracy Assessment

The reliability of any thematic LULC map depends on both its overall accuracy and the class-specific accuracy of individual land-cover categories (Warrens, 2015). Accuracy assessment typically employs several well-established metrics, including overall accuracy (OA), producer's accuracy (PA), and user's accuracy (UA) (Appendix C). In this study, OA, PA, and UA were computed for each reference year, while the kappa coefficient was excluded due to its widely documented limitations in reflecting true map reliability (Foody, 2020).

To provide a more robust class-specific measure of accuracy, the F1-score was also calculated, which synthesizes PA and UA into a single metric ranging from 0 to 100% (Congalton & Green, 2019). The F1-score for class *i* was computed as:

$$F1_i = \frac{2 \times PA_i \times UA_i}{PA_i + UA_i} \quad (5)$$

Given ongoing concerns regarding the interpretability and statistical limitations of the kappa coefficient in thematic accuracy assessment (Foody, 2020), two complementary disagreement metrics, quantity disagreement (QD) and allocation disagreement (AD), were incorporated, as proposed by Pontius and Millones (2011). QD quantifies discrepancies between observed and predicted class proportions, whereas AD captures differences in the spatial allocation of predicted versus observed samples. Together, these metrics provide a more nuanced and reliable characterization of classification performance.

### 3.3.5. Land Use/Land Cover (LULC) Change Detection

LULC dynamics were quantified by comparing classified maps across time. The proportional change in each LULC category was computed following the approach in (Anand and Oinam, 2020) using:

$$C = \frac{C_2 - C_1}{C_1} \times 100 \qquad (6)$$

where $C_1$ and $C_2$ represent class areas in the baseline and comparison years, respectively.

Transition matrices were generated to quantify gains, losses, persistence, and class-to-class conversions. Changes were evaluated for the periods 1995–2008, 2008–2021, and 1995–2021, thereby capturing both medium-term and long-term landscape dynamics.

#### 3.3.6. Land Use/Land Cover (LULC) Transition Mapping

To analyze spatial patterns of change, transition maps and matrices were generated using ArcGIS Pro 3.6, following established LULC transformation approaches (Nath et al., 2018; Barnieh et al., 2020). Classified maps from 1995, 2008, and 2021 were overlaid to identify class-to-class transitions over 13-year and 26-year intervals. This approach enabled a detailed assessment of the direction, magnitude, and spatial distribution of land-cover transformations within ENFR.

Overall, the LULC classification framework was designed to ensure cross-sensor comparability, temporal independence, and reproducibility. Comparable spectral bands were selected across sensors, all samples were verified against year-specific imagery, and each reference year was classified using independent training and validation datasets. These steps reduced classification uncertainty and improved the reliability and consistency of spatio-temporal LULC comparisons.

### 3.4. Evaluation of Changes in Woody Species Composition, Diversity, and Regeneration under Climatic Variability and Anthropogenic Pressures (Objective 3)

This objective evaluates temporal changes in woody species composition, stand structure, diversity, and regeneration status within the Elnour Natural Forest Reserve (ENFR) using repeated measurements from a permanent sample-plot network. This approach enables a direct, consistent, and reliable assessment of ecological change over time and supports the interpretation of vegetation dynamics in relation to climatic variability and anthropogenic pressures.

#### 3.4.1. Data Collection

The spatial distribution and temporal dynamics of woody species composition, diversity, and regeneration were assessed using a network of 229 permanent sample plots established across Elnour Natural Forest Reserve (ENFR). Each plot had a radius of 17.84 m, corresponding to an area of 1,000 m². The plots were systematically arranged along 18 transects, with a spacing of

100 m between adjacent plots and 200 m between transects. This sampling design ensures adequate spatial coverage and representation of vegetation heterogeneity within the reserve.

The permanent plots were first established and surveyed in 2008 and subsequently revisited in 2021 using identical plot locations and measurement protocols. The use of consistent plot locations and standardized field procedures ensures comparability between survey periods and allows robust assessment of temporal changes in forest structure and species composition (Fig. 3.7).

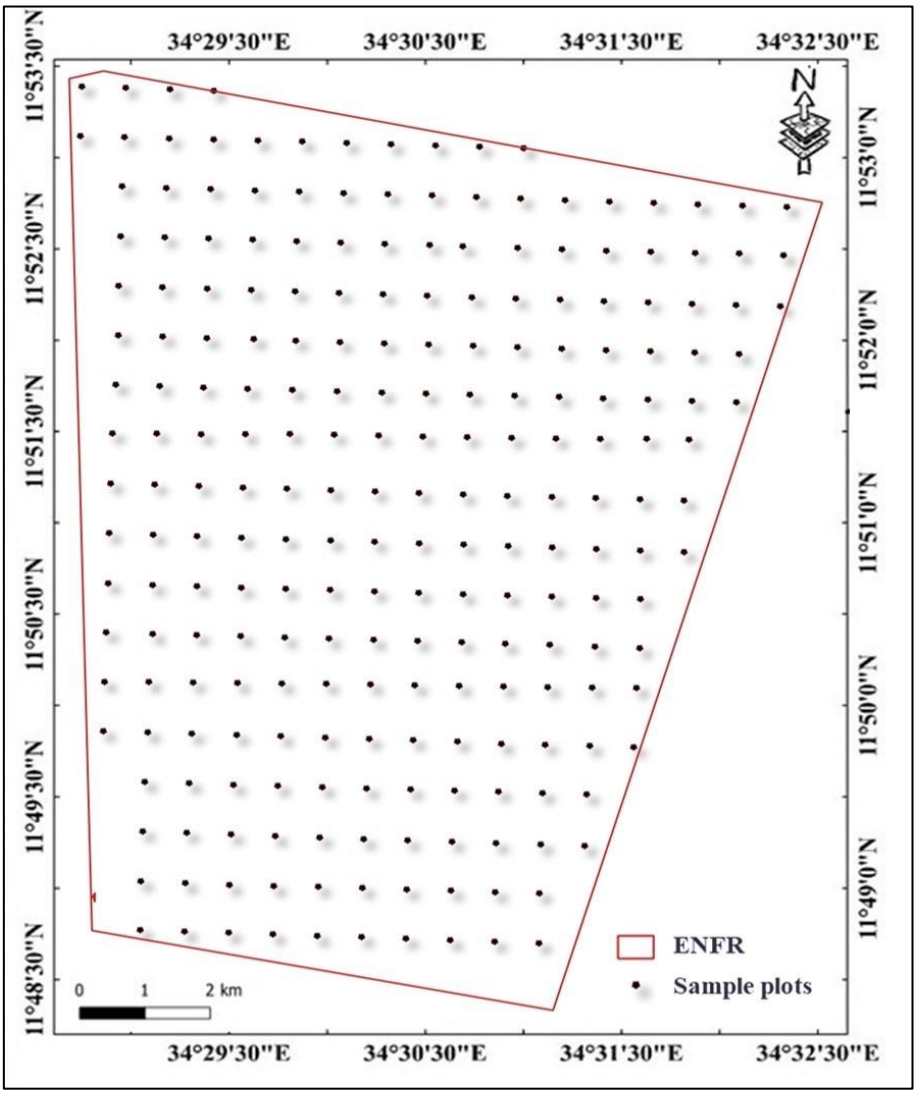


Fig. 3.7. Spatial distribution of sampling plots within Elnour Natural Forest Reserve (ENFR), Blue Nile State, Sudan.

Within each plot, all woody plant species were identified in the field by a professional botanist to ensure taxonomic accuracy. Individual plants were classified into three regeneration and growth classes based on stem diameter: seedlings (stem diameter < 3 cm), saplings (3 cm ≤ stem diameter < 7 cm), and adult trees (diameter at breast height (DBH) ≥ 7 cm) (Mohammed et al., 2021a; Yasin and Mulyana, 2022). For seedlings and saplings, diameter was measured at

the stem collar due to their small size (Ibrahim and Hassan, 2015; Maua et al., 2020), whereas DBH for adult trees was measured at 1.3 m above ground level using calipers. Tree height was measured using a Suunto hypsometer following standard forestry procedures (Ouedraogo et al., 2019; Ibrahim et al., 2018). All plots were georeferenced using a handheld GPS to ensure accurate spatial positioning and facilitate consistent relocation during remeasurement.

### 3.4.2. Data Analysis

Field data were analyzed to quantify changes in woody species composition, stand structure, diversity, and regeneration status in the ENFR. Initial data processing and organization were conducted using Microsoft Excel 2016, while statistical analyses were performed in R (version 4.5.2) and Statistica 13.0. Descriptive statistics were computed for key structural variables, including tree diameter, height, and density. Data normality was assessed using the Shapiro–Wilk test to ensure the validity of subsequent statistical interpretations.

The ecological importance of each species was evaluated using the Importance Value Index (IVI), which integrates three key structural parameters: Relative Frequency (RF), Relative Density (RDe), and Relative Dominance (RDo), following established phytosociological approaches (Mohammed et al., 2021a; Ibrahim et al., 2014; Assogbadjo et al., 2010). Frequency was calculated as the number of plots in which a species occurred, density as the number of individuals per unit sampled area, and dominance as the total basal area contributed by each species. Relative values were computed to standardize these measures across species, and IVI was derived as the sum of RF, RDe, and RDo. In addition, Relative Abundance (RA) was calculated to represent the proportional contribution of each species within the sampled plots, although it was not included in the IVI computation (Yasin and Mulyana, 2022; Gurashi et al., 2024a).

Regeneration status was assessed based on the population structure of seedlings, saplings, and adult individuals. Species were categorized into four regeneration classes: good, fair, poor, and no regeneration, following criteria proposed by Maua et al. (2020) and Mohammed et al. (2021a). Good regeneration was defined as species with more seedlings than saplings and more saplings than adult trees. Fair regeneration included species with more seedlings than saplings but fewer saplings than adults. Poor regeneration referred to species represented only by saplings and adult individuals, while species recorded exclusively in the adult stage were classified as having no regeneration. Seedling, sapling, and adult tree densities were calculated by dividing the number of individuals in each class by the total sampled area (Mohammed et al., 2021a; Idrissa et al., 2018).

Basal area was calculated using standard forestry equations based on diameter at breast height (DBH), and these values were used to derive dominance and relative dominance (Ibrahim et al., 2014; Assogbadjo et al., 2010). Biodiversity was assessed using widely accepted diversity indices, including Simpson's Diversity Index, Shannon–Wiener Diversity Index, Margalef Species Richness Index, and species evenness, which together provide complementary measures of species diversity, richness, and distribution patterns within the forest community (Idrissa et al., 2018; Assogbadjo et al., 2010; Listopad et al., 2018; Ghanbari et al., 2021; Asbeck et al., 2021).

To support ecological interpretation and conservation prioritization, species were further categorized based on their Relative Density (RDe) into abundance classes: abundant (RDe ≥ 5.00), frequent (4.00 ≤ RDe < 5.00), occasional (3.00 ≤ RDe < 4.00), rare (1.00 ≤ RDe < 3.00), and threatened (RDe < 1.00), following Ogwu et al. (2016). This classification facilitates the identification of dominant, declining, and vulnerable species within the ecosystem.

Overall, the structural attributes, ecological importance, and diversity of woody species in the ENFR were quantified using standard phytosociological and biodiversity metrics. The combined application of these indices provides a comprehensive, consistent, and reproducible framework for assessing vegetation structure, species composition, and regeneration dynamics under changing environmental conditions (Table 3.2).

Table 3.2. Equations and indices used for calculating stand structure, species importance, and biodiversity of woody species in the Elnour Natural Forest Reserve (ENFR).

| Equation | Reference |
|---|---|
| Tree basal area (Ba) = $\frac{\pi(DBH)^2}{4}$ | (Ibrahim and Hassan, 2015) |
| Frequency (F) = Number of plots in which a species occurs | (Mohammed et al., 2021a) |
| Relative frequency (RF) = $\left(\frac{Tree\ species\ frequency}{Total\ frequency\ for\ all\ species}\right) \times 100$ | (Idrissa et al., 2018) |
| Dominance (Do) = Total basal area of the species | (Ibrahim et al., 2015) |
| Relative dominance (RDo) = $\left(\frac{Species\ dominance}{Total\ dominance\ for\ all\ species}\right) \times 100$ | (Ibrahim and Osman, 2014) |
| Density (De) = Number of individuals of a species per unit sampled | (Maua et al., 2020 |
| Relative Density (RDe) = $\left(\frac{Density\ of\ a\ species}{Total\ density\ for\ all\ species}\right) \times 100$ | (Mohammed et al., 2021a) |
| Abundance (A) = Number of individuals of a species per sampled | (Maua et al., 2020) |
| Relative abundance (RA) = $\left(\frac{Tree\ species\ abundance}{Total\ abundance\ for\ all\ species}\right) \times 100$ | (Mohammed et al., 2021a) |
| IVI = Relative frequency + Relative dominance + Relative density | (Mohammed, 2019) |

| | |
|---|---|
| Simpson's Species Diversity index (D) = $(\frac{\Sigma n(n-1)}{N(N-1)})$ | (Frerebeau, 2019) |
| Simpson's Species Diversity index (1-D) = 1-D | (Frerebeau, 2019) |
| Margalef species richness index (M) = $\frac{(s-1)}{lnN}$ | (Gamito, 2010) |
| Species Evenness Index; EH = H / Hmax = $\sum_{i=1}^{S} \frac{piln(pi)}{ln(S)}$ | (Okpiliya, 2012) |
| Shannon-Weiner diversity index (H') = - $\Sigma^{s}_{i=1} P_i \ln P_i$ | (Shannon and Weaver, 1949) |

## 3.5. Mapping of Dominant Tree Species Using Multi-Source Remote Sensing Data and Machine Learning Approaches (Objective 4)

This objective integrates field observations and multi-source remote sensing data to map dominant woody species in the Elnour Natural Forest Reserve (ENFR) across four reference years (2008, 2013, 2018, and 2021). The approach combines multi-temporal satellite imagery, ecological field data, and machine learning techniques to produce spatially explicit and temporally consistent maps of species distribution.

### 3.5.1. Data Collection and Analysis

Understanding the spatio-temporal dynamics of forest composition and dominant tree species requires a structured and reproducible framework integrating remote sensing data, field observations, and machine learning classification (Fig. 3.8) (Gorelick et al., 2017; Belgiu and Drăguţ, 2016). Data were compiled for four reference years (2008, 2013, 2018, and 2021) to capture temporal changes in forest composition under varying environmental and anthropogenic conditions.

The workflow includes remote sensing data acquisition, preprocessing, feature dataset construction, classification using multiple machine learning algorithms, feature importance analysis, accuracy assessment, and final mapping of dominant tree species. This integrated framework ensures methodological consistency, comparability across years, and reproducibility of results (Fassnacht et al., 2016; Axelsson et al., 2021).

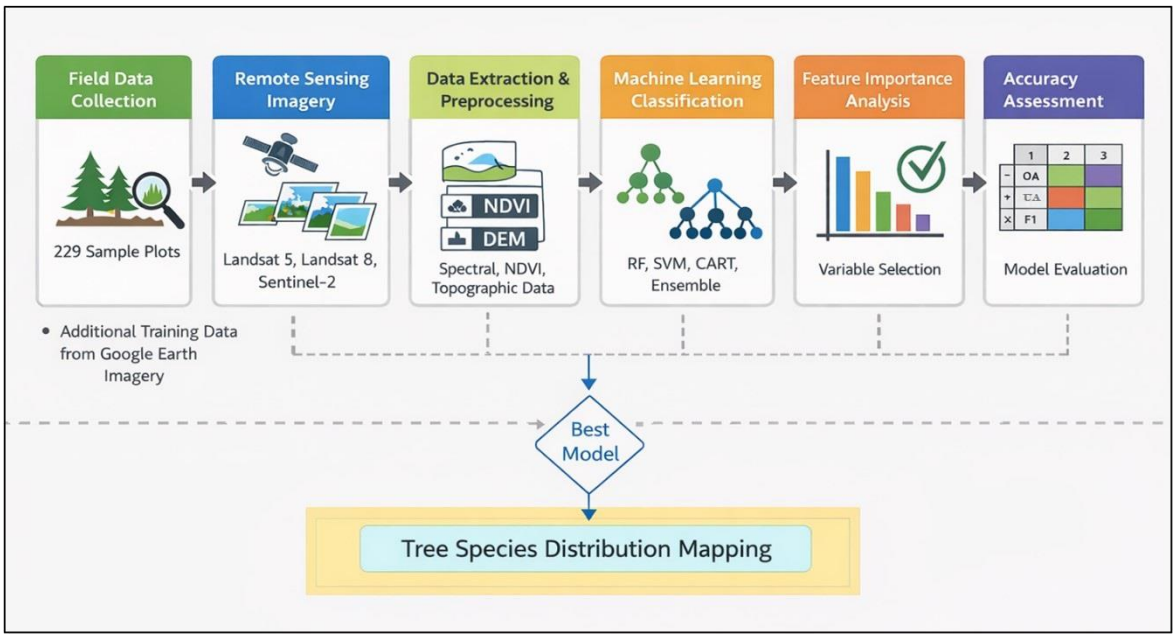


Fig. 3.8. Illustrates the overall workflow of the study, including data collection, preprocessing, feature construction, classification (RF, SVM, CART, and ensemble), feature importance analysis, and accuracy assessment.

### 3.5.2. Remote Sensing Data Collection and Processing

Satellite imagery was acquired for each reference year to ensure consistent spatial coverage of the Elnour Natural Forest Reserve (ENFR). Landsat 5 TM imagery was used for 2008, Landsat 8 OLI for 2013, and Sentinel-2 MSI for 2018 and 2021. The use of Sentinel-2 imagery for recent years is justified by its higher spatial resolution (10 m), which improves the discrimination of heterogeneous vegetation structures and enhances species separability. In contrast, Landsat data were used for earlier years to maintain long-term temporal consistency and ensure continuity in multi-temporal analysis (Fassnacht et al., 2016; Persson et al., 2018).

All available cloud-free images acquired between 1 January and 31 December for each reference year were utilized. After quality filtering, approximately 23 images were retained for 2008, 24 images for 2013, and 45 images for both 2018 and 2021. The variation in the number of retained images reflects differences in sensor revisit frequency and atmospheric conditions. Landsat sensors have a revisit interval of 16 days, whereas Sentinel-2 provides more frequent observations (5–10 days), resulting in a higher number of available images in recent years. Additionally, interannual variability in cloud covers influences the number of usable images after filtering. This full-year data acquisition approach ensures robust temporal representation and effectively captures intra-annual variability in vegetation conditions (Griffiths et al., 2013; Hermosilla et al., 2015).

All preprocessing was conducted in Google Earth Engine (GEE) using surface reflectance datasets (Landsat Collection 2 Level-2 and Sentinel-2 Level-2A), which include atmospheric correction. Additional preprocessing steps included cloud and cloud-shadow masking using quality assurance (QA) bands, image filtering based on cloud cover thresholds, and geometric alignment to ensure consistency across sensors and acquisition dates (Gorelick et al., 2017; Wang et al., 2020).

To characterize vegetation phenology, monthly greenest-pixel composites were generated using a Normalized Difference Vegetation Index (NDVI)-based quality mosaic approach. For each month, the pixel with the highest NDVI value was selected, representing peak vegetation conditions while minimizing the effects of cloud contamination, atmospheric noise, and residual shadows (Huete et al., 2002; Belgiu and Drăguţ, 2016; Praticò et al., 2021). This process resulted in 12 NDVI layers (NDVI1–NDVI12) per year, effectively capturing intra-annual vegetation dynamics.

To ensure spectral consistency across sensors, only comparable spectral bands were used. These included the blue, green, red, near-infrared (NIR), and shortwave infrared bands (SWIR1 and SWIR2) from Landsat sensors, along with the corresponding bands (B2, B3, B4, B8, B11, and B12) from Sentinel-2. Landsat imagery (30 m spatial resolution) was resampled to 10 m to match the spatial resolution of Sentinel-2. This resampling ensured geometric compatibility and seamless dataset integration, although it did not increase the intrinsic spatial detail of the Landsat data.

Topographic variables, including elevation, slope, and aspect, were derived from the Shuttle Radar Topography Mission (SRTM) digital elevation model at 30 m resolution and subsequently resampled to 10 m. These variables were incorporated to represent terrain-driven environmental gradients that influence species distribution and habitat variability (Farr et al., 2007; Sesnie et al., 2008; Smith et al., 2019).

For each reference year, spectral bands, monthly NDVI layers, and topographic variables were combined into year-specific feature datasets. In this study, the term *multi-temporal* refers to the integration of intra-annual (monthly) information within each individual year, rather than combining multiple years into a single dataset. Consequently, four independent feature datasets were generated and classified separately to ensure temporal consistency and avoid inter-annual bias (Axelsson et al., 2021; Zhong et al., 2024).

### 3.5.3. Training Samples Collection and Dataset Preparation

A total of 229 permanent sample plots (1,000 m² each) were used as the primary source of training and validation data. These plots were initially established and surveyed in 2008 and subsequently revisited in 2013, 2018, and 2021 using identical locations and measurement protocols to ensure temporal consistency.

Within each plot, all woody species were identified by a professional botanist to ensure taxonomic accuracy (Abdelrahim, 2015; Abdou et al., 2016). These field data were complemented by additional training samples derived from high-resolution Google Earth imagery, particularly in areas not accessible during field surveys, thereby improving spatial coverage and representativeness (Congalton & Green, 2019; Fassnacht et al., 2016).

All samples were carefully cross-checked against the corresponding satellite imagery for each reference year to ensure spectral consistency, spatial accuracy, and class homogeneity. Only homogeneous and clearly identifiable species patches were retained to minimize classification uncertainty and mixed-pixel effects.

Samples were labeled using species codes and organized into year-specific datasets, ensuring that each reference year had independent training and validation datasets. A stratified sampling strategy was applied to ensure balanced representation of dominant species classes. Each dataset was divided into 70% for training and 30% for independent validation, thereby ensuring robust and unbiased model evaluation.

Predictor variables, including spectral bands, monthly NDVI layers, and topographic variables, were extracted for each sample using Google Earth Engine, ensuring standardized and consistent input data for all classification models (Pal, 2005; Belgiu and Drăguţ, 2016).

### 3.5.4. Variable Selection and Feature Importance

Predictor variables included spectral bands, monthly NDVI layers, and topographic variables, representing the combined influence of physiological, phenological, and environmental factors on species distribution. The integration of multi-source predictors enhances the ability to capture structural and functional variability in dryland forest ecosystems.

Monthly NDVI variables were particularly important for capturing intra-annual vegetation dynamics, thereby improving species discrimination in dryland environments where spectral similarity among species is high (Huete et al., 2002; Persson et al., 2018). Topographic variables derived from the digital elevation model (DEM), including elevation, slope, and aspect, were incorporated to represent environmental gradients influencing soil moisture availability, microclimatic conditions, and species composition (Sesnie et al., 2008).

Feature importance was evaluated using algorithm-specific approaches. In Random Forest (RF), importance was assessed using permutation-based methods that quantify the impact of each variable on model performance (Breiman, 2001). In Classification and Regression Trees (CART), importance was derived from split frequency and hierarchical structure within the decision tree, reflecting the contribution of variables to class separation (Breiman et al., 1984). For Support Vector Machines (SVM), sensitivity analysis was applied to evaluate the influence of predictor variables on class discrimination (Cortes and Vapnik, 1995; Ramezan et al., 2019).

To enhance robustness and reduce algorithm-specific bias, feature importance results were compared and aggregated across classifiers using an ensemble approach (James et al., 2013; Kuhn and Johnson, 2013; Chung et al., 2021). This integrative strategy ensures a more consistent and reliable interpretation of variable contributions across study years and supports the identification of ecologically meaningful predictors (Zhong et al., 2024).

**3.5.5. Machine Learning Algorithms**

Google Earth Engine provides an integrated platform for supervised classification using various machine learning algorithms. In this study, four classification approaches were implemented: Random Forest (RF), Support Vector Machine (SVM), Classification and Regression Trees (CART), and an ensemble voting approach.

Random Forest was selected as the primary classifier due to its strong predictive performance, robustness to noise, and ability to handle high-dimensional datasets (Breiman, 2001; Vorpahl et al., 2012; Ließ et al., 2012). Support Vector Machine was included due to its effectiveness in non-linear classification using a radial basis function (RBF) kernel (Cortes and Vapnik, 1995; Bishop & Nasrabadi, 2006; Chung et al., 2021). CART was applied for its interpretability and simplicity (Breiman et al., 1984).

An ensemble voting approach was implemented to combine predictions from RF, SVM, and CART using a majority voting scheme. This approach was included to evaluate whether combining classifiers could improve classification robustness and reduce the influence of individual model biases under heterogeneous dryland conditions (Ali et al., 2023).

Hyperparameter tuning was performed for all classifiers using a grid search approach combined with stratified k-fold cross-validation (Stromann et al., 2019; Kuhn and Johnson, 2013). Key parameters included the number of trees and variables per split for Random Forest, cost and gamma parameters for SVM, and tree complexity parameters for CART.

### 3.5.6. Accuracy Assessment

Classification performance was evaluated using independent validation datasets and confusion matrix-based accuracy metrics, including overall accuracy (OA), producer's accuracy (PA), user's accuracy (UA), kappa coefficient, and F1-score.

Stratified 5-fold cross-validation was applied to ensure robust and unbiased model evaluation (Fathizad et al., 2020; Ramezan et al., 2019; Kuhn and Johnson, 2013; James et al., 2013). Overall accuracy represents the proportion of correctly classified samples, while producer's and user's accuracy indicate omission and commission errors, respectively. The kappa coefficient measures agreement beyond chance, and the F1-score provides a balanced measure of classification performance (Praticò et al., 2021; Lu & Weng, 2007; Lee et al., 2016). All accuracy metrics were calculated using standard equations to ensure consistency and comparability across classifiers and reference years as follow:

$$OA = \frac{1}{N}\sum_{i=j=1}^{n} C_{ij} \quad (7)$$

$$PA = \frac{C_{ij}}{\sum_{i=j=1}^{n} C_j} \quad (8)$$

$$UA = \frac{C_{ij}}{\sum_{i=j=1}^{n} C_i} \quad (9)$$

$$F = \frac{2 \times PA \times UA}{PA + UA} \quad (10)$$

$$\text{Kappa} = \frac{N\sum_{i=j=1}^{n} C_{ij} - \sum_{i=j=1}^{n} C_i\, C_j}{N^2 - \sum_{i=j=1}^{n} C_i\, C_j} \quad (11)$$

Where $N$ is the total number of validation samples, and $n$ is the number of classes. $C_{ij}$ represents the number of samples belonging to reference class $i$ and classified as class $j$, while $C_{ii}$ denotes correctly classified samples (diagonal elements of the confusion matrix). $C_{i+}$ and $C_{+i}$ represent the row and column totals, corresponding to the total reference and classified samples for class $i$, respectively.

Overall, the species-mapping workflow was designed as a set of independent year-specific classifications using harmonized spectral bands, monthly NDVI composites, and DEM-derived terrain variables. This design ensures temporal consistency, reduces inter-annual bias, and

improves the interpretability and robustness of multi-source remote sensing data for dominant tree-species discrimination in heterogeneous dryland environments.

## 3.6. Modeling and Prediction of the Current and Future Potential Distribution of *Acacia seyal* (Delile) under Climate Change Scenarios (Objective 5)

This objective model and predicts the current and future habitat suitability of *Acacia seyal* across Sudan using species occurrence records and environmental predictor variables. The approach integrates field observations, secondary occurrence data, environmental variables, and species distribution modelling to assess spatial patterns and future shifts under climate change scenarios.

### 3.6.1. Establishing species occurrence records

Occurrence records for *Acacia seyal* (Delile) were assembled from multiple complementary sources to build a comprehensive distribution dataset (Fig. 3.9). The primary dataset originated from field campaigns conducted between August 2022 and March 2023 in Blue Nile, North Darfur, North Kordofan, Sinnar, White Nile, West Kordofan, and West Darfur States. During field surveys, individual trees were located and opportunistically georeferenced using a handheld Garmin GPS receiver.

Additional presence records were compiled from multiple secondary sources, including the National Forest Inventory (NFI) (n = 215; FNC, 2021), the Global Biodiversity Information Facility (GBIF; n = 22; https://www.gbif.org; accessed 10 October 2025), and the International Union for Conservation of Nature (IUCN; n = 22; http://www.iucnredlist.org; accessed 10 October 2025). Further occurrence data were obtained from the Faculty of Forestry, University of Khartoum (Students' Working Plans; n = 1,254), as well as from previously published studies reporting confirmed occurrences of *Acacia seyal* (Delile) (n = 275; Gibreel, 2008; FNC, 2021; Gamal et al., 2022; Hasoba et al., 2025). After compilation and initial screening, these sources yielded a total of 1,988 presence locations for *Acacia seyal* (Delile).

All coordinates were converted to decimal degrees and subsequently matched to a 1 × 1 km spatial grid to minimize spatial redundancy and reduce the effects of inflated sampling density. This grid-based filtering also ensured full compatibility with the environmental predictor variables used in the species distribution modelling workflow. The spatial accuracy and consistency of each presence record were evaluated using ArcGIS Pro 3.6, and any points falling outside Sudan's geopolitical boundaries were excluded to eliminate errors related to mislabelled or inaccurately georeferenced locations.

To further mitigate sampling bias and spatial autocorrelation, the occurrence dataset was subjected to spatial thinning using the *spThin* package in R. A conservative minimum nearest-neighbour distance of 1 km was applied, ensuring that only spatially independent records were retained. Following this filtering procedure, 448 unique and spatially independent presence points remained and were used to model habitat suitability for *Acacia seyal* (Delile) across Sudan. The final sample size exceeds standard thresholds for robust species distribution modelling, thereby improving model stability, predictive accuracy, and ecological reliability.

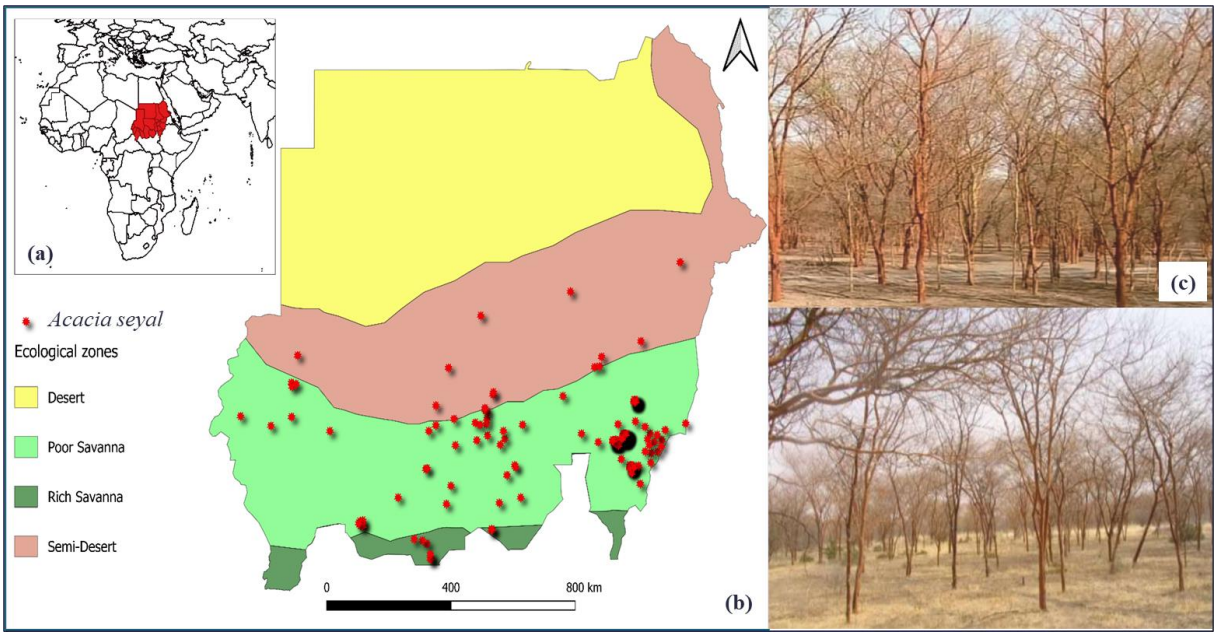


Fig. 3.9. Geographic distribution of Acacia seyal (Delile) and ecological zones in Sudan. (a) Location of Sudan within Africa; (b) distribution of *Acacia seyal* occurrence points overlaid on major ecological zones (Desert, Semi-desert, Poor Savanna, and Rich Savanna); (c) representative field photographs of *Acacia seyal* stands in the savanna woodlands.

### 3.6.2. Environmental predictor variables

A suite of environmental predictors representing climatic conditions, edaphic characteristics, and elevation was assembled to support modelling the potential distribution of *Acacia seyal* (Delile) in Sudan (Appendix B). The climatic component consisted of the full set of 19 bioclimatic variables, together with elevation, all provided at 30-arc-second resolution (≈1 km²) from the WorldClim 2.1 database (https://www.worldclim.org/). These bioclimatic layers are derived from long-term interpolations of monthly precipitation and temperature extremes, summarizing near-present climate conditions averaged over the period 1970–2000 (Fick and Hijmans, 2017).

Complementary soil information was obtained from the World Inventory of Soil Emission Potentials (WISE) dataset, available through ISRIC's SoilGrids and linked to the FAO Harmonized World Soil Database (https://www.isric.org/explore/wise-databases). The most recent WISE products provide globally harmonized estimates of soil properties at 30-arc-second spatial resolution, offering critical baseline inputs for environmental modelling (ISRIC, 2016; Batjes, 2016). All spatial layers were clipped to the Sudan boundary using ArcGIS Pro 3.6 (ESRI, 2025) to ensure consistency across datasets.

To reduce the influence of redundant predictors and mitigate multicollinearity, a variance inflation factor (VIF) analysis was conducted as a screening step prior to model calibration. VIF values were computed using R (v.4.4.2), following the standard interpretation that values greater than 10 indicate substantial inflation due to linear dependence among predictors (Bhandari, 2020; Guisande et al., 2017). Variables exceeding this threshold were flagged for exclusion to improve statistical robustness and model interpretability. After assessment, predictors with VIF > 7.5 were removed due to strong cross-correlation. This resulted in the exclusion of twelve variables: bio1, bio4, bio5, bio6, bio7, bio8, bio9, bio11, bio12, bio13, bio16, and bio17.

The final predictor set for MaxEnt consisted of seven low-correlation variables capturing temperature (bio2, bio3, bio10), precipitation (bio14, bio15, bio18, bio19), elevation, and soil properties. Based on the model's relative contribution metrics, this refined set of predictors most effectively represented the environmental gradients associated with the distribution of *Acacia seyal* (Delile) (Appendix B).

### 3.6.3. Projection of the Future Distribution of *Acacia seyal* (Delile) under Shared Socioeconomic Pathways (SSP) Scenarios

Future climatic variables used in this study were derived from the CMIP6 climate projection framework (Eyring et al., 2016). To capture a representative range of potential future climate conditions, two Shared Socioeconomic Pathway (SSP) scenarios, SSP2-4.5 and SSP5-8.5, were selected for the periods 2021–2040 (near future) and 2081–2100 (late century). SSP2-4.5 represents an intermediate stabilization pathway with moderate mitigation efforts, whereas SSP5-8.5 reflects a high-emission, fossil fuel–intensive development trajectory (Riahi et al., 2017). The selection of these contrasting scenarios enables the assessment of species distribution responses under both moderate and extreme climate forcing, thereby improving the robustness and policy relevance of projections for *Acacia seyal* (Delile).

To enhance the reliability of future climate projections, outputs from three CMIP6 global climate models (GCMs) were incorporated: HadGEM3-GC31-LL (UK Met Office), MPI-

ESM1-2-HR (Max Planck Institute), and IPSL-CM6A-LR (Institut Pierre-Simon Laplace). These models were selected based on their demonstrated performance and availability of bias-corrected datasets, which have shown high reliability in previous climate assessments across Sudan and the broader East African and MENA regions (Mesgari et al., 2022; Hamadalnel et al., 2022; Omay et al., 2023; Babiker et al., 2024). Their inclusion ensures that the analysis captures a range of climate sensitivities and structural differences among models.

To reduce uncertainty associated with individual model outputs, an ensemble mean of the three GCMs was calculated. Ensemble averaging is widely recommended in climate impact studies as it minimizes model-specific biases and enhances the stability and robustness of projected climatic patterns. This approach leverages the complementary strengths of individual models, resulting in more consistent and reliable inputs for ecological modelling and species distribution projections.

#### 3.6.4. Modeling procedure and variable contributions

The MaxEnt framework was adopted in this study due to its well-established performance in linking environmental predictors with species occurrence data, as demonstrated by Elith et al. (2010), Phillips et al. (2022), and Koreň et al. (2011). MaxEnt is specifically designed for presence-only datasets (Elith et al., 2006), making it highly suitable for modelling the realized distribution of *Acacia seyal* (Delile). By integrating observed presence records with spatially explicit environmental variables, the algorithm generates robust and reliable estimates of habitat suitability (Phillips et al., 2006a; Pearson et al., 2007). A key methodological advantage of MaxEnt is its robustness to multicollinearity among predictors; even when strongly correlated variables are included, the algorithm reduces their influence internally, thereby mitigating overfitting and redundancy during model calibration (Phillips et al., 2006a; Elith et al., 2010). Following the variance inflation factor (VIF) assessment, a set of nine environmental predictors was retained and combined with the occurrence records of *Acacia seyal* (Delile). These inputs were implemented in MaxEnt version 3.4.4 (https://biodiversityinformatics.amnh.org/open_source/MaxEnt/; Phillips et al., 2006a). For model development, 80% of the occurrence records were randomly allocated for training, while the remaining 20% were used for testing and independent validation. The logistic output format was selected, as it provides continuous probability values (ranging from 0 to 1) representing habitat suitability for each grid cell, which are intuitive for ecological interpretation (Elith et al., 2011). Model configuration included 10,000 maximum iterations, 10 replicate runs, a 20% test proportion, a 10% training presence threshold, and logistic output settings. The final

prediction surface was generated by averaging the outputs of all replicates, thereby reducing stochastic variability and improving model stability.

Model performance was evaluated using the Area Under the Receiver Operating Characteristic Curve (AUC) and the True Skill Statistic (TSS) (Duan et al., 2023; Warren et al., 2021). AUC is widely applied in species distribution modelling because it assesses the model's discriminatory ability independent of a specific threshold, with values ranging from 0 to 1, where 0.5 indicates performance no better than random and 1 represents perfect discrimination between presence and absence (Phillips et al., 2006b). However, for presence-only models, the maximum achievable AUC is typically less than 1 due to inherent sampling limitations (Elith et al., 2011). TSS, derived from the confusion matrix, incorporates both sensitivity (true positive rate) and specificity (true negative rate), providing a threshold-dependent and balanced measure of model performance. TSS values range from −1 to +1, where values greater than 0 indicate predictive performance better than random.

$$TSS = Sensitivity\ (TruePresence) + Specificity\ (TrueAbsence) - 1 \qquad (12)$$

To identify the predictors that most strongly influence the current distribution of *Acacia seyal* (Delile), a Jackknife analysis was conducted. This resampling approach, widely used in ecological niche modelling (Peterson et al., 2007), evaluates variable importance based on two complementary metrics: percent contribution and permutation importance. Permutation importance reflects the dependence of the model on each predictor by randomly permuting its values across presence and background samples and measuring the resulting decrease in AUC; larger decreases indicate higher variable importance (Howse et al., 2020). In addition, percent contribution values were calculated to quantify the relative influence of each predictor on the modeled distribution patterns of *Acacia seyal* (Delile).

**3.6.5. Species habitat suitability categorization**

MaxEnt produces a continuous suitability surface ranging from 0 to 1, representing the favorability of environmental conditions for *Acacia seyal* (Delile). These outputs were converted into discrete habitat suitability classes using the threshold scheme outlined in Table 3.3. The 10th percentile training presence threshold was applied to distinguish suitable from unsuitable areas, following standard practice in presence-only ecological modelling.

The resulting binary layer (1 = suitable, 0 = unsuitable) was further reclassified into Low, Medium, and High suitability categories. Areas with suitability values ≥ 0.60 were considered

highly suitable, indicating strong agreement between environmental conditions and the ecological niche of the species (Elith et al., 2011; Merow et al., 2013).

To evaluate how suitability may change under future climate scenarios, proportional habitat gains or losses were computed by comparing projected and present distributions. Following the method of Hussein & Estifanos (2023), changes were expressed using:

$$SACH = \frac{FSA - CSA}{CSA} \times 100 \qquad (13)$$

where SACH is the percentage change in suitable area, FSA is the future suitable area, and CSA is the current suitable area.

Habitat suitability maps were further classified into four change categories to capture the dynamics of habitat suitability under future climate scenarios. The *loss* class represents areas that are currently suitable but are projected to become unsuitable in the future, indicating potential habitat contraction. The *stable* class includes areas that remain suitable under both current and future conditions, reflecting environmental resilience. The *gain* class identifies areas that are currently unsuitable but are projected to become suitable, suggesting potential range expansion. The *persistent unsuitable* class comprises areas that remain unsuitable across both time periods. Total suitable areas for current and future scenarios under both SSP pathways were calculated using R-based geospatial packages, while raster classification and spatial analyses were performed in ArcGIS Pro 3.6.

Table 3.3. Habitat Suitability Classes Based on Threshold Categories

| No. | Threshold Value | Threshold Description |
|---|---|---|
| 01 | 0.00–0.20 | Unsuitable |
| 02 | 0.21–0.40 | Low |
| 03 | 0.41–0.60 | Medium |
| 04 | ≥ 0.60 | High |

# 4. RESULTS AND DISCUSSION

## 4.1. Overview

This chapter presents and discusses the main findings of the study in relation to existing literature. The results are organized into five main components: (a) long-term climatic variability, trends, and drought dynamics in the savanna woodlands of southeastern Sudan (1950–2024); (b) spatio-temporal land use/land cover (LULC) changes; (c) woody species composition, diversity, and regeneration; (d) mapping of dominant tree species using remote sensing and machine learning; and (e) current and future potential distribution of *Acacia seyal* (Delile) in Sudan.

## 4.2. Analysis of Long-Term Climatic Variability, Trends, and Drought Patterns in Savanna Woodlands of Southeastern Sudan (1950–2024) (Objective 1)

This section presents a comprehensive analysis of long-term climatic variability, drought dynamics, and temperature trends in the Blue Nile savanna based on multiple indicators, including Standardized Precipitation Evapotranspiration Index (SPEI), precipitation, temperature, and dry-spell metrics. The results are structured to capture interannual variability, seasonal and decadal trends, and integrated climate regime shifts, providing a detailed assessment of hydroclimatic changes and their implications for drought processes in semi-arid ecosystems.

### 4.2.1. Interannual and Multi-Decadal Standardized Precipitation Evapotranspiration Index (SPEI) Dynamics

The SPEI, evaluated across multiple accumulation scales (1–48 months), reveals pronounced interannual variability, characterized by alternating wet and dry periods between 1950 and 2022 (Fig. 4.1). A distinct shift is evident after the 1970s, with drought events becoming more frequent and persistent.

At short accumulation scales, significant negative trends are observed. SPEI-1 and SPEI-3 exhibit consistent declines (SPEI-1: $y = -0.0085x + 0.2748$, $R^2 = 0.2515$; SPEI-3: $y = -0.0084x + 0.2694$, $R^2 = 0.2635$), indicating an increase in drought frequency. Distinct drought episodes are identified during the late 1980s, early 2000s, and after 2010.

At intermediate scales, drought conditions persist over longer durations. SPEI-6 and SPEI-9 show sustained negative trends ($R^2 \approx 0.27$), with extended dry periods from the late 1970s to the early 2000s.

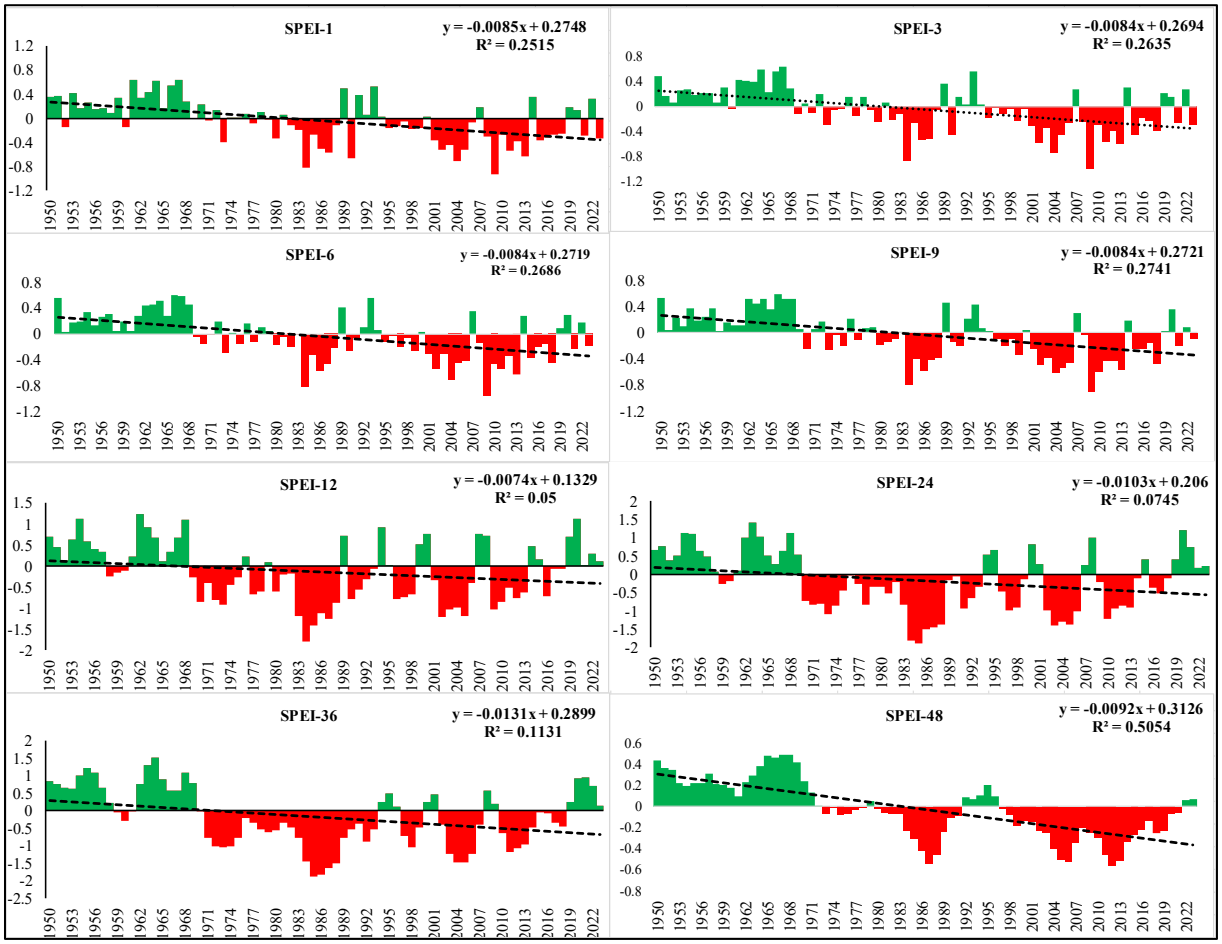


Fig. 4.1. Interannual variability and long-term trends of the SPEI across multiple accumulation scales (1–48 months) in savanna woodland, Blue Nile, Sudan, during 1950–2024. The figure illustrates alternating wet and dry periods and an increasing frequency and persistence of drought conditions over time.

At annual and multi-year scales, drought signals remain evident despite lower explained variance ($R^2$ = 0.05–0.0745). SPEI-12 highlights prolonged dry periods, whereas SPEI-24 captures multi-year drought events, indicating cumulative and sustained moisture deficits.

At longer accumulation scales, drought persistence becomes more pronounced. SPEI-36 shows a clear downward trend ($y = -0.0131x + 0.2899$, $R^2 = 0.1131$), while SPEI-48 exhibits the strongest long-term signal ($y = -0.0092x + 0.3126$, $R^2 = 0.5054$). These results indicate sustained and intensifying drying conditions, particularly after the 1980s. Overall, the results demonstrate that drought frequency and persistence have increased across all time scales, with stronger and more consistent signals at longer accumulation periods, indicating a progressive intensification of hydroclimatic stress.

To further illustrate the spatial dimension of these drought dynamics, decadal SPEI maps were generated to examine the spatial distribution and temporal evolution of moisture conditions across Blue Nile State (Fig. 4.2), highlighting the emergence of spatial heterogeneity and shifting drought patterns over time.

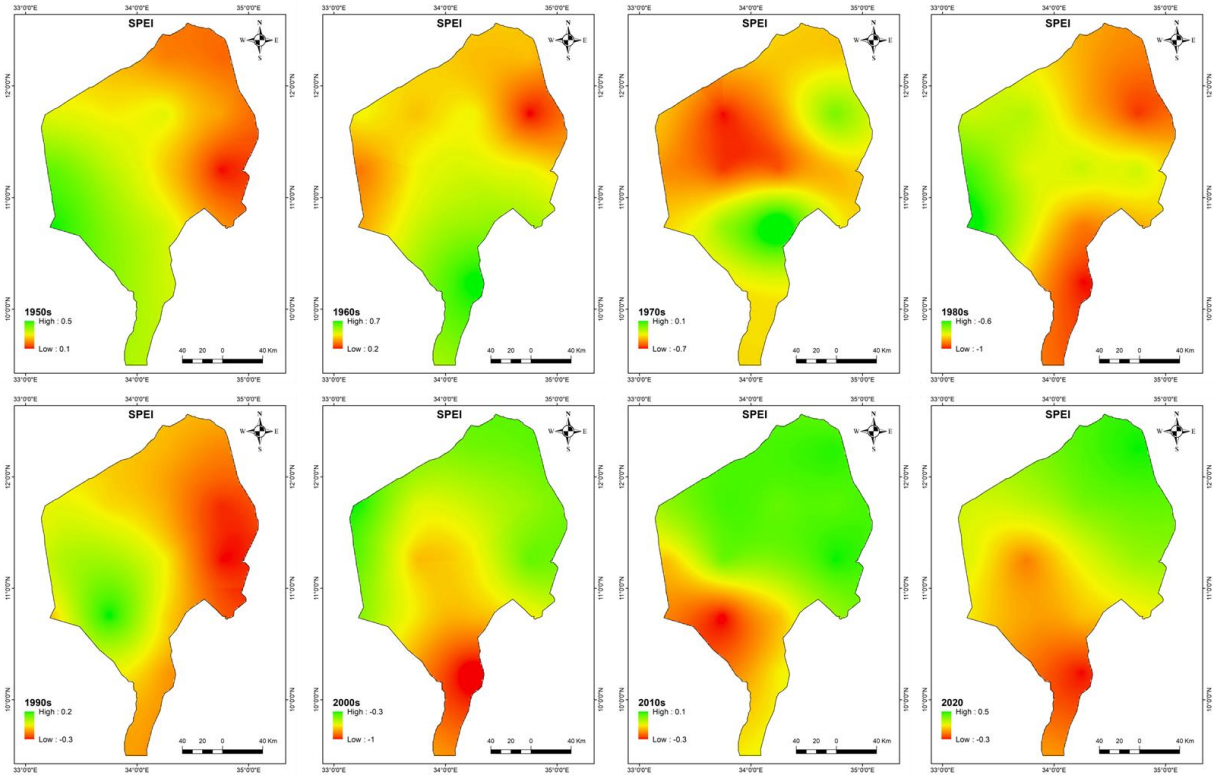


Fig. 4.2. Decadal spatial distribution of the SPEI in Blue Nile State, Sudan, from the 1950s to 2020. The maps show the spatial variability and temporal evolution of moisture conditions, with green indicating wetter conditions and red indicating increasing drought severity.

The observed intensification indicates a transition toward a more variable and drier hydroclimatic regime in the Blue Nile savanna. In particular, the increasing frequency of short-term droughts suggests that rainfall has become more irregular and insufficient to meet atmospheric water demand, reflecting enhanced moisture stress associated with rising temperatures.

These findings are consistent with previous studies reporting intensified drought frequency and declining rainfall in Sudan since the 1970s (Zhang et al., 2012; Ana, 2013). Increasing rainfall variability has also been documented by El Gamri et al. (2021), while Alriah et al. (2022) linked these fluctuations to large-scale climate drivers such as the Atlantic Multidecadal Oscillation (AMO), which may explain the observed alternation between wet and dry periods.

At intermediate time scales, the persistence of drought highlights the importance of cumulative moisture deficits, which exert stronger control on vegetation dynamics and agricultural productivity than short-term variability. Similar patterns have been reported in other semi-arid regions (Wambua et al., 2015; Modarres & Sarhadi, 2010) and support drought frameworks emphasizing duration and intensity as key characteristics (Wilhite, 2016; Tate & Gustard, 2000).

At longer accumulation scales, the strengthening of drought signals reflects long-term hydrological imbalance and chronic moisture depletion. Comparable multi-year drought patterns have been reported in Sudan and other dryland systems (Zhang et al., 2012) and are consistent with projections of increasing drought persistence under future climate scenarios (Ji et al., 2023). Long-term meteorological droughts are also known to significantly influence ecosystem functioning and agricultural systems (Wang et al., 2022).

The pronounced decline in SPEI-36 and SPEI-48 further confirms multi-decadal drying trends in the region (Ana, 2013; Zhang et al., 2012; Alriah et al., 2022), with direct implications for water resources, food security, and ecosystem resilience (FAO, 2021; Mbogo, 2014).

Overall, these findings confirm that drought dynamics in the Blue Nile savanna are intensifying in both frequency and duration, with significant implications for vegetation resilience, water availability, and long-term ecosystem sustainability.

#### 4.2.2. Seasonal and Annual Drought Frequency (1950–2024)

The frequency distribution of drought categories in the Blue Nile savanna indicates that non-drought conditions dominate across all seasons and at the annual scale; however, drought remains a recurrent and significant climatic feature (Table 4.1). Annually, no-drought conditions account for 69.22% of the period, while total drought occurrence reaches 30.78%, indicating that nearly one-third of the years were affected by drought. Mild drought is the most frequent category (13.89%), followed by moderate drought (11.44%), whereas severe (4.44%) and extreme (1.00%) droughts occur less frequently.

Seasonally, drought frequency exhibits pronounced variability. Autumn records the highest total drought occurrence (32.44%), primarily driven by mild (15.56%) and moderate drought (14.22%). Summer shows the highest proportion of severe drought (5.78%), while extreme drought remains relatively low (0.89%). In contrast, winter has the lowest total drought frequency (27.11%) but the highest proportion of extreme drought (2.22%).

Table 4.1. Percentage distribution of seasonal and annual drought frequency in the Blue Nile State during 1950–2024, based on the Standardized Precipitation Evapotranspiration Index (SPEI) classification.

| Drought category | SPEI % | | | |
|---|---|---|---|---|
| | Winter | Summer | Autumn | Annual |
| No drought | 72.89 | 69.33 | 67.56 | 69.22 |
| Mild drought | 12.89 | 15.11 | 15.56 | 13.89 |
| Moderate drought | 9.78 | 8.89 | 14.22 | 11.44 |
| Severe drought | 2.22 | 5.78 | 2.67 | 4.44 |
| Extreme drought | 2.22 | 0.89 | 0.00 | 1.00 |
| Total drought | 27.11 | 30.67 | 32.44 | 30.78 |

Overall, the results indicate that drought is a frequent and seasonally variable phenomenon, with mild and moderate droughts dominating, while severe and extreme events occur less frequently but remain significant.

The observed seasonal variability indicates that drought dynamics in the Blue Nile savanna are strongly influenced by seasonal climatic conditions. The high drought frequency in autumn likely reflects shortened or interrupted rainy seasons, suggesting increased rainfall variability and early cessation of precipitation. Similar patterns have been reported in Sudan, where rainfall variability has intensified in recent decades (El Gamri et al., 2021; Alriah et al., 2022).

The dominance of mild and moderate drought conditions is consistent with drought climatology reported in Sudan and East Africa, where these categories occur more frequently, whereas severe and extreme droughts are less common but are associated with greater environmental impacts (Zhang et al., 2012; Ana, 2013; Yagoub et al., 2017; Wambua et al., 2015; Hussien, 2024).

The higher occurrence of severe drought during summer indicates increased climatic stress during the main growing season, when vegetation water demand is highest. This seasonal sensitivity has also been observed in Sudan and neighboring regions, where drought impacts are most pronounced during peak vegetation growth periods (Mbogo, 2014; FAO, 2021). Although extreme drought events are relatively rare in summer, their occurrence under high evaporative demand may intensify moisture deficits and increase vegetation mortality.

In winter, although overall drought frequency is lower, the relatively higher proportion of extreme drought reflects the inherently dry nature of the season, where even small moisture deficits can lead to extreme drought classification. This pattern supports drought frameworks that emphasize the importance of seasonal context in determining drought severity and impacts (Tate & Gustard, 2000; Wilhite, 2016; Sheffield & Wood, 2020).

Overall, these findings demonstrate that drought in the study area is both frequent and seasonally uneven, with important implications for vegetation productivity, ecosystem functioning, and increasing climate vulnerability in savanna ecosystems.

#### 4.2.3. Trends in Maximum Consecutive Dry Days (CDDmax) (1950–2024)

The annual maximum number of consecutive dry days (CDDmax) in the Blue Nile savanna exhibits pronounced interannual variability and distinct multi-year fluctuations (Fig. 4.3).

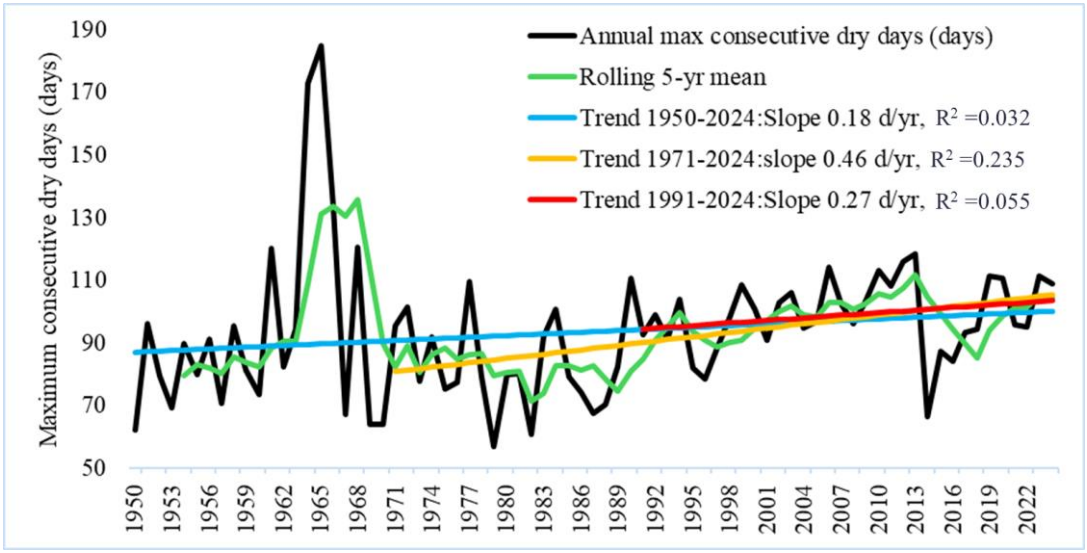


Fig. 4.3. Interannual variability and temporal trends in annual maximum consecutive dry days (CDDmax) in savanna woodland, Blue Nile, Sudan, during 1950–2024. The figure shows annual values, a 5-year moving average, and linear trends for 1950–2024, 1971–2024, and 1991–2024, highlighting increasing dry-spell persistence.

Extreme dry spells exceeding 180 days are observed during the mid-1960s, whereas markedly shorter dry spells (<70 days) occur during parts of the 1970s and 1980s. The 5-year moving average highlights clear decadal patterns, including relatively short dry spells with occasional long events in the 1950s, a pronounced peak during 1964–1966 followed by a rapid decline in the early 1970s, generally shorter and more variable dry spells during the 1970s–1980s, and a gradual increase in dry-spell duration from the early 1990s onward.

Trend analysis indicates a weak and non-significant increase over the full period (1950–2024; +0.18 days $yr^{-1}$, $R^2 = 0.032$), reflecting the high interannual variability characteristic of semi-arid climates. In contrast, a stronger increasing trend is observed for the post-1970 period (+0.46 days $yr^{-1}$, $R^2 = 0.235$), indicating a more consistent rise in dry-spell duration in recent decades. A continued, but weaker, positive trend is also evident during 1991–2024 (+0.27 days $yr^{-1}$, $R^2 = 0.055$). Although the explanatory power of these trends remains moderate to low, the consistently positive slopes indicate a gradual increase in dry-spell persistence since the early 1970s.

Overall, the results show that, despite high interannual variability, the duration of dry spells has increased over time, particularly in recent decades.

The observed increase in dry-spell duration indicates a shift in rainfall dynamics toward longer rain-free intervals rather than a simple reduction in total rainfall. This temporal pattern is consistent with documented hydroclimatic changes in Sudan, including the major rainfall regime shift during the late 1960s–early 1970s and the subsequent increase in rainfall variability and altered seasonality (Ana, 2013; Zhang et al., 2012).

The increasing dry-spell duration since the 1990s further suggests that rainfall is becoming more concentrated into fewer, more intense events, rather than being evenly distributed throughout the rainy season. Similar patterns have been reported in Sudan and across Eastern Africa (El Gamri et al., 2021; Alriah et al., 2022; Muthoni et al., 2019; Kimani et al., 2017).

The stronger post-1970 increase in CDDmax supports the concept of rainfall redistribution, whereby drought manifests through longer intervals between rainfall events rather than reduced annual totals (Sheffield & Wood, 2020). This behavior is consistent with drought frameworks that emphasize duration as a critical component of drought processes (Tate & Gustard, 2000; Wilhite, 2016). Comparable increases in dry-spell persistence have also been reported in other semi-arid regions, including Iran and Kenya (Modarres & Sarhadi, 2010; Wambua et al., 2015), suggesting a broader dryland response to climate variability.

From an ecological perspective, the increasing duration of dry spells implies enhanced soil moisture depletion and increased evaporative stress between rainfall events, even in years with near-normal precipitation. These conditions may constrain vegetation recovery, reduce seedling establishment, and favor drought-tolerant species and functional traits in Sudanese savannas (Mohamed et al., 2016). In addition, prolonged dry intervals intensify agricultural drought impacts and reduce water availability for both ecosystems and livelihoods (FAO, 2021; Mbogo, 2014).

Overall, these findings highlight that changes in rainfall distribution and dry-spell persistence are critical drivers of climate stress in the Blue Nile savanna, with important implications for ecosystem resilience, agricultural productivity, and long-term sustainability.

#### 4.2.4. Trends in Hot–Humid Conditions

The annual number of days with a heat index (HI) exceeding 35 °C indicates a clear increase in hot–humid exposure in the Blue Nile savanna over the period 1950–2024 (Fig. 4.4). During the mid-20th century, such conditions were rare, with many years recording no events. From the early 1990s onward, both the frequency and magnitude of HI > 35 °C days have increased markedly.

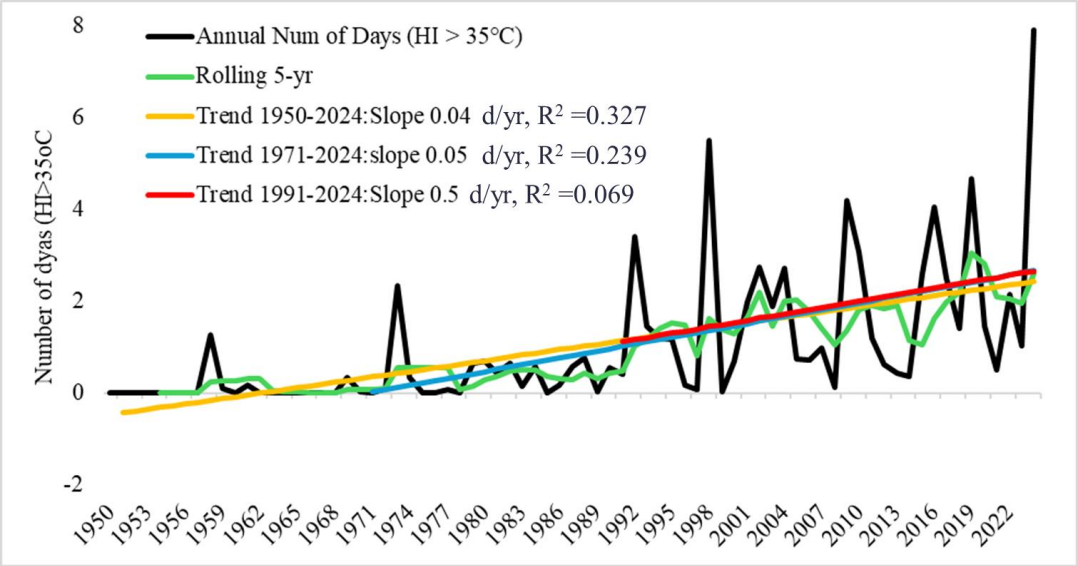


Fig. 4.4. Interannual variability and temporal trends in hot–humid conditions (days with heat index > 35 °C) in savanna woodland, Blue Nile, Sudan, during 1950–2024. The figure shows annual values, a 5-year moving average, and linear trends for multiple periods, indicating increasing frequency and intensity of humid-heat events.

The distribution of hot–humid days is highly skewed, ranging from 0 to 7.91 days in 2024 (mean = 0.99 days $yr^{-1}$; median = 0.43; SD = 1.48), reflecting the episodic nature of extreme humid-heat events. Decadal patterns show a clear transition, with near-zero occurrence in the 1950s–1960s, modest increases during the 1970s–1980s, and a pronounced rise from the 1990s onward. Extreme years exceeding the 95th percentile are concentrated in recent decades, particularly in 1998, 2009, 2019, and 2024, indicating increasingly frequent and intense humid-heat conditions.

Trend analysis confirms a consistent increase in HI > 35 °C days across all evaluated periods. The long-term trend (1950–2024) shows a moderate positive increase (+0.04 days $yr^{-1}$; $R^2 = 0.327$), indicating a relatively strong relationship compared to other climate indicators in

this study. Post-1970 trends remain positive (+0.05 days $yr^{-1}$; $R^2 = 0.239$), while the 1991–2024 period shows continued, but more variable, growth (+0.05 days $yr^{-1}$; $R^2 = 0.069$). Despite this variability, the consistently positive trends indicate a clear intensification of humid-heat conditions. Overall, the results show that hot–humid conditions have increased in both frequency and intensity, particularly since the early 1990s.

The observed increase in humid-heat exposure reflects broader warming and hydroclimatic changes in Sudan, including rising temperatures and altered moisture regimes since the late 20th century (Ana, 2013; Zhang et al., 2012). The marked increase in hot–humid conditions after 1990 is consistent with evidence that recent rainfall changes are characterized by higher intensity and increased atmospheric moisture, rather than uniform distribution (El Gamri et al., 2021; Alriah et al., 2022). Similar increases in climate extremes associated with warming have been reported across Eastern Africa (Muthoni et al., 2019; Kimani et al., 2017; Dinku et al., 2018).

The combined effect of elevated temperatures and episodic moisture availability supports drought–heat interaction frameworks, where compound climate extremes amplify environmental stress (Hao et al., 2018; Wilhite, 2016). In semi-arid ecosystems such as the Blue Nile savanna, these conditions increase evapotranspiration, reduce soil moisture availability, and intensify physiological stress on vegetation. Previous studies in Sudan have highlighted the growing ecological and agricultural impacts of temperature-driven stress (Mohamed et al., 2016; Yagoub et al., 2017; FAO, 2021; Mbogo, 2014; Hussien, 2024).

Overall, these findings demonstrate that humid-heat extremes are emerging as a distinct and increasingly important climate risk in the Blue Nile savanna, with significant implications for ecosystem resilience, water availability, and human and agricultural systems.

#### 4.2.5. Decadal Trends in Precipitation and Temperature

Decadal Mann–Kendall (M–K) trend analysis reveals pronounced temporal variability and strong contrasts in precipitation and temperature across decades in the Blue Nile savanna (Table 4.2). Statistically significant trends ($p < 0.05$) occur in specific decades, indicating distinct phases of hydroclimatic variability and thermal change.

During the 1950s, annual precipitation shows a statistically significant increasing trend ($Z = 2.33$, $p = 0.02$), while maximum temperature exhibits a significant decreasing trend ($Z = -2.68$, $p = 0.01$), and minimum temperature remains stable ($p = 0.86$). In contrast, the 1960s and 1970s show no statistically significant trends across all variables, indicating relatively stable climatic conditions.

Table 4.2. Decadal Mann–Kendall trend statistics (Z-values and corresponding p-values) for annual precipitation, maximum temperature, and minimum temperature in savanna woodland, Blue Nile, Sudan during 1950–2024. Statistically significant trends ($p < 0.05$) are shown in bold. Positive Z-values indicate increasing trends, while negative Z-values indicate decreasing trends.

| Index period | Precipitation (mm) | | Maximum temperature (C) | | Minimum temperature (C) | |
|---|---|---|---|---|---|---|
| | Z value | P value | Z value | P value | Z value | P value |
| 1950-1959 | **2.33** | **0.02** | -2.68 | **0.01** | -0.18 | 0.86 |
| 1960-1969 | -0.18 | 0.86 | -1.43 | 0.15 | -1.43 | 0.15 |
| 1970-1979 | 0.36 | 0.72 | -0.54 | 0.59 | 0.00 | 1.00 |
| 1980-1989 | -1.25 | 0.21 | 1.79 | 0.07 | **2.15** | **0.03** |
| 1990-1999 | 0.36 | 0.72 | -1.43 | 0.15 | -1.07 | 0.28 |
| 2000-2009 | 1.43 | 0.15 | **-1.97** | **0.05** | **-2.86** | **0.00** |
| 2010-2019 | 0.54 | 0.59 | -0.81 | 0.42 | -0.18 | 0.86 |
| 2020-2024 | 1.25 | 0.21 | -0.89 | 0.37 | 0.00 | 1.00 |

A clear shift emerges in the 1980s. Precipitation shows a non-significant declining tendency ($Z = -1.25$, $p = 0.21$), while minimum temperature increases significantly ($Z = 2.15$, $p = 0.03$), and maximum temperature shows a near-significant increase ($Z = 1.79$, $p = 0.07$). During the 1990s, trends remain non-significant but exhibit high variability. In the 2000s, precipitation shows a positive but non-significant trend ($Z = 1.43$, $p = 0.15$), while both temperature indices indicate decreasing tendencies. Minimum temperature shows a statistically significant decline ($Z = -2.86$, $p < 0.01$), whereas maximum temperature shows a marginally significant decrease ($Z = -1.97$, $p = 0.05$). The 2010s and early 2020s show no statistically significant trends across the analyzed variables.

Overall, the results indicate strong decadal variability, with significant changes occurring in specific decades rather than forming consistent long-term linear trends.

These results indicate distinct phases of climatic variability in the region. The wetter and relatively cooler conditions observed in the 1950s are consistent with regional studies identifying this period as a humid phase across eastern Sudan and the Sahel (Ana, 2013; Zhang et al., 2012; El Gamri et al., 2021). The absence of significant trends during the 1960s and 1970s

suggests a transitional period dominated by interannual variability rather than directional change, as reported in previous studies (Mohamed et al., 2016; Alriah et al., 2022).

The shift observed in the 1980s marks the onset of thermal intensification, particularly through increasing minimum temperatures. This warming signal has been widely documented across Sudanese savanna systems and broader East African drylands (Zhang et al., 2012; Yagoub et al., 2017; Muthoni et al., 2019; Hussien, 2024). Although the 1990s and 2000s do not show consistent statistically significant trends, the high variability and contrasting signals indicate increasing climatic instability.

Importantly, the apparent cooling tendencies observed in the 2000s, particularly in minimum temperature, do not contradict the overall pattern of increasing drought stress identified in previous analyses. This suggests that moisture stress is more strongly influenced by rainfall distribution, intensity, and evaporative demand than by total precipitation alone, consistent with established drought frameworks (FAO, 2021; Sheffield & Wood, 2020; Wilhite, 2016).

Although recent decades (2010s–2020s) show no statistically significant trends, the cumulative effects of earlier warming and increasing variability continue to influence drought dynamics and ecological stress in the region. These results highlight the importance of considering decadal variability, rather than relying solely on long-term averages, to better understand climate dynamics and their impacts on savanna ecosystems.

#### 4.2.6. Seasonal Standardized Precipitation Evapotranspiration Index (SPEI) Trends

Decadal seasonal SPEI analysis reveals pronounced temporal variability and strong seasonal contrasts, indicating that drought dynamics in the Blue Nile savanna are highly season-dependent rather than uniform throughout the year (Table 4.3). Statistically significant trends ($p \leq 0.05$) occur only in specific decades and seasons, highlighting the episodic nature of drought behavior.

During the 1950s, winter SPEI shows a statistically significant increasing trend ($Z = 1.98$, $p = 0.05$), indicating wetter winter conditions, while summer and autumn exhibit no significant changes. In contrast, the 1960s and 1970s show weak and non-significant trends across all seasons, reflecting relatively stable climatic conditions dominated by interannual variability.

A shift becomes evident in the 1980s. Summer SPEI shows a declining tendency ($Z = -1.61$, $p = 0.11$), while autumn exhibits a positive but non-significant trend ($Z = 1.25$, $p = 0.21$), indicating emerging seasonal divergence. In the 1990s, autumn continues to show a positive

tendency (Z = 1.25, p = 0.21), whereas winter and summer remain weakly variable. During the 2000s, no statistically significant trends are observed across seasons, although summer SPEI maintains a slight negative tendency (Z = −0.36, p = 0.72). The 2010s show minimal variability, with all seasonal trends remaining non-significant. In the early 2020s, summer SPEI shows a statistically significant increasing trend (Z = 1.97, p = 0.05), while autumn also shows a positive but non-significant tendency (Z = 1.61, p = 0.11).

Table 4.3. Decadal Mann–Kendall trend statistics for seasonal SPEI (winter, summer, and autumn) in Blue Nile State during 1950–2024. Statistically significant trends ($p \leq 0.05$) are highlighted in bold.

| Decade | Winter | | Summer | | Autumn | |
|---|---|---|---|---|---|---|
| | Z value | P value | Z value | P value | Z value | P value |
| 1950-1959 | **1.98** | **0.05** | 0.72 | 0.47 | 0.18 | 0.86 |
| 1960-1969 | -1.43 | 0.15 | 1.43 | 0.15 | 0.00 | 1.00 |
| 1970-1979 | 0.00 | 1.00 | 0.00 | 1.00 | -0.54 | 0.59 |
| 1980-1989 | 0.36 | 0.72 | -1.61 | 0.11 | 1.25 | 0.21 |
| 1990-1999 | -0.36 | 0.72 | 0.36 | 0.72 | 1.25 | 0.21 |
| 2000-2009 | 0.54 | 0.59 | -0.36 | 0.72 | 0.00 | 1.00 |
| 2010-2019 | 0.72 | 0.47 | 0.00 | 1.00 | 0.00 | 1.00 |
| 2020-2024 | -1.25 | 0.21 | **1.97** | **0.05** | 1.61 | 0.11 |

Overall, the results indicate strong seasonal asymmetry in drought behavior, with summer showing the greatest sensitivity to variability and change.

These results reflect regional climatic patterns. The wetter winter conditions observed in the 1950s are consistent with studies identifying this period as relatively humid across Sudan and the Sahel (Ana, 2013; Zhang et al., 2012; El Gamri et al., 2021). The absence of significant trends during the 1960s and 1970s suggests a transitional phase dominated by interannual variability rather than sustained climatic change (Abuelbashar et al., 2022; Mohamed et al., 2016).

The emerging divergence in the 1980s, particularly the decline in summer SPEI, indicates increasing moisture stress during the main growing season. This pattern is consistent with documented drought intensification across Sudanese savannas (Yagoub et al., 2017; Muthoni et al., 2019). The continued variability observed in the 1990s and 2000s reflects fluctuating wet and dry conditions, driven by rainfall variability and changes in atmospheric

demand rather than total precipitation alone (El Gamri et al., 2021; Hao et al., 2018; FAO, 2021; Sheffield & Wood, 2020).

The short-term increase in summer SPEI during the early 2020s suggests a temporary improvement in moisture availability; however, this does not offset the longer-term pattern of variability and drought risk. Seasonal differences in drought behavior emphasize that ecological processes, particularly vegetation growth and regeneration, are strongly influenced by conditions during the growing season.

Overall, these findings demonstrate that drought dynamics in the Blue Nile savanna are seasonally uneven and highly variable, with important implications for ecosystem functioning, climate vulnerability, and adaptation strategies in dryland environments.

#### 4.2.7. Long-Term Precipitation Variability

Annual precipitation in the Blue Nile savanna exhibits strong interannual variability, ranging from less than 400 mm to more than 1,100 mm (Fig. 4.5).

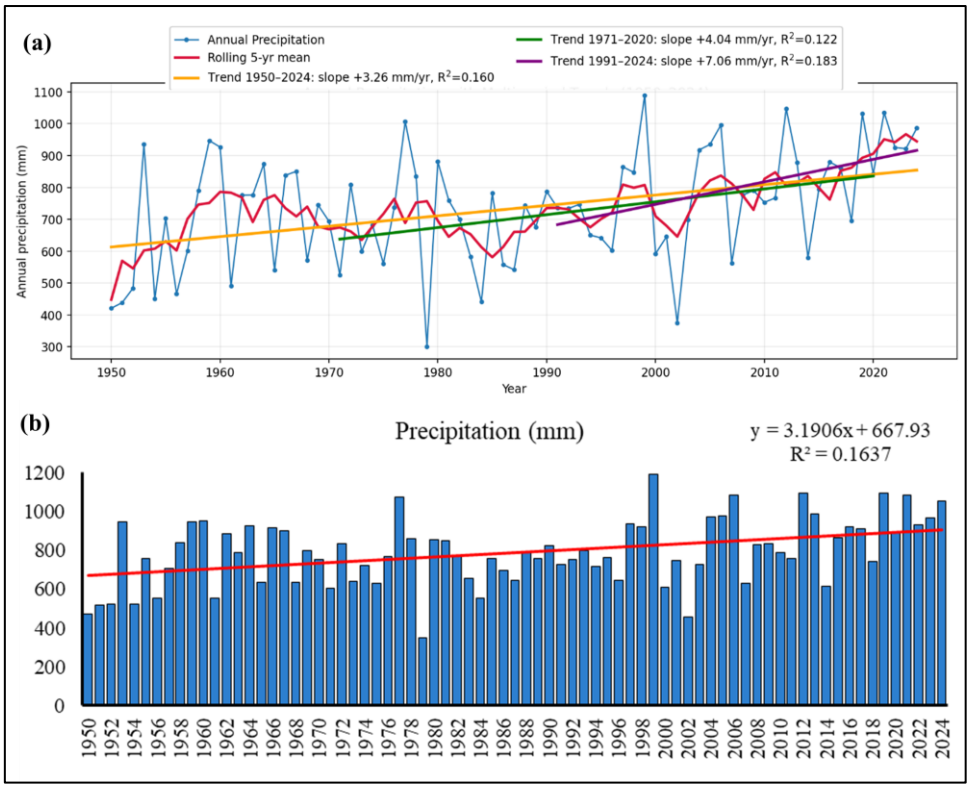


Fig. 4.5. Long-term variability and trends in annual precipitation in savanna woodland, Blue Nile, Sudan, during 1950–2024. (a) Annual precipitation time series with a 5-year moving average and linear trend analyses for 1950–2024, 1971–2020, and 1991–2024, illustrating interannual variability and regime shifts. (b) Annual precipitation distribution with a fitted linear trend, showing overall variability and gradual increase in rainfall over time.

A modest long-term increasing trend is observed (+3.26 mm $yr^{-1}$), indicating a gradual increase in precipitation over the study period. However, this increase is accompanied by substantial variability, with alternating wet and dry years throughout the record.

A clearer shift emerges from the early 1990s onward, when precipitation shows a more sustained increase. Sub-period analysis confirms this pattern, with a stronger trend during 1991–2024 (+7.06 mm $yr^{-1}$). Despite this increase, extreme dry years remain evident across the entire period, indicating that variability persists even during phases of higher rainfall.

Overall, the results indicate that, although annual precipitation has increased slightly over time, variability remains high and dry years continue to occur.

These results are consistent with previous studies documenting strong rainfall variability and alternating wet–dry phases across Sudan and the Sahel (Ana, 2013; Zhang et al., 2012). The more pronounced increase in precipitation after the 1990s aligns with recent wetting trends reported in parts of East Africa and Sudan (Muthoni et al., 2019; El Gamri et al., 2021).

However, the persistence of extreme dry years indicates that increasing mean precipitation does not necessarily reduce drought risk. This reflects changes in rainfall characteristics, where precipitation becomes more variable and unevenly distributed, often occurring in fewer but more intense events. Such behavior has been linked to large-scale climate drivers, including the Atlantic Multidecadal Oscillation (Alriah et al., 2022), and is consistent with studies showing that rainfall concentration can intensify drought conditions even when total precipitation increases (Sheffield & Wood, 2020; Hao et al., 2018).

These findings are consistent with the SPEI analysis, which shows that moisture stress in the region is influenced more by rainfall distribution and evaporative demand than by total precipitation alone (Wilhite, 2016; Wilks, 2006; Guenang & Kamga, 2014). This indicates that drought in the Blue Nile savanna is increasingly driven by irregular rainfall patterns and prolonged dry intervals rather than sustained declines in annual precipitation.

#### 4.2.8. Temperature Trends and Ecological Implications

Annual temperature analysis in the Blue Nile savanna shows a clear warming trend in both minimum (Tmin) and maximum (Tmax) temperatures, with a more pronounced and consistent increase in Tmin (Fig. 4.6). The time series and distribution plots illustrate both interannual variability and long-term warming patterns.

Minimum temperature (Tmin) exhibits a strong and consistent upward trend (+0.0259 °C $yr^{-1}$, $R^2 = 0.504$), corresponding to an increase of approximately 1.9 °C since 1950. The

warming signal intensifies after the 1990s, with a higher rate during 1991–2024 (+0.0504 °C $yr^{-1}$), indicating accelerated nighttime warming in recent decades.

Maximum temperature (Tmax) also shows a positive trend (+0.0177 °C $yr^{-1}$, $R^2$ = 0.288), equivalent to an increase of approximately 1.3 °C since 1950. Stronger warming is observed after 1990 (+0.0337 °C $yr^{-1}$ for 1991–2024), although the trend is more variable compared to Tmin.

Overall, the results indicate a consistent warming trend, with minimum temperatures increasing more rapidly than maximum temperatures.

These results are consistent with regional studies reporting stronger increases in minimum temperatures across Sudan and the Sahel (Ana, 2013; Zhang et al., 2012). The transition from relatively stable conditions before the late 1970s to sustained warming after the 1990s reflects broader climate changes associated with greenhouse forcing and atmospheric circulation variability (Alriah et al., 2022; Dinku et al., 2018).

The observed difference between Tmin and Tmax trends indicates an asymmetric warming pattern, characterized by faster increases in nighttime temperatures. This asymmetry has important ecological implications. Rising Tmin reduces nocturnal cooling, leading to increased respiration rates and limiting recovery periods for vegetation. At the same time, increasing Tmax enhances evaporative demand and vapor pressure deficit, intensifying water stress even in the absence of a significant decline in rainfall (Hao et al., 2018; Wilhite, 2016).

The combined effect of increasing temperature and variable precipitation reinforces the role of temperature as a key driver of drought processes in semi-arid environments. This interaction supports drought–heat frameworks, where thermal stress amplifies moisture deficits (Hao et al., 2018; Wilhite, 2016). Ecologically, these conditions may reduce regeneration, increase mortality of sensitive species, and promote a shift toward drought-tolerant vegetation, ultimately altering savanna structure and ecosystem functioning (Ji et al., 2023; Wilks, 2006; Sheffield & Wood, 2020; Wang et al., 2022).

Overall, these findings demonstrate that warming, particularly nighttime warming, is a dominant climatic signal in the Blue Nile savanna and a key factor intensifying ecological stress. This highlights the importance of integrating temperature-based indicators with precipitation and drought metrics in climate impact assessments and adaptation planning.

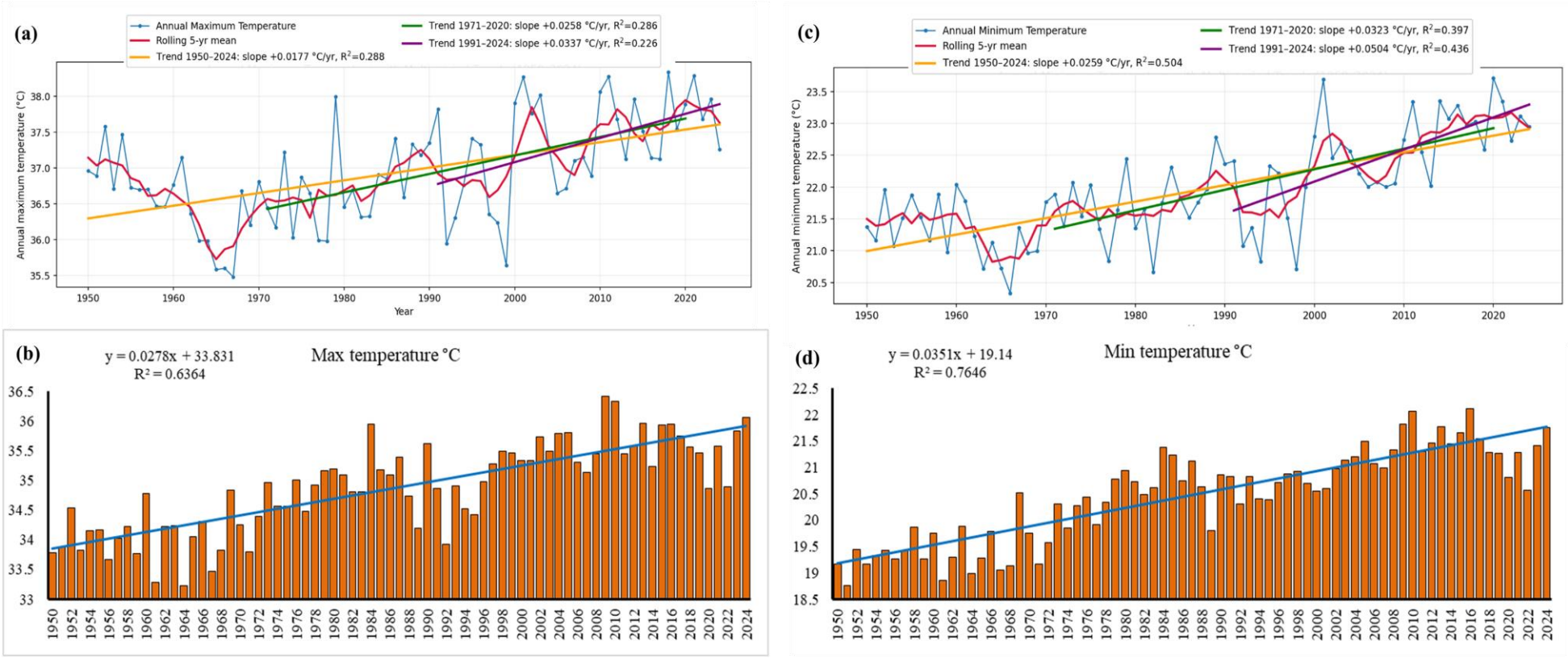


Fig. 4.6. Long-term trends and variability in annual maximum (Tmax) and minimum (Tmin) temperatures in savanna woodland, Blue Nile, Sudan, during 1950–2024. (a) Tmax time series with a 5-year moving average and linear trend analyses for 1950–2024, 1971–2020, and 1991–2024; (b) Tmax distribution with a fitted linear trend; (c) Tmin time series with a 5-year moving average and multiple linear trends; and (d) Tmin distribution with a fitted linear trend, illustrating consistent warming trends, particularly for minimum temperature.

### 4.2.9. Integrated Climate Regime Shifts

Mutation analysis reveals a clear regime shift toward higher mean annual temperatures in the late 1990s (Fig. 4.7). In contrast, the Standardized Precipitation Evapotranspiration Index (SPEI) shows repeated oscillations between wet and dry phases without a sustained directional trend, while precipitation exhibits weak long-term change combined with high variability. These results indicate a divergence between steadily increasing temperature and highly variable moisture conditions.

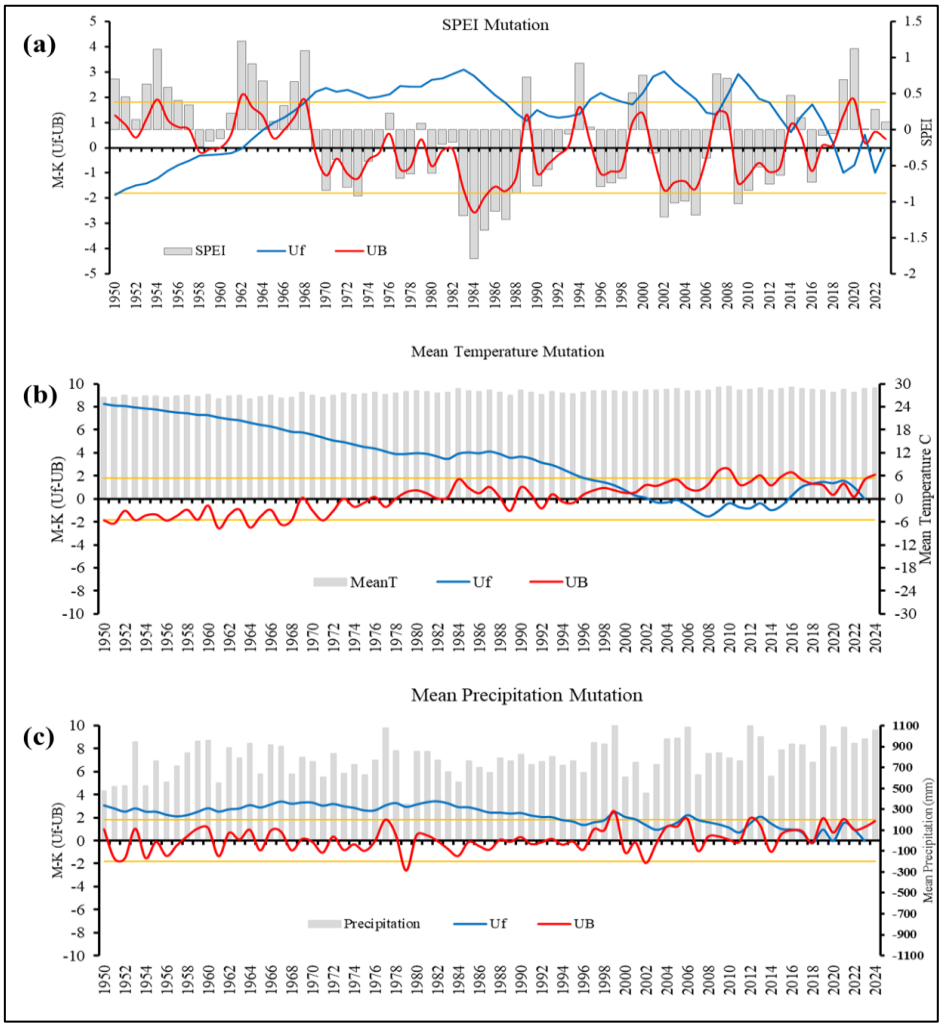


Fig. 4.7. Mutation analysis of mean temperature, SPEI, and precipitation in savanna woodland, Blue Nile, Sudan, during 1950–2024. The figure shows change points and long-term variability in (a) SPEI, (b) temperature, and (c) precipitation.

Overall, the results demonstrate a distinct climatic asymmetry, characterized by persistent warming accompanied by non-directional variability in precipitation and drought indices.

These results are consistent with regional evidence of accelerated warming across Sudan and East Africa since the late 20th century (Ana, 2013; Zhang et al., 2012), with stronger warming trends reported after the 1990s due to greenhouse forcing and land–atmosphere feedbacks (El Gamri et al., 2021; Muthoni et al., 2019). The continuous increase in temperature reinforces the role of warming as a dominant climate signal in the region, often exceeding changes in precipitation (Alriah et al., 2022; Ji et al., 2023).

The absence of a clear long-term trend in SPEI and precipitation highlights the dominant role of rainfall variability and evaporative demand in controlling drought dynamics. Similar findings indicate that drought in Sudan is governed more by rainfall distribution and temperature-driven evapotranspiration than by total precipitation alone (Sheffield & Wood, 2020; Hao et al., 2018). The weak directional change in precipitation further supports studies showing that rainfall remains highly variable and does not exhibit consistent long-term trends comparable to temperature (Dinku et al., 2018; Abuelbashar et al., 2022).

This decoupling between increasing temperature and variable precipitation implies that drought risk is intensifying due to rising evaporative demand, even during periods of rainfall recovery. This interpretation is consistent with established drought frameworks emphasizing the role of temperature and atmospheric demand in amplifying moisture deficits (Wilhite, 2016; Wilks, 2006).

Overall, these findings highlight the importance of integrating temperature, precipitation, and drought indices when assessing hydroclimatic stress and ecosystem resilience, as reliance on precipitation alone may underestimate the increasing climate risk in savanna ecosystems (FAO, 2021; Sheffield & Wood, 2020).

### 4.3. Assessment of Spatio-Temporal Land Use/Land Cover (LULC) Changes and Their Interaction with Climatic Variability (Objective 2)

This section presents a comprehensive analysis of spatio-temporal land use/land cover (LULC) dynamics in the Elnour Natural Forest Reserve (ENFR) and examines their interactions with climatic factors. The analysis integrates multi-temporal LULC mapping, transition dynamics, landscape condition assessment, and socio-economic drivers, supported by accuracy evaluation of classified images. Together, these components provide a detailed understanding of land-cover change processes, degradation pathways, and their underlying drivers in a semi-arid savanna ecosystem.

#### 4.3.1. Accuracy Assessment of Classified Images

The accuracy assessment indicates that the land use/land cover (LULC) classifications for 1995, 2008, and 2021 are reliable and suitable for subsequent spatial and temporal analyses (Table 4.4; Appendix C). Overall accuracy (OA) exceeds 85% for all years, and Kappa coefficients indicate strong to near-perfect agreement between classified results and reference data.

In 1995, the classification achieves an overall accuracy of 89.0% and a Kappa coefficient of 83.81%. User's accuracy ranges from 75.0% for Bareland to 91.67% for Light Forest, while producer's accuracy varies between 85.71% and 90.63%. In 2008, classification performance improved, with an overall accuracy of 91.60% and a Kappa coefficient of 88.0%, and all classes showing user's and producer's accuracies above 89%. The highest accuracy is observed in 2021, with an overall accuracy of 93.02% and a Kappa coefficient of 93.60%. In this year, Semi-bareland and Light Forest both exceed 95% in user's and producer's accuracies.

Overall, the results indicate a progressive improvement in classification accuracy over time, with consistently high performance across all land-cover classes.

Table 4.4. Classification Accuracy Assessment (UA, PA, OA, and Kappa) of LULC Classes for 1995, 2008, and 2021

| Year | Class name | UA % | PA % | OA % | Kappa % |
|---|---|---|---|---|---|
| 1995 | Bareland | 75 | 85.71 | 89 | 83.81 |
| | Semi-bareland | 90.63 | 90.63 | | |
| | Light Forest | 91.67 | 88.71 | | |
| | Dense Forest | 86.67 | 89.04 | | |
| 2008 | Bareland | 90.63 | 89.66 | 91.6 | 88 |
| | Semi-bareland | 93.9 | 92.77 | | |
| | Light Forest | 92.54 | 92.54 | | |
| | Dense Forest | 94.53 | 91.04 | | |
| 2021 | Bareland | 91.67 | 91.67 | 93.02 | 93.6 |
| | Semi-bareland | 96.32 | 95.45 | | |
| | Light Forest | 95.45 | 96.36 | | |
| | Dense Forest | 93.02 | 93.02 | | |

These results confirm the robustness of the classification approach and the suitability of the generated maps for long-term LULC analysis. The relatively lower accuracy for Bareland in 1995 is likely due to spectral confusion with Semi-bareland and sparsely vegetated areas, which is a well-documented limitation in semi-arid environments where exposed soil and sparse vegetation exhibit similar spectral responses (Fassnacht et al., 2016; Persson et al., 2018).

The improvement in classification accuracy over time reflects enhanced image quality, improved preprocessing, and advances in classification methods and algorithms (Gorelick et al., 2017; Belgiu & Drăguţ, 2016). The high accuracy achieved for forest classes, particularly Light Forest and Dense Forest, indicates reliable discrimination of vegetation types, which is critical for assessing forest dynamics and degradation processes (Lu & Weng, 2007; Griffiths et al., 2013).

Overall, the strong agreement between classified and reference data provides confidence in the use of these maps for analyzing spatial patterns and long-term changes in the ENFR.

### 4.3.2. Long-Term Land Use/Land Cover Dynamics (1995–2021)

Analysis of land use/land cover (LULC) in the Elnour Natural Forest Reserve (ENFR) for 1995, 2008, and 2021 (Fig. 4.8; Table 4.5) reveals substantial structural changes over time. Between 1995 and 2008, bareland increased from 5.1% to 6.3%, followed by a decline to 4.36% in 2021. In contrast, semi-bareland expanded markedly from 23.1% to 37.8% during 1995–2008 and further increased to 40.0% by 2021, becoming the dominant land cover class.

Forest cover classes show contrasting trends. Light forest declined sharply from 45.1% in 1995 to 31.7% in 2008, followed by a partial recovery to 39.9% in 2021. In contrast, dense forest shows a continuous decline from 26.7% in 1995 to 15.7% in 2021, indicating substantial canopy loss over the study period.

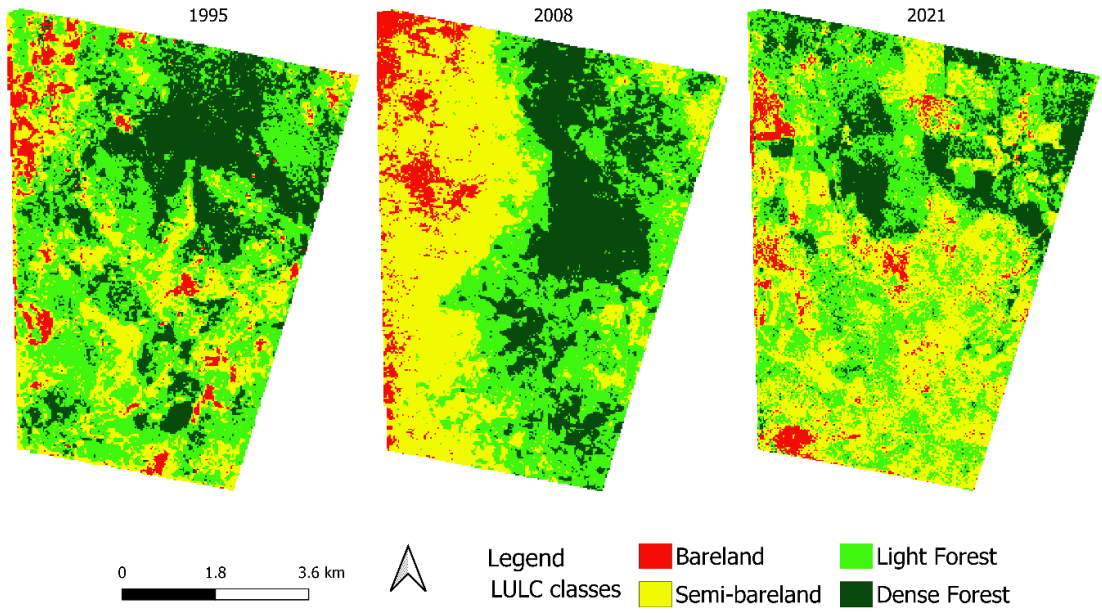


Fig. 4.8. Land use/land cover (LULC) change maps of the ENFR for 1995, 2008, and 2021.

Table 4.5. Land use/land cover (LULC) changes in the ENFR (1995–2021), including area and percentage distribution.

| Class | 1995 | | 2008 | | 2021 | |
|---|---|---|---|---|---|---|
| | Area(ha) | % | Area(ha) | % | Area(ha) | % |
| Bareland | 242.6 | 5.1 | 297.2 | 6.3 | 206.3 | 4.4 |
| Semi-bareland | 1091.0 | 23.1 | 1788.5 | 37.8 | 1893.8 | 40.0 |
| Light Forest | 2132.6 | 45.1 | 1500.2 | 31.7 | 1887.9 | 39.9 |
| Dense Forest | 1264.9 | 26.7 | 1145.2 | 24.2 | 743.2 | 15.7 |
| Total | 4731.1 | 100 | 4731.1 | 100 | 4731.1 | 100 |

Overall, the results indicate a clear shift from dense and light forest toward semi-bareland, reflecting increasing landscape degradation and structural simplification.

These results are consistent with broader patterns of land transformation in dryland ecosystems driven by anthropogenic pressures and environmental variability (Arfat, 2010; MacDicken, 2015; Gorelick et al., 2017; Tamiminia et al., 2020; Yasin et al., 2022). The increase in bareland during the early period reflects intensified land degradation, similar to trends observed in northern Kordofan and eastern Sudan (Dafalla et al., 2014; Sulieman, 2018). The subsequent decline in bareland by 2021 may indicate localized vegetation recovery or redistribution of land-use pressures, as reported in other semi-arid systems (Pelletier et al., 2016; Phan et al., 2020).

The strong expansion of semi-bareland suggests a transition toward intermediate degradation states, which is a common trajectory in dryland landscapes under sustained human pressure (Munthali et al., 2019; Tong et al., 2020). The partial recovery of light forest reflects opportunistic regrowth under fluctuating disturbance regimes or favorable climatic conditions, as documented in similar environments (Zurqani et al., 2018; Pelletier et al., 2016; Phan et al., 2020). In contrast, the continuous decline in dense forest indicates persistent canopy loss and fragmentation, consistent with regional and global observations of forest degradation (Sulieman & Elagib, 2012; Yasin & Mulyana, 2022; Winkler et al., 2021; Bourgoin et al., 2024). The dominant transition from forest classes to semi-bareland highlights a shift toward degraded and simplified vegetation structures, aligning with established models of dryland degradation (Lambin & Meyfroidt, 2011; Basse et al., 2014). Similar transitions toward open and degraded

land cover have been reported in Ethiopia and China (Zewdie & Csaplovics, 2016; Zhang et al., 2017). Overall, these findings demonstrate progressive fragmentation, declining canopy integrity, and increasing ecological vulnerability in the ENFR. Although the partial recovery in light forest suggests some resilience, it remains insufficient to offset the continued loss of dense forest. This underscores the need for targeted conservation and sustainable land management strategies supported by continuous monitoring (Hano, 2013; Biro et al., 2013).

### 4.3.3. LULC Transition Dynamics and Forest Degradation Pathways in ENFR

LULC transition analysis in the Elnour Natural Forest Reserve (ENFR) reveals substantial changes between 1995–2008 and 2008–2021, indicating dynamic and uneven landscape transformation (Fig. 4.9; Table 4.6). Dense forest shows very low persistence, declining from 10.9% during 1995–2008 to 3.5% in 2008–2021, indicating high instability and continuous loss. The dominant transitions involve the conversion of both dense and light forest into semi-bareland, with a marked increase during 1995–2008 (Δ +14.7%). Light forest exhibits moderate persistence (14.3% in 1995–2008 and 13.1% in 2008–2021), with gains from semi-bareland (15.2%) but also substantial losses to semi-bareland (18.5%). Bareland shows very low persistence (<1%) and functions primarily as a transitional class.

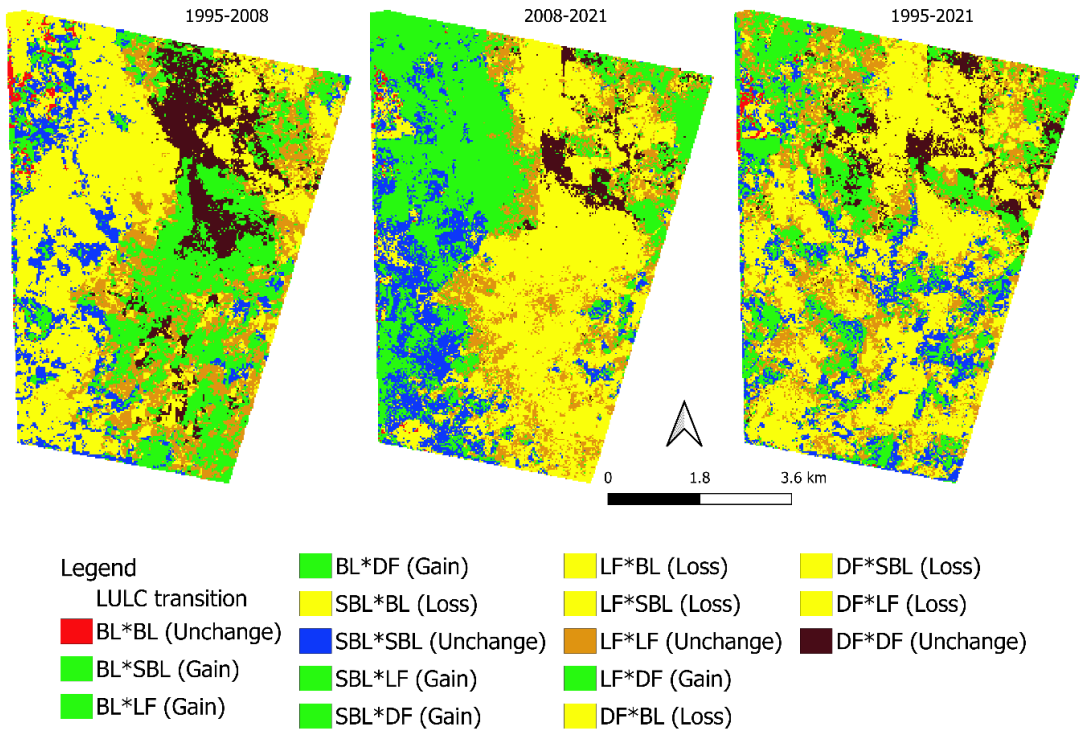


Fig. 4.9. Land use/land cover (LULC) change trajectories in the ENFR from 1995 to 2021 based on transition matrix analysis.

Table 4.6. Land use/land cover (LULC) transition matrices in the ENFR between 1995 and 2021 (in %). Columns represent the land-cover class at the beginning of the period, and rows represent the class at the end of the period.

| Period | From / To | Bareland | Semi-bareland | Light Forest | Dense Forest | End % |
|---|---|---|---|---|---|---|
| 1995-2008 | Bareland | 1.0 | 2.1 | 2.7 | 0.6 | 6.3 |
| | Semi-bareland | 2.7 | 9.9 | 18.5 | 6.7 | 37.8 |
| | Light Forest | 1.0 | 7.8 | 14.3 | 8.6 | 31.7 |
| | Dense Forest | 0.4 | 3.3 | 9.7 | 10.9 | 24.2 |
| | Start % | 5.1 | 23.1 | 45.1 | 26.7 | 100 |
| 2008-2021 | Bareland | 0.4 | 2.5 | 0.7 | 0.8 | 4.4 |
| | Semi-bareland | 2.3 | 13.3 | 13.4 | 11.1 | 40.1 |
| | Light Forest | 2.6 | 15.2 | 13.1 | 8.9 | 39.8 |
| | Dense Forest | 1.0 | 6.8 | 4.4 | 3.5 | 15.7 |
| | Start % | 6.3 | 37.8 | 31.6 | 24.3 | 100 |
| 1995-2021 | Bareland | 0.6 | 1.5 | 1.6 | 0.7 | 4.4 |
| | Semi-bareland | 2.2 | 10.9 | 18.3 | 8.6 | 40 |
| | Light Forest | 1.6 | 8.6 | 17.9 | 11.7 | 39.9 |
| | Dense Forest | 0.7 | 2 | 7.2 | 5.8 | 15.7 |
| | Start % | 5.1 | 23.1 | 45.1 | 26.8 | 100 |

Overall, the results indicate that forest areas are progressively being converted into semi-bareland, reflecting a shift toward more degraded and simplified land-cover states.

These results reflect the combined influence of sustained anthropogenic pressures and environmentally constrained recovery processes, as commonly observed in semi-arid and savanna ecosystems (Arfat, 2010; Sulieman & Elagib, 2012; Hano, 2013; Dafalla et al., 2014; Sulieman, 2018). The extremely low persistence of dense forest confirms its high vulnerability to disturbance, particularly from fuelwood extraction, agricultural expansion, and grazing.

The expansion of semi-bareland highlights its role as a persistent degradation stage, consistent with dryland degradation models in which intermediate vegetation states expand under continuous pressure before transitioning to more degraded conditions (Basse et al., 2014; Lambin & Meyfroidt, 2011). Similar transitions toward semi-degraded classes have been reported in Sudan, Ethiopia, and the Sahel (Biro et al., 2013; Zewdie & Csaplovics, 2016; Tong et al., 2020).

Light forest dynamics indicate a dual role as both a degradation pathway and a recovery stage. Gains from semi-bareland suggest localized regeneration under favorable conditions or reduced disturbance, as reported in other semi-arid systems (Pelletier et al., 2016; Phan et al., 2020; Zurqani et al., 2018). However, the substantial losses of light forest to semi-bareland demonstrate that such recovery is unstable and often reversible, consistent with findings from savanna woodlands (Hasoba et al., 2020; Yasin & Mulyana, 2022; Yasin et al., 2023).

The very low persistence of bareland further supports its role as a transitional class, where exposed surfaces fluctuate rapidly in response to land-use pressure and short-term vegetation dynamics (Zakaria, 2010; Sulieman & Ahmed, 2013; Munthali et al., 2019). Over the full period, the net increase in semi-bareland (~17%), combined with substantial losses of dense forest (−11%) and light forest (−5.2%), indicates long-term fragmentation and structural simplification. These trajectories are consistent with regional and global assessments showing that dryland forests are highly vulnerable to human-driven degradation (MacDicken, 2015; Winkler et al., 2021; Bourgoin et al., 2024).

Overall, these findings confirm that the ENFR landscape is shifting toward degraded, open vegetation states with limited resilience. The persistence of semi-bareland and the continued decline of dense forest highlight the need for targeted restoration, improved land use management, and continuous monitoring using remote sensing approaches (FAO, 2016; Gorelick et al., 2017; Tamiminia et al., 2020; Yasin et al., 2025).

#### 4.3.4. Trends in ENFR Condition During 1995–2021

Analysis of LULC dynamics in the Elnour Natural Forest Reserve (ENFR) from 1995 to 2021 reveals substantial changes in landscape condition (Fig. 4.10). Bareland increased markedly during 1995–2008 by 24.9% (+1.92% $yr^{-1}$), followed by a decrease of 25.7% (−1.98% $yr^{-1}$) during 2008–2021. In contrast, semi-bareland increased significantly in the later period (+18.9%), resulting in a net gain of 17.0% over the entire study period. Light forest shows a net decline of 5.2%, while dense forest decreases by 11.0%, indicating a reduction in forest cover and canopy density.

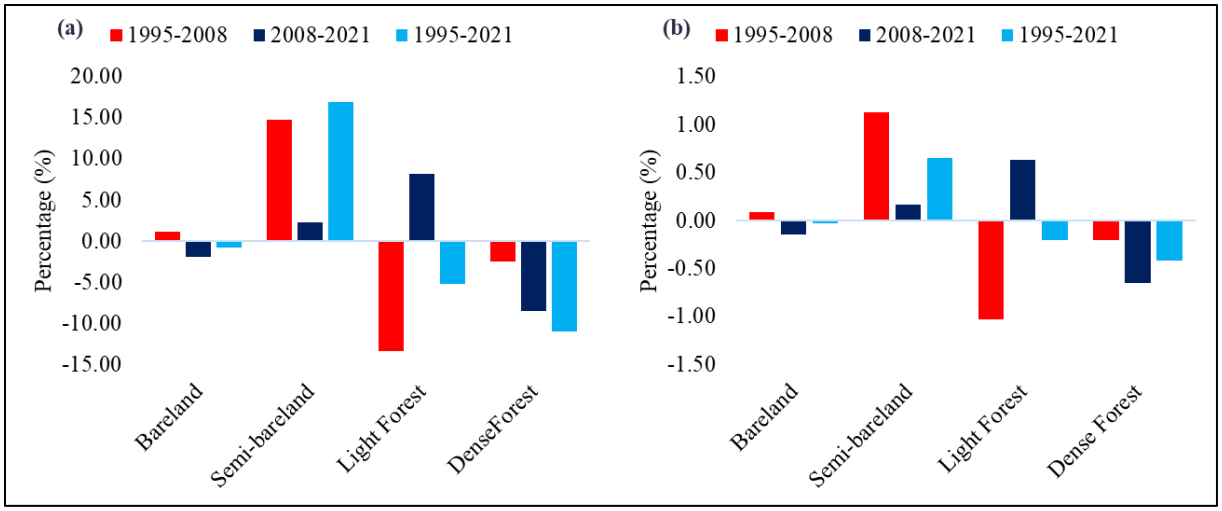


Fig. 4.10. Spatio-temporal dynamics of LULC change in the ENFR between 1995 and 2021: (a) direction of change and (b) annual rate of change.

Overall, the results indicate a clear transition toward more open and sparsely vegetated land-cover classes, accompanied by a decline in dense and continuous forest cover.

These results reflect the combined effects of ecological pressures and anthropogenic disturbances. The initial expansion of bareland during 1995–2008 is associated with increased land degradation driven by deforestation, agricultural expansion, and resource overexploitation, consistent with findings from Sudanese drylands and other tropical regions (Sulieman, 2010; Glover & Elsiddig, 2012; Biro et al., 2013; Zewdie & Csaplovics, 2016; Yasin et al., 2022). The subsequent decline in bareland during 2008–2021 suggests partial vegetation recovery or redistribution of land-use pressure, similar to regeneration patterns observed in fragmented dry forests under reduced disturbance or restoration efforts (Hemida et al., 2023; de Almeida et al., 2025).

The substantial increase in semi-bareland indicates a persistent shift toward intermediate degradation states, which is a common trajectory in dryland ecosystems experiencing sustained disturbance (Sulieman, 2018; Yasin et al., 2023; Tamiminia et al., 2020; Winkler et al., 2021). The continued decline of light and dense forest highlights the vulnerability of closed-canopy systems to ongoing disturbance and fragmentation (FAO, 2015; MacDicken, 2015; Bourgoin et al., 2024; Yasin & Mulyana, 2022).

Overall, these findings demonstrate progressive canopy reduction and structural simplification in the ENFR, reflecting increasing ecological vulnerability. This underscores the need for targeted restoration, improved land-use governance, and continuous monitoring using remote sensing approaches (Gorelick et al., 2017; Potapov et al., 2022).

#### 4.3.5. Major Drivers of Forest Degradation in ENFR

The integrated socio-economic assessment indicates that forest degradation in the Elnour Natural Forest Reserve (ENFR) is predominantly driven by human activities, with environmental factors acting as secondary influences (Table 4.7). Illegal tree cutting and charcoal production represent the largest share of pressure (35%), followed by overgrazing (25%). Governance and institutional limitations contribute 15%, while socioeconomic factors account for 10%. Land-use expansion contributes 8%, and environmental factors, such as prolonged dry seasons, account for 5%.

Overall, the results indicate that anthropogenic drivers dominate the degradation process, with resource extraction and grazing representing the primary pressures.

These results reflect broader patterns observed in dryland ecosystems. The high contribution of illegal tree cutting and charcoal production indicates a transition from

subsistence use to more intensive, market-driven extraction, driven by poverty and increasing urban energy demand. Similar dynamics have been widely reported across Sudan and other dryland regions (Sulieman, 2018; Yasin et al., 2022; Yasin et al., 2025; Eltohami, 2018; UNEP, 2007).

Table 4.7. Relative contribution of major drivers to forest degradation in the ENFR, expressed as percentage shares of total pressure.

| Driver Category | Specific Driver | Contribution (%) | Evidence Type |
|---|---|---|---|
| Human-Induced | Illegal tree cutting & charcoal production | 35% | Field observation, literature. |
| | Overgrazing by livestock | 25% | Field observation. |
| | Weak governance & enforcement | 15% | Institutional assessment, literature. |
| | Socioeconomic pressures | 10% | Field observation, literature. |
| | Agricultural expansion & settlement | 8% | Land cover change detection. |
| Environmental | Climatic variability (rainfall and drought) | 5% | Climate pattern observation, literature. |
| Ecological Consequences | Fragmentation & species composition changes | 2% | Long-term result of persistent human and climatic pressures. |

Overgrazing plays a major role by limiting vegetation recovery through browsing and trampling, which reduce seedling establishment and favor disturbance-tolerant species. This process has been documented in Sudanese woodlands and other semi-arid pastoral systems (Sulieman & Elagib, 2012; Gadallah et al., 2020; Hasoba et al., 2020; Yasin et al., 2024).

Governance-related factors further exacerbate degradation. Weak enforcement, unclear land tenure systems, and limited institutional capacity enable unsustainable resource use, consistent with findings from other dryland regions (Munthali et al., 2019; Lambin & Meyfroidt, 2011). Socioeconomic pressures, including dependence on forest resources and low agricultural productivity, intensify resource extraction, particularly during periods of climatic stress (Mohmmed et al., 2018; Tamiminia et al., 2020).

Land-use expansion contributes to fragmentation and habitat loss at forest margins, reflecting broader trends of agricultural encroachment in Sudan (Biro et al., 2013; Hano, 2013). Although environmental factors play a smaller role, prolonged dry seasons reduce regeneration

capacity and ecosystem resilience, thereby reinforcing the impacts of human activities (Sulieman & Elagib, 2012; Tran et al., 2019).

Overall, these findings demonstrate that forest degradation in the ENFR is primarily human-driven, with environmental stress acting as a reinforcing factor. This interaction creates a feedback loop that accelerates forest decline. Addressing this challenge requires integrated management approaches that combine improved governance, sustainable land-use practices, alternative energy solutions, and climate-adaptive restoration strategies.

## 4.4. Evaluation of Changes in Woody Species Composition, Diversity, and Regeneration under Climatic Variability and Anthropogenic Pressures (Objective 3)

This section presents a detailed assessment of changes in woody species composition, diversity, population structure, and regeneration status in the Elnour Natural Forest Reserve (ENFR) between 2008 and 2021. The analysis integrates species-level metrics, structural attributes, and ecological indicators, including basal area, density, and Importance Value Index (IVI), to evaluate shifts in forest composition and function. These results are interpreted in relation to climatic variability and anthropogenic pressures to provide a comprehensive understanding of ecological change and forest degradation processes in the study area.

### 4.4.1. Changes in Tree Species Diversity, Frequency, and Regeneration (2008–2021)

The woody species composition of the Elnour Natural Forest Reserve (ENFR) shows substantial changes between 2008 and 2021 in terms of diversity, abundance, and regeneration (Tables 4.8 and 4.9). In 2021, a total of 1,498 individual trees representing 18 species across nine families were recorded. Fabaceae is the most species-rich family, comprising six species, followed by Combretaceae with five species, while Anacardiaceae and Rhamnaceae each include two species. In terms of abundance, Fabaceae dominates with 838 individuals, followed by Malvaceae (188), Zygophyllaceae (160), Combretaceae (148), Rhamnaceae (81), and Anacardiaceae (63).

In contrast, the 2008 inventory recorded 16,979 individuals representing 35 species across 16 families. Species richness declined across most families, with Fabaceae decreasing from 12 to 6 species and Combretaceae from 7 to 5 species, while Anacardiaceae and Rhamnaceae remained unchanged. Growth-form composition also declined, from 21 tree species and 14 shrub species in 2008 to 13 tree species and 5 shrub species in 2021.

Table 4.8. Tree and shrub species type, presence, frequency (FR), and regeneration status in ENFR in 2008 and 2021

| ***Family*** | ***Species*** | **Vern.names** | ***Presence*** | | | **Regeneration status** | | | |
|---|---|---|---|---|---|---|---|---|---|
| | | | **Type** | ***2008*** | ***2021*** | **FR (%, 2008)** | **Reg. 2008** | **FR (%, 2021)** | **Reg. 2021** |
| *Fabaceae* | *Acacia seyal Delile* | Talih Ahmar - Talih | Tree | ✓ | ✓ | 75.55 | Good | 28.82 | Good |
| *Fabaceae* | *Acacia seyal var. fistula (Schweinf.) Kyal. & Boatwr.* | Sufar Abiad | Tree | ✓ | - | 70.74 | Fair | 0.00 | None |
| *Fabaceae* | *Acacia polyacantha Willd.* | Kakamoot | Tree | ✓ | | 21.40 | Fair | 0.00 | None |
| *Fabaceae* | *Acacia senegal (L.) Willd.* | Hashab | Tree | ✓ | ✓ | 40.17 | Good | 9.61 | Poor |
| *Fabaceae* | *Dichrostachys cinerea (L.) Wight & Arn.* | Kadad | Shrub | ✓ | - | 17.47 | Poor | 0.00 | None |
| *Zygophyllaceae* | *Balanites aegyptiaca (L.) Delile* | Hegleeg (Laloub) | Tree | ✓ | ✓ | 38.86 | Poor | 21.40 | Poor |
| *Fabaceae* | *Acacia mellifera (Vahl) Benth.* | Kitir | Shrub | ✓ | ✓ | 3.49 | Fair | 4.80 | Good |
| *Fabaceae* | *Acacia nubica Benth.* | Laut | Shrub | ✓ | ✓ | 0.87 | Poor | 20.09 | Good |
| *Malvaceae* | *Sterculia setigera Delile* | Tartar | Tree | ✓ | ✓ | 68.12 | Poor | 31.88 | Fair |
| *Combretaceae* | *Anogeissus leiocarpus (DC.) Guill. & Perr.* | Sahab – seilk | Tree | ✓ | ✓ | 17.90 | Poor | 9.61 | Fair |
| *Combretaceae* | *Terminalia laxiflora Engl.* | Subagh – Darut | Tree | ✓ | ✓ | 15.28 | Poor | 6.99 | Poor |
| *Combretaceae* | *Terminalia brownii Fresen.* | Subagh – Shaf | Tree | ✓ | ✓ | 11.79 | Good | 5.68 | Fair |
| *Combretaceae* | *Combretum hartmannianum Schweinf.* | Habeel Al Gabal | Tree | ✓ | ✓ | 39.74 | Good | 14.85 | Poor |
| *Combretaceae* | *Combretum aculeatum Vent.* | Habeel Shehait | Shrub | ✓ | - | 6.55 | Good | 0.00 | None |
| *Combretaceae* | *Combretum molle R.Br. ex G.Don* | Habeel Khrisha Kabeira | Tree | ✓ | - | 11.35 | Good | 0.00 | None |
| *Combretaceae* | *Combretum glutinosum Perr. ex DC.* | Habeel Khrisha | Tree | ✓ | ✓ | 7.42 | Good | 3.93 | Good |
| *Anacardiaceae* | *Lannea fruticosa (Hochst. ex A.Rich.) Engl.* | Leyun-Ghallub | Shrub | ✓ | ✓ | 17.90 | Poor | 13.10 | Good |
| *Anacardiaceae* | *Sclerocarya birrea (A.Rich.) Hochst.* | Humeid | Tree | ✓ | ✓ | 4.80 | Poor | 3.93 | Good |
| *Rhamnaceae* | *Ziziphus spina-christi (L.) Desf.* | Siddir - Nabag | Tree | ✓ | ✓ | 8.73 | Poor | 8.73 | Good |
| *Rhamnaceae* | *Ziziphus abyssinica Hochst. ex A.Rich.* | Siddir Al Feel | Shrub | ✓ | ✓ | 7.86 | Poor | 6.99 | Good |
| *Rubiaceae* | *Xeromphis nilotica (Stapf) Keay* | Shidr el Marfein | Shrub | ✓ | ✓ | 6.11 | Poor | 4.37 | Fair |
| *Bignoniaceae* | *Stereospermum kunthianum Cham.* | Khashkash Abiad | Tree | ✓ | ✓ | 3.93 | Poor | 1.75 | None |
| *Fabaceae* | *Lonchocarpus laxiflorus Guill. & Perr.* | Khashkash Azrag | Tree | ✓ | ✓ | 5.24 | Good | 2.18 | Poor |
| *Fabaceae* | *Dalbergia melanoxylon Guill. & Perr.* | Abnos - Babanos | Tree | ✓ | - | 2.18 | Poor | 1.31 | Good |
| *Malvaceae* | *Grewia tenax (Forssk.) Fiori* | Guddeim | Shrub | ✓ | - | 2.62 | Good | 0.00 | None |

| | | | | | | | | | |
|---|---|---|---|---|---|---|---|---|---|
| *Malvaceae* | *Grewia flavescens Juss.* | Guddeim Abou Dlouae | Shrub | ✓ | - | 0.87 | Good | 0.00 | None |
| *Ochnaceae* | *Ochna afzelii R.Br. ex Oliv.* | Lessan El kalib | Shrub | ✓ | - | 1.31 | Good | 0.00 | None |
| *Capparaceae* | *Maerua angolensis DC.* | Shagar ElZaraf | Shrub | ✓ | - | 1.31 | Poor | 0.00 | None |
| *Fabaceae* | *Cassia arereh Delile* | Al Gaga | Tree | ✓ | - | 0.44 | Poor | 0.00 | None |
| *Loganiaceae* | *Strychnos innocua Delile* | Um Bukheisa | Shrub | ✓ | - | 1.75 | Good | 0.00 | None |
| *Fabaceae* | *Tamarindus indica L.* | Aradaib | Tree | ✓ | - | 0.44 | Poor | 0.00 | None |
| *Fabaceae* | *Piliostigma reticulatum (DC.) Hochst.* | Kharub | Shrub | ✓ | - | 0.44 | Good | 0.00 | None |
| *Capparaceae* | *Capparis decidua (Forssk.) Edgew.* | Tundub | Shrub | ✓ | - | 3.06 | Poor | 0.00 | None |
| *Malvaceae* | *Adansonia digitata L.* | Tabaldi (Gongulis) | Tree | ✓ | - | 1.31 | Poor | 0.00 | None |
| *Burseraceae* | *Boswellia papyrifera (Delile) Hochst.* | Trag Trag | Tree | ✓ | - | 1.31 | Poor | 0.00 | None |

Table 4.9. Number of genera, number of species and relative frequency (RF) of genus and species within identified families in ENFR in 2008 and 2021.

| ***Family*** | ***2008*** | | | | ***2021*** | | | |
|---|---|---|---|---|---|---|---|---|
| | ***No. of Genera*** | ***No. of Species*** | ***Genus RF (%)*** | ***Species RF (%)*** | ***No. of Genera*** | ***No. of Species*** | ***Genus RF (%)*** | ***Species RF (%)*** |
| Fabaceae | 7 | 12 | 28.00 | 34.29 | 3 | 6 | 23.08 | 31.58 |
| Combretaceae | 3 | 7 | 12.00 | 20.00 | 3 | 5 | 23.08 | 26.32 |
| Malvaceae | 4 | 4 | 16.00 | 11.43 | 1 | 1 | 7.69 | 5.26 |
| Anacardiaceae | 2 | 2 | 8.00 | 5.71 | 2 | 2 | 15.38 | 10.53 |
| Rhamnaceae | 1 | 2 | 4.00 | 5.71 | 1 | 2 | 7.69 | 10.53 |
| Zygophyllaceae | 1 | 1 | 4.00 | 2.86 | 1 | 1 | 7.69 | 5.26 |
| Rubiaceae | 1 | 1 | 4.00 | 2.86 | 1 | 1 | 7.69 | 5.26 |
| Bignoniaceae | 1 | 1 | 4.00 | 2.86 | 1 | 1 | 7.69 | 5.26 |
| Capparaceae | 2 | 2 | 8.00 | 5.71 | 0 | 0 | 0.00 | 0.00 |
| Ochnaceae | 1 | 1 | 4.00 | 2.86 | 0 | 0 | 0.00 | 0.00 |
| Loganiaceae | 1 | 1 | 4.00 | 2.86 | 0 | 0 | 0.00 | 0.00 |
| Burseraceae | 1 | 1 | 4.00 | 2.86 | 0 | 0 | 0.00 | 0.00 |
| ***Total*** | ***25*** | ***35*** | | | ***13*** | ***19*** | | |

Species dominance patterns changed markedly. *Acacia seyal* declined from 63.3% of individuals in 2008 to 16.7% in 2021. Similarly, species frequency declined for several dominant species, including *Acacia seyal* (75.6% to 28.8%), *Acacia senegal* (40.2% to 9.6%), and *S. setigera* (68.1% to 31.9%). Several subdominant and rare species, including *Acacia seyal* var. *fistula*, *Acacia polyacantha*, *Dichrostachys cinerea*, and some *Combretum* and *Grewia* species, were not recorded in 2021.

In contrast, disturbance-tolerant species increased in relative importance. *Acacia nubica* increased from 0.87% to 20.1%, while *Acacia mellifera* increased from 3.5% to 4.8%. Other species, such as *Lannea fruticosa* (17.9% to 13.1%) and *Sclerocarya birrea* (4.8% to 3.9%), show relatively stable or moderate changes. Overall, approximately 54% of species declined, while only about 14% increased. Regeneration patterns also deteriorated, with the number of species classified as having "good" regeneration decreasing from 11 to 6, and 15 species showing no regeneration capacity (Appendix D). Overall, the results indicate a marked decline in species richness, structural diversity, and regeneration capacity, accompanied by a shift toward dominance by disturbance-tolerant species.

These results reflect significant ecological degradation in the ENFR and are consistent with patterns observed in other dryland forests, where anthropogenic pressure leads to loss of species diversity and structural complexity (Dereje & Duguma, 2019; Masresha et al., 2024; Chepkoech et al., 2024). The dominance of Fabaceae is typical of savanna ecosystems, where nitrogen-fixing species are relatively resilient under dry conditions (Abdou et al., 2016; Assogbadjo et al., 2010). However, the reduction in Fabaceae species richness indicates that even resilient functional groups are affected under sustained disturbance (Gebeyehu et al., 2019; Ghanbari et al., 2021).

The sharp decline of dominant and subdominant species, along with the disappearance of rare species, reflects the loss of disturbance-sensitive taxa. Similar patterns have been reported in dry Afromontane forests and other protected areas, where continuous disturbance leads to local species loss (Ghanbari et al., 2021; Gebeyehu et al., 2019; Rahman et al., 2020; Maua et al., 2020).

The increase in disturbance-tolerant species further confirms a shift in species composition toward more resilient but less diverse vegetation communities, as observed in other degraded savanna systems (Oke & Jamala, 2013; Kikoti & Mligo, 2015; Abdullahi, 2021). The decline in regeneration capacity is particularly critical, as it indicates reduced ecosystem resilience and limited potential for natural recovery. This pattern is likely driven by a

combination of reduced seed sources, grazing pressure, and climatic stress affecting seedling establishment (Canham & Murphy, 2016; Díaz et al., 2021).

Overall, these findings demonstrate a transition toward a simplified and degraded ecosystem, highlighting the urgent need for targeted conservation and restoration interventions to maintain biodiversity and ecosystem functioning in the ENFR.

#### 4.4.2. Population Structure of Woody species

Based on the 2021 inventory, tree diameter at breast height (DBH) ranges from 5 to 146 cm, with a mean of 22.83 cm (SD = 13.52 cm), while tree height ranges from 1 to 36 m, with a mean of 7.96 m (SD = 6.04 m) (Table 4.10). In comparison, the 2008 inventory records DBH values between 5 and 80 cm (mean = 21.76 cm; SD = 11.39 cm) and tree heights between 1 and 35 m (mean = 8.93 m; SD = 6.14 m).

The higher maximum DBH observed in 2021 reflects structural changes in the forest stand overtime rather than inconsistencies in sampling. Although the same permanent plots were revisited, tree populations are dynamic, and individual trees may have undergone growth, mortality, or replacement through recruitment processes. The presence of larger diameter classes in 2021 can therefore be attributed to the survival and continued growth of older trees, combined with selective removal or mortality of smaller individuals, which alters overall stand structure. These results indicate the presence of both mature trees and younger individuals, reflecting a mixed population structure.

Table 4.10. Summary statistics of tree growth variables (DBH and height) in Elnour Natural Forest Reserve (ENFR)

| Variables | 2008 | | 2021 | |
|---|---|---|---|---|
| | DBH (cm) | Height (m) | DBH (cm) | Height (m) |
| Maximum | 80.00 | 35.00 | 146.00 | 36.00 |
| Minimum | 5.00 | 1.00 | 5.00 | 1.00 |
| Mean | 21.76 | 8.93 | 22.83 | 7.96 |
| SD | 11.39 | 6.14 | 13.52 | 6.04 |

DBH distribution in 2008 is strongly skewed toward smaller size classes (Fig. 4.11a). The 6–10 cm class dominates with 32.34% of individuals, followed by 21–25 cm (20.13%), 16–20 cm (17.46%), and 26–30 cm (16.49%), while larger trees (>40 cm) represent only 4.07%. In 2021, the dominance of smaller diameter classes becomes more pronounced, with the 6–10 cm class increasing to 43.05% and the 11–15 cm class representing 21.30%. Intermediate classes (16–25 cm) account for approximately 24% of individuals, while larger diameter classes (>25 cm) decline to less than 12%. Tree height distribution shows a similar pattern (Fig. 4.11b). In 2008, the 1–3 m class accounts for 47.99% of individuals, followed by 4–6 m (21.03%), 7–

9 m (10.43%), and 10–12 m (10.11%), while taller classes (>13 m) are less frequent. In 2021, the 1–3 m class increases to 50.24%, followed by 4–6 m (21.46%), 7–9 m (10.24%), and 10–12 m (8.29%), with taller classes remaining the least represented.

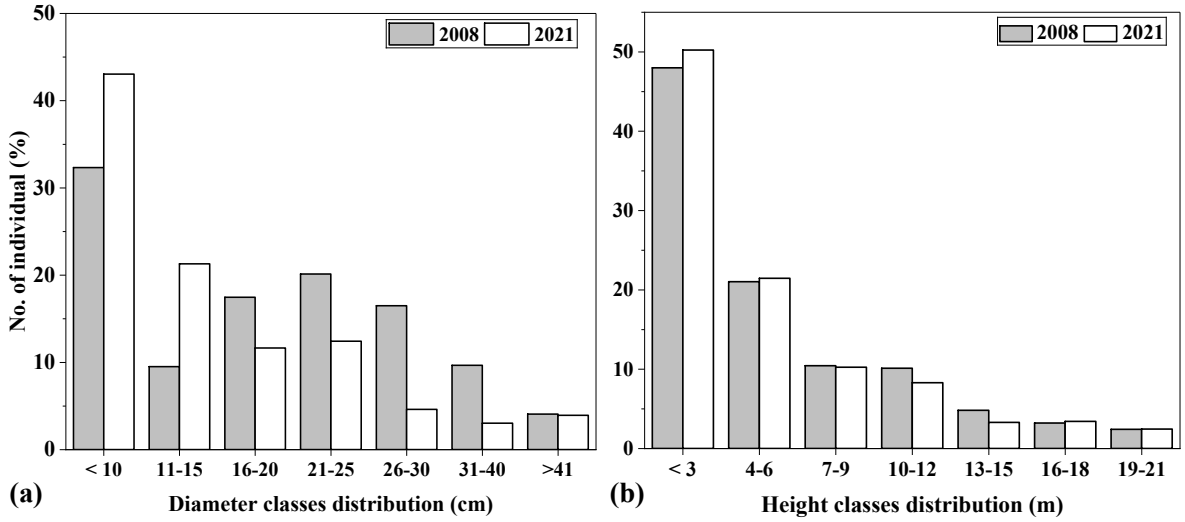


Fig. 4.11. Size-class distribution of woody species in the ENFR (2008 and 2021): (a) Diameter at breast height (DBH) classes distribution of individual trees and (b) Height classes distribution of individual trees.

Overall, the results show a clear dominance of smaller diameter and height classes, indicating strong recruitment alongside a reduction in larger and taller trees. These results are characteristic of disturbed forest systems. The dominance of smaller DBH classes reflects continuous recruitment, which is common in tropical and savanna forests where juvenile and sub-adult individuals dominate population structure (Adekunle & Olagoke, 2008; Adekunle et al., 2013; Aigbe et al., 2014). However, the sharp decline in larger diameter classes indicates selective removal of mature trees, a pattern widely reported in disturbed forests and dryland woodlands (Edet et al., 2012; Oke & Jamala, 2013; Kikoti & Mligo, 2015; Abdullahi, 2021; Gebeyehu et al., 2019; Ijomah et al., 2022).

The predominance of shorter height classes further indicates a regenerating but structurally simplified forest. Similar patterns have been observed in degraded forest reserves, where reduced canopy height reflects the loss of mature individuals and decreased structural complexity (Gogoi & Sahoo, 2018; Mohammed et al., 2021a; Musa et al., 2024; Asbeck et al., 2021).

The low proportion of large trees (particularly >50 cm DBH) is likely the result of selective logging and harvesting for fuelwood, timber, and other uses, as documented in comparable tropical forest ecosystems (Hadi et al., 2009). Such selective removal reduces canopy cover, alters microclimatic conditions, and limits regeneration potential, leading to long-term

structural changes (Pokhriyal et al., 2010; Yakubu et al., 2020; Aigbe et al., 2014; Rajasugunasekar et al., 2023). While the presence of both small and large individuals indicates ongoing regeneration and some level of structural continuity, the overall pattern reflects a shift toward younger cohorts and reduced canopy complexity. This has important ecological implications, as large trees play a critical role in biomass storage, habitat provision, and ecosystem stability (Adekunle & Olagoke, 2008; Aigbe et al., 2014; Gauthier et al., 2015; Asbeck et al., 2021; Gebeyehu et al., 2019).

Overall, these findings indicate that the ENFR forest structure is increasingly dominated by smaller and younger individuals, reflecting ongoing disturbance and selective removal of mature trees despite continued recruitment.

#### 4.4.3. Mean Basal Area, Density, Importance Value Index (IVI), and Conservation Status of Woody Species in the Elnour Natural Forest Reserve (ENFR)

The 2021 inventory (Table 4.11) shows substantial interspecific variation in tree density, basal area, and dominance across the ENFR. Mean density ranges from 0.17 to 22.93 trees $ha^{-1}$, while basal area varies from 0.00 to 0.35 $m^2$ $ha^{-1}$, indicating marked structural heterogeneity among species. *Acacia seyal* remains the most dominant species, with the highest mean density (22.93 trees $ha^{-1}$), basal area (0.35 $m^2$ $ha^{-1}$), and Importance Value Index (IVI = 71.99). Other species, including *Balanites aegyptiaca*, *Sterculia setigera*, *Acacia nubica*, and *Ziziphus spina-christi*, contribute to stand structure, whereas most remaining species exhibit low densities and IVI values below 15.

In contrast, the 2008 inventory reflects a denser and more structurally complex forest. Mean density reaches 469.21 trees $ha^{-1}$, and basal area reaches up to 8.83 $m^2$ $ha^{-1}$. *Acacia seyal* strongly dominates (IVI = 125.79), along with *Sterculia setigera*, *Acacia senegal*, and *Dichrostachys cinerea.* Between 2008 and 2021, there is a marked decline in density, basal area, and IVI, accompanied by the disappearance of several species and a shift in dominance patterns. The relative density of *Acacia seyal* decreases from 63.29% to 16.72%, while disturbance-tolerant species such as *Acacia mellifera*, *Acacia nubica*, *Dalbergia melanoxylon*, *Balanites aegyptiaca*, and *Z. spina-christi* increased in relative abundance. Although the Shannon–Wiener diversity index increases from $H' = 1.56$ to 2.46, species richness, total number of individuals, and basal area decline substantially. Regeneration patterns also change, with relatively stable seedling numbers but sharp declines in saplings and adult trees (Table 4.12). Overall, the results indicate a significant reduction in forest density and structural complexity, with a shift toward dominance by disturbance-tolerant species and a decline in mature tree populations.

Table 4.11. Tree species density, basal area, and Importance Value Index (IVI) in the ENFR for 2008 and 2021

| *Species* | 2008 | | | | 2021 | | | |
|---|---|---|---|---|---|---|---|---|
| | Mean density No. $ha^{-1}$ | Mean BA ($m^2/ha^{-1}$) | IVI | Classification Based on RD | Mean density No. $ha^{-1}$ | Mean BA ($m^2/ha^{-1}$) | IVI | ClassificationBased on RD |
| *Acacia seyal* | 469.21 | 8.83 | 125.79 | Abundant | 22.93 | 0.35 | 71.99 | Abundant |
| *Acacia seyal var. fistulal* | 27.73 | 0.31 | 20.11 | Occasional | 0.00 | 0.00 | 0.00 | - |
| *Acacia polycantha* | 13.28 | 0.26 | 10.31 | Rare | 0.00 | 0.00 | 0.00 | - |
| *Acacia Senegal* | 42.40 | 2.35 | 19.80 | Abundant | 2.53 | 0.25 | 15.12 | Abundant |
| *Dichrostachys cinerea* | 44.24 | 0.87 | 14.65 | Abundant | 0.00 | 0.00 | 0.00 | - |
| *Balanites aegyptiaca* | 17.73 | 0.24 | 10.02 | Rare | 6.99 | 0.15 | 53.16 | Abundant |
| *Acacia mellifera* | 0.74 | 0.01 | 0.93 | Threatened | 1.66 | 0.01 | 7.09 | Abundant |
| *Acacia nubica* | 0.13 | 0.00 | 0.19 | Threatened | 8.78 | 0.13 | 25.32 | Abundant |
| *Sterculia setigera* | 48.78 | 2.32 | 43.18 | Abundant | 8.21 | 0.19 | 44.88 | Abundant |
| *Anogeissus leiocarpus* | 5.24 | 0.24 | 5.60 | Threatened | 1.66 | 0.06 | 9.40 | Occasional |
| *Terminalia laxiflora* | 4.45 | 0.16 | 5.06 | Threatened | 1.09 | 0.02 | 5.29 | Occasional |
| *Terminalia brownii* | 3.01 | 0.06 | 4.38 | Threatened | 0.92 | 0.02 | 5.72 | Occasional |
| *Combretum hartmannianum* | 28.30 | 1.24 | 12.56 | Occasional | 2.10 | 0.05 | 10.78 | Rare |
| *Combretum aculeatum* | 3.80 | 0.09 | 1.82 | Threatened | 0.00 | 0.00 | 0.00 | - |
| *Combretum molle* | 4.06 | 0.08 | 2.76 | Threatened | 0.00 | 0.00 | 0.00 | - |
| *Combretum glutinosum* | 2.75 | 0.05 | 1.89 | Threatened | 0.70 | 0.01 | 5.35 | Occasional |
| *Lannea fruticosa* | 4.59 | 0.04 | 4.50 | Threatened | 1.83 | 0.02 | 10.29 | Rare |
| *Sclerocarya birrea* | 1.14 | 0.02 | 1.53 | Threatened | 0.92 | 0.03 | 6.80 | Frequent |
| *Ziziphus spina-christi* | 10.57 | 0.23 | 3.32 | Rare | 2.49 | 0.10 | 11.28 | Abundant |
| *Ziziphus abyssinica* | 2.75 | 0.19 | 2.03 | Threatened | 1.05 | 0.04 | 5.62 | Occasional |
| *Stereospermum kunthianum* | 2.40 | 0.07 | 2.58 | Threatened | 0.70 | 0.01 | 5.57 | Occasional |
| *Lonchocarpus laxiflorus* | 0.61 | 0.00 | 0.86 | Threatened | 0.17 | 0.00 | 1.26 | Rare |
| *Dalbergia melanoxylon* | 1.09 | 0.14 | 1.49 | Threatened | 0.26 | 0.00 | 3.30 | Rare |
| *Grewia tenax* | 0.35 | 0.00 | 0.47 | Threatened | 0.44 | 0.00 | 1.63 | Abundant |
| *Grewia flavescens* | 0.44 | 0.00 | 0.57 | Threatened | 0.00 | 0.00 | 0.00 | - |
| *Xeromphis nilotica* | 0.09 | 0.00 | 0.22 | Threatened | 0.00 | 0.00 | 0.00 | - |
| *Ochna afzelii* | 0.26 | 0.01 | 0.43 | Threatened | 0.00 | 0.00 | 0.00 | - |
| *Maerua angolensis* | 0.13 | 0.01 | 0.37 | Threatened | 0.00 | 0.00 | 0.00 | - |
| *Cassia arereh* | 0.04 | 0.00 | 0.11 | Threatened | 0.00 | 0.00 | 0.00 | - |
| *Strychons innocua* | 0.22 | 0.00 | 0.43 | Threatened | 0.00 | 0.00 | 0.00 | - |
| *Tamarindus indica* | 0.04 | 0.00 | 0.14 | Threatened | 0.00 | 0.00 | 0.00 | - |
| *Piliostigma reticulatum* | 0.04 | 0.00 | 0.11 | Threatened | 0.00 | 0.00 | 0.00 | - |
| *Capparis decidua* | 0.57 | 0.01 | 0.88 | Threatened | 0.00 | 0.00 | 0.00 | - |
| *Adansonia digitata* | 0.13 | 0.03 | 0.66 | Threatened | 0.00 | 0.00 | 0.00 | - |
| *Boswellia papyrifera* | 0.13 | 0.00 | 0.32 | Threatened | 0.00 | 0.00 | 0.00 | - |
| *Total* | 741.44 | 17.88 | | | 65.41 | 1.44 | | |

Table 4.12. Summary of stand structural variables and diversity indices in Elnour Natural Forest Reserve (ENFR) in 2008 and 2021

| Growth variables and diversity indices | 2008 | 2021 |
|---|---|---|
| Number of families | 16 | 9 |
| Genera | 25 | 13 |
| Number of tree species | 35 | 19 |
| Density (Tree $ha^{-1}$) | 741.44 | 65.41 |
| Number of trees | 16979 | 1498 |
| Number of seedlings | 8285 | 8265 |
| Number of saplings | 5491 | 645 |
| Number of adults | 13128 | 853 |
| Total basal area ($m^2$ $ha^{-1}$) | 17.88 | 1.44 |
| Basal area ($m^2$ $ha^{-1}$) | 0.51 | 0.07 |
| Abundant (Relative density; RD ≥ 5) | 4 (11.43%) | 8 (42.11%) |
| Frequent (4.00 ≤ RD ≥ 4.99) | - | 1 (5.26%) |
| Occasional (3.00 ≤ RD ≥ 3.99) | 2 (5.71%) | 6 (31.58%) |
| Rare (1.00 ≤ RD ≥ 2.99) | 3 (8.57%) | 4 (21.05%) |
| Threatened/ Endangered (0.00 < RD ≤ 1) | 26 (74.29%) | - |
| Shannon–Wiener (Diversity index (H) | 1.56 | 2.21 |
| Margalef's index (Species Richness) | 3.49 | 2.46 |
| Species Evenness index ($E_H$) | 0.44 | 0.75 |
| Simpson's Species Diversity index | 0.58 | 0.82 |
| Index of Dominance | 0.42 | 0.18 |

These results are consistent with structural degradation observed in dryland forests subjected to sustained anthropogenic pressure. The dominance of a few resilient species and the low IVI values of most others reflect competitive advantages under disturbance, as reported in Sudanese and African dryland ecosystems (Ibrahim & Hassan, 2015; Mohammed et al., 2021a; Musa et al., 2024; Abdullahi, 2021; Assogbadjo et al., 2010; Gebeyehu et al., 2019; Maua et al., 2020; Yahya et al., 2023; Hido et al., 2020). The substantial decline in density and basal area between 2008 and 2021 indicates intense harvesting, fuelwood extraction, and grazing pressure, which reduce stem density and canopy cover (Hadi et al., 2009; Eltayb & Magid, 2012; Gamoun et al., 2015; Kikoti & Mligo, 2015; Ghanbari et al., 2021; Gogoi & Sahoo, 2018). Similar degradation patterns have been documented in East African and Sahelian woodlands under comparable pressures (Assogbadjo et al., 2010; Gebeyehu et al., 2019; Maua et al., 2020; Abdullahi, 2021).

The disappearance of several species suggests local extirpation of disturbance-sensitive taxa, consistent with findings from fragmented and overexploited forest systems (Tesfaye et al., 2010; Pokhriyal et al., 2010; Rahman et al., 2020; Joshi et al., 2024; Zhong et al., 2024). The increase in disturbance-tolerant species reflects competitive release under degraded conditions, a pattern widely observed in dryland ecosystems (Maua et al., 2020; Ibrahim & Hassan, 2015; Musa et al., 2024; Abdullahi, 2021; Yahya et al., 2023; Hido et al., 2020; Ayele et al., 2024; Masresha et al., 2024).

The increase in the Shannon–Wiener diversity index, despite declining species richness, reflects reduced dominance of previously dominant species rather than true ecological recovery. This pattern is consistent with ecological theory and empirical evidence from disturbed forests (Gamito, 2010; Okpiliya, 2012; Yeom & Kim, 2011; Siddig, 2019; Serbouti et al., 2023; Gunawan et al., 2024; Wilfahrt et al., 2023; Stritih et al., 2024). The observed regeneration bottleneck, characterized by stable seedling numbers but declining saplings and adult trees, indicates impaired recruitment and long-term instability, as reported in degraded tropical and dry forests (Cueva-Ortiz et al., 2020; Petrie et al., 2023; Bentz et al., 2022; Lalor et al., 2023; Crockett & Hurteau, 2024).

Overall, these findings demonstrate substantial restructuring of species composition and forest function in the ENFR, driven by selective loss of disturbance-sensitive species and increasing dominance of resilient taxa. This highlights the urgent need for conservation measures, including protection of declining species, regulation of resource extraction, assisted regeneration, and sustainable management strategies to restore forest complexity and long-term resilience (FAO, 2010; Vizzarri, 2024; Yasin et al., 2024; Hasoba et al., 2025; Osewe et al., 2024; Rajasugunasekar et al., 2023; Chaturvedi et al., 2024; de Oliveira et al., 2024; Volis, 2024; Zhao et al., 2024).

## 4.5. Mapping of Dominant Tree Species Using Multi-Source Remote Sensing Data and Machine Learning Approaches (Objective 4)

This section presents the mapping and analysis of dominant tree species in the Elnour Natural Forest Reserve (ENFR) using multi-temporal and multi-source remote sensing data combined with machine learning techniques. The performance of different classification algorithms is evaluated, and their outputs are compared in terms of accuracy, spatial consistency, and temporal stability. The results provide a detailed assessment of species distribution patterns and their changes over time, contributing to a better understanding of forest composition dynamics and the applicability of machine learning approaches in dryland ecosystems.

### 4.5.1. Machine Learning–Based Classification of Dominant Tree Species

Machine learning classifiers successfully mapped dominant tree species in the dryland forest ecosystem across four time periods (2008, 2013, 2018, and 2021) using multi-temporal and multi-source satellite data within Google Earth Engine. Random Forest (RF), Support Vector Machine (SVM), Classification and Regression Trees (CART), and an ensemble approach all produced reliable classification outputs. RF and SVM consistently demonstrate

strong performance across all years, while CART provides stable and interpretable results. The ensemble approach improves overall classification accuracy but introduces higher uncertainty for less-represented species.

Across all years, *Acacia seyal* is consistently identified as the dominant canopy species. Secondary species, including *Sterculia setigera* and *Combretum hartmannianum*, are also detected, although their spatial distribution varies over time.

Overall, the results indicate that machine learning approaches are effective for mapping dominant tree species in dryland ecosystems, with higher classification accuracy for dominant species and lower reliability for minor or less-represented classes.

These results are consistent with previous studies demonstrating the effectiveness of Google Earth Engine for large-scale vegetation monitoring (Gorelick et al., 2017; Wang et al., 2020). The strong performance of RF reflects its ability to handle high-dimensional and multi-source data, while SVM performs well under limited sample conditions (Pal, 2005; Belgiu & Drăguţ, 2016; Cortes & Vapnik, 1995; Halldorsson et al., 2003). The effectiveness of CART further supports its applicability in ecological classification tasks (De'ath & Fabricius, 2000; Sesnie et al., 2008).

The improved performance of the ensemble approach is consistent with studies showing that combining classifiers can enhance overall accuracy; however, the increased uncertainty for minor species highlights the influence of class imbalance and spectral overlap (Breiman et al., 1984; Ramezan et al., 2020). The consistent dominance of *Acacia seyal* aligns with ecological studies in Sudan's dryland forests, where this species plays a central structural role (Harrison & Jackson, 1958; Fahmi, 2017; Mohammed et al., 2021a).

The variability observed in mapping secondary species reflects known challenges in species-level classification, particularly in dryland environments where spectral similarity and phenological variation reduce class separability (Fassnacht et al., 2016; Persson et al., 2018; Liu et al., 2021).

Overall, these findings demonstrate that machine learning–based classification provides a robust and scalable approach for mapping dominant tree species in dryland forests, while also highlighting the need for improved methods to better capture minor and spectrally similar species.

#### 4.5.2. Comparison of Algorithm Performance for Dominant Tree Species Mapping

Across all years (2008, 2013, 2028, and 2021), Support Vector Machine (SVM) and Random Forest (RF) show the most stable and reliable performance for mapping dominant tree

species, with overall accuracies ranging from 89% to 96% and Kappa coefficients between 0.84 and 0.93 (Fig. 4.12). In contrast, Classification and Regression Trees (CART) exhibit more variable performance, particularly for less distinct species such as *Dichrostachys cinerea*, *Balanites aegyptiaca*, and *Combretum molle*. The ensemble classifier shows lower overall accuracy (69–89%) and reduced Kappa values (0.55–0.80), with inconsistent detection of minor species and a tendency to overestimate dominant classes. Overall, the results indicate that RF and SVM outperform CART and the ensemble approach, providing more consistent and reliable classification results across all time periods.

These results are consistent with previous studies demonstrating the robustness of RF and SVM in forest classification tasks (Belgiu & Drăguţ, 2016; Raczko & Zagajewski, 2017; Sabins & Ellis, 2020). The strong performance of RF reflects its ability to handle high-dimensional spectral data and reduce overfitting, as widely reported in remote sensing applications (Pal, 2005; Immitzer et al., 2012; Du et al., 2015). Similarly, the stability of SVM confirms its effectiveness in separating spectrally overlapping classes through margin optimization (Cortes & Vapnik, 1995; Halldorsson et al., 2003; Axelsson et al., 2021).

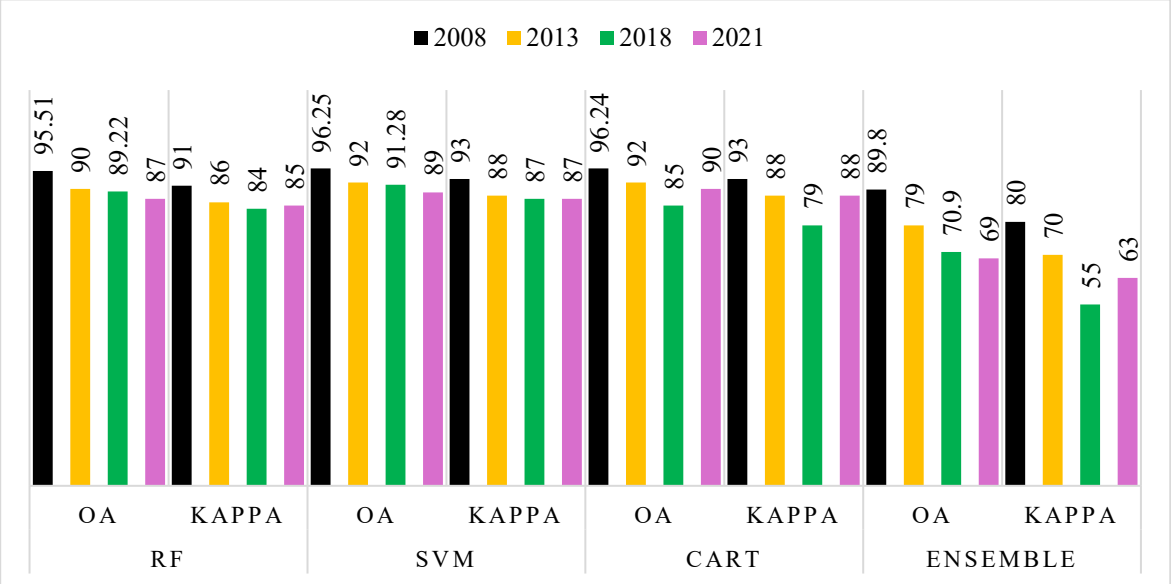


Fig. 4.12. Comparative performance of machine learning classifiers (RF, SVM, CART, and ensemble) for dominant tree species mapping in the ENFR during 2008–2021, based on overall accuracy and Kappa statistics.

The moderate performance of CART reflects its sensitivity to class imbalance and spectral overlap, which limits its effectiveness in complex vegetation environments (De'ath & Fabricius, 2000; Breiman et al., 1984; Ließ et al., 2012). Similar limitations of single decision-tree models have been reported in heterogeneous forest systems (Lu & Weng, 2007; Fassnacht et al., 2016).

The lower performance of the ensemble classifier is likely due to majority-voting bias and correlated errors among base classifiers, which can reduce classification accuracy and spatial detail, particularly for rare species (Hu et al., 2021; Ramezan et al., 2019; Chung et al., 2021). This finding is consistent with studies showing that ensemble approaches may lead to overgeneralization and reduced spatial realism when class imbalance is present (Sabat-Tomala et al., 2020; Strömann et al., 2019; Persson et al., 2018).

Overall, these findings demonstrate that individual classifiers, particularly RF and SVM, provide more accurate and reliable outputs than the ensemble approach for mapping dominant tree species. This supports their suitability for long-term monitoring of savanna woodland composition, consistent with findings in remote sensing and machine learning studies (Fassnacht et al., 2016; Wang et al., 2020; Zhong et al., 2024).

#### 4.5.3. Spatial Distribution and Area Estimates of Dominant Tree Species

Spatial distribution maps reveal clear and consistent ecological patterns across all study years (Figures 4.13–4.16; Tables 4.13–4.17). *Acacia seyal* dominates the central and lowland areas of the Elnour Natural Forest Reserve (ENFR), forming the most continuous and extensive canopy cover. In contrast, *Sterculia setigera* and *Combretum hartmannianum* occur in more fragmented patches, typically associated with transitional or disturbed zones. Minor species are confined to localized and discontinuous patches, indicating limited spatial extent and lower ecological dominance.

Random Forest (RF) and Support Vector Machine (SVM) produce more spatially coherent, continuous, and ecologically consistent distribution patterns across all years. In contrast, Classification and Regression Trees (CART) and the ensemble approach exhibit greater spatial fragmentation and less consistent class distribution, particularly for minor species. Overall, the results indicate that dominant species exhibit stable and spatially structured distribution patterns, whereas secondary and minor species show fragmented and variable spatial dynamics.

##### 4.5.3.1. Distribution of Dominant Tree Species in 2008

The spatial distribution and proportional coverage of dominant tree species in 2008 vary among the classification algorithms, reflecting differences in model sensitivity and class assignment behavior (Fig. 4.13; Table 4.13).

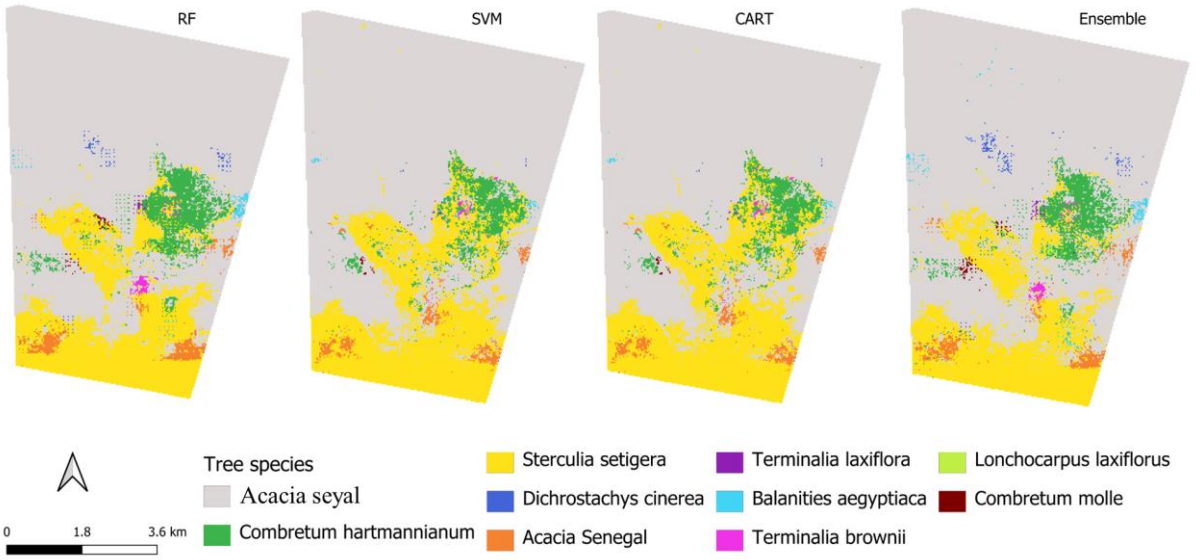


Fig. 4.13. Spatial distribution of dominant tree species in the Elnour Natural Forest Reserve (ENFR) using RF, SVM, CART, and ensemble models in 2008.

Table 4.13. Estimated area (ha) and relative proportion (%) of dominant tree species in the study area derived from RF, SVM, CART, and ensemble classifications in 2008.

| Species | RF | | SVM | | CART | | Ensemble | |
|---|---|---|---|---|---|---|---|---|
| | Area(ha) | % | Area(ha) | % | Area(ha) | % | Area(ha) | % |
| *Acacia seyal* | 3372.81 | 71.29 | 3313.92 | 70.05 | 3313.92 | 70.05 | 3482.36 | 73.61 |
| *Combretum hartmannianum* | 250.24 | 5.29 | 193.35 | 4.09 | 193.35 | 4.09 | 222.92 | 4.71 |
| *Sterculia setigera* | 979.79 | 20.71 | 1144.10 | 24.18 | 1144.10 | 24.18 | 887.99 | 18.77 |
| *Dichrostachys cinerea* | 9.86 | 0.21 | 0.68 | 0.01 | 0.68 | 0.01 | 17.77 | 0.38 |
| *Acacia Senegal* | 77.64 | 1.64 | 64.57 | 1.36 | 64.57 | 1.36 | 69.87 | 1.48 |
| *Terminalia laxiflora* | 3.09 | 0.07 | 0.98 | 0.02 | 0.98 | 0.02 | 3.41 | 0.07 |
| *Balanities aegyptiaca* | 13.71 | 0.29 | 4.14 | 0.09 | 4.14 | 0.09 | 18.56 | 0.39 |
| *Terminalia brownii* | 13.55 | 0.29 | 6.93 | 0.15 | 6.93 | 0.15 | 13.31 | 0.28 |
| *Lonchocarpus laxiflorus* | 4.44 | 0.09 | 0.30 | 0.01 | 0.30 | 0.01 | 7.00 | 0.15 |
| *Combretum molle* | 5.95 | 0.13 | 2.11 | 0.04 | 2.11 | 0.04 | 7.88 | 0.17 |

Across all classifiers, *Acacia seyal* is consistently identified as the dominant species, covering the largest proportion of the study area. Estimated coverage ranges from 70.05% under SVM and CART to 73.61% under the ensemble classifier, while RF provides an intermediate estimate of 71.29%. These results indicate stable and consistent detection of this structurally dominant species across algorithms.

*Sterculia setigera* is the second most extensive species, although its estimated area varies among classifiers. SVM and CART produce higher estimates (24.18%) than RF (20.71%) and the ensemble classifier (18.77%). *Combretum hartmannianum* occupies a moderate proportion of the landscape, with RF estimating the largest area (5.29%), SVM and CART

producing lower estimates (4.09%), and the ensemble approach yielding an intermediate value (4.71%).

Minor and sparsely distributed species, including *Dichrostachys cinerea*, *Terminalia laxiflora*, *Lonchocarpus laxiflorus*, and *Combretum molle*, consistently occupy less than 1% of the total area across all classifiers. However, the ensemble classifier generally produces slightly higher estimates for these rare species than SVM and CART. Overall, SVM and CART generate highly similar estimates for most species, RF shows slightly greater variability among minor classes, and the ensemble classifier consistently reports higher area estimates for both dominant and rare species. Overall, the results confirm the strong spatial dominance of *Acacia seyal* and demonstrate consistent classification performance for dominant species across algorithms, while highlighting greater variability in the estimation of secondary and minor species.

These results are consistent with the ecological and structural dominance of *Acacia seyal* in Sudanese dryland woodlands (Harrison & Jackson, 1958; Fahmi, 2017; Mohammed et al., 2021a). The relatively stable estimates across classifiers indicate that dominant canopy species with distinct spectral and structural characteristics can be mapped reliably using machine learning approaches, particularly RF and SVM (Belgiu & Drăguţ, 2016; Cortes & Vapnik, 1995; Pal, 2005).

The greater variability observed for *Sterculia setigera* and *Combretum hartmannianum* reflects the difficulty of separating secondary species with overlapping spectral responses and patchier distributions, which is a common challenge in tree-species classification using multi-source imagery (Fassnacht et al., 2016; Persson et al., 2018; Liu et al., 2021; Wan et al., 2021). The slightly higher coverage assigned by the ensemble classifier to both dominant and rare species suggests aggregation bias associated with majority voting, particularly under conditions of class imbalance (Hu et al., 2021; Ramezan et al., 2019; Chung et al., 2021).

#### 4.5.3.2. Distribution of Dominant Tree Species in 2013

The spatial distribution and proportional coverage of dominant tree species in 2013 show clear variation among classification algorithms, reflecting differences in model sensitivity and class assignment behavior (Fig. 4.14; Table 4.14). *Acacia seyal* remains the dominant species across all classifiers, occupying the largest proportion of the study area. Estimated coverage ranges from (60.37%) under RF and (67.37%) under both SVM and CART, while the ensemble classifier provides an intermediate estimate of (63.86%).

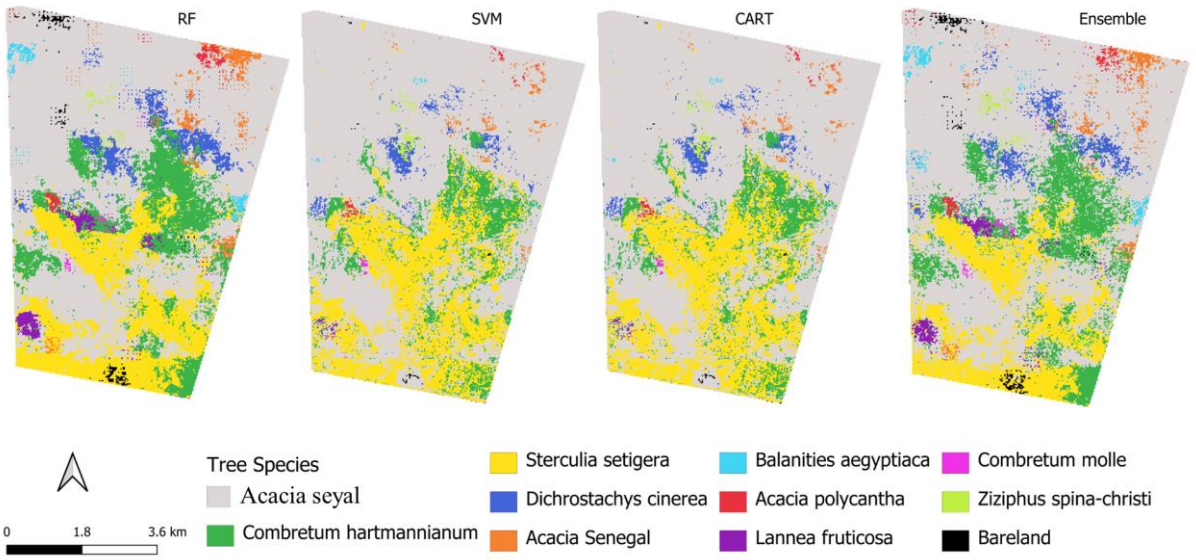


Fig. 4.14. Spatial distribution of dominant tree species in the Elnour Natural Forest Reserve (ENFR) using RF, SVM, CART, and ensemble models in 2013.

Table 4.14. Estimated area (ha) and relative proportion (%) of dominant tree species in the study area derived from RF, SVM, CART, and ensemble classifications in 2013.

| Species name | RF | | SVM | | CART | | Ensemble | |
|---|---|---|---|---|---|---|---|---|
| | Area(ha) | % | Area(ha) | % | Area(ha) | % | Area(ha) | % |
| *Acacia seyal* | 2856.01 | 60.37 | 3187.33 | 67.37 | 3187.33 | 67.37 | 3021.29 | 63.86 |
| *Combretum hartmannianum* | 616.59 | 13.03 | 409.01 | 8.65 | 409.01 | 8.65 | 605.10 | 12.79 |
| *Sterculia setigera* | 841.63 | 17.79 | 976.23 | 20.63 | 976.23 | 20.63 | 709.99 | 15.01 |
| *Dichrostachys cinerea* | 161.00 | 3.40 | 77.75 | 1.64 | 77.75 | 1.64 | 134.40 | 2.84 |
| *Acacia Senegal* | 89.96 | 1.90 | 31.11 | 0.66 | 31.11 | 0.66 | 83.62 | 1.77 |
| *Balanities aegyptiaca* | 32.47 | 0.69 | 3.69 | 0.08 | 3.69 | 0.08 | 39.84 | 0.84 |
| *Acacia polycantha* | 29.53 | 0.62 | 11.90 | 0.25 | 11.90 | 0.25 | 27.84 | 0.59 |
| *Lannea fruticosa* | 55.68 | 1.18 | 6.93 | 0.15 | 6.93 | 0.15 | 47.81 | 1.01 |
| *Combretum molle* | 8.51 | 0.18 | 4.07 | 0.09 | 3.77 | 0.08 | 11.03 | 0.23 |
| *Ziziphus spina-christi* | 14.77 | 0.31 | 20.19 | 0.43 | 20.19 | 0.43 | 23.20 | 0.49 |
| Bareland | 24.94 | 0.53 | 2.86 | 0.06 | 3.16 | 0.07 | 26.97 | 0.57 |

*Sterculia setigera* remains the second most extensive species; however, its estimated area varies substantially among classifiers. SVM and CART produce higher estimates (20.63%) than RF (17.79%) and the ensemble approach (15.01%). *Combretum hartmannianum* occupies a moderate proportion of the forest landscape, with RF (13.03%) and the ensemble classifier (12.79%) generating higher estimates than SVM and CART (8.65%).

Minor and sparsely distributed species, including *Dichrostachys cinerea*, *Acacia senegal*, *Balanites aegyptiaca*, *Acacia polyacantha*, *Lannea fruticosa*, *Combretum molle*, and *Ziziphus spina-christi*, consistently occupy less than 4% of the total area across all models. Bareland occupies a negligible proportion in all classifications, ranging from 0.06% under SVM

to 0.57% under the ensemble classifier. Overall, SVM and CART produce highly comparable area estimates, RF yields more conservative predictions for several secondary and minor species, and the ensemble approach tends to assign slightly higher areas to multiple classes.

Overall, the results confirm the continued dominance of *Acacia seyal*, while indicating increased variability in the spatial distribution of secondary and minor species across classification algorithms.

These results indicate that *Acacia seyal* maintains structural dominance in 2013 despite a reduction in its spatial extent relative to 2008. This decline likely reflects increasing ecological pressure, localized disturbance, or temporal variation in canopy condition affecting spectral separability. Similar trends have been reported in Sudanese dryland forests under continued anthropogenic and climatic stress (Abuelbashar et al., 2022; Gurashi et al., 2024a; Yasin et al., 2024).

The increased representation of *Combretum hartmannianum*, particularly under RF and ensemble classification, suggests expansion into mixed or transitional canopy conditions. In contrast, the variability observed in *Sterculia setigera* estimates highlights the difficulty of mapping species with partially overlapping spectral and structural characteristics (Fassnacht et al., 2016; Ferreira et al., 2019; Axelsson et al., 2021). The more conservative estimates produced by RF for several secondary species are consistent with its ability to reduce overfitting and maintain robust classification performance in complex datasets (Belgiu & Drăguţ, 2016; Du et al., 2015; Soleimannejad et al., 2019).

The negligible extent of bareland indicates that changes in 2013 are primarily driven by transitions among vegetation classes rather than large-scale conversion to non-vegetated land. The slightly higher estimates produced by the ensemble classifier again suggest majority-voting effects, particularly for less represented classes (Hu et al., 2021; Ramezan et al., 2019).

#### 4.5.3.3. Distribution of Dominant Tree Species in 2018

The spatial distribution and proportional coverage of dominant tree species in 2018 show pronounced variation among classification algorithms, reflecting differences in model sensitivity and class assignment behavior (Fig. 4.15; Table 4.15). *Acacia seyal* remains the dominant species across all classifiers, although its estimated area varies substantially. CART produces the lowest estimate (47.26%), while the ensemble classifier reports the highest coverage (73.99%). RF and SVM yield identical intermediate estimates of (68.29%), indicating strong agreement between these two algorithms.

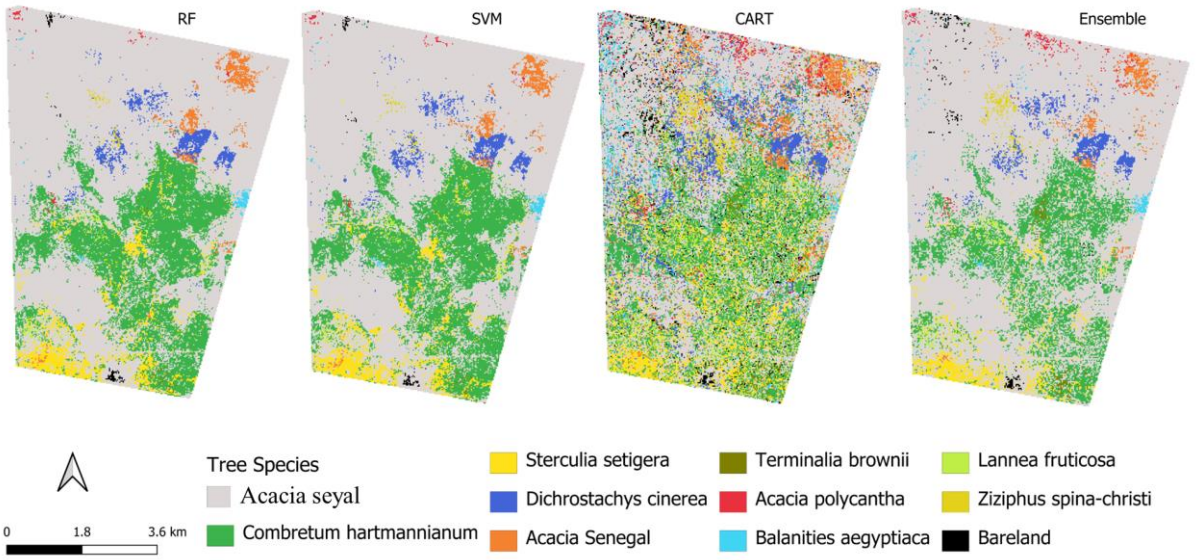


Fig. 4.15. Spatial distribution of dominant tree species in the Elnour Natural Forest Reserve (ENFR) using RF, SVM, CART, and ensemble models in 2018.

Table 4.15. Estimated area (ha) and relative proportion (%) of dominant tree species in the study area derived from RF, SVM, CART, and ensemble classifications in 2018.

| Species | RF | | SVM | | CART | | Ensemble | |
|---|---|---|---|---|---|---|---|---|
| | Area(ha) | % | Area(ha) | % | Area(ha) | % | Area(ha) | % |
| *Acacia seyal* | 3230.70 | 68.29 | 3230.70 | 68.29 | 2235.87 | 47.26 | 3500.48 | 73.99 |
| *Combretum hartmannianum* | 1029.13 | 21.75 | 1029.13 | 21.75 | 928.53 | 19.63 | 750.44 | 15.86 |
| *Sterculia setigera* | 219.01 | 4.63 | 219.01 | 4.63 | 402.56 | 8.51 | 157.51 | 3.33 |
| *Dichrostachys cinerea* | 103.14 | 2.18 | 103.14 | 2.18 | 275.83 | 5.83 | 105.94 | 2.24 |
| *Acacia Senegal* | 75.41 | 1.59 | 75.41 | 1.59 | 237.41 | 5.02 | 68.56 | 1.45 |
| *Terminalia brownii* | 5.35 | 0.11 | 5.35 | 0.11 | 66.45 | 1.40 | 19.70 | 0.42 |
| *Acacia polycantha* | 8.81 | 0.19 | 8.81 | 0.19 | 107.97 | 2.28 | 28.37 | 0.60 |
| *Balanities aegyptiaca* | 14.69 | 0.31 | 14.69 | 0.31 | 141.42 | 2.99 | 22.94 | 0.48 |
| *Lannea fruticosa* | 28.10 | 0.59 | 28.10 | 0.59 | 109.55 | 2.32 | 31.61 | 0.67 |
| *Ziziphus spina-christi* | 8.66 | 0.18 | 8.66 | 0.18 | 127.63 | 2.70 | 28.19 | 0.60 |
| Bareland | 8.06 | 0.17 | 8.06 | 0.17 | 97.87 | 2.07 | 17.34 | 0.37 |

*Combretum hartmannianum* occupies a substantial proportion of the forest landscape, with RF and SVM both estimating (21.75%), CART producing slightly lower coverage (19.63%), and the ensemble classifier assigning a smaller area (15.86%). *Sterculia setigera* also shows considerable inter-algorithm variability, with CART reporting the highest estimate (8.51%), RF and SVM producing identical values (4.63%), and the ensemble classifier assigning the lowest coverage (3.33%).

Minor and sparsely distributed species generally occupy less than 6% of the total forest area. CART tends to assign higher coverage to several rare classes, such as *Dichrostachys cinerea* (5.83%). Bareland remains minimal across all models (≤2.07%). Overall, RF and SVM

produce closely aligned estimates, CART underestimates the dominant species and overestimates several minor species, and the ensemble classifier inflates the coverage of dominant species.

Overall, the results confirm the continued dominance of *Acacia seyal*, while highlighting increased variability among algorithms in estimating secondary and minor species.

These results indicate that the strong agreement between RF and SVM in 2018 is likely associated with improved species discrimination enabled by Sentinel-2 imagery, whose higher spatial and spectral resolution enhances the separation of spectrally similar vegetation classes (Drusch et al., 2012; Persson et al., 2018; Liu et al., 2021). This supports previous studies demonstrating that multi-temporal Sentinel-2 data improve tree-species mapping performance in heterogeneous forest environments (Axelsson et al., 2021; Praticò et al., 2021; Zhong et al., 2024).

The lower estimate of *Acacia seyal* under CART, combined with higher estimates for rare species, reflects the sensitivity of single-tree methods to class imbalance and spectral overlap in ecologically complex landscapes (De'ath & Fabricius, 2000; Breiman et al., 2017; Ließ et al., 2012). In contrast, RF and SVM are better able to handle multidimensional feature space and complex class boundaries, which explains their closer agreement and greater stability (Belgiu & Drăguţ, 2016; Cortes & Vapnik, 1995; Raczko & Zagajewski, 2017).

The high estimate of *Acacia seyal* under the ensemble classifier indicates that majority voting can amplify dominant classes when component classifiers share similar tendencies. This confirms that ensemble outputs should be interpreted cautiously in imbalanced species datasets (Hu et al., 2021; Ramezan et al., 2019; Sabat-Tomala et al., 2020).

#### 4.5.3.4. Distribution of Dominant Tree Species in 2021

The spatial distribution and proportional coverage of dominant tree species in 2021 show pronounced variation among classification algorithms, reflecting differences in model sensitivity and class assignment behavior (Fig. 4.16; Table 4.16). *Acacia seyal* remains a dominant species; however, its estimated coverage declines markedly compared to earlier years. Area estimates range from (33.79%) under SVM and CART to (37.73%) under the ensemble classifier, while RF provides an intermediate estimate of (34.23%).

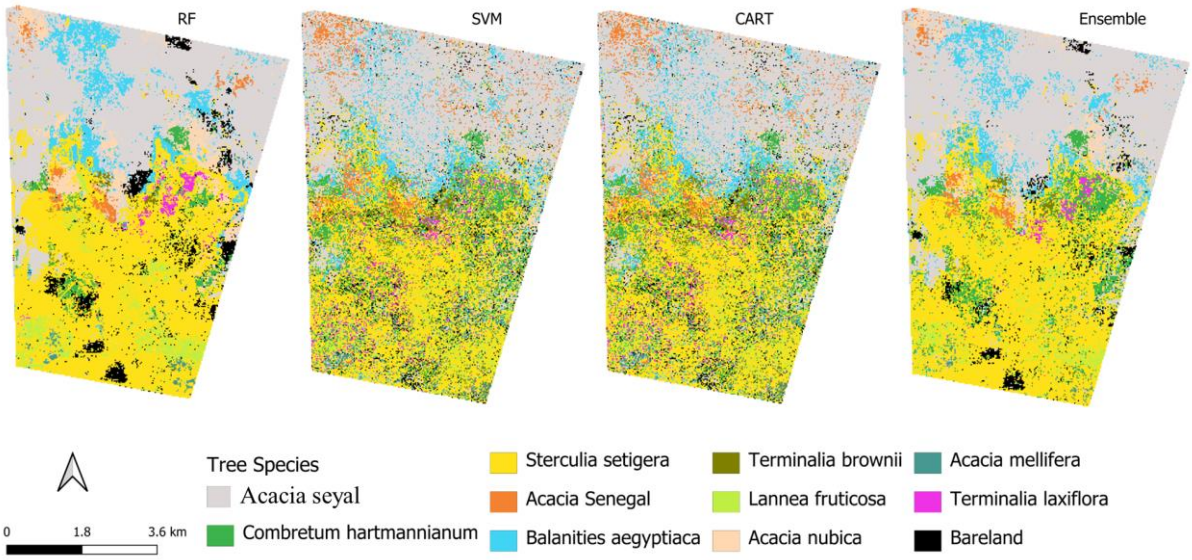


Fig. 4.16. Spatial distribution of dominant tree species in the Elnour Natural Forest Reserve (ENFR) using RF, SVM, CART, and ensemble models in 2021.

Table 4.16. Estimated area (ha) and relative proportion (%) of dominant tree species in the study area derived from RF, SVM, CART, and ensemble classifications in 2021.

| Species | RF | | SVM | | CART | | Ensemble | |
|---|---|---|---|---|---|---|---|---|
| | Area(ha) | % | Area(ha) | % | Area(ha) | % | Area(ha) | % |
| *Acacia seyal* | 1619.61 | 34.23 | 1598.85 | 33.79 | 1598.85 | 33.79 | 1784.91 | 37.73 |
| *Combretum hartmannianum* | 104.63 | 2.21 | 390.07 | 8.24 | 390.07 | 8.24 | 324.83 | 6.87 |
| *Sterculia setigera* | 1821.20 | 38.49 | 1315.93 | 27.81 | 1315.93 | 27.81 | 1731.68 | 36.60 |
| *Acacia Senegal* | 62.52 | 1.32 | 186.93 | 3.95 | 186.93 | 3.95 | 74.25 | 1.57 |
| *Balanities aegyptiaca* | 336.73 | 7.12 | 328.89 | 6.95 | 328.89 | 6.95 | 292.09 | 6.17 |
| *Terminalia brownii* | 24.11 | 0.51 | 153.48 | 3.24 | 153.48 | 3.24 | 42.20 | 0.89 |
| *Lannea fruticosa* | 190.51 | 4.03 | 164.26 | 3.47 | 164.26 | 3.47 | 132.03 | 2.79 |
| *Acacia nubica* | 274.66 | 5.81 | 212.93 | 4.50 | 212.93 | 4.50 | 163.73 | 3.46 |
| *Acacia mellifera* | 31.64 | 0.67 | 125.00 | 2.64 | 125.00 | 2.64 | 24.17 | 0.51 |
| *Terminalia laxiflora* | 47.01 | 0.99 | 107.37 | 2.27 | 107.37 | 2.27 | 31.17 | 0.66 |
| Bareland | 218.46 | 4.62 | 147.38 | 3.12 | 147.38 | 3.12 | 130.02 | 2.75 |

In contrast, *Sterculia setigera* emerges as a co-dominant species in 2021. RF estimates the largest coverage (38.49%), followed by the ensemble classifier (36.60%), while SVM and CART generate lower but identical estimates (27.81%). *Combretum hartmannianum* shows a clear decline compared with 2018, with estimates ranging from (2.21%) under RF to (8.24%) under SVM and CART.

Other minor and sparsely distributed species, including *Acacia senegal*, *Balanites aegyptiaca*, *Terminalia brownii*, *Lannea fruticosa*, *Acacia nubica*, *Acacia mellifera*, and *Terminalia laxiflora*, consistently occupy less than 7% of the total area across all algorithms. CART tends to assign relatively higher coverage to several rare classes, such as *Terminalia*

*brownii* (3.24%). Bareland remains low across all models (≤4.62%). Overall, SVM and CART produce closely aligned estimates, RF yields more conservative predictions for secondary and minor species, and the ensemble classifier produces slightly higher estimates for both dominant and rare classes.

Overall, the results indicate a clear shift in species dominance, with a decline in *Acacia seyal* and the emergence of *Sterculia setigera* as a co-dominant species, accompanied by increased variability in the distribution of secondary and minor species.

These results indicate substantial ecological restructuring by 2021. The decline of *Acacia seyal* and the rise of *Sterculia setigera* likely reflect changes in competitive dynamics under increasing disturbance pressure, selective resource extraction, and altered site conditions. Similar compositional shifts toward disturbance-tolerant and opportunistic species have been reported in Sudanese forest reserves under sustained ecological stress (Abuelbashar et al., 2022; Gurashi et al., 2024b; Musa et al., 2024).

The decline of *Combretum hartmannianum* relative to 2018 suggests sensitivity to disturbance intensity or reduced competitiveness under changing canopy structure. The moderate increase of other secondary species further indicates a transition toward a more heterogeneous and structurally simplified vegetation state, characteristic of dryland forests undergoing ecological reorganization (Smith et al., 2019; Yasin et al., 2024; Yasin et al., 2025).

As observed in previous years, RF produces more conservative and spatially coherent estimates, whereas CART shows a tendency to overestimate minor classes. The ensemble classifier again smooths class distributions and slightly inflates selected areas, confirming that majority voting can bias final area estimates under conditions of class imbalance (Hu et al., 2021; Chung et al., 2021; Ramezan et al., 2019).

#### 4.5.4. Temporal Dynamics of Dominant Tree Species Composition (2008–2021)

The analysis of dominant tree species from 2008 to 2021 reveals pronounced temporal changes in forest structure and spatial composition, together with clear algorithm-dependent variability across all study years (Table 4.17).

*Acacia seyal* remains the dominant species throughout the study period; however, its spatial extent fluctuates substantially over time. In 2008, its estimated area ranges from (70.05%) under SVM and CART to (73.61%) under the ensemble classifier. By 2013, coverage declines to (60.37–67.37%). In 2018, estimates range from (47.26%) under CART to (73.99%) under the ensemble classifier. In 2021, RF, SVM, and CART converge at approximately (33.79–34.23%), while the ensemble classifier again reports slightly higher coverage (37.73%).

Table 4.17. Percentage area of the top three species across 2008, 2013, 2018, and 2021 for all four classifiers (RF, SVM, CART, and ensemble).

| Year | Species | RF (%) | SVM (%) | CART (%) | Ensemble (%) |
|---|---|---|---|---|---|
| 2008 | *Acacia seyal* | 71.29 | 70.05 | 70.05 | 73.61 |
| | *Sterculia setigera* | 20.71 | 24.18 | 24.18 | 18.77 |
| | *Combretum hartmannianum* | 5.29 | 4.09 | 4.09 | 4.71 |
| 2013 | *Acacia seyal* | 60.37 | 67.37 | 67.37 | 63.86 |
| | *Sterculia setigera* | 17.79 | 20.63 | 20.63 | 15.01 |
| | *Combretum hartmannianum* | 13.03 | 8.65 | 8.65 | 12.79 |
| 2018 | *Acacia seyal* | 68.29 | 68.29 | 47.26 | 73.99 |
| | *Sterculia setigera* | 4.63 | 4.63 | 8.51 | 3.33 |
| | *Combretum hartmannianum* | 21.75 | 21.75 | 19.63 | 15.86 |
| 2021 | *Acacia seyal* | 34.23 | 33.79 | 33.79 | 37.73 |
| | *Sterculia setigera* | 38.49 | 27.81 | 27.81 | 36.6 |
| | *Combretum hartmannianum* | 2.21 | 8.24 | 8.24 | 6.87 |

*Sterculia setigera* shows marked temporal variability. In 2008, its estimated area ranges from (18.77–24.18%). It remains moderate in 2013 (15.01–20.63%), declines sharply in 2018 (3.33–8.51%), and then increases substantially in 2021 to (27.81–38.49%).

*Combretum hartmannianum* follows a different trajectory. It occupies (4.09–5.29%) in 2008, increases in 2013 to (8.65–13.03%), peaks in 2018 at (15.86–21.75%), and then declines sharply in 2021 to (2.21–8.24%). Minor and sparsely distributed species consistently occupy small proportions of the forest, generally below 6%, while bareland remains below 5% throughout the study period.

Overall, the results indicate substantial temporal shifts in species dominance and composition, characterized by a long-term decline in *Acacia seyal*, strong fluctuations in *S. setigera* and *Combretum hartmannianum*, and low but persistent representation of minor species.

These results indicate that the long-term decline in *Acacia seyal*, particularly by 2021, reflects a weakening of its previously dominant position in the ENFR. Although it remains one of the leading species overall, the reduction in area indicates substantial structural change in the forest. This likely reflects continued disturbance, shifts in competitive balance, and changing environmental conditions affecting canopy dominance. Similar structural changes have been reported in dryland forest systems under increasing ecological stress (Abuelbashar et al., 2022; Musa et al., 2024; Yasin et al., 2024).

The strong increase in *Sterculia setigera* in 2021 suggests possible competitive release or a successional response following the decline of *Acacia seyal*. In contrast, the rise and

subsequent decline of *Combretum hartmannianum* indicate that its distribution is sensitive to disturbance intensity, canopy structure, and habitat variability over time. Such temporal dynamics are consistent with the behavior of secondary species in heterogeneous dryland ecosystems (Smith et al., 2019; Mohammed et al., 2021a).

The consistently low proportion of bareland indicates that forest change is primarily driven by internal reorganization of species composition rather than large-scale conversion to non-vegetated land. At the same time, the recurrent overestimation of both dominant and rare species under ensemble classification confirms that algorithm choice strongly influences temporal interpretation. This supports broader remote-sensing evidence that classifier selection is a critical component of long-term ecological monitoring (Congalton & Green, 2019; Gorelick et al., 2017; Zhong et al., 2024).

Overall, these findings demonstrate that the ENFR has undergone substantial compositional restructuring between 2008 and 2021. They further show that multi-temporal species mapping in dryland forests requires careful algorithm selection to minimize bias and improve ecological interpretation.

## 4.6. Modeling and Prediction of the Current and Future Potential Distribution of *Acacia seyal* (Delile) under Climate Change Scenarios (Objective 5)

To understand the current and future spatial distribution of Acacia seyal under changing climatic conditions, a species distribution modeling approach was applied using the MaxEnt algorithm. This section presents the evaluation of model performance, the identification of key environmental drivers, and the spatial patterns of habitat suitability under both current and projected climate scenarios.

The analysis is structured to first assess model reliability, followed by the contribution of environmental variables, and then to examine the current distribution of suitable habitats. Subsequently, future projections under different emission scenarios (SSP2–4.5 and SSP5–8.5) are analyzed to identify potential shifts in species distribution. Finally, state-level assessments are provided to highlight regional differences in suitability and to support spatially explicit conservation and management strategies.

### 4.6.1. Model accuracy and prediction performance

The MaxEnt simulations demonstrate strong discriminatory performance, with mean AUC values of 0.950 for the training dataset and 0.944 for the evaluation dataset across ten replicated runs (Fig. 4.17). The model also achieves a mean True Skill Statistic (TSS) of 0.838 ± 0.02, indicating a high level of agreement between predicted suitability patterns and observed

occurrence records. These results confirm that the model reliably distinguishes suitable from unsuitable habitats, with performance well above the commonly accepted threshold of 0.7 for ecological niche models.

Model calibration is further supported by the close agreement between observed omission rates and those expected under cumulative threshold criteria, indicating that the model predictions are neither overfitted nor overly generalized. In addition, the low standard deviation across replicate runs demonstrates strong model stability and consistency, suggesting that the predictions are robust despite variability in training data partitioning.

Overall, the results indicate that MaxEnt effectively captures the ecological niche of *Acacia seyal* under both historical climatic conditions (1970–2000) and future climate scenarios (2021–2040 and 2081–2100) under SSP2–4.5 and SSP5–8.5.

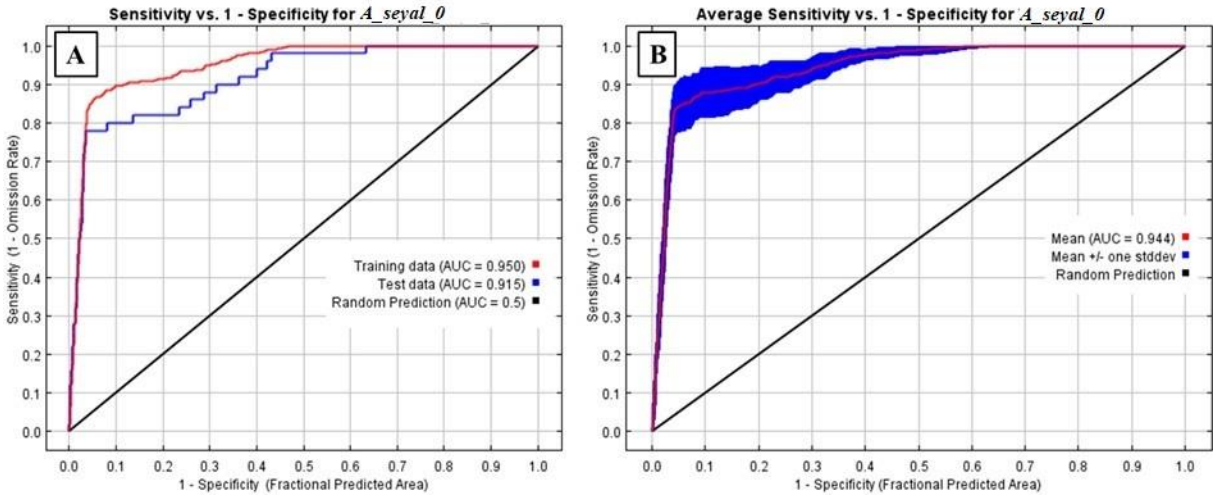


Fig. 4. 17. The AUC results from the MaxEnt model for Acacia seyal SDM in Sudan. (A) The red line represents model performance on training data, indicating how well the model fits the data it was trained on. The blue line represents performance on testing data, serving as the real test of the model's predictive power. (B) The average AUC per formance across multiple replicate runs, with the red line showing the mean AUC and the blue shaded area representing the standard deviation, reflecting model stability and reliability. The diagonal black line in both panels represents random prediction (AUC = 0.5).

These results are consistent with previous studies demonstrating the effectiveness of MaxEnt for presence-only species distribution modeling (Jiménez-Valverde, 2014; Elith et al., 2011; Merow et al., 2013; Phillips et al., 2017). Similar high AUC values have been reported for tree species in dryland and tropical environments, including *Acacia* species and other savanna trees, confirming the suitability of this approach for climate-driven habitat modeling (Tesfamariam et al., 2022; Hosseini et al., 2024; Montoya-Jimenez et al., 2022). Comparable

results have also been reported for species such as *Acacia Senegal* (Alhassan et al., 2024), *Tamarindus indica* (Gufi et al., 2023), and *Adansonia digitata* (Gadallah et al., 2025), further supporting the robustness and transferability of MaxEnt in predicting species distributions under changing climatic conditions.

The high predictive performance reflects the model's ability to represent complex, nonlinear relationships between species occurrence and environmental gradients, which is particularly important in heterogeneous dryland ecosystems (Elith et al., 2011; Merow et al., 2013). Although MaxEnt may yield slightly lower AUC values compared to presence–absence models for ecologically tolerant species, the performance observed in this study remains high and reliable (Phillips et al., 2006; Elith et al., 2006).

Overall, these findings confirm that the MaxEnt model provides a robust and scientifically sound basis for assessing the current and future potential distribution of *Acacia seyal* in the Blue Nile savanna under climate change scenarios.

#### 4.6.2. Key Environmental Variables Shaping *Acacia seyal* (Delile) Habitat Distribution

A total of nine environmental predictors were retained after applying the Variance Inflation Factor (VIF) screening procedure, ensuring minimal multicollinearity among variables. These include bio2, bio3, bio10, bio14, bio15, bio18, bio19, altitude, and soil characteristics. Their relative contributions and permutation importance values are presented in Table 4.18.

Table 4.18. Relative percent contribution and permutation importance of all environmental variables retained in the MaxEnt analysis, presented in order of decreasing contribution to model performance.

| Variable | Bioclimatic Description | Percent Contribution (%) | Permutation Importance (%) |
|---|---|---|---|
| bio3 | Isothermality (BIO2/BIO7 × 100) | 37.6 | 4.9 |
| bio18 | Precipitation of warmest quarter | 24.7 | 37.8 |
| bio15 | Precipitation seasonality | 14.2 | 24.2 |
| bio2 | Mean diurnal range | 11.1 | 0.8 |
| bio10 | Mean temperature of warmest quarter | 8.8 | 10.2 |
| Altitude | Elevation | 1.9 | 18.6 |
| Soil | Physical and chemical characteristics | 1.0 | 0.5 |
| bio19 | Precipitation of coldest quarter | 0.8 | 3.0 |
| bio14 | Precipitation of driest month | 0 | 0 |

Among all predictors, isothermality (bio3) emerges as the most influential variable, accounting for 37.6% of the total model contribution. This is followed by precipitation of the warmest quarter (bio18) and precipitation seasonality (bio15), contributing 24.7% and 14.2%,

respectively. Notably, bio18 also shows the highest permutation importance (37.8%), indicating a strong independent influence on model predictions. Although altitude contributes only 1.9% during model training, its relatively high permutation importance (18.6%) highlights its distinct role in shaping habitat suitability. The Jackknife test further confirms the importance of bio3, bio18, and bio15, as these variables produce the highest model gain when used independently (Fig. 4.18).

Overall, the results indicate that the distribution of *Acacia seyal* is primarily controlled by climatic variability, particularly temperature stability and water availability during the warmest period of the year.

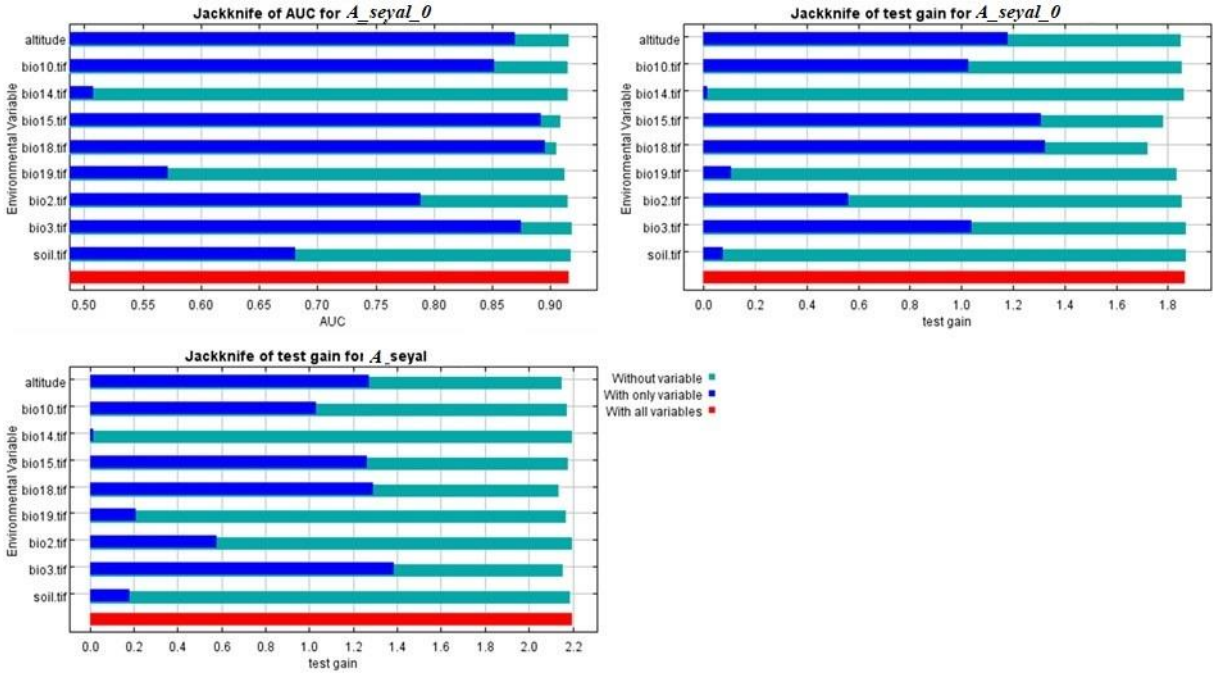


Fig. 4.18. The jackknife test for evaluating the relative importance of environmental variables for Acacia seyal distribution. The green bar represents the decrease in total gain when excluding that particular variable from the model. The blue bar illustrates the gain achieved by using only the variable in question, with all other variables excluded, and the red bar indicates the gain realized through the inclusion of all variables in the model.

These results indicate that the dominant role of isothermality (bio3) reflects strong sensitivity of the species to the balance between diurnal and annual temperature fluctuations, which directly influence physiological processes such as growth, transpiration, and survival. The strong influence of precipitation during the warmest quarter (bio18) highlights the importance of moisture availability during critical growth periods, particularly for seedling establishment and early development in dryland environments.

These findings are consistent with ecological studies indicating that *Acacia seyal* is well adapted to semi-arid and savanna ecosystems, where seasonal rainfall patterns and temperature variability strongly regulate species distribution (Ahanger et al., 2021; Acharya et al., 2025). Similar results have been reported in Ethiopia and other parts of East Africa, where precipitation availability plays a key role in regeneration and spatial distribution of *Acacia* species (Semu et al., 2021). Temperature-related variables also contribute significantly, as extreme variability can limit physiological performance and reproductive success (Elhassan et al., 2024).

Although altitude shows a relatively low contribution during model fitting, its high permutation importance suggests that it exerts an indirect but critical influence by modifying local climatic and edaphic conditions. Elevation affects temperature gradients, moisture availability, and soil properties, all of which are essential for species establishment and persistence (Acharya et al., 2025; Martínez-Villa et al., 2023). The strong performance of key variables in the Jackknife test further confirms their central role in determining habitat suitability, as model performance declines substantially when these variables are excluded.

Overall, these findings indicate that *Acacia seyal* distribution is governed by the interaction between temperature stability, seasonal precipitation, and topographic controls. This climatic sensitivity suggests that future changes in rainfall patterns and temperature regimes may significantly alter the spatial distribution of the species. Similar climate-driven distribution shifts have been reported for other African woody species, indicating potential range contraction or redistribution under future climate scenarios (Mtsetfwa et al., 2023; Moradi et al., 2025).

#### 4.6.3. Current potential habitat distribution of *Acacia seyal* in Sudan

The model predicts that approximately 20.22% of Sudan's total land area offers suitable habitat for *Acacia seyal* under current conditions. This area includes different suitability levels (unsuitable, low, medium, and high), with approximately 0.48% classified as high, 2.03% as medium, and 17.71% as low habitat suitability. The remaining 79.78% is currently considered unsuitable for *Acacia seyal* presence.

Further, the current distribution of baobab in Sudan varies significantly across the regions, with distinct patterns of habitat suitability. Northern and western, parts of Sudan show the largest areas classified as unsuit able, while the south and eastern regions show suitability with different degrees (Fig. 4.19).

Overall, the results indicate that suitable habitats for *Acacia seyal* are concentrated in the southern and eastern parts of Sudan, while large areas in the north and west remain environmentally unsuitable.

These results indicate that the distribution of *Acacia seyal* is strongly controlled by climatic gradients, particularly precipitation availability and temperature regimes. The concentration of suitable habitats in southern and eastern Sudan is consistent with the ecological requirements of the species, which prefers semi-arid to sub-humid environments with moderate rainfall and suitable soil conditions (Wickens, 1995; Siddig, 2014; Sankaran et al., 2005). Similar spatial patterns have been reported in dryland ecosystems, where vegetation distribution closely follows moisture availability and soil characteristics (D'Odorico & Bhattachan, 2012; Smith et al., 2019).

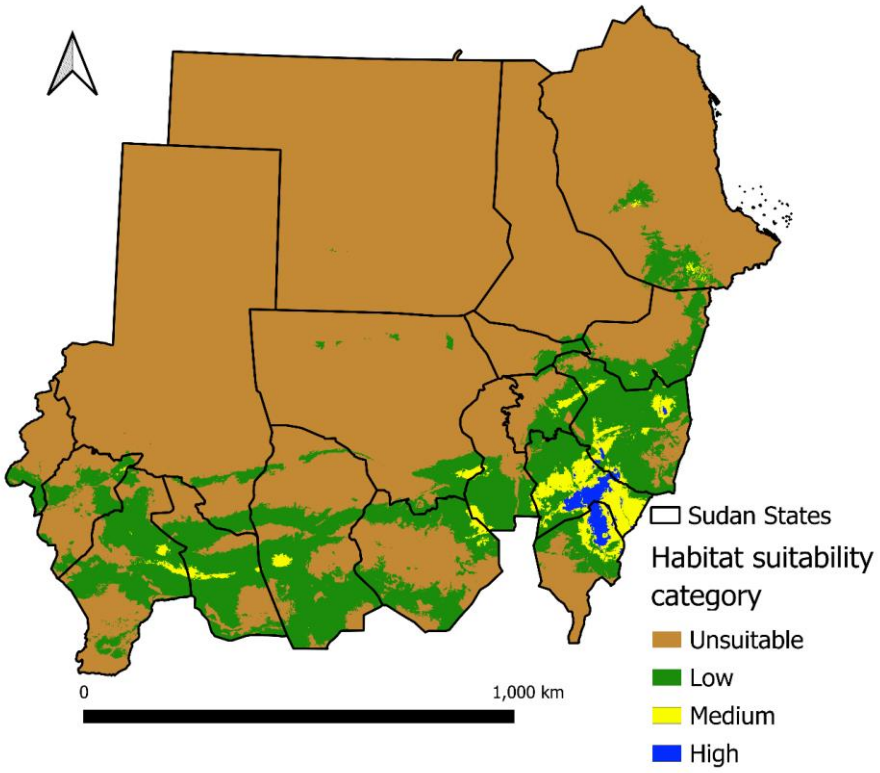


Fig. 4.19. Map showing the spatial distribution of potential current habitat suitability for Acacia seyal across Sudan, categorized by suitability degrees ranging from unsuitable to high.

The identification of southern and eastern regions as high- and medium-suitability zones suggests that these areas function as ecological strongholds for *Acacia seyal*. These zones likely support more stable populations and may serve as important reservoirs of genetic diversity and adaptive capacity under future climate change. Comparable patterns have been reported in other studies, where climatically favorable regions act as refugia for species persistence and adaptation (Aguirre-Liguori et al., 2021; Lawlor et al., 2024; Lyam et al., 2021).

From a management perspective, these high-suitability areas represent priority zones for conservation, restoration, and sustainable forest management. They offer strong potential for assisted natural regeneration, enrichment planting, and long-term ecosystem resilience. In

contrast, northern and western regions are largely unsuitable due to extreme aridity, high temperatures, and limited soil moisture, which constrain both natural regeneration and plantation success (Gamreldin & Hamadalnel, 2024).

Given these constraints, management strategies in marginal areas should focus on alternative approaches, including ex situ conservation, drought-resilient land-use systems, and diversified livelihood strategies. Such approaches are increasingly recommended under climate change scenarios, where species distributions are expected to shift and unsuitable areas may expand (IPCC, 2022; Sanchez et al., 2023; Mtsetfwa et al., 2023; Ahanger et al., 2021; Umuhoza et al., 2025).

Overall, these findings demonstrate that the current distribution of *Acacia seyal* is strongly climate-driven, with clear regional differentiation in habitat suitability. This provides a robust baseline for assessing future distribution changes and for guiding spatially targeted conservation and management interventions under changing environmental conditions.

#### 4.6.4. Predicted future habitat distribution

Future projections (Table 4.19; Fig. 4.20) reveal clear and consistent shifts in the potential distribution of *Acacia seyal* across Sudan under different climate change scenarios. Suitable habitat does not remain stable but fluctuates over time, reflecting both contraction and expansion driven by changing climatic conditions and species-specific ecological tolerance.

Table 4.19. Distribution of Acacia seyal habitat in Sudan under current and future projections with rates of change

| Time slice | Total suitable area (ha) | Total suitable area (%) | Unsuitable area (%) | Gain (%) | Loss (%) | Stable (%) |
|---|---|---|---|---|---|---|
| Current | 38,089063 | 20.22 | 79.78 | 0 | 0 | 20.22 |
| **SSP245_2021–2040** | 17,724019 | 9.41 | 78.33 | 1.45 | 12.26 | 7.96 |
| *Change Rate* | **-20,365044** | **-10.81** | **-1.45** | **1.45** | **12.26** | **-12.26** |
| **SSP245_2081–2100** | 25,548220 | 13.56 | 83.50 | 7.10 | 2.94 | 6.47 |
| *Change Rate* | **7,824201** | **4.15** | **5.17** | **5.64** | **-9.32** | **-1.49** |
| **SSP585_2021–2040** | 35,077569 | 18.62 | 77.21 | 2.57 | 4.17 | 16.05 |
| *Change Rate* | **-3,011494** | **-1.6** | **-2.57** | **2.57** | **4.17** | **-4.17** |
| **SSP585_2081–2100** | 30,692326 | 16.29 | 76.25 | 5.13 | 7.46 | 11.16 |
| *Change Rate* | **-4,385243** | **-2.33** | **-0.96** | **2.56** | **3.29** | **-4.89** |

Gain (areas newly becoming suitable in future scenarios); Loss (areas currently suitable that become unsuitable); Stable (areas remaining suitable across different time periods); Unsuitable (areas remaining unsuitable across current and future periods) Change rates are shown in italics, and their corresponding values are presented in bold.

Under the SSP2–4.5 scenario, suitable habitat declines markedly from 20.22% under current conditions to 9.41% during 2021–2040, representing a reduction of 10.81%. By the late century (2081–2100), suitable habitat partially recovers to 13.56%, indicating a gain of 4.15%

relative to mid-century conditions. Although some currently suitable areas become unsuitable (2.94%), gains (7.10%) suggest spatial redistribution rather than complete habitat loss.

Under the SSP5–8.5 scenario, a different trajectory is observed. During 2021–2040, suitable habitat decreases slightly to 18.62%, representing a modest decline of 1.6%, with gains (2.57%) partially offsetting losses (4.17%). However, by 2081–2100, suitable habitat declines further to 16.29%, with losses (7.46%) exceeding gains (5.13%), indicating increasing instability under prolonged warming.

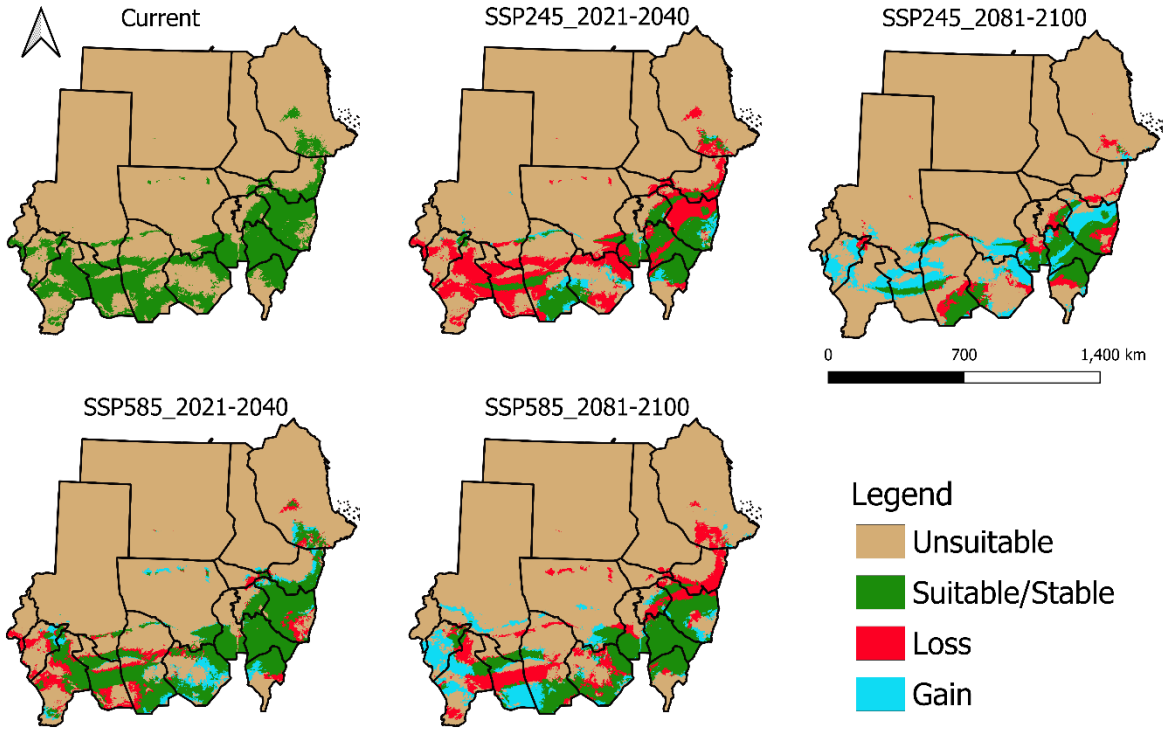


Fig. 4.20. Spatial patterns illustrating the directional trends of spatial distribution of habitat suitability for Acacia seyal under current and future climate scenarios in Sudan. The current map shows the present distribution of suitable vs. unsuitable habitats, while the future maps depict habitat change under different scenarios. Future suitability is categorized as: (i) stable (areas remaining suitable), (ii) lost (currently suitable areas projected to become unsuitable), (iii) gained (newly suitable areas not currently occupied), and (iv) unsuitable (persistently unsuitable areas).

Overall, the results demonstrate that suitable habitat for *Acacia seyal* is projected to decline in the near future, with partial recovery under moderate emission scenarios but continued reduction under high-emission pathways. The high turnover between habitat gains and losses highlights a shift toward spatial redistribution rather than uniform decline.

These results indicate that the projected changes are primarily driven by increasing climatic stress, particularly rising temperatures, drought intensity, and irregular rainfall patterns. Although *Acacia seyal* is adapted to semi-arid environments, its regeneration and survival depend strongly on moisture availability during critical growth periods (Ahanger et al., 2021; Elzaki et al., 2023). Increased temperature and evaporative demand can intensify water stress even when total precipitation remains relatively stable, thereby reducing recruitment and increasing mortality risk (Wan et al., 2021; D'Odorico & Bhattachan, 2012).

The contrasting responses between SSP2–4.5 and SSP5–8.5 highlight the role of climate extremes in shaping species distributions. Moderate warming may allow partial adaptation and expansion into newly suitable areas, whereas severe warming leads to habitat contraction and the exceeding of ecological tolerance thresholds (Mtsetfwa et al., 2023; Acharya et al., 2025). Similar redistribution patterns have been reported across African savanna systems, where climate-driven shifts alter species ranges and ecosystem structure (Semu et al., 2021; Patrut et al., 2018).

The observed balance between habitat gain and loss, particularly under SSP5–8.5, indicates high spatial turnover and instability. Such dynamics are commonly associated with increased mortality, reduced regeneration, and fragmentation of suitable habitats under extreme climatic stress (Sanchez et al., 2023; Zerbo et al., 2023; Atakpama et al., 2023). In addition, reduced landscape connectivity and genetic diversity may further increase vulnerability to climatic shocks (Sanchez et al., 2023).

Overall, these findings demonstrate that *Acacia seyal* may persist under moderate climate change scenarios but is likely to experience increasing vulnerability under high-emission pathways. These results highlight the importance of climate-informed management strategies, including conservation of suitable habitats, assisted regeneration, maintenance of genetic diversity, and preservation of landscape connectivity to support long-term ecosystem resilience (Semu et al., 2021; Sanchez et al., 2023; IPCC, 2022).

#### 4.6.5. State-Level Habitat Suitability of *Acacia seyal* under Current and Future Climates

Future projections (Figs. 4.21 and 4.22) reveal pronounced spatial variability and consistent redistribution patterns in the potential distribution of *Acacia seyal* across Sudan under current and future climatic conditions. Suitable habitats are not uniformly distributed but vary substantially across regions, reflecting both contraction and expansion driven by changing climatic conditions and species-specific ecological tolerance.

Under current climatic conditions, northern and hyper-arid regions are overwhelmingly dominated by unsuitable habitats. Northern State (36.8 Mha), North Darfur (31.5 Mha), and Red Sea State (20.2 Mha) remain largely inhospitable. In contrast, central and southeastern regions exhibit comparatively higher suitability. Blue Nile contains 1.2 Mha of low suitability, 588.7 Kha of medium suitability, and 392.6 Kha of high suitability. Similarly, Al Gedaref includes 4.7 Mha (low), 643.9 Kha (medium), and 86.4 Kha (high), while South Kordofan supports 3.4 Mha (low), 138.3 Kha (medium), and 795 ha (high). Sennar also shows notable suitability, with 2.1 Mha of low, 1.9 Mha of medium, and 536.8 Kha of high suitability. These patterns demonstrate a clear concentration of suitable habitats in southern and eastern Sudan.

Projected near-future conditions (2021–2040) indicate continued spatial redistribution while maintaining the north–south gradient. Under SSP2–4.5, unsuitable areas remain dominant. West Kordofan comprises 7.8 Mha of unsuitable land, 3.5 Mha of low suitability, and 73.8 Kha of medium suitability. Blue Nile maintains strong suitability (1.0 Mha low, 550.8 Kha medium, and 371.2 Kha high), while Al Gedaref shows moderate increases in medium suitability (245.6 Kha), and Sennar retains substantial medium (653.9 Kha) and high suitability (359.2 Kha). In contrast, North Kordofan, Kassala, and parts of Darfur exhibit reductions in medium and high suitability.

Under SSP5–8.5 for the same period, redistribution becomes more pronounced. Blue Nile remains relatively stable (420.1 Kha medium and 327.9 Kha high), while South Kordofan shows increases in medium (1.1 Mha) and high suitability (86.6 Kha). Kassala exhibits substantial gains (1.4 Mha medium and 440.6 Kha high), and River Nile shows emerging areas of suitability (365.5 Kha medium and 27.0 Kha high). Conversely, western regions, including Central Darfur and West Darfur, remain largely unsuitable, while Red Sea State is predominantly characterized by low suitability.

By the late century (2081–2100), these trends persist and intensify. Under SSP2–4.5, southeastern regions show further expansion, with Al Gedaref increasing to 582.1 Kha of medium and 121.2 Kha of high suitability, and Sennar reaching 1.5 Mha of medium and 979.9 Kha of high suitability. Blue Nile maintains consistent suitability (407.9 Kha medium and 328.3 Kha high). Under SSP5–8.5, Sennar contains 1.7 Mha of medium and 826.7 Kha of high suitability, while Blue Nile, Kassala, and South Kordofan maintain moderate suitability. Northern and western regions remain predominantly unsuitable across all scenarios.

Overall, the results indicate that the future distribution of *Acacia seyal* will be characterized by spatial redistribution toward southeastern and eastern Sudan rather than a

uniform decline. This pattern is supported by the high predictive performance of the MaxEnt model (mean AUC ≈ 0.94 ± 0.02), indicating strong model reliability.

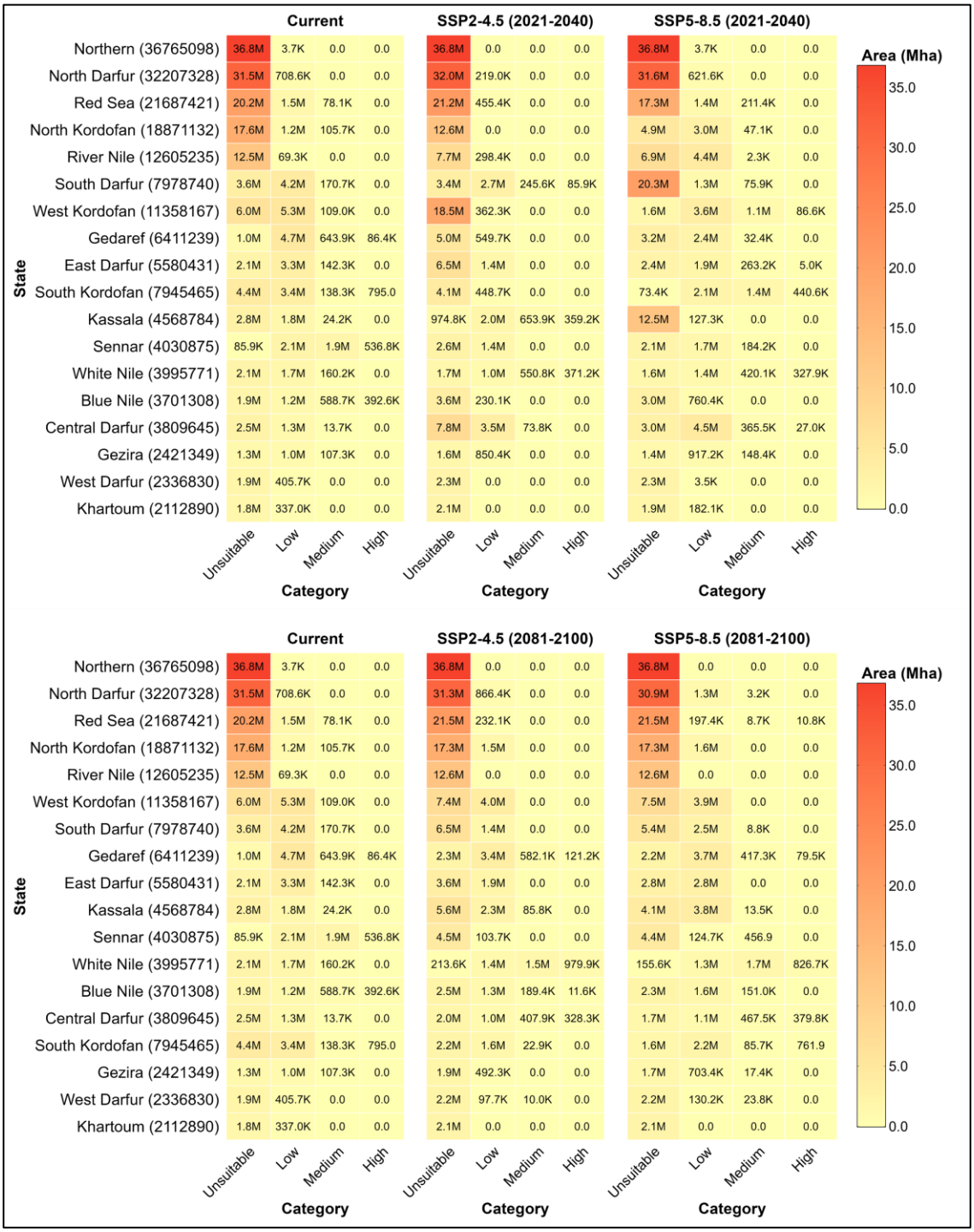


Fig. 4.21. Current and projected habitat suitability of Acacia seyal across Sudanese states under current climate and future scenarios SSP2-4.5 and SSP5-8.5. The figure categorizes areas into Unsuitable, Low, Medium, and High suitability classes based on area (ha). Colored gradients represent the magnitude of area in each category.

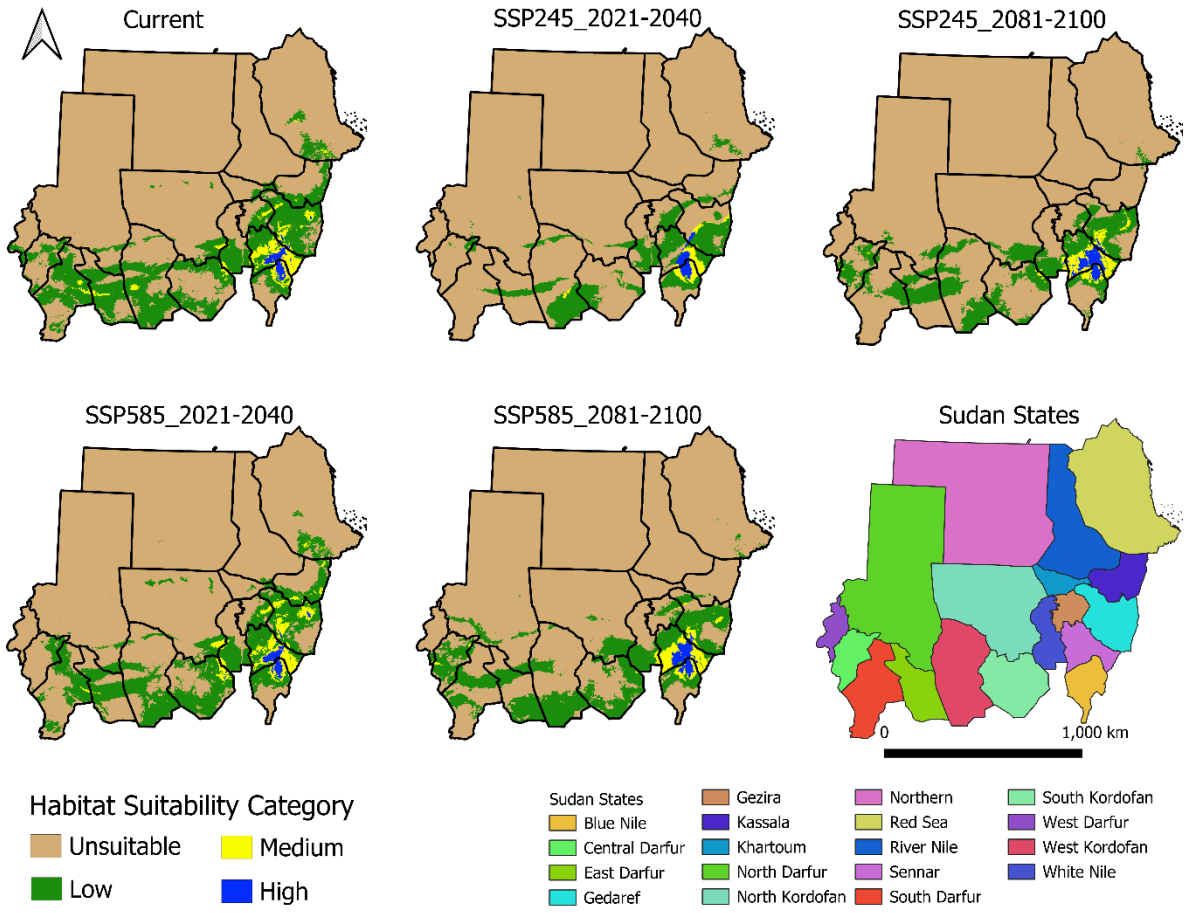


Fig. 4.22. Spatial distribution of Acacia seyal habitat suitability across Sudan states under current and future climate projections. State boundaries are over laid for regional reference, and suitability categories range from “unsuitable” to “high.”

These patterns are primarily driven by climatic gradients, particularly temperature regimes and moisture availability (Sankaran et al., 2005; Ahanger et al., 2021; Mtsetfwa et al., 2023). The dominant influence of isothermality (bio3) and precipitation of the warmest quarter (bio18) highlights the sensitivity of *Acacia seyal* to seasonal moisture balance and thermal stability. These variables regulate key physiological processes, including water-use efficiency, seedling establishment, and drought tolerance. Increasing aridity and thermal stress are therefore likely to constrain regeneration and survival, particularly in marginal environments (Atakpama et al., 2023).

The persistence of the north–south gradient reflects a broader ecohydrological transition across Sudan, where increasing temperature and evaporative demand intensify moisture deficits in northern and western regions, while southern and eastern areas retain relatively favorable conditions. Similar patterns have been reported across savanna ecosystems, where climate-

driven gradients strongly control species distribution and ecosystem structure (Semu et al., 2021; Patrut et al., 2018).

In addition to climatic drivers, land-use dynamics further influence these patterns. Regions such as Kassala and Central Darfur are affected by agricultural expansion, overgrazing, and deforestation, which amplify climate-induced stress and accelerate habitat degradation (Foden et al., 2007; Siddig, 2014; Yasin et al., 2025).

Despite the strong model performance, uncertainties remain, including limitations related to spatial resolution, the assumption of species–climate equilibrium in MaxEnt, and the exclusion of biotic interactions and future land-use changes. These factors may influence the accuracy of projected distributions.

Overall, these findings demonstrate that *Acacia seyal* is likely to persist in climatically favorable regions of southeastern and eastern Sudan but may experience increasing vulnerability in marginal environments under future climate change. This highlights the importance of climate-informed management strategies, including conservation of suitable habitats, restoration of degraded areas, and the maintenance of ecosystem resilience.

# 5. CONCLUSION AND RECOMMENDATIONS

This study demonstrates that the Elnour Natural Forest Reserve (ENFR) is undergoing significant long-term ecological degradation, primarily driven by anthropogenic activities, including illegal tree cutting, charcoal production, and overgrazing. Despite ongoing recruitment, the ecosystem has experienced substantial declines in species richness, structural complexity, and regeneration capacity, accompanied by a marked reduction in dense forest and the expansion of semi-bareland as the dominant land-cover class.

Machine learning analysis confirmed that Random Forest (RF) and Support Vector Machine (SVM) provide the most reliable approaches for mapping dominant tree species in heterogeneous savanna environments. In addition, species distribution modeling of *Acacia seyal* indicates future contraction and spatial redistribution of suitable habitats under changing climatic conditions.

Overall, these findings highlight the urgent need for integrated, climate-informed conservation and restoration strategies that combine improved governance, sustainable resource use, and adaptive ecosystem management. The results provide a robust scientific basis to support policymakers, conservation agencies, and local stakeholders in prioritizing targeted interventions to enhance forest resilience and biodiversity conservation in Sudan's dryland ecosystems.

## 5.1. Conclusion

This study provides a comprehensive and integrated assessment of climate variability, land-use/land-cover (LULC) dynamics, forest structure, biodiversity change, and species distribution in the Elnour Natural Forest Reserve (ENFR). By combining remote sensing, field inventory data, socio-economic analysis, machine learning, and species distribution modeling, the research establishes a robust, multi-dimensional framework for understanding the processes driving forest degradation and climate vulnerability in Sudan's dryland savanna ecosystems.

The climate analysis reveals a clear warming trend, primarily driven by increasing minimum temperatures, accompanied by rising rainfall variability, prolonged dry spells, and more frequent hot–humid extremes. Although total precipitation shows a modest recovery in recent decades, moisture stress has intensified due to uneven rainfall distribution and increased evaporative demand. These findings demonstrate that drought dynamics in the Blue Nile savanna are increasingly governed by rainfall variability and temperature-driven processes rather than total precipitation alone.

LULC analysis indicates substantial and persistent landscape transformation between 1995 and 2021. Dense and light forest classes declined markedly, while semi-bareland expanded to become the dominant land-cover class. Transition analysis confirms that semi-bareland represents a major degradation pathway and a relatively stable endpoint, reflecting progressive fragmentation and structural simplification of the ecosystem. Although localized recovery in light forest is observed, it remains unstable and insufficient to compensate for the continuous loss of dense forest.

The results clearly identify anthropogenic activities as the primary drivers of degradation. Illegal tree cutting and charcoal production account for approximately 35% of total pressure, followed by overgrazing (25%), governance limitations (15%), and socio-economic factors (18%). Environmental stressors, including prolonged dry seasons and climate variability, act primarily as amplifying factors rather than initiating drivers.

Field-based vegetation analysis demonstrates substantial ecological decline. Species richness decreased from 35 to 18 species, accompanied by significant reductions in abundance, basal area, and regeneration capacity. Many species exhibit poor or absent regeneration, indicating a high risk of local extinction under continued disturbance. The observed shift toward disturbance-tolerant species reflects declining ecosystem resilience and functional integrity.

Structural analysis further reveals persistent simplification of forest architecture. Diameter and height distributions are increasingly dominated by smaller size classes, while large trees have declined significantly. Although recruitment persists, selective removal of mature trees prevents canopy recovery, limits biomass accumulation, and reduces ecosystem stability, resulting in long-term structural degradation.

Machine learning analysis demonstrates that Random Forest (RF) and Support Vector Machine (SVM) provide the most accurate and stable approaches for mapping dominant tree species in heterogeneous dryland environments. Multi-temporal analysis reveals a shift in species dominance, with *Acacia seyal* declining and secondary species such as *Sterculia setigera* increasing in relative importance, indicating ecological restructuring driven by disturbance and environmental change.

Species distribution modeling further highlights the strong climatic sensitivity of *Acacia seyal*, particularly to isothermality and precipitation of the warmest quarter. Future projections indicate contraction and spatial redistribution of suitable habitats under climate change scenarios. Southern and eastern regions, including Blue Nile, Gedaref, Sennar, and West Kordofan, are identified as potential climate refugia, while northern and western regions remain largely unsuitable due to extreme aridity.

Overall, the ENFR is undergoing a transition toward a degraded, structurally simplified, and less resilient ecosystem. This transformation is primarily driven by anthropogenic pressures, reinforced by climate variability and warming-induced moisture stress. The combined effects of forest loss, biodiversity decline, structural simplification, and climate-driven habitat shifts underscore the urgency of implementing integrated, climate-adaptive management strategies.

This study advances the understanding of dryland forest dynamics by demonstrating that ecosystem degradation in Sudanese savannas is primarily driven by anthropogenic pressures, with climate variability acting as a secondary but amplifying factor. It further provides a novel, integrated methodological framework that combines remote sensing, field data, machine learning, and species distribution modeling to assess ecosystem change in data-scarce dryland environments. In addition, the study offers new insights into the climate sensitivity and future redistribution of *Acacia seyal*, identifying potential refugia and areas of vulnerability under different climate scenarios.

These contributions provide both a scientific and practical foundation for improving the monitoring, management, and conservation of dryland forest ecosystems under ongoing and future climate change.

### 5.2. Recommendations

Based on the findings of this study, the following recommendations are proposed:

1. Enhance climate and drought monitoring: Improve projections using high-resolution regional climate models (RCMs) and incorporate indicators such as soil moisture, evapotranspiration, and heatwave frequency.
2. Establish long-term ecological monitoring systems: Develop permanent sample plots to monitor vegetation structure, species composition, regeneration, and mortality.
3. Integrate socio-economic drivers into management frameworks: Incorporate livelihood analysis and resource-use assessments to design context-specific interventions.
4. Improve species mapping and monitoring accuracy: Integrate multi-sensor remote sensing data (LiDAR, SAR, hyperspectral, UAV) with advanced machine learning and deep learning approaches.
5. Support eco-physiological and genetic research: Investigate drought tolerance and adaptive capacity of key species, particularly *Acacia seyal*.
6. Incorporate disturbance dynamics into modeling frameworks: Include grazing, fire regimes, land-use change, and fragmentation in predictive models.

7. Implement targeted restoration and conservation strategies: Prioritize climatically suitable regions such as Blue Nile, Gedaref, Sennar, and West Kordofan using assisted natural regeneration and climate-adaptive approaches.
8. Develop integrated monitoring and decision-support systems: Establish platforms combining remote sensing, field data, and socio-economic information for real-time monitoring and policy support.

Priority should be given to strengthening climate monitoring, improving governance and socio-economic integration, and establishing long-term ecological monitoring systems, as these form the foundation for effective restoration and sustainable management of dryland forest ecosystems.

## 6. SUMMARY

Savanna ecosystems in Sudan are undergoing rapid transformation under the combined influence of climate variability and intensified anthropogenic pressures, resulting in land degradation, biodiversity loss, and declining ecosystem resilience. This thesis provides a comprehensive and integrated assessment of these interacting drivers by explicitly linking climatic trends, land-use dynamics, vegetation structure, and species-level responses, with a particular focus on the Elnour Natural Forest Reserve (ENFR) and the ecological dynamics of *Acacia seyal* as a representative keystone species.

The primary aim of this research was to understand and predict the impacts of climate change and human disturbance on savanna ecosystems using an integrated geospatial and ecological modeling framework. Specifically, the study (i) quantified long-term climatic variability and drought dynamics; (ii) analyzed spatio-temporal land use/land cover (LULC) changes and their interaction with climate; (iii) assessed changes in woody species composition, diversity, and regeneration; (iv) mapped dominant tree species using multi-source remote sensing and machine learning approaches; and (v) modeled current and future habitat suitability of *Acacia seyal* under different climate change scenarios.

To achieve these objectives, a multidisciplinary framework was developed, integrating long-term climate datasets, multi-temporal satellite imagery, field-based ecological surveys, machine learning classification, and species distribution modeling. This integrated approach represents a key contribution of the thesis, enabling a consistent and spatially explicit evaluation of climate, land-use, and ecological processes in a data-scarce dryland environment.

The results reveal a clear and statistically significant warming trend, primarily driven by increasing minimum temperatures, alongside rising rainfall variability and more frequent

and persistent droughts. Despite a modest increase in total precipitation, moisture stress has intensified due to increased evaporative demand and irregular rainfall distribution, indicating a shift toward temperature-driven drought dynamics.

LULC analysis demonstrates substantial landscape transformation between 1995 and 2021, characterized by continuous forest decline and expansion of semi-bareland as the dominant land-cover class. Transition analysis identifies semi-bareland as a persistent degradation pathway and ecological endpoint, reflecting progressive fragmentation and structural simplification. Anthropogenic activities, particularly illegal logging and charcoal production (~35%) and overgrazing (~25%), were identified as the primary drivers, while climatic variability acts as a secondary amplifier of degradation.

Field-based ecological analysis reveals severe ecosystem deterioration, with species richness declining from 35 to 18 species, accompanied by sharp reductions in density, basal area, and regeneration capacity. Many species exhibit poor or absent regeneration, indicating a high risk of local extinction. Structural analysis further shows dominance of smaller diameter classes and a significant decline in mature trees, confirming persistent structural simplification and reduced ecosystem stability.

Machine learning analysis demonstrates that Random Forest (RF) and Support Vector Machine (SVM) provide the most accurate and stable approaches for mapping dominant tree species in heterogeneous dryland environments. Multi-temporal mapping reveals a clear ecological shift, with declining dominance of *Acacia seyal* and increasing importance of disturbance-tolerant species such as *Sterculia setigera*, indicating ongoing ecosystem restructuring under combined anthropogenic and climatic pressures.

Species distribution modeling using MaxEnt shows high predictive performance (AUC $\approx$ 0.94) and identifies isothermality and precipitation of the warmest quarter as key environmental drivers. Future projections indicate contraction and spatial redistribution of suitable habitats under climate change, particularly under SSP5–8.5. Southern and eastern regions, including Blue Nile, Gedaref, Sennar, and West Kordofan, are identified as potential climate refugia, while northern and western regions remain largely unsuitable.

Overall, this thesis demonstrates that Sudanese savanna ecosystems are transitioning toward a degraded, structurally simplified, and less resilient state, driven primarily by anthropogenic pressures and reinforced by climate variability and warming-induced moisture stress. The study makes a significant contribution by developing an integrated, multi-scale framework that links climate dynamics, land-use change, ecological degradation, and species

distribution, providing robust, spatially explicit evidence to support climate-informed management, conservation planning, and adaptation strategies in dryland ecosystems.

## 7. NEW SCIENTIFIC RESULTS

This dissertation presents original scientific contributions to understanding land degradation processes, biodiversity dynamics, forest structural change, and climate-driven species distribution in Sudanese savanna ecosystems. These findings are derived from an integrated multi-scale framework combining climate analysis, remote sensing, field observations, and modeling approaches, and are summarized as follows:

### 7.1. Climate–Drought Mechanism

I demonstrate that drought dynamics in Sudanese savannas are primarily driven by increasing temperature and rainfall variability rather than by total precipitation alone. I quantify how rising temperatures enhance evaporative demand, intensifying moisture stress even under stable or slightly increasing rainfall. This provides region-specific empirical evidence that drought processes are increasingly temperature-driven and establishes the climatic mechanism underlying the observed patterns of vegetation degradation and ecosystem change.

### 7.2. Semi-Bareland as a Degradation Pathway

I demonstrate that semi-bareland has become the dominant and persistent land-use/land-cover class in Elnour Natural Forest Reserve (ENFR) between 1995 and 2021. I establish that it is not a transitional stage but a stable and self-reinforcing degradation endpoint, representing a terminal pathway of forest degradation in dryland ecosystems.

### 7.3. Drivers of Forest Degradation

I establish that anthropogenic activities are the primary drivers of forest degradation in ENFR. Illegal logging and charcoal production account for approximately 35% of degradation, followed by overgrazing (25%) and other socio-economic drivers, while climatic factors act primarily as secondary amplifiers.

### 7.4. Biodiversity Loss and Regeneration Failure

I demonstrate a substantial decline in woody species richness from 35 to 18 species between 2008 and 2021, accompanied by widespread regeneration failure and the absence of successful recruitment in several species. This establishes regeneration collapse as a key mechanism driving biodiversity loss and reduced ecosystem resilience.

### 7.5. Structural Simplification of Forests

I demonstrate that forest structure is increasingly dominated by small diameter classes (exceeding 43%), while large trees (below 12%) have declined significantly. I show that selective removal of mature trees disrupts cohort development and prevents canopy recovery despite ongoing recruitment, revealing a decoupling between regeneration and structural recovery as a key driver of persistent forest degradation.

### 7.6. Machine Learning Robustness in Species Mapping

I demonstrate that, under heterogeneous dryland conditions characterized by class imbalance and multi-temporal multi-sensor data, Random Forest (RF) and Support Vector Machine (SVM) provide more robust and consistent species-level classification performance (85–96%) than CART and unweighted ensemble approaches. This establishes that reliable species mapping in Sudanese savanna ecosystems depends critically on algorithm robustness to minority classes and landscape heterogeneity, rather than on overall accuracy alone.

### 7.7. Climate-Driven Redistribution of *Acacia seyal*

I demonstrate that the distribution of *Acacia seyal* is primarily controlled by isothermality and precipitation during the warmest quarter. I further show that climate change will drive habitat contraction in northern regions and expansion in southern and eastern regions, identifying these areas as climate refugia that are critical for conservation and climate adaptation planning.

**ACKNOWLEDGMENTS**

I would like to express my sincere and profound gratitude to my supervisor, Prof. Dr.. Kornel Czimber, for his outstanding academic guidance, continuous support, and invaluable expertise throughout the course of my doctoral studies. His constructive feedback, professional dedication, and ethical commitment have been essential to the successful completion of this research.

This doctoral work was made possible through the financial support provided by the Tempus Public Foundation, Hungary, and the Ministry of Higher Education, Sudan, whose scholarships enabled me to pursue and accomplish my PhD studies.

I am especially grateful to Dr. Hytham Hashim Gibreel for providing the time-series survey data (2008–2021), which constituted a critical component of this research. I also extend my sincere appreciation to Dr. Ahmed A. H. Siddig for his valuable academic advice, insightful discussions, and continuous encouragement.

Furthermore, I would like to acknowledge Dr. Milan Koren for hosting me during my study mobility supported by the Pannonia Scholarship in June 2025 at the Department of Forest Resources Planning and Informatics, Technical University in Zvolen, Slovakia, and for his professional guidance and support during that period.

My gratitude is also extended to my colleagues and the staff of the Institute of Geomatics and Civil Engineering, University of Sopron, for providing a supportive academic environment and encouragement throughout my study period.

Above all, I owe my deepest gratitude to my wife and my family for their unwavering moral and financial support, patience, and encouragement during the entire doctoral journey.

Finally, I would like to express my sincere thanks to all individuals who contributed to this research in any way but could not be mentioned personally. Their assistance is greatly appreciated.

## REFERENCES


Abbasnezhad, B., Abrams, J. B., & Hepinstall-Cymerman, J. (2023). Incorporating Social and policy drivers into land-use and land-cover projection. *Sustainability*, *15*(19), 14270.

Abdelrahim, M. (2015). Contribution of non-wood forest products in support of livelihoods of rural people living in the area south of Blue Nile State, Sudan. *International Journal of Agriculture, Forestry and Fisheries, 3*(5), 189–194.

Abdou, L., Morou, B., Abasse, T., & Mahamane, A. (2016). Analysis of the structure and diversity of Prosopis africana (G. et Perr.) Taub. tree stands in the southeastern Niger. *Journal of Plant Studies; 5*(1) 58. https://doi.org/10.5539/jps.v5n1p58

Abdullahi, I. N. (2021). Parkland trees under severe drought: An assessment of species diversity and abundance across three agroecological zones of Northern Nigeria. *Open Journal of Forestry*, *11*(2), 117-134. https://doi.org/10.4236/ojf.2021.112009

Abuelbashar, A. I., Ahmed, D. A. M. D. A., Siddig, A. A. H., Yagoub, Y. E., & Gibreel, H. H. (2022). Analysis of Composition and Diversity of Natural Regeneration of Woody Species in Jebel El Gerrie Dry Land Forest East of Blue Nile State, Sudan. *Journal of forest and environmental science*, *38*(2), 90-101. https://doi.org/10.7747/JFES.2022.38.2.90

Acharya, S., Joshi, R., Maraseni, T. N., & Bhattarai, P. (2025). Unraveling Elevation-Driven Variations in Forest Structure and Composition in Western Nepal. *Diversity*, *17*(8), 588. https://doi.org/10.3390/d17080588

Adane, A., & Asmerom, B. (2025). Analysis of spatiotemporal distribution, variability, and trends of rainfall in Wollo area, Northeastern Ethiopia. *PloS one*, *20*(1), e0312889. https://doi.org/10.1371/journal.pone.0312889

Adekunle, V. A. J., & Olagoke, A. O. (2008). Diversity and biovolume of tree species in natural forest ecosystem in the bitumen-producing area of ondo state, Nigeria: a baseline study. *Biodiversity and Conservation*, *17*(11), 2735-2755. https://doi.org/10.1007/s10531-007-9279-y

Adekunle, V. A. J., & Olagoke, A. O. (2013). Tree species diversity and structure of a Nigerian strict nature reserve. *Tropical Ecology*, *54*(3), 275-289.

Aguirre-Liguori, J. A., Ramírez-Barahona, S., & Gaut, B. S. (2021). The evolutionary genomics of species' responses to climate change. *Nature Ecology & Evolution*, *5*(10), 1350-1360. https://doi.org/10.1038/s41559-021-01526-9

Agustino, S., Mataya, B., Senelwa, K., & Achigan-Dako, E. G. (2011). Non-wood forest products and services for socio-economic development. In *A compendium for technical and professional forestry education. The African Forest Forum, Nairobi, Kenya* (219). https://www.researchgate.net/publication/233399241.

Ahanger, M. A., Siddique, K. H., & Ahmad, P. (2021). Understanding drought tolerance in plants. *Physiologia Plantarum*, *172*(2), 286-288. https://doi.org/10.1111/ppl.13442

Aigbe, H. I., Akindele, S. O., & Onyekwelu, J. C. (2014). Tree species diversity and density pattern in Afi River Forest Reserve, Nigeria. *International Journal of Scientific and Technology Research*, *3*(10), 178-185. https://doi.org/10.5296/jas.v3i1.6461

Ali, Y. A., Awwad, E. M., Al-Razgan, M., & Maarouf, A. (2023). Hyperparameter search for machine learning algorithms for optimizing the computational complexity. *Processes*, *11*(2), 349. https://doi.org/10.3390/pr11020349

Alriah, M. A. A., Bi, S., Nkunzimana, A., Elameen, A. M., Sarfo, I., & Ayugi, B. (2022). Multiple gridded-based precipitation products' performance in Sudan's different topographical

features and the influence of the Atlantic Multidecadal Oscillation on rainfall variability in recent decades. *International Journal of Climatology*, *42*(16), 9539-9566. https://doi.org/10.1002/joc.7700

Alriah, M. A. A., Bi, S., Shahid, S., Nkunzimana, A., Ayugi, B., Ali, A., ... & Elameen, A. M. (2021). Summer monsoon rainfall variations and its association with atmospheric circulations over Sudan. *Journal of Atmospheric and Solar-Terrestrial Physics*, *225*, 105751. https://doi.org/10.1016/j.jastp.2021.105751

Ana, J. (2013). *Changes in long term variability of the rains of Sudan* (Ph.D. Thesis). University of Reading.

Anand, V., & Oinam, B. (2020). Future land use land cover prediction with special emphasis on urbanization and wetlands. *Remote Sensing Letters*, *11*(3), 225-234. https://doi.org/10.1080/2150704X.2019.1704304

Arfat, Y. (2010). Land use/land cover change detection and quantification: A case study in Eastern Sudan. Lund University, Department of Physical Geography, Seminar Paper Series; University of Lund: Lund, Sweden. https://lup.lub.lu.se/luur/download?func=downloadFile&recordOId=2255865&fileOId=2256453

Asaye, T. S., Amare, Z. Y., & Abebe, M. G. (2025). Spatio-temporal analysis of rainfall variability and seasonality over Tekeze River Basin, Ethiopia. *Geocarto International*, *40*(1), 2537382. https://doi.org/10.1080/10106049.2025.2537382

Asbeck, T., Großmann, J., Paillet, Y., Winiger, N., & Bauhus, J. (2021). The use of tree-related microhabitats as forest biodiversity indicators and to guide integrated forest management. *Current Forestry Reports*, *7*(1), 59-68. https://doi.org/10.1007/s40725-020-00132-5

Assogbadjo, A. E., Kakaï, R. L. G., Sinsin, B., & Pelz, D. (2010). Structure of Anogeissus leiocarpa Guill., Perr. natural stands in relation to anthropogenic pressure within Wari-Maro Forest Reserve in Benin. *African Journal of Ecology*, *48*(3), 644-653. https://doi.org/10.1111/j.1365-2028.2009.01160.x

Atakpama, W., Gouwakinnou, G. N., Dimobe, K., Batawila, K., Natta, A. K., & Akpagana, K. (2023). Habitat suitability of subpopulations of Adansonia digitata L. in West Africa: Implications for conservation and domestication. *Trees, Forests and People*, *12*, 100397. https://doi.org/10.1016/j.tfp.2023.100397

Atique, L., Mahmood, I., & Atique, F. (2014). Disturbances in atmospheric radiative balance due to anthropogenic activities and its implications for climate change. *American-Eurasian Journal of Agricultural & Environmental Sciences, 14*, 73–84.

Axelsson, A., Lindberg, E., Reese, H., & Olsson, H. (2021). Tree species classification using Sentinel-2 imagery and Bayesian inference. *International Journal of Applied Earth Observation and Geoinformation*, *100*, 102318. https://doi.org/10.1016/j.jag.2021.102318

Ayele, A., Seid, A., Mekonnen, A. B., Wassie, W. A., Yemata, G., Yihune, E., ... & Shimeles, L. (2024). Woody species diversity, structure and regeneration status of the church forests in West Gojjam Zone, Northwestern Ethiopia. *Trees, Forests and People*, *16*, 100570. https://doi.org/10.1016/j.tfp.2024.100570

Babatolu, J. S., & Akinnubi, R. T. (2013). Surface temperature anomalies in the river Niger basin development authority areas, Nigeria. *Atmospheric and Climate Sciences, 3*(4), 532-537. https://doi.org/10.4236/acs.2013.34056

Babiker, W., Tan, G., Alriah, M. A. A., & Elameen, A. M. (2024). Evaluation and correction analysis of the regional rainfall simulation by CMIP6 over Sudan. *Geographica Pannonica, 28*, 53–70. https://doi.org/10.5937/gp28-46565

Barnieh, B. A., Jia, L., Menenti, M., Zhou, J., & Zeng, Y. (2020). Mapping land use land cover transitions at different spatiotemporal scales in West Africa. *Sustainability*, *12*(20), 8565. https://doi.org/10.3390/su12208565

Basse, R. M., Omrani, H., Charif, O., Gerber, P., & Bódis, K. (2014). Land use changes modelling using advanced methods: Cellular automata and artificial neural networks. The spatial and explicit representation of land cover dynamics at the cross-border region scale. *Applied Geography*, *53*, 160-171. https://doi.org/10.1016/j.apgeog.2014.06.016

Batjes, N. H. (2016). Harmonized soil property values for broad-scale modelling (WISE30sec) with estimates of global soil carbon stocks. Geoderma 269:61–68. https://doi.org/10.1016/j.geoderma.2016.01.034

Beguería, S., Vicente-Serrano, S. M., Reig, F., & Latorre, B. (2014). Standardized Precipitation Evapotranspiration Index (SPEI) revisited: Parameter fitting, evapotranspiration models, tools, datasets and drought monitoring. *International Journal of Climatology*, **34**(10), 3001–3023. https://doi.org/10.1002/joc.3887

Belgiu, M., & Drăguţ, L. (2016). Random forest in remote sensing: A review of applications and future directions. *ISPRS journal of photogrammetry and remote sensing*, *114*, 24-31. https://doi.org/10.1016/j.isprsjprs.2016.01.011

Bentz, B. J., Millar, C. I., Vandygriff, J. C., & Hansen, E. M. (2022). Great Basin bristlecone pine mortality: Causal factors and management implications. *Forest Ecology and Management*, *509*, 120099. https://doi.org/10.1016/j.foreco.2022.120099

Berry, L. B. (2015). *Sudan: A country study* (5th ed.). Library of Congress, Washington D.C., USA.

Beyene, T., Lettenmaier, D. P., & Kabat, P. (2010). Hydrologic impacts of climate change on the Nile River Basin: implications of the 2007 IPCC scenarios. *Climatic change*, *100*(3), 433-461. https://doi.org/10.1007/s10584-009-9693-0

Bhandari, A. (2020). What is multicollinearity? Understand causes, effects and detection using VIF. In *Analytics Vidhya*. https://www.analyticsvidhya.com/blog/2020/03/what-is-multicollinearity/. (Accessed date: 15.01.2026).

Biro, K., Pradhan, B., Buchroithner, M., & Makeschin, F. (2013). Land use/land cover change analysis and its impact on soil properties in the northern part of Gadarif region, Sudan. *Land Degradation & Development*, *24*(1), 90-102. https://doi.org/10.1002/ldr.1116

Bishop, C. M., & Nasrabadi, N. M. (2006). *Pattern recognition and Machine Learning*. Springer New York, NY, 4(4), p. 738.

Bourgoin, C., Ceccherini, G., Girardello, M., Vancutsem, C., Avitabile, V., Beck, P. S. A., ... & Achard, F. (2024). Human degradation of tropical moist forests is greater than previously estimated. *Nature*, *631*(8021), 570-576. https://doi.org/10.1038/s41586-024-07629-0

Breiman, L. (2001). Random forests. Machine Learning. *Springer Nature*, *45*(1), 5–32. https://doi.org/10.1023/A:1010933404324

Breiman, L., Friedman, J., Olshen, R.A., & Stone, C.J. (1984). Classification and Regression Trees (1st ed.). Chapman and Hall/CRC. https://doi.org/10.1201/9781315139470

Canham, C. D., & Murphy, L. (2016). The demography of tree species response to climate: seedling recruitment and survival. *Ecosphere*, *7*(8), e01424. https://doi.org/10.1002/ECS2.1424

Chaturvedi, R. K., Pandey, S. K., Tripathi, A., Goparaju, L., Raghubanshi, A. S., & Singh, J. S. (2024). Variations in the plasticity of functional traits indicate the differential impacts of

abiotic and biotic factors on the structure and growth of trees in tropical dry forest fragments. *Frontiers in Plant Science*, *14*, 1181293. https://doi.org/10.3389/fpls.2023.1181293

Chepkoech, E. K., Agevi, H., Lung'ayia, H., & Tsingalia, H. M. (2024). Woody Species Composition, Stand Structure and Regeneration Status of Londiani Forest in Kenya. *Forests*, *15*(4), 653. https://doi.org/10.3390/f15040653

Chung, L. C. H., Xie, J., & Ren, C. (2021). Improved Machine Learning mapping of local climate zones in metropolitan areas using composite Earth observation data in Google Earth Engine. *Building and environment*, *199*, 107879. https://doi.org/10.1016/j.buildenv.2021.107879

Coleine, C., Delgado-Baquerizo, M., DiRuggiero, J., Guirado, E., Harfouche, A. L., Perez-Fernandez, C., ... & Egidi, E. (2024). Dryland microbiomes reveal community adaptations to desertification and climate change. *The ISME journal*, *18*(1), wrae056. https://doi.org/10.1093/ismejo/wrae056

Colwell, R. K., Brehm, G., Cardelús, C. L., Gilman, A. C., & Longino, J. T. (2008). Global warming, elevational range shifts, and lowland biotic attrition in the wet tropics. *science*, *322*(5899), 258-261. https://doi.org/10.1126/science.1162547

Congalton, R. G., & Green, K. (2019). *Assessing the accuracy of remotely sensed data: principles and practices (3rded)*. CRC press.

Conway, D. (2000). The climate and hydrology of the upper Blue Nile River. *Geographical Journal, 166*, 49–62. https://doi.org/10.1111/j.1475-4959.2000.tb00006.x

Cortes, C., & Vapnik, V. (1995). Support-vector networks. *Machine Learning*, *20*(3), 273-297. https://doi.org/10.1023/A:1022627411411

Crockett, J. L., & Hurteau, M. D. (2024). Ability of seedlings to survive heat and drought portends future demographic challenges for five southwestern US conifers. *Tree Physiology*, *44*(1), tpad136. https://doi.org/10.1093/treephys/tpad136

Cueva-Ortiz, J., Espinosa, C. I., Aguirre-Mendoza, Z., Gusmán-Montalván, E., Weber, M., & Hildebrandt, P. (2020). Natural regeneration in the Tumbesian dry forest: identification of the drivers affecting abundance and diversity. *Scientific reports*, *10*(1), 9786. https://doi.org/10.1038/s41598-020-66743-x

Dafalla, M. S., Abdel-Rahman, E. M., Siddig, K. H., Ibrahim, I. S., & Csaplovics, E. (2014). Land use and land cover changes in Northern Kordofan state of Sudan: A remotely sensed data analysis. In *Nile River Basin: Ecohydrological Challenges, Climate Change and Hydropolitics* (pp. 269-283). Cham: Springer International Publishing. https://doi.org/10.1007/978-3-319-02720-3_15

Darbyshire, I., Kordofani, M., Farag, I., et al. (2015). *The plants of Sudan and South Sudan – an annotated checklist*. Kew Publishing, Royal Botanic Gardens, Kew, UK.

de Almeida, D. R., Vedovato, L. B., Fuza, M., Molin, P., Cassol, H., Resende, A. F., ... & Brancalion, P. H. (2025). Remote sensing approaches to monitor tropical forest restoration: Current methods and future possibilities. *Journal of Applied Ecology*, *62*(2), 188-206. https://doi.org/10.1111/1365-2664.14830

de Oliveira, A. C. P., Nunes, A., Oliveira, M. A., Oliveira, R. S., Rodrigues, R. G., & Branquinho, C. (2024). Shifts in plant functional groups along an aridity gradient in a tropical dry forest. *Science of the Total Environment*, *924*, 171695. https://doi.org/10.1016/j.scitotenv.2024.171695

de Sousa, C., Fatoyinbo, L., Neigh, C., Boucka, F., Angoue, V., & Larsen, T. (2020). Cloud-computing and Machine Learning in support of country-level land cover and ecosystem extent mapping in Liberia and Gabon. *PLoS One*, *15*(1), e0227438. https://doi.org/10.1371/journal.pone.0227438

De'ath, G., & Fabricius, K. E. (2000). Classification and regression trees: a powerful yet simple technique for ecological data analysis. *Ecology*, *81*(11), 3178-3192. https://doi.org/10.1890/0012-9658(2000)081[3178:CARTAP]2.0.CO;2

Dereje, O. A., & Duguma, I. D. (2019). Woody species composition and natural regeneration status of Ades Forest, Oromia Regional State, West Hararghe Zone, Ethiopia. *Journal of Tropical Forestry and Environment, 9*(1):27-36. https://doi.org/10.31357/jtfe.v9i1.3947

Deutsch, C. A., Tewksbury, J. J., Huey, R. B., Sheldon, K. S., Ghalambor, C. K., Haak, D. C., & Martin, P. R. (2008). Impacts of climate warming on terrestrial ectotherms across latitude. *Proceedings of the National Academy of Sciences*, *105*(18), 6668-6672. https://doi.org/10.1073/pnas.0709472105

Díaz, M., Sánchez-Mejía, T., & Morán-López, T. (2021). Long-term tree regeneration of fragmented agroforestry systems under varying climatic conditions. *Frontiers in Ecology and Evolution*, *9*, 640143. https://doi.org/10.3389/fevo.2021.640143

Dinku, T., Funk, C., Peterson, P., Maidment, R., & Tadesse, T. (2018). Validation of the CHIRPS satellite rainfall estimates over Eastern Africa. *Quarterly Journal of the Royal Meteorological Society, 144*, 292–312. https://doi.org/10.1002/qj.3244

Djosetro, M., & Behagel, J. (2024). Including local knowledge in conservation planning: the case of the western coastal protected areas in Suriname. *Ecosystems and People*, *20*(1), 2361683. https://doi.org/10.1080/26395916.2024.2361683

D'Odorico, P., & Bhattachan, A. (2012). Hydrologic variability in dryland regions: impacts on ecosystem dynamics and food security. *Philosophical Transactions of the Royal Society B: Biological Sciences*, *367*(1606), 3145-3157. https://doi.org/10.1098/rstb.2012.0016

Drusch, M., Del Bello, U., Carlier, S., Colin, O., Fernandez, V., Gascon, F., ... & Bargellini, P. (2012). Sentinel-2: ESA's optical high-resolution mission for GMES operational services. *Remote sensing of Environment*, *120*, 25-36. https://doi.org/10.1016/j.rse.2011.11.026

Du, P., Samat, A., Waske, B., Liu, S., & Li, Z. (2015). Random forest and rotation forest for fully polarized SAR image classification using polarimetric and spatial features. *ISPRS journal of photogrammetry and remote sensing*, *105*, 38-53. https://doi.org/10.1016/j.isprsjprs.2015.03.002

Duan, P., Fu, R., Nottingham, A. T., Domeignoz-Horta, L. A., Yang, X., Du, H., ... & Li, D. (2023). Tree species diversity increases soil microbial carbon use efficiency in a subtropical forest. *Global Change Biology*, *29*(24), 7131-7144. https://doi.org/10.1111/gcb.16971

Edet, D. I., Ijeomah, H. M., & Ogogo, A. U. (2012). Preliminary assessment of tree species diversity in Afi Mountain Wildlife Sanctuary, Southern Nigeria. *Agriculture and biology journal of North America*, *3*(12), 486-492. https://doi.org/10.5251/abjna.2012.3.12.486.492

El Gamri, T., Saeed, A. B., & Abdalla, A. (2021). Rainfall of the Sudan: Characteristics and prediction. *Journal of Faculty of Arts, University of Khartoum, 27*, 17–35. https://doi.org/10.53332/jfa.v27i.624

Elagib, N. A., & Mansell, M. G. (2000). Recent trends and anomalies in mean seasonal and annual temperatures over Sudan. *Journal of Arid Environments*, *45*(3), 263-288. https://doi.org/10.1006/jare.2000.0639

Elhassan, F. A. A., Kouassi, E. K., Abrha, H., Laamarni, A., & Siddig, A. A. H. (2024). Response of Species to the Impact of Climate Change in the Gum Arabic Belt, Sudan: A Case Study in Acacia senegal. *International Journal of Environment and Climate Change, 14*(5), 305-323. https://doi.org/10.9734/ijecc/2024/v14i54191

Elith, J., Graham, H., Anderson, C. P. R., et al. (2006). Novel methods improve prediction of species' distributions from occurrence data. *Ecography, 29*, 129–151. https://doi.org/10.1111/j.2006.0906-7590.04596.x

Elith, J., Kearney, M., & Phillips, S. (2010). The art of modelling range-shifting species. *Methods in ecology and evolution*, *1*(4), 330-342. https://doi.org/10.1111/j.2041-210X.2010.00036.x

Elith, J., Phillips, S. J., Hastie, T., Dudík, M., Chee, Y. E., & Yates, C. J. (2011). A statistical explanation of MaxEnt for ecologists. *Diversity and distributions*, *17*(1), 43-57. https://doi.org/10.1111/j.1472-4642.2010.00725.x

Eltayb, M.T.A., Magid, T.D.A., 2012. Assessing the effect of timing and felling techniqueson the susceptibility of Acacia. *Journal of Forest Products and Industries* 1, 26–34.

Eltohami, A. B. E. S. A. (2018). Threats to green gum arabic production in Sudan. *Biomedical Journal of Scientific & Technical Research*, *3*(5), 3526-3530. https://doi.org/10.26717/BJSTR.2018.03.000951

Elzaki, I. A., Siddig, A. A., Yasin, E. H. E., et al. (2023). Effect of simulated drought and rainfall fluctuation on seedling growth of two savannah tree species in Sudan: An experimental exploration. *Acta Silvatica et Lignaria Hungarica, 19*, 37–50. https://doi.org/10.37045/aslh-2023-0003

ESRI (Environmental Systems Research Institute). (2025). ArcGIS Pro, Release 3.6. Redlands, CA: Esri.

Eyring, V., Bony, S., Meehl, G. A., Senior, C. A., Stevens, B., Stouffer, R. J., & Taylor, K. E. (2016). Overview of the Coupled Model Intercomparison Project Phase 6 (CMIP6) experimental design and organization. *Geoscientific Model Development*, *9*(5), 1937-1958. https://doi.org/10.5194/gmd-9-1937-2016

Fahmi, M. K. M. (2017). Climate, trees and agricultural practices: Implications for food Security in the semi-arid zone of Sudan. Univ. Helsinki Tropic. Forest. Dep., Helsinki.

FAO. (2010). Global Forest Resources Assessment Food and Agriculture Organization of the United Nations, Rome, 2010.

FAO. (2015). Global Forest Resources Assessment 2015: How are the world's forests changing? Rome: FAO. https://www.fao.org/forest-resources-assessment/. (Access date: 20 November 2025).

FAO. (2016). Trees, forests and land use in drylands: The first global assessment. Rome, Italy: FAO.

FAO. (2021). *The impact of disasters and crises on agriculture and food security: 2021*. FAO.

Farr, T. G., Rosen, P. A., Caro, E., Crippen, R., Duren, R., Hensley, S., ... & Alsdorf, D. (2007). The Shuttle Radar Topography Mission. *Reviews of Geophysics, 45*(2). https://doi.org/10.1029/2005RG000183

Fassnacht, F. E., Latifi, H., Stereńczak, K., Modzelewska, A., Lefsky, M., Waser, L. T., ... & Ghosh, A. (2016). Review of studies on tree species classification from remotely sensed data. *Remote sensing of environment*, *186*, 64-87. https://doi.org/10.1016/j.rse.2016.08.013

Fathizad, H., Ardakani, M. A. H., Sodaiezadeh, H., Kerry, R., & Taghizadeh-Mehrjardi, R. (2020). Investigation of the spatial and temporal variation of soil salinity using random forests in the central desert of Iran. *Geoderma*, *365*, 114233. https://doi.org/10.1016/j.geoderma.2020.114233

Feng, W., Ma, C., Zhao, G., Zhang, R.. (2020). Fsrf: An improved random forest for classification. In: 2020 IEEE International Conference on Advances in Electrical Engineering and Computer Applications (AEECA), IEEE, pp. 173–178. https://doi.org/10.1109/AEECA49918.2020.9213456

Ferreira, M. P., Wagner, F. H., Aragão, L. E., Shimabukuro, Y. E., & de Souza Filho, C. R. (2019). Tree species classification in tropical forests using visible to shortwave infrared WorldView-3 images and texture analysis. *ISPRS journal of photogrammetry and remote sensing*, *149*, 119-131. https://doi.org/10.1016/j.isprsjprs.2019.01.019

Fick, S. E., & Hijmans, R. J. (2017). WorldClim 2: new 1-km spatial resolution climate surfaces for global land areas. *International journal of climatology*, *37*(12), 4302-4315. https://doi.org/10.1002/joc.5086

FNC of S. (2021). *Sudan National Forest Inventory*. Food and Agriculture Organization of the United Nations and Forests National Corporation of Sudan, Khartoum, Sudan.

Foden, W., Midgley, G. F., Hughes, G., Bond, W. J., Thuiller, W., Hoffman, M. T., ... & Hannah, L. (2007). A changing climate is eroding the geographical range of the Namib Desert tree Aloe through population declines and dispersal lags. *Diversity and Distributions*, *13*(5), 645-653. https://doi.org/10.1111/j.1472-4642.2007.00391.x

Fonseka, H. P. U., Zhang, H., Sun, Y., Su, H., Lin, H., & Lin, Y. (2019). Urbanization and its impacts on land surface temperature in Colombo metropolitan area, Sri Lanka, from 1988 to 2016. *Remote sensing*, *11*(8), 957. https://doi.org/10.3390/rs11080957

Foody, G. M. (2020). Explaining the unsuitability of the kappa coefficient in the assessment and comparison of the accuracy of thematic maps obtained by image classification. *Remote sensing of environment*, *239*, 111630. https://doi.org/10.1016/j.rse.2019.111630

Frerebeau N. (2019). Diversity Measures. http://cran.univ-paris1.fr/web/packages/tabula/vignettes/diversity.html. (Access data 28.05.2025).

Gadallah, N. A. H., Hano, A., & Yagoub, Y. (2020). Characterizing forest cover changes based on satellite images cum forest dependents' data. *Agriculture & Forest Journal, 4*, 63–70. https://doi.org/10.5281/zenodo.4310945

Gadallah, N. A., Gone, B. Z. B., Hakam, O., Siddig, A. A., & Ongoma, V. (2025). Modeling the impacts of climate change on the current and future distribution of baobab (Adansonia digitata L.) in Sudan. *Modeling Earth Systems and Environment*, *11*(6), 1-18. https://doi.org/10.1007/s40808-025-02574-x

Gamal, H. M. S., Abdalla, A. M. A., Salih, R. R. M., & Abualgasim, M. R. (2022). Suitability of using *Acacia seyal* var. *seyal* for forest-based industries development in Sudan. *Academia Journal of Agricultural Research, 10*(2), 19-30. https://www.researchgate.net/publication/366593671

Gamito, S. (2010). Caution is needed when applying Margalef diversity index. *Ecological Indicators*, *10*(2), 550-551. https://doi.org/10.1016/j.ecolind.2009.07.006

Gamoun, M., Patton, B., & Hanchi, B. (2015). Assessment of vegetation response to grazing management in arid rangelands of southern Tunisia. *International Journal of Biodiversity Science, Ecosystem Services & Management*, *11*(2), 106-113. https://doi.org/10.1080/21513732.2014.998284

Gamreldin, E., & Hamadalnel, M. (2024). Spatial and temporal analysis of maximum and minimum temperature trends in northern Sudan during (1990-2019). *Journal of Geoscience and Environment Protection*, *12*(5), 266-288. https://doi.org/10.4236/gep.2024.125015

Gauthier, S., Bernier, P., Kuuluvainen, T., Shvidenko, A. Z., & Schepaschenko, D. G. (2015). Boreal forest health and global change. *Science*, *349*(6250), 819-822. https://doi.org/10.1126/science.aaa9092

Ge, Y., Hu, S., Ren, Z., Jia, Y., Wang, J., Liu, M., ... & Chen, Y. (2019). Mapping annual land use changes in China's poverty-stricken areas from 2013 to 2018. *Remote Sensing of Environment*, *232*, 111285. https://doi.org/10.1016/j.rse.2019.111285

Gebeyehu, G., Soromessa, T., Bekele, T., & Teketay, D. (2019). Species composition, stand structure, and regeneration status of tree species in dry Afromontane forests of Awi Zone, northwestern Ethiopia. *Ecosystem Health and Sustainability*, *5*(1), 199-215. https://doi.org/10.1080/20964129.2019.1664938

Ghanbari, S., Sefidi, K., Kern, C. C., & Álvarez-Álvarez, P. (2021). Population structure and regeneration status of woody plants in relation to the human interventions, Arasbaran Biosphere Reserve, Iran. *Forests*, *12*(2), 191. https://doi.org/10.3390/f12020191

Ghimire, B., Rogan, J., Galiano, V. R., Panday, P., & Neeti, N. (2012). An evaluation of bagging, boosting, and random forests for land-cover classification in Cape Cod, Massachusetts, USA. *GIScience & Remote Sensing*, *49*(5), 623-643. https://doi.org/10.2747/1548-1603.49.5.623

Gibreel, H. (2008). A taxonomic Study on Trees and Shrubs of El Nour Natural Forest Reserve, Blue Nile State-Sudan. Master thesis. University of Khartoum.

Gibreel, H. H., Kordofani, M. A. I., Warrag, E. I., & Ahmed, H. O. (2013). Medicinal value and ecotaxonomy of the flora of Blue Nile State-Sudan. *Journal of Chemical and Pharmaceutical Research*, *5*(2), 36-43. https://www.researchgate.net/profile/Haytham-Gibreel/publication/289794047

Glover, E. K., & Elsiddig, E. A. (2012). The causes and consequences of environmental changes in Gedaref, Sudan. *Land Degradation & Development*, *23*(4), 339-349. https://doi.org/10.1002/ldr.2167

Gogoi, A., & Sahoo, U. K. (2018). Impact of anthropogenic disturbance on species diversity and vegetation structure of a lowland tropical rainforest of eastern Himalaya, India. *Journal of Mountain Science*, *15*(11), 2453-2465. https://doi.org/10.1007/s11629-017-4713-4

Gorelick, N., Hancher, M., Dixon, M., Ilyushchenko, S., Thau, D., & Moore, R. (2017). Google Earth Engine: Planetary-scale geospatial analysis for everyone. *Remote sensing of Environment*, *202*, 18-27. https://doi.org/10.1016/j.rse.2017.06.031

Griffiths, P., van der Linden, S., Kuemmerle, T., & Hostert, P. (2013). A pixel-based Landsat compositing algorithm for large area land cover mapping. *IEEE Journal of Selected Topics in Applied Earth Observations and Remote Sensing*, *6*(5), 2088-2101. https://doi.org/10.1109/JSTARS.2012.2228167

Guan, Y., Zhang, X., Zheng, F., & Wang, B. (2015). Trends and variability of daily temperature extremes during 1960–2012 in the Yangtze River Basin, China. *Global and Planetary Change*, *124*, 79-94. https://doi.org/10.1016/j.gloplacha.2014.11.008

Guenang, G. M., & Kamga, F. M. (2014). Computation of the standardized precipitation index (SPI) and its use to assess drought occurrences in Cameroon over recent decades. *Journal of Applied Meteorology and Climatology, 53*, 2310–2324. https://doi.org/10.1175/JAMC-D-14-0032.1

Gufi, Y., Manaye, A., Tesfamariam, B., Abrha, H., Tesfaye, M., & Hintsa, S. (2023). Modeling impacts of climate change on the geographic distribution and abundances of Tamarindus

indica in Tigray region, Ethiopia. *Heliyon*, *9*(7). https://doi.org/10.1016/j.heliyon.2023.e17471

Guiller, A., Decocq, G., Kichey, T., Poli, P., Vandepitte, K., Dubois, F., ... & Closset-Kopp, D. (2023). Spatial genetic structure of two forest plant metapopulations in dynamic agricultural landscapes. *Landscape and Urban Planning*, *231*, 104648. https://doi.org/10.1016/j.landurbplan.2022.104648

Guisande, C., García-Roselló, E., Heine, J., González-Dacosta, J., Vilas, L. G., Pérez, B. J. G., & Lobo, J. M. (2017). SPEDInstabR: an algorithm based on a fluctuation index for selecting predictors in species distribution modeling. *Ecological Informatics*, *37*, 18-23. https://doi.org/10.1016/j.ecoinf.2016.11.004

Gunawan, H., Setyawati, T., Atmoko, T., Kwatrina, R. T., Yeny, I., Yuwati, T. W., ... & Kuswanda, W. (2024). A review of forest fragmentation in Indonesia under the DPSIR framework for biodiversity conservation strategies. *Global Ecology and Conservation*, *51*, e02918. https://doi.org/10.1016/j.gecco.2024.e02918

Guo, P., Wang, H., Qin, F., Miao, C., & Zhang, F. (2023). Coupled MOP and PLUS-SA model research on land use scenario simulations in zhengzhou metropolitan area, Central China. *Remote Sensing*, *15*(15), 3762. https://doi.org/10.3390/rs15153762

Gurashi, N. A., Yasin, E. H. E., & Czimber, K. (2024a). Changes in Structure, Tree Species Composition, and Diversity of the Abu Geili Riverine Forest Reserve, Sinnar State, Sudan. *Acta Silvatica Et Lignaria Hungarica: An International Journal In Forest, Wood and Environmental Sciences, 20*(2), 55-70. https://doi.org/10.37045/aslh-2024-0004

Gurashi, N. A., Yasin, E. H., & Czimber, K. (2024b). Assessment of tree species availability based on sawmilling and timber markets survey in Sinnar State, Sudan. *Acta Silvatica et Lignaria Hungarica: An International Journal In Forest, Wood and Environmental Sciences, 20*, 39–51. https://doi.org/10.37045/aslh-2024-0003

Gusman, A., & Supriyadi, S. (2024). Analysis of Participatory Approaches of Community-Based Sustainable Marine Protected Area Management Groups. *Jurnal Indonesia Sosial Sains*, *5*(03), 342-350. https://doi.org/10.59141/jiss.v5i03.1026

Haddeland, I., Heinke, J., Voß, F., Eisner, S., Chen, C., Hagemann, S., & Ludwig, F. (2012). Effects of climate model radiation, humidity and wind estimates on hydrological simulations. *Hydrology and Earth System Sciences*, *16*(2), 305-318. https://doi.org/10.5194/hess-16-305-2012

Hadi, S., Ziegler, T., Waltert, M., & Hodges, J. K. (2009). Tree diversity and forest structure in northern Siberut, Mentawai islands, Indonesia. *Tropical Ecology 50*(2), 315–327.

Halldorsson, G. H., Benediktsson, J. A., & Sveinsson, J. R. (2003). Support Vector Machines in multisource classification. In *Proceedings of the IGARSS 2003 IEEE International Geoscience and Remote Sensing Symposium*. *IEEE*, *3*, pp. 2054–2056. https://doi.org/10.1109/IGARSS.2003.1294337

Hamadalnel, M., Zhu, Z., Gaber, A., Iyakaremye, V., & Ayugi, B. (2022). Possible changes in Sudan's future precipitation under the high and medium emission scenarios based on bias adjusted GCMs. *Atmospheric Research*, *269*, 106036. https://doi.org/10.1016/j.atmosres.2022.106036

Hano, A. I. (2013). Assessment of impacts of changes in land use patterns on land degradation/desertification in the semi-arid zone of White Nile State, Sudan, by means of remote sensing and GIS. Ph.D. Thesis, TU Dresden, Germany.

Hansen, M. C., Roy, D. P., Lindquist, E., Adusei, B., Justice, C. O., & Altstatt, A. (2008). A method for integrating MODIS and Landsat data for systematic monitoring of forest cover and change in the Congo Basin. *Remote Sensing of Environment*, *112*(5), 2495-2513. https://doi.org/10.1016/j.rse.2007.11.012

Hao, Z., Singh, V. P., & Xia, Y. (2018). Seasonal drought prediction: Advances, challenges, and future prospects. *Reviews of Geophysics, 56*, 108–141. https://doi.org/10.1002/2016RG000549

Haq, B., Jamshed, M. A., Ali, K., Kasi, B., Arshad, S., Kasi, M. K., ... & Ur-Rehman, M. (2024). Tech-driven forest conservation: combating deforestation with internet of things, artificial intelligence, and remote sensing. *IEEE Internet of Things Journal*, *11*(14), 24551-24568. https://doi.org/10.1109/JIOT.2024.3378671

Harris, I., Osborn, T. J., Jones, P., & Lister, D. (2020). Version 4 of the CRU TS monthly high-resolution gridded multivariate climate dataset. *Scientific data*, *7*(1), 109. https://doi.org/10.1038/s41597-020-0453-3

Harrison, M. N., & Jackson, J. K. (1958) Ecological classification of the vegetation of the Sudan. *Forests Bulletin, Forest Department, Ministry of Agriculture, Khartoum, Sudan 1958*(2), 45.

Hasoba, A. M., Siddig, A. A., & Yagoub, Y. E. (2020). Exploring tree diversity and stand structure of savanna woodlands in southeastern Sudan. *Journal of Arid Land*, *12*(4), 609-617. https://doi.org/10.1007/s40333-020-0076-8

Hasoba, A. M., Siddig, A. A., Czimber, K., Omer, A., Gadallah, N. A., Adam, M., & Plotkin, A. B. (2025). Synthesizing knowledge about tree diversity, density, and distribution in the savanna woodlands of Sudan. *Trees, Forests and People*, *21*, 100906. https://doi.org/10.1016/j.tfp.2025.100906

Hemida, M., Yasin, E. H. E., Kheiry, M. A., Hammad, Z. M., & Vityi, A. (2023). Assessment of Taungya agroforestry system in dryland forests rehabilitation in Sudan. Journal of Degraded and Mining Lands Management, 10, 4495–4507. https://doi.org/10.15243/jdmlm.2023.103.4495

Hermosilla, T., Wulder, M. A., White, J. C., Coops, N. C., & Hobart, G. W. (2015). An integrated Landsat time series protocol for change detection and generation of annual gap-free surface reflectance composites. *Remote Sensing of Environment*, *158*, 220-234. https://doi.org/10.1016/j.rse.2014.11.005

Hido, A., Tolera, M., Lemma, B., & Evangelista, P. H. (2020). Population status and resin quality of frankincense Boswellia neglecta (burseraceae) growing in South omo, southwestern Ethiopia. *Journal of Sustainable Forestry*, *39*(6), 620-634. https://doi.org/10.1080/10549811.2020.1721302

Hosseini, N., Ghorbanpour, M., & Mostafavi, H. (2024). Habitat potential modelling and the effect of climate change on the current and future distribution of three Thymus species in Iran using MaxEnt. *Scientific Reports*, *14*(1), 3641. https://doi.org/10.1038/s41598-024-53405-5

Howse, M. W., Haywood, J., & Lester, P. J. (2020). Bioclimatic modelling identifies suitable habitat for the establishment of the invasive European paper wasp (Hymenoptera: Vespidae) across the southern hemisphere. *Insects*, *11*(11), 784. https://doi.org/10.3390/insects11110784

https://doi.org/10.3390/su151914270

Hu, B., Li, Q., & Hall, G. B. (2021). A decision-level fusion approach to tree species classification from multi-source remotely sensed data. *ISPRS Open Journal of Photogrammetry and Remote Sensing*, *1*, 100002. https://doi.org/10.1016/j.ophoto.2021.100002

Huber, J. M., Newig, J., & Loos, J. (2023). Participation in protected area governance: A systematic case survey of the evidence on ecological and social outcomes. *Journal of Environmental Management*, *336*, 117593. https://doi.org/10.2139/ssrn.4286771

Huete, A., Didan, K., Miura, T., Rodriguez, E. P., Gao, X., & Ferreira, L. G. (2002). Overview of the radiometric and biophysical performance of the MODIS vegetation indices. *Remote sensing of environment*, *83*(1-2), 195-213. https://doi.org/10.1016/S0034-4257(02)00096-2

Hughes, T. P., Baird, A. H., Bellwood, D. R., Card, M., Connolly, S. R., Folke, C., ... & Roughgarden, J. (2003). Climate change, human impacts, and the resilience of coral reefs. *science*, *301*(5635), 929-933. https://doi.org/10.1126/science.1085046

Hulme, M., Doherty, R., Ngara, T., New, M., & Lister, D. (2001). African climate change: 1900-2100. *Climate research*, *17*(2), 145-168. https://doi.org/10.3354/cr017145

Hussein, A., & Estifanos, S. (2023). Modeling impacts of climate change on the distribution of invasive Opuntia ficus-indica (L.) Mill. in Ethiopia: Implications on biodiversity conservation. *Heliyon*, *9*(4), e14927. https://doi.org/10.1016/j.heliyon.2023.e14927

Hussien, A. (2024). Analysis of the Drought Impact as an Extreme Climatic Event in Sudan. Journal of Geoscience and Environment Protection, 12, 38-47. https://doi.org/10.4236/gep.2024.126003

Ibrahim, E. M. I., & Osman, E. H. (2014). Diameter at Breast Height-Crown Width Prediction Models for Anogeissus Leiocarpus (DC.) Guill &Perr and Combretum Hartmannianum Schweinf. *Journal of Forest Products & Industries, 3*(4), 191-197.

Ibrahim, E. M. M., Paity, B. E., Hassan, T. T., Idris, E. Z. A., & Yousif, T. A. (2018). Effect of tree species, tree variables and topography on CO2 concentration in badous riverine forest reserve–Blue Nile, Sudan. *University of Kordofan Journal of Natural Resources & Enviromental Studies*, *5*(01), 1-12.

Ibrahim, E., Osman, E., & Idris, E. (2014). Modelling the Relationship between Crown width and Diameter at Breast Height for Naturally grown Terminalia tree species. *Journal of Natural Resources and Environmental Studies, 6456*, 42-49.

Ibrahim, E., Osman, E., Idris, E., & Yousif, T. (2015). Linear and non-linear regression equations for estimating the crown diameter of three Sudanese edible trees. *Journal of Forest Products & Industries*, *4*(2), 44–52.

Ibrahim, E.M., & Hassan, T.T. (2015). Factors affecting natural regeneration and distribution of trees species in El-Nour natural forest reserve. *Journal of Natural Resources and Environmental Studies*, *6456*, 16-21.

Idreas, A. E. L. A. (2015). Effect of mechanized rain-fed farming on vegetation cover and effect of shelter belts on environment at Ghadambaliya Area Gedaref State (Sudan). Ph.D. Thesis, Sudan University of Science and Technology, Sudan.

Idrissa, B., Idrissa, S., Issiaka, Y., Karimou, A. J., Mahamane, A., Mahamane, S., & Weber, J. C. (2018). Trend and Structure of Populations of Balanites Aegyptiaca in Parkland Agroforestsin Western Niger. *Annual Research & Review in Biology,* 22 (4), 1-12. https://doi.org/10.9734/ARRB/2018/38650.

Ijomah, J. U., Igiri, M. R., & Okey, I. B. (2022). Evaluation of Trees Species Diversity, Abundance and Soil Physicochemical Properties of Ukpon River Forest Reserves, Cross River,

Nigeria. *Asian Journal of Research in Agriculture and Forestry*, *8*(4), 109-122. https://doi.org/10.9734/ajraf/2022/v8i4170

Immitzer, M., Atzberger, C., & Koukal, T. (2012). Tree species classification with random forest using very high spatial resolution 8-band WorldView-2 satellite data. *Remote sensing*, *4*(9), 2661-2693. https://doi.org/10.3390/rs4092661

IPCC. (2007a). Climate Change 2007: Impacts, Adaptation and Vulnerability. Contribution of Working Group II to the Fourth Assessment Report of the Intergovernmental Panel on Climate Change, AnnexI., In M.L. Parry, O.F. Canziani, J.P. Palutikof, P.J. van der Linden and C.E. Hanson, Eds., Cambridge, Cambridge University Press,

IPCC. (2007b). Climate change 2007: The physical science basis. Contribution of Working Group I to the Fourth Assessment Report of the IPCC. Online at: http://www.ipcc.ch/ipccreports/ar4-wg1.htm

IPCC. (2013). Climate Change 2013: The Physical Science Basis. Working Group 1 Contribution to the Fifth Assessment Report of the Intergovernmental Panel on Climate Change (IPCC). http://www.ipcc.ch/report/ar5/wg1/

IPCC. (2014). Climate Change 2014: Impacts, Adaptation, and Vulnerability. Part A: Global and Sectoral Aspects. Contribution of Working Group II to the Fifth Assessment Report of the Intergovernmental Panel on Climate Change. Cambridge University Press.

IPCC. (2022). *Climate Change 2022: Impacts, Adaptation and Vulnerability. Contribution of Working Group II to the Sixth Assessment Report of the Intergovernmental Panel on Climate Change*. In H. O. Pörtner, D. C. Roberts, M. Tignor, E. S. Poloczanska, K. Mintenbeck, A. Alegría, M. Craig, S. Langsdorf, S. Löschke, V. Möller, A. Okem, & B. Rama (Eds.). Cambridge University Press.

ISRIC. (2016). *World Inventory of Soil Emission Potentials (WISE)*. https://www.isric.org/projects/world-inventory-soil-emission-potentials-wise. (Accessed 30 August 2025).

James, G., Witten, D., Hastie, T., & Tibshirani, R. (2013). *An introduction to statistical learning: with applications in R*. *Springer New York Heidelberg Dordrecht London, 103*. https://doi.org/10.1007/978-1-4614-7138-7

Jensen, J.R. (2009). Remote sensing of the environment: An earth resource perspective. *Cartography and Geographic Information Science,* 27(4), 311. https://doi.org/10.1559/1523040200.

Ji, Y., Fu, J., Lu, Y., & Liu, B. (2023). Three-dimensional-based global drought projection under global warming tendency. *Atmospheric Research, 291*, 106812. https://doi.org/10.1016/j.atmosres.2023.106812

Jiménez-Valverde, A. (2014). Threshold-dependence as a desirable attribute for discrimination assessment: Implications for the evaluation of species distribution models. *Biodiversity and Conservation, 23*, 369–385. https://doi.org/10.1007/s10531-013-0606-1

Joshi, V. C., Negi, V. S., Sundriyal, R. C., & Arya, D. (2024). Temporal changes in species richness, composition and diversity of the forest stands over 36-year period, Western Himalaya, India. *Trees, Forests and People*, *16*, 100572. https://doi.org/10.1016/j.tfp.2024.100572

Jump, A. S., & Peñuelas, J. (2005). Running to stand still: adaptation and the response of plants to rapid climate change. *Ecology letters*, *8*(9), 1010-1020. https://doi.org/10.1111/j.1461-0248.2005.00796.x

Karlson, M., Reese, H., & Ostwald, M. (2014). Tree crown mapping in managed woodlands (parklands) of semi-arid West Africa using WorldView-2 imagery and geographic object based image analysis. *Sensors*, *14*(12), 22643-22669. https://doi.org/10.3390/s141222643

Kendall, M. G. (1975). *Rank Correlation Methods* (4th ed.). London: Charles Griffin

Kikoti, I. A., & Mligo, C. (2015). Impacts of livestock grazing on plant species composition in montane forests on the northern slope of Mount Kilimanjaro, Tanzania. *International Journal of Biodiversity Science, Ecosystem Services & Management*, *11*(2), 114-127. https://doi.org/10.1080/21513732.2015.1031179

Kim, U., & Kaluarachchi, J. J. (2009). Climate change impacts on water resources in the upper blue Nile River Basin, Ethiopia 1. *JAWRA Journal of the American Water Resources Association*, *45*(6), 1361-1378. https://doi.org/10.1111/j.1752-1688.2009.00369.x

Kimani, M. W., Hoedjes, J. C. B., & Su, Z. (2017). An assessment of satellite-derived rainfall products relative to ground observations over East Africa. *Remote Sensing, 9*, 430. https://doi.org/10.3390/rs9050430

Koreň, M., Find'o, S., Skuban, M., & Kajba, M. (2011). Habitat suitability modelling from non-point data: the case study of brown bear habitat in Slovakia. *Ecological Informatics*, *6*(5), 296-302. https://doi.org/10.1016/j.ecoinf.2011.05.002

Kuhn, M., & Johnson, K. (2013). *Applied predictive modeling*. Springer New York, NY. PP. 600. https://doi.org/10.1007/978-1-4614-6849-3

Lalor, A. R., Law, D. J., Breshears, D. D., Falk, D. A., Field, J. P., Loehman, R. A., ... & Barron-Gafford, G. A. (2023). Mortality thresholds of juvenile trees to drought and heatwaves: implications for forest regeneration across a landscape gradient. *Frontiers in Forests and Global Change*, *6*, 1198156. https://doi.org/10.3389/ffgc.2023.1198156

Lambin, E. F., & Meyfroidt, P. (2011). Global land use change, economic globalization, and the looming land scarcity. Proceedings of the National Academy of Sciences, 108, 3465–3472. https://doi.org/10.1073/pnas.1100480108

Lawlor, J. A., Comte, L., Grenouillet, G., Lenoir, J., Baecher, J. A., Bandara, R. M. W. J., ... & Sunday, J. (2024). Mechanisms, detection and impacts of species redistributions under climate change. *Nature Reviews Earth & Environment*, *5*(5), 351-368. https://doi.org/10.1038/s43017-024-00527-z

Lee, J. S. H., Wich, S., Widayati, A., & Koh, L. P. (2016). Detecting industrial oil palm plantations on Landsat images with Google Earth Engine. *Remote Sensing Applications: Society and Environment*, *4*, 219-224. https://doi.org/10.1016/j.rsase.2016.11.003

Lee, S., Moriasi, D. N., Mehr, A. D., & Mirchi, A. (2024). Sensitivity of Standardized Precipitation and Evapotranspiration Index (SPEI) to the choice of SPEI probability distribution and evapotranspiration method. *Journal of Hydrology: Regional Studies*, *53*, 101761. https://doi.org/10.1016/j.ejrh.2024.101761

Ließ, M., Glaser, B., & Huwe, B. (2012). Uncertainty in the spatial prediction of soil texture: comparison of regression tree and Random Forest models. *Geoderma*, *170*, 70-79. https://doi.org/10.1016/j.geoderma.2011.10.010

Lin, L., Hao, Z., Post, C. J., Mikhailova, E. A., Yu, K., Yang, L., & Liu, J. (2020). Monitoring land cover change on a rapidly urbanizing island using Google Earth Engine. *Applied Sciences*, *10*(20), 7336. https://doi.org/10.3390/app10207336

Listopad, C. M., Köbel, M., Príncipe, A., Gonçalves, P., & Branquinho, C. (2018). The effect of grazing exclusion over time on structure, biodiversity, and regeneration of high nature value

farmland ecosystems in Europe. *Science of the Total Environment*, *610*, 926-936. https://doi.org/10.1016/j.scitotenv.2017.08.018

Liu, M., Liu, J., Atzberger, C., Jiang, Y., Ma, M., & Wang, X. (2021). Zanthoxylum bungeanum Maxim mapping with multi-temporal Sentinel-2 images: The importance of different features and consistency of results. *ISPRS Journal of Photogrammetry and Remote Sensing*, *174*, 68-86. https://doi.org/10.1016/j.isprsjprs.2021.02.003

Lu, D., & Weng, Q. (2007). A survey of image classification methods and techniques for improving classification performance. *International journal of Remote sensing*, *28*(5), 823-870. https://doi.org/10.1080/01431160600746456

Lu, Y., Zhang, B., Zhang, M., Jie, M., Guo, S., & Wang, Y. (2023). Relict plants are better able to adapt to climate change: evidence from desert shrub communities. *Plants*, *12*(23), 4065. https://doi.org/10.3390/plants12234065

Ludwig, F., Supit, I., Franssen, W., & Biemans, H. (2013). *Climate change impacts on hydrological and meteorological extremes: Executive summary of COMBINE project.*

Lyam, P. T., Duque-Lazo, J., Hauenschild, F., Schnitzler, J., Muellner-Riehl, A. N., Greve, M., ... & Durka, W. (2022). Climate change will disproportionally affect the most genetically diverse lineages of a widespread African tree species. *Scientific Reports*, *12*(1), 7035. https://doi.org/10.1038/s41598-022-11182-z

MacDicken, K. (2015). Introduction to the Changes in Global Forest Resources from 1990 to 2015. *Forest Ecology and Management*, *352*, 1-2. https://doi.org/10.1016/j.foreco.2015.06.018

Maclean, I. M., & Wilson, R. J. (2011). Recent ecological responses to climate change support predictions of high extinction risk. *Proceedings of the National Academy of Sciences*, *108*(30), 12337-12342. https://doi.org/10.1073/pnas.1017352108

Mann, H. B. (1945). Nonparametric tests against trend. *Econometrica*, **13**(3), 245–259. https://doi.org/10.2307/1907187

Martínez-Villa, J. A., Durán, S. M., Enquist, B. J., Duque, A., Messier, C., & Paquette, A. (2024). Temporal shifts in the functional composition of Andean forests at different elevations are driven by climate change. *Global Ecology and Biogeography*, *33*(1), 85-99. https://doi.org/10.1111/geb.13774

Masresha, G., Melkamu, Y., & Mulu, G. (2024). Woody Species Composition, Structure, and Status of Regeneration in Pugnido Forest, Gambella Region, Western Ethiopia. *Scientifica*, *2024*(1), 3961434. https://doi.org/10.1155/2024/3961434

Maua, J. O., MugatsiaTsingalia, H., Cheboiwo, J., & Odee, D. (2020). Population structure and regeneration status of woody species in a remnant tropical forest: A case study of South Nandi forest, Kenya. *Global Ecology and Conservation*, *21*, e00820. https://doi.org/10.1016/j.gecco.2019.e00820

Mbogo, I. N. (2014). *Drought conditions and management strategies in Kenya*. Namibia Meteorological Services.

Merow, C., Smith, M. J., & Silander Jr, J. A. (2013). A practical guide to MaxEnt for modeling species' distributions: what it does, and why inputs and settings matter. *Ecography*, *36*(10), 1058-1069. https://doi.org/10.1111/j.1600-0587.2013.07872.x

Mesgari, E., Hosseini, S. A., Hemmesy, M. S., Houshyar, M., & Partoo, L. G. (2022). Assessment of CMIP6 models' performances and projection of precipitation based on SSP scenarios over the MENAP region. *Journal of Water and Climate Change*, *13*(10), 3607-3619. https://doi.org/10.2166/wcc.2022.195

Modarres, R., & Sarhadi, A. (2010). Frequency distribution of extreme hydrologic drought of southeastern semiarid region, Iran. *Journal of Hydrologic Engineering, 15*, 255–264. https://doi.org/10.1061/(ASCE)HE.1943-5584.0000186

Mohamed, N. A. H., Bannari, A., Fadul, H. M., & Zakieldeen, S. (2016). Ecological zones degradation analysis in central sudan during a half century using remote sensing and GIS. *Advances in remote sensing*, *5*(4), 355-371. https://doi.org/10.4236/ars.2016.54025

Mohammed, E. M. I. (2019). Impact of land use practices on the natural forest in Dinder Biosphere Reserve and it's surrounding areas - Sudan. University of Bahri, Sudan.

Mohammed, E. M., Hassan, T. T., Idris, E. A., & Abdel-Magid, T. D. (2021a). Tree population structure, diversity, regeneration status, and potential disturbances in Abu Gadaf natural reserved forest, Sudan. *Environmental Challenges*, *5*, 100366. https://doi.org/10.1016/j.envc.2021.100366

Mohammed, E. M., Ndakidemi, P. A., & Treydte, A. C. (2021b). Anthropogenic pressure on tree species diversity, composition, and growth of Balanites aegyptiaca in Dinder Biosphere Reserve, Sudan. *Plants*, *10*(3), 483. https://doi.org/10.3390/plants10030483

Mohmmed, A., Li, J., Elaru, J., Elbashier, M. M., Keesstra, S., Artemi, C., ... & Teffera, Z. (2018). Assessing drought vulnerability and adaptation among farmers in Gadaref region, Eastern Sudan. *Land use policy*, *70*, 402-413. https://doi.org/10.1016/j.landusepol.2017.11.027

Montoya-Jimenez, J. C., Valdez-Lazalde, J. R., Ángeles-Perez, G., De Los Santos-Posadas, H. M., & Cruz-Cárdenas, G. (2022). Predictive capacity of nine algorithms and an ensemble model to determine the geographic distribution of tree species. *iForest-Biogeosciences and Forestry*, *15*(5), 363. https://doi.org/10.3832/ifor4084-015

Moradi, S., Moradi, H., & Rezvani, A. (2025). Integrating remote sensing and species distribution modeling to assess the impacts of flood disturbance on the species habitat in the central Zagros. *Discover Applied Sciences*, *7*(9), 935. https://doi.org/10.1007/s42452-025-07582-1

Moss, R. H., Edmonds, J. A., Hibbard, K. A., Manning, M. R., Rose, S. K., Van Vuuren, D. P., ... & Wilbanks, T. J. (2010). The next generation of scenarios for climate change research and assessment. *Nature*, *463*(7282), 747-756. https://doi.org/10.1038/nature08823

Mtsetfwa, F. P., Kruger, L., & McCleery, R. A. (2023). Climate change decouples dominant tree species in African savannas. *Scientific Reports*, *13*(1), 7619. https://doi.org/10.1038/s41598-023-34550-9

Munthali, M. G., Davis, N., Adeola, A. M., Botai, J. O., Kamwi, J. M., Chisale, H. L., & Orimoogunje, O. O. (2019). Local perception of drivers of land-use and land-cover change dynamics across Dedza District, Central Malawi Region. *Sustainability*, *11*(3), 832. https://doi.org/10.3390/su11030832

Musa, F. I., & Sahoo, U. K. (2023). Role of sustainable forest management in poverty reduction and livelihood improvement in Sudan: A review. *International Journal of Ecology and Environmental Sciences*, *49*, 449-456. https://doi.org/10.55863/ijees.2023.3036

Musa, F. I., Mohammed, M. H., Fragallah, S. D., Adam, H. E., & Sahoo, U. K. (2024). Current status of tree species diversity at Abu Gadaf Natural Forest Reserve, Blue Nile Region–Sudan. *Vegetos*, *37*(5), 1760-1771. https://doi.org/10.1007/s42535-024-00931-2

Musiyiwa, K., Leal Filho, W., Harris, D., & Nyamangara, J. (2014). Implications of climate variability and change for smallholder crop production in different areas of Zimbabwe. *Research Journal of Environmental and Earth Sciences*, *6*(8), 394-401. https://doi.org/10.19026/rjees.6.5249

Muthoni, F. K., Odongo, V. O., Ochieng, J., Mugalavai, E. M., Mourice, S. K., Hoesche-Zeledon, I., Mwila, M., & Bekunda, M. (2019). Long-term spatial-temporal trends and variability of rainfall over Eastern and Southern Africa. *Theoretical and Applied Climatology, 137*, 1869–1882. https://doi.org/10.1007/s00704-018-2712-1

Naidoo, R., & Hill, K. (2006). Emergence of indigenous vegetation classifications through integration of traditional ecological knowledge and remote sensing analyses. *Environmental Management*, *38*(3), 377-387. https://doi.org/10.1007/s00267-004-0338-9

Nath, B., Niu, Z., & Singh, R. P. (2018). Land Use and Land Cover changes, and environment and risk evaluation of Dujiangyan city (SW China) using remote sensing and GIS techniques. *Sustainability*, *10*(12), 4631. https://doi.org/10.3390/su10124631

Nicholson, S. E. (2009). A revised picture of the structure of the "monsoon" and land ITCZ over West Africa. *Climate Dynamics*, *32*(7), 1155-1171. https://doi.org/10.1007/s00382-008-0514-3

Ogwu, M. C., Osawaru, M. E., & Obayuwana, O. K. (2016). Diversity and abundance of tree species in the University of Benin, Benin City, Nigeria. *Applied Tropical Agriculture*, *21*(3), 46-54.

Oke, D. O., & Jamala, G. Y. (2013). Traditional agroforestry practices and woody species conservation in the derived savanna ecosystem of Adamawa state, Nigeria. *Biodiversity Journal*, *4*(3), 427-434. https://doi.org/10.5897/JSSEM2013.0400

Okpiliya, F. I. (2012). Ecological diversity indices: Any hope for one again. *Journal of Environment and Earth Science*, *2*(10), 45-52.

Omay, P. O., Muthama, N. J., Oludhe, C., Kinama, J. M., Artan, G., & Atheru, Z. (2023). Evaluation of CMIP6 historical simulations over IGAD region of Eastern Africa. *Discover Environment*, *1*(1), 11. https://doi.org/10.1007/s44274-023-00012-2

Osewe, E. O., Popa, B., Vacik, H., Osewe, I., & Abrudan, I. V. (2024). Review of forest ecosystem services evaluation studies in East Africa. *Frontiers in Ecology and Evolution*, *12*, 1385351. https://doi.org/10.3389/fevo.2024.1385351

Osman, A. K., & Ali, A. M. (2021). *Sudan–Land, climate, energy, agriculture and development: A study in the Sudano-Sahel initiative for regional development, jobs, and food security*. zef Working Paper 203, Center for Development Research, University of Bonn, German. https://doi.org/10.2139/ssrn.3769148

Osman, M. A., Abdel-Rahman, E. M., Onono, J. O., Olaka, L. A., Elhag, M. M., Adan, M., & Tonnang, H. E. (2023). Mapping, intensities and future prediction of land use/land cover dynamics using google earth engine and CA-artificial neural network model. *PLoS One*, *18*(7), e0288694. https://doi.org/10.1371/journal.pone.0288694

Ouedraogo, I., Tigabu, M., Savadogo, P., Compaoré, H., Oden, P. C., & Ouadba, J. M. (2010). Land cover change and its relation with population dynamics in Burkina Faso, West Africa. *Land Degradation & Development*, *21*(5), 453-462. https://doi.org/10.1002/ldr.981

Pal, M. (2005). Random forest classifier for remote sensing classification. *International journal of remote sensing*, *26*(1), 217-222. https://doi.org/10.1080/01431160412331269698

Patrut, A., Woodborne, S., Patrut, R. T., Rakosy, L., Lowy, D. A., Hall, G., & Von Reden, K. F. (2018). The demise of the largest and oldest African baobabs. *Nature Plants*, *4*(7), 423-426. https://doi.org/10.1038/s41477-018-0170-5

Peacock, M. M. (2025). Negotiating a Fragmented World: What Do We Know, How Do We Know It, and Where Do We Go from Here?. *Diversity*, *17*(3), 200. https://doi.org/10.3390/d17030200

Pearson, R. G., Raxworthy, C. J., Nakamura, M., & Townsend Peterson, A. (2007). Predicting species distributions from small numbers of occurrence records: a test case using cryptic geckos in Madagascar. *Journal of biogeography*, *34*(1), 102-117. https://doi.org/10.1111/j.1365-2699.2006.01594.x

Pelletier, C., Valero, S., Inglada, J., Champion, N., & Dedieu, G. (2016). Assessing the robustness of Random Forests to map land cover with high resolution satellite image time series over large areas. *Remote Sensing of Environment*, *187*, 156-168. https://doi.org/10.1016/j.rse.2016.10.010

Persson, M., Lindberg, E., & Reese, H. (2018). Tree species classification with multi-temporal Sentinel-2 data. *Remote Sensing*, *10*(11), 1794. https://doi.org/10.3390/rs10111794

Peterson, A. T., Papeş, M., & Eaton, M. (2007). Transferability and model evaluation in ecological niche modeling: A comparison of GARP and MaxEnt. *Ecography, 30*, 550–560. https://doi.org/10.1111/j.0906-7590.2007.05102.x

Petrie, M. D., Hubbard, R. M., Bradford, J. B., Kolb, T. E., Noel, A., Schlaepfer, D. R., ... & Moser, W. K. (2023). Widespread regeneration failure in ponderosa pine forests of the southwestern United States. *Forest Ecology and Management*, *545*, 121208. https://doi.org/10.1016/j.foreco.2023.121208

Phan, N. T., Kuch, V., & Lehnert, L. W. (2020). Land cover classification using Google Earth Engine and Random Forest classifier—The role of image composition. Remote Sensing, 12(15), 2411. https://doi.org/10.3390/rs12152411

Phillips, J. S., Dudík, M., & Schapire, R. (2017). *MaxEnt software for modeling species niches and distributions* (Version 3.4.1). http://biodiversityinformatics.amnh.org/open_source/MaxEnt/

Phillips, S. J., Anderson, R. P., & Schapire, R. E. (2006a). Maximum entropy modeling of species geographic distributions. *Ecological Modelling, 190*, 231–259. https://doi.org/10.1016/j.ecolmodel.2005.03.026

Phillips, S. J., Anderson, R. P., & Schapire, R. E. (2006b). Maximum entropy modeling of species geographic distributions. *Ecological Modelling, 190*, 231–259. https://doi.org/10.1016/j.ecolmodel.2005.03.026

Phillips, S. J., Dudík, M., & Schapire, R. E. (2022). MaxEnt software for modeling species niches and distributions. http://biodiversityinformatics.amnh.org/open_source/MaxEnt/

Pokhriyal, P., Uniyal, P., Chauhan, D. S., & Todaria, N. P. (2010). Regeneration status of tree species in forest of Phakot and Pathri Rao watersheds in Garhwal Himalaya. *Current science*, 171-175.

Pontius, R. G., & Millones, M. (2011). Death to Kappa: Birth of quantity disagreement and allocation disagreement for accuracy assessment. *International Journal of Remote Sensing, 32*, 4407–4429. https://doi.org/10.1080/01431161.2011.552923

Potapov, P., Hansen, M. C., Pickens, A., Hernandez-Serna, A., Tyukavina, A., Turubanova, S., ... & Kommareddy, A. (2022). The global 2000-2020 land cover and land use change dataset derived from the Landsat archive: first results. *Frontiers in Remote Sensing*, *3*, 856903. https://doi.org/10.3389/frsen.2022.856903

Pradhan, B., Elias, P. J., & Almazroui, M. (2024). Evaluating and Predicting Meteorological Drought Using Different Climate Reanalysis Datasets over New South Wales, Australia. *Earth Systems and Environment*, *8*(4), 1657-1672. https://doi.org/10.1007/s41748-024-00507-9

Praticò, S., Solano, F., Di Fazio, S., & Modica, G. (2021). Machine Learning classification of mediterranean forest habitats in google earth engine based on seasonal sentinel-2 time-series and input image composition optimisation. *Remote sensing*, *13*(4), 586. https://doi.org/10.3390/rs13040586

Price, D. T., Alfaro, R. I., Brown, K. J., Flannigan, M. D., Fleming, R. A., Hogg, E. H., ... & Venier, L. A. (2013). Anticipating the consequences of climate change for Canada's boreal forest ecosystems. *Environmental Reviews*, *21*(4), 322-365. https://doi.org/10.1139/er-2013-0042

Qi, J., Chehbouni, A., Huete, A. R., Kerr, Y. H., & Sorooshian, S. (1994). A modified soil adjusted vegetation index. *Remote sensing of environment*, *48*(2), 119-126. https://doi.org/10.1016/0034-4257(94)90134-1

Qu, L. A., Chen, Z., Li, M., Zhi, J., & Wang, H. (2021). Accuracy improvements to pixel-based and object-based lulc classification with auxiliary datasets from Google Earth engine. *Remote Sensing*, *13*(3), 453. https://doi.org/10.3390/rs13030453

Raczko, E., & Zagajewski, B. (2017). Comparison of Support Vector Machine, Random Forest and neural network classifiers for tree species classification on airborne hyperspectral APEX images. *European Journal of Remote Sensing*, *50*(1), 144-154. https://doi.org/10.1080/22797254.2017.1299557

Rahman, M. R., Rahman, M. M., & Chowdhury, M. A. (2020). Assessment of natural regeneration status: the case of Durgapur hill forest, Netrokona, Bangladesh. *Geology, Ecology, and Landscapes*, *4*(2), 121-130. https://doi.org/10.1080/24749508.2019.1600911

Rajasugunasekar, D., Patel, A. K., Devi, K. B., Singh, A., Selvam, P., & Chandra, A. (2023). An Integrative Review for the Role of Forests in Combating Climate Change and Promoting Sustainable Development. *International Journal of Environment and Climate Change* *13*(11), 4331-4341. https://doi.org/10.9734/ijecc/2023/v13i113614

Ramezan, C.A.; Warner, T.A.; Maxwell, A.E. (2019). Evaluation of sampling and cross-validation tuning strategies for regional-scale Machine Learning classification. *Remote Sensing*, *11*(2), 185. https://doi.org/10.3390/rs11020185

Riahi, K., Van Vuuren, D. P., Kriegler, E., Edmonds, J., O'neill, B. C., Fujimori, S., ... & Tavoni, M. (2017). The Shared Socioeconomic Pathways and their energy, land use, and greenhouse gas emissions implications: An overview. *Global environmental change*, *42*, 153-168. https://doi.org/10.1016/j.gloenvcha.2016.05.009

Sabat-Tomala, A., Raczko, E., & Zagajewski, B. (2020). Comparison of Support Vector Machine and Random Forest algorithms for invasive and expansive species classification using airborne hyperspectral data. *Remote Sensing*, *12*(3), 516. https://doi.org/10.3390/rs12030516

Sabins, F. F., Jr., & Ellis, J. M. (2020). Remote sensing: Principles, interpretation, and applications. *Waveland Press: Long Grove, IL*, USA.

Sanchez, G. M., Petrasova, A., Skrip, M. M., Collins, E. L., Lawrimore, M. A., Vogler, J. B., ... & Meentemeyer, R. K. (2023). Spatially interactive modeling of land change identifies location-specific adaptations most likely to lower future flood risk. *Scientific Reports*, *13*(1), 18869. https://doi.org/10.1038/s41598-023-46195-9

Sankaran, M., Hanan, N. P., Scholes, R. J., Ratnam, J., Augustine, D. J., Cade, B. S., ... & Zambatis, N. (2005). Determinants of woody cover in African savannas. *Nature*, *438*(7069), 846-849. https://doi.org/10.1038/nature04070

Semu, A. A., Bekele, T., Lulekal, E., Cariñanos, P., & Nemomissa, S. (2021). Projected impact of climate change on habitat suitability of a vulnerable endemic Acacia negrii (Pic. Serm.)

Kyal. & Boatwr (Fabaceae) in Ethiopia. *Sustainability*, *13*(20), 11275. https://doi.org/10.3390/su132011275

Sen, P. K. (1968). Estimates of the regression coefficient based on Kendall's tau. *Journal of the American Statistical Association*, 63(324), 1379–1389. https://doi.org/10.1080/01621459.1968.10480934

Serbouti, S., Ettaqy, A., Boukcim, H., Mderssa, M. E., El Ghachtouli, N., & Abbas, Y. (2023). Forests and woodlands in Morocco: Review of historical evolution, services, priorities for conservation measures and future research. *International Forestry Review*, *25*(1), 121-145. https://doi.org/10.1505/146554823836838745

Sesnie, S. E., Gessler, P. E., Finegan, B., & Thessler, S. (2008). Integrating Landsat TM and SRTM-DEM derived variables with decision trees for habitat classification and change detection in complex neotropical environments. *Remote Sensing of Environment*, *112*(5), 2145-2159. https://doi.org/10.1016/j.rse.2007.08.025

Shannon, C. E. & Weaver, W. 1949. The Mathematical Theory of Communication. Urbana, IL: The University of Illinois Press, USA, 1–117.

Sheffield, J., & Wood, E. F. (2020). What is drought? *Drought*, 23–30.

Siddig, A. A. H. (2014). Biodiversity of Sudan: Between the harsh conditions, political instability and civil wars. *Biodiversity Journal*, *5*(4), 545-555.

Siddig, A. A. H. (2019). Why is biodiversity data-deficiency an ongoing conservation dilemma in Africa?. *Journal for Nature Conservation*, *50*, 125719. https://doi.org/10.1016/j.jnc.2019.125719

Siddig, A. A., Magid, T. D. A., EL-Nasry, H. M., Hano, A. I., & Mohammed, A. A. (2018). Biodiversity in Sudan. In *Global biodiversity*. Apple Academic Press. pp. 273-294. https://doi.org/10.1201/9780429469800-10

Simba, F. M., Chikodzi, D., & Murwendo, T. (2012). Climate change scenarios, perceptions and crop production: a case study of Semi-arid Masvingo Province in Zimbabwe. *Journal of Earth Science and Climate Change*, *3*(124), 2.

Smith, W. K., Dannenberg, M. P., Yan, D., Herrmann, S., Barnes, M. L., Barron-Gafford, G. A., ... & Yang, J. (2019). Remote sensing of dryland ecosystem structure and function: Progress, challenges, and opportunities. *Remote Sensing of Environment*, *233*, 111401. https://doi.org/10.1016/j.rse.2019.111401

Soleimannejad, L., Ullah, S., Abedi, R., Dees, M., & Koch, B. (2019). Evaluating the potential of sentinel-2, landsat-8, and irs satellite images in tree species classification of hyrcanian forest of iran using random forest. *Journal of Sustainable Forestry*, *38*(7), 615-628. https://doi.org/10.1080/10549811.2019.1598443

Solomon, S. D. (2007). Climate change: The physical science basis. IPCC, Contribution of Working Group I to the Fourth Assessment Report of the Intergovernmental Panel on Climate Change. *Cambridge University Press*.

Stritih, A., Senf, C., Kuemmerle, T., Munteanu, C., Dzadzamia, L., Stritih, J., ... & Seidl, R. (2024). Same, but different: similar states of forest structure in temperate mountain regions of Europe despite different social-ecological forest disturbance regimes. *Landscape Ecology*, *39*(6), 114. https://doi.org/10.1007/s10980-024-01908-x

Stromann, O., Nascetti, A., Yousif, O., & Ban, Y. (2019). Dimensionality reduction and feature selection for object-based land cover classification based on Sentinel-1 and Sentinel-2 time series using Google Earth Engine. *Remote Sensing*, *12*(1), 76. https://doi.org/10.3390/rs12010076

Stromann, O., Nascetti, A., Yousif, O., & Ban, Y. (2019). Dimensionality reduction and feature selection for object-based land cover classification based on Sentinel-1 and Sentinel-2 time series using Google Earth Engine. *Remote Sensing*, *12*(1), 76. https://doi.org/10.3390/rs12010076

Sulieman, H. M. (2010). Expansion of mechanised rain fed agriculture and land use/land cover change in southern Gadarif, Sudan. *African Journal of Agricultural Research, 5*(11), 1609–1615. https://doi.org/10.5897/AJAR09.078

Sulieman, H. M. (2018). Exploring drivers of forest degradation and fragmentation in Sudan: The case of Erawashda forest and its surrounding community. *Science of the total environment*, *621*, 895-904. https://doi.org/10.1016/j.scitotenv.2017.11.210

Sulieman, H. M., & Ahmed, A. G. M. (2013). Monitoring changes in pastoral resources in eastern Sudan: A synthesis of remote sensing and local knowledge. *Pastoralism: Research, Policy and Practice*, *3*(1), 22. https://doi.org/10.1186/2041-7136-3-22

Sulieman, H. M., & Elagib, N. A. (2012). Implications of climate, land-use and land-cover changes for pastoralism in eastern Sudan. *Journal of arid environments*, *85*, 132-141. https://doi.org/10.1016/j.jaridenv.2012.05.001

SUSIS-ARC. (2016). Sudanese Soil Information System and Digital Soil Mapping. Food and Agriculture Organization of the United Nations. https://www.fao.org/soils-portal/data-hub/national-soil-information-systems/susis-sudan/en/

Tamiminia, H., Salehi, B., Mahdianpari, M., Quackenbush, L., Adeli, S., & Brisco, B. (2020). Google Earth Engine for geo-big data applications: A meta-analysis and systematic review. *ISPRS journal of photogrammetry and remote sensing*, *164*, 152-170. https://doi.org/10.1016/j.isprsjprs.2020.04.001

Tate, E. L., & Gustard, A. (2000). Drought definition: A hydrological perspective. In J. V. Vogt & F. Somma (Eds.), *Drought and drought mitigation in Europe* (pp. 23–48). Springer. https://doi.org/10.1007/978-94-015-9472-1_3

Taye, M. T., Ntegeka, V., Ogiramoi, N. P., & Willems, P. (2011). Assessment of climate change impact on hydrological extremes in two source regions of the Nile River Basin. *Hydrology and Earth System Sciences*, *15*(1), 209-222. https://doi.org/10.5194/hess-15-209-2011

Tegos, A., Stefanidis, S., Cody, J., & Koutsoyiannis, D. (2023). On the sensitivity of standardized-precipitation-evapotranspiration and aridity indexes using alternative potential evapotranspiration models. *Hydrology*, *10*(3), 64. https://doi.org/10.3390/hydrology10030064

Tesfamariam, B. G., Gessesse, B., & Melgani, F. (2022). MaxEnt-based modeling of suitable habitat for rehabilitation of Podocarpus forest at landscape-scale. *Environmental Systems Research*, *11*(1), 4. https://doi.org/10.1186/s40068-022-00248-6

Tesfaye, G., Teketay, D., Fetene, M., & Beck, E. (2010). Regeneration of seven indigenous tree species in a dry Afromontane forest, southern Ethiopia. *Flora-Morphology, Distribution, Functional Ecology of Plants*, *205*(2), 135-143. https://doi.org/10.1016/j.flora.2008.12.006

Tesfaye, W., Elias, E., Warkineh, B., Tekalign, M., & Abebe, G. (2024). Modeling of land use and land cover changes using Google Earth Engine and Machine Learning approach: implications for landscape management. *Environmental Systems Research*, *13*(1), 31. https://doi.org/10.1186/s40068-024-00366-3

Thornthwaite, C. W. (1948). An approach toward a rational classification of climate. *Geographical Review*, 38(1), 55–94. https://doi.org/10.2307/210739

Tolessa, T., Senbeta, F., & Kidane, M. (2017). The impact of land use/land cover change on ecosystem services in the central highlands of Ethiopia. *Ecosystem services*, *23*, 47-54. https://doi.org/10.1016/j.ecoser.2016.11.010

Tong, X., Brandt, M., Hiernaux, P., Herrmann, S., Rasmussen, L. V., Rasmussen, K., ... & Fensholt, R. (2020). The forgotten land use class: Mapping of fallow fields across the Sahel using Sentinel-2. *Remote Sensing of Environment*, *239*, 111598. https://doi.org/10.1016/j.rse.2019.111598

Torres, R., Snoeij, P., Geudtner, D., Bibby, D., Davidson, M., Attema, E., ... & Brown, M. (2012). GMES Sentinel-1 mission. *Remote Sensing of Environment, 120*, 9–24. https://doi.org/10.1016/j.rse.2011.05.028

Tran, T. V., Tran, D. X., Myint, S. W., Latorre-Carmona, P., Ho, D. D., Tran, P. H., & Dao, H. N. (2019). Assessing spatiotemporal drought dynamics and its related environmental issues in the Mekong River Delta. *Remote Sensing*, *11*(23), 2742. https://doi.org/10.3390/rs11222742

Tripathi, K., & Verma, A. (2024). Remote sensing and Machine Learning fusion: A robust framework for land use and land cover change detection. In *2024 IEEE International Conference for Women in Innovation, Technology & Entrepreneurship (ICWITE)*. IEEE. pp. 434-439. https://doi.org/10.1109/ICWITE59797.2024.10503360

Tucker, C. J. (1979). Red and photographic infrared linear combinations for monitoring vegetation. *Remote Sensing of Environment, 8*(2), 127–150. https://doi.org/10.1016/0034-4257(79)90013-0

Umuhoza, J., Jiapaer, G., Tao, Y., Bai, J., Hakorimana, E., Zhang, L., ... & Ju, T. (2025). Impacts of climate extremes on vegetation health in the tropical savannas of Africa. *Global Ecology and Conservation*, e03649. https://doi.org/10.1016/j.gecco.2025.e03649

UNEP. (2007). Sudan post conflict environmental assessment. Nairobi: United Nations Environment Programme. https://postconflict.unep.ch/publications (Access date: 20 November 2025).

UNEP. (2020). Sudan first state of environment and outlook report 2020. Khartoum, Sudan.

Vicente-Serrano, S. M., Beguería, S., & López-Moreno, J. I. (2010). A multiscalar drought index sensitive to global warming: The Standardized Precipitation Evapotranspiration Index (SPEI). *Journal of Climate*, **23**(7), 1696–1718. https://doi.org/10.1175/2009JCLI2909.1

Vizzarri, M. (2024). Managing Global Forests in View of Multiple Goals: An Evidence-Based Perspective. *Land*, *13*(12), 2169. https://doi.org/10.3390/land13122169

Volis, S. (2024). Effect of intra-seasonal variation in precipitation on seed germination and seedling growth in Iris atrofusca: implications for conservation. *Israel Journal of Ecology and Evolution*, *70*(3), 123-129. https://doi.org/10.1163/22244662-bja10074

Vorpahl, P., Elsenbeer, H., Märker, M., & Schröder, B. (2012). How can statistical models help to determine driving factors of landslides?. *Ecological Modelling*, *239*, 27-39. https://doi.org/10.1016/j.ecolmodel.2011.12.007

Wambua, R. M., Mutua, B. M., & Raude, J. M. (2015). Spatio-temporal drought characterization for the Upper Tana River Basin, Kenya using standardized precipitation index (SPI). *World Journal of Environmental Engineering, 3*, 111–120.

Wan, H., Tang, Y., Jing, L., Li, H., Qiu, F., & Wu, W. (2021). Tree species classification of forest stands using multisource remote sensing data. *Remote Sensing*, *13*(1), 144. https://doi.org/10.3390/rs13010144

Wan, J. N., Mbari, N. J., Wang, S. W., Liu, B., Mwangi, B. N., Rasoarahona, J. R., ... & Wang, Q. F. (2021). Modeling impacts of climate change on the potential distribution of six endemic baobab species in Madagascar. *Plant Diversity*, *43*(2), 117-124. https://doi.org/10.1016/j.pld.2020.07.001

Wang, F., Lai, H., Li, Y., Feng, K., Zhang, Z., Tian, Q., Zhu, X., & Yang, H. (2022). Dynamic variation of meteorological drought and its relationships with agricultural drought across China. *Agricultural Water Management, 261*, 107301. https://doi.org/10.1016/j.agwat.2021.107301

Wang, L., Diao, C., Xian, G., Yin, D., Lu, Y., Zou, S., & Erickson, T. A. (2020). A summary of the special issue on remote sensing of land change science with Google earth engine. *Remote Sensing of Environment*, *248*, 112002. https://doi.org/10.1016/j.rse.2020.112002

Wang, X., Wang, B., & Cui, F. (2024). Exploring ecosystem services interactions in the dryland: Socio-ecological drivers and thresholds for better ecosystem management. *Ecological Indicators*, *159*, 111699. https://doi.org/10.1016/j.ecolind.2024.111699

Warren, D. L., Matzke, N. J., Cardillo, M., Baumgartner, J. B., Beaumont, L. J., Turelli, M., ... & Dinnage, R. (2021). ENMTools 1.0: an R package for comparative ecological biogeography. *Ecography*, *44*(4), 504-511. https://doi.org/10.1111/ecog.05485

Warrens, M. J. (2015). Properties of the quantity disagreement and the allocation disagreement. *International Journal of Remote Sensing*, *36*(5), 1439-1446. https://doi.org/10.1080/01431161.2015.1011794

Wickens, G. E. (1995). Role of Acacia Species in the Rural Economy of Dry Africa and the Near East. Conservation Guide 27. Rome: FAO.

Wilfahrt, P. A., Seabloom, E. W., Bakker, J. D., Biederman, L., Bugalho, M. N., Cadotte, M. W., ... & Borer, E. T. (2023). Nothing lasts forever: Dominant species decline under rapid environmental change in global grasslands. *Journal of Ecology*, *111*(11), 2472-2482. https://doi.org/10.1111/1365-2745.14198

Wilhite, D. A. (2016). Managing drought risk in a changing climate. *Climate Research, 70*, 99–102. https://doi.org/10.3354/cr01430

Wilks, D. (2006). *Statistical methods in the atmospheric sciences* (3rd ed.). Elsevier.

Wilks, D. S. (2011). *Statistical methods in the atmospheric sciences* (3rd ed.). Academic Press.

Winkler, K., Fuchs, R., Rounsevell, M., & Herold, M. (2021). Global land use changes are four times greater than previously estimated. *Nature communications*, *12*(1), 2501. https://doi.org/10.1038/s41467-021-22702-2

World Meteorological Organization (WMO). (2023). Guidelines on the Calculation of Climate Normals (1991–2020) (WMO-No. 1203). Geneva, Switzerland: World Meteorological Organization.

Xu, Y., Yang, Z., Zhang, L., & Zhang, J. (2025). An Evaluation of the Capability of Global Meteorological Datasets to Capture Drought Events in Xinjiang. *Land*, *14*(2), 219. https://doi.org/10.3390/land14020219

Xu, Z., Shen, X., Cao, L., Coops, N. C., Goodbody, T. R., Zhong, T., ... & Wu, X. (2020). Tree species classification using UAS-based digital aerial photogrammetry point clouds and multispectral imageries in subtropical natural forests. *International Journal of Applied Earth Observation and Geoinformation*, *92*, 102173. https://doi.org/10.1016/j.jag.2020.102173

Yagoub, Y. E., Li, Z. Q., Musa, O. S., Wang, F., Anjum, M. N., Bo, Z., & Ji, D. (2017). Detection of drought pattern in sudan using standardized precipitation-evapotranspiration index (spei). *International Journal of Recent Advances in Multidisciplinary Research*, *4*(4), 2546.

Yahya, N., Abdelkadir, A., Teshome, B., Abebe, M., & Kassa, H. (2023). Gum and resin bearing dryland forests of the Somali region, Southeastern Ethiopia: Diversity, structure and spatial distribution. *International Journal of Agricultural Research, Innovation and Technology (IJARIT)*, *13*(2), 6-13. https://doi.org/10.3329/ijarit.v13i2.70848

Yakubu, M., Saka, M. G., Sa'idu, I., Mahmud, W. A., & Yunus, A. U. (2020). Assessment of the Checklist and Regeneration Status Potential of Species Seedlings and Saplings of Baturiya Hadejia Wetland Game Reserve, Jigawa State, Nigeria. *Global Advanced Research Journal of Agricultural Science*, *9*, 19-26.

Yasin, E. H. E, Siddig, A. A. H., Diab, E. E., & Czimber, K. (2025). Evaluating the Efficiency of Two Ecological Indices in Monitoring Forest Degradation in the Drylands of Sudan. *Remote Sensing*, *17*(13), 2298. https://doi.org/10.3390/rs17132298

Yasin, E. H. E., & Mulyana, B. (2022). Spatial distribution of tree species composition and carbon stock in Tozi tropical dry forest, Sinnar State, Sudan. *Biodiversitas, 23*, 2359–2368. https://doi.org/10.13057/biodiv/d230513

Yasin, E. H. E., Siddig, A. A. H., & Kornel, C. (2024). Forests at the Crossroads: Biodiversity Conservation in the Era of Climate Change. In S. N. Kulshreshtha (Ed.). Sustainable Forest Management - Surpassing Climate Change and Land Degradation. *Intech Open*. https://doi.org/10.5772/intechopen.1004224

Yasin, E. H., Kamil, O. H., & Mulyana, B. (2022). Multi-temporal satellite images analysis for assessing and mapping deforestation in Um Hataba Forest, South Kordofan, Sudan. *Jurnal Sylva Indonesiana*, 5, 81–92. https://doi.org/10.32734/jsi.v5i01.7504

Yasin, E. H., Kornel, C., & Hemida, M. (2023). Assessment and mapping of forest cover change in dryland, Sudan using remote sensing. In Conservation, Exploitation and Restoration of Mountain Ecosystem (pp. 65–79). *IntechOpen*. https://doi.org/10.5772/intechopen.113862

Yeom, D. J., & Kim, J. H. (2011). Comparative evaluation of species diversity indices in the natural deciduous forest of Mt. Jeombong. *Forest Science and Technology*, *7*(2), 68-74. https://doi.org/10.1080/21580103.2011.573940

Zakaria, H. E. A. (2010). Integration of remote sensing and GIS in studying vegetation trends and conditions in the Gum Arabic belt in North Kordofan, Sudan (MSc thesis). University of Hamburg.

Zerbo, I., Salako, K. V., Hounkpevi, A., Zozoda, D., Kakai, R. G., & Thiombiano, A. (2023). Impact of climate patterns, land-use types and exploitation on the population structure of Bombax costatum Pellegr. and Vuillet in West African semi-arid savannas. *Global Ecology and Conservation*, *43*, e02434. https://doi.org/10.1016/j.gecco.2023.e02434

Zewdie, W., & Csaplovics, E. (2016). Identifying categorical land use transition and land degradation in northwestern drylands of Ethiopia. *Remote Sensing*, *8*(5), 408. https://doi.org/10.3390/rs8050408

Zhang, B., Zhang, Q., Feng, C., Feng, Q., & Zhang, S. (2017). Understanding land use and land cover dynamics from 1976 to 2014 in Yellow River Delta. *Land*, *6*(1), 20. https://doi.org/10.3390/land6010020

Zhang, Z., Xu, C. Y., Yong, B., Hu, J., & Sun, Z. (2012). Understanding the changing characteristics of droughts in Sudan and the corresponding components of the hydrologic cycle. *Journal of Hydrometeorology, 13*, 1520–1535. https://doi.org/10.1175/JHM-D-11-0109.1

Zhao, J., Yu, L., Newbold, T., Shen, X., Liu, X., Hua, F., ... & Ma, K. (2024). Biodiversity responses to agricultural practices in cropland and natural habitats. *Science of the Total Environment*, *922*, 171296. https://doi.org/10.1016/j.scitotenv.2024.171296

Zhong, L., Dai, Z., Fang, P., Cao, Y., & Wang, L. (2024). A review: Tree species classification based on remote sensing data and classic deep learning-based methods. *Forests*, *15*(5), 852. https://doi.org/10.3390/f15050852

Zhong, X., Li, W., Li, Z., Huang, Y., Chen, X., Huang, L., ... & Chen, Y. (2024). Decadal changes in population structures of rare oak species Quercus chungii. *Ecology and Evolution*, *14*(10), e70479. https://doi.org/10.1002/ece3.70479

Zhou, B., Okin, G. S., & Zhang, J. (2020). Leveraging Google Earth Engine (GEE) and Machine Learning algorithms to incorporate in situ measurement from different times for rangelands monitoring. *Remote Sensing of Environment*, *236*, 111521. https://doi.org/10.1016/j.rse.2019.111521

Zohrabi, N., Bavani, A. M., Goodarzi, E., & Eslamian, S. (2014). Attribution of temperature and precipitation changes to greenhouse gases in northwest Iran. *Quaternary International*, *345*, 130-137. https://doi.org/10.1016/j.quaint.2014.01.026

Zurqani, H. A., Post, C. J., Mikhailova, E. A., Schlautman, M. A., & Sharp, J. L. (2018). Geospatial analysis of land use change in the Savannah River Basin using Google Earth Engine. *International journal of applied earth observation and geoinformation*, *69*, 175-185. https://doi.org/10.1016/j.jag.2017.12.006

## APPENDICES

Appendix A. Sudan Ecological Zones

| Zone | Description |
|---|---|
| Desert | Hyper-arid landscapes found in northern Sudan, characterized by extremely low annual rainfall (<75 mm), very high evapotranspiration, and sparse vegetation cover. Plant life is largely restricted to wadi systems, rocky outcrops, and isolated microhabitats capable of retaining minimal moisture. Vegetation consists mainly of highly stress-tolerant shrubs, ephemeral herbs, and scattered xerophytes adapted to extreme water deficit. Soil surfaces are dominated by desert pavements, sand sheets, and dune systems, with biological activity concentrated along temporary watercourses. |
| Semi-desert | A broad transition belt between hyper-arid desert and savanna regions, characterized by high rainfall variability (100–300 mm/year) and shallow, often degraded soils. Vegetation forms shrub–grass mosaics dominated by drought-tolerant species such as Acacia tortilis, Acacia seyal (Delile), and Commiphora africana. Productivity is strongly linked to short, irregular rainy seasons, and the zone is highly sensitive to overgrazing, wind erosion, and climate fluctuations. This zone supports pastoralism and limited rain-fed agriculture. |
| Poor Savanna woodland | Semi-arid savanna characterized by nutrient-poor soils, seasonal water deficits, and strong ecological drivers such as drought, fire, and grazing pressure. Vegetation consists of open woodlands, scattered deciduous trees, and mixed perennial grasses. Trees such as Acacia seyal (Delile), Balanites aegyptiaca, and Combretum spp. are common. The zone marks a shift from predominantly pastoral to agro-pastoral land use and experiences significant land degradation along grazing routes. |
| Rich Savanna woodlan | A mesic savanna system with higher rainfall (600–1000 mm/year), deeper and more fertile soils, and greater biomass production than the poor savanna. Vegetation forms woodland–grassland mosaics, often dominated by broad-leaved species such as Terminalia brownii, Anogeissus leiocarpa, and tall grasses including Hyparrhenia spp. This zone supports intensive agriculture, wildlife habitats, and relatively stable hydrological processes. Its higher productivity makes it a key area for both biodiversity and rural livelihoods. |

**Source:** Adopted from (Berry, 2015; Misachi, 2017; Siddig et al., 2018; Gunn, 2021; Alriah et al., 2022)

Appendix B. Initial bioclimatic variables selected for modelling the habitat suitability distribution of *Acacia seyal* (Delile), and eventually only ones shown in bold font, were chosen for the MaxEnt modeling

| Code | Bioclimatic Variable | Unit |
|---|---|---|
| Bio01 | Annual Mean Temperature | °C |
| **Bio02** | **Mean Diurnal Range** | **°C** |
| **Bio03** | **Isothermality (BIO2/BIO7) (* 100)** | **%** |
| Bio04 | Temperature Seasonality | °C |
| Bio05 | Max Temperature of Warmest Month | °C |
| Bio06 | Min Temperature of Coldest Month | °C |
| Bio07 | Temperature Annual Range | °C |
| Bio08 | Mean Temperature of Wettest Quarter | °C |
| Bio09 | Mean Temperature of Driest Quarter | °C |
| **Bio10** | **Mean Temperature of Warmest Quarter** | **°C** |
| Bio11 | Mean Temperature of Coldest Quarter | °C |
| Bio12 | Annual Precipitation | mm |
| Bio13 | Precipitation of Wettest Month | mm |
| **Bio14** | **Precipitation of Driest Month** | **mm** |
| **Bio15** | **Precipitation Seasonality** | **mm** |
| Bio16 | Precipitation of Wettest Quarter | mm |
| Bio17 | Precipitation of Driest Quarter | mm |
| **Bio18** | **Precipitation of Warmest Quarter** | **mm** |
| **Bio19** | **Precipitation of Coldest Quarter** | **mm** |
| **Altitude** | **Elevation** | **m** |
| **Soil** | **Physical and chemical characteristics** | **-** |

Appendix C. Accuracy assessment of classified maps of 1995, 2008, and 2021.

| Year | Class name | Bareland | Semi-bareland | Light Forest | Dense Forest | Total | UA % | PA % | OA % | Kappa % |
|---|---|---|---|---|---|---|---|---|---|---|
| 1995 | Bareland | 12.00 | 1.00 | 1.00 | 0.00 | 14.00 | 75.00 | 85.71 | 89.00 | 83.81 |
| | Semi-bareland | 1.00 | 58.00 | 3.00 | 2.00 | 64.00 | 90.63 | 90.63 | | |
| | Light Forest | 2.00 | 4.00 | 110.00 | 8.00 | 124.00 | 91.67 | 88.71 | | |
| | Dense Forest | 1.00 | 1.00 | 6.00 | 65.00 | 73.00 | 86.67 | 89.04 | | |
| | Total | 16.00 | 64.00 | 120.00 | 75.00 | 275.00 | | | | |
| 2008 | Bareland | 52.00 | 3.00 | 2.00 | 1.00 | 58.00 | 90.63 | 89.66 | 91.60 | 88.00 |
| | Semi-bareland | 77.00 | 3.00 | 2.00 | 1.00 | 83.00 | 93.90 | 92.77 | | |
| | Light Forest | 1.00 | 2.00 | 62.00 | 2.00 | 67.00 | 92.54 | 92.54 | | |
| | Dense Forest | 1.00 | 1.00 | 4.00 | 61.00 | 67.00 | 94.53 | 91.04 | | |
| | Total | 82.00 | 58.00 | 70.00 | 65.00 | 275.00 | | | | |
| 2021 | Bareland | 11.00 | 1.00 | 0.00 | 0.00 | 12.00 | 91.67 | 91.67 | 93.02 | 93.60 |
| | Semi-bareland | 1.00 | 105.00 | 3.00 | 1.00 | 110.00 | 96.32 | 95.45 | | |
| | Light Forest | 0.00 | 2.00 | 106.00 | 2.00 | 110.00 | 95.45 | 96.36 | | |
| | Dense Forest | 0.00 | 1.00 | 2.00 | 40.00 | 43.00 | 93.02 | 93.02 | | |
| | Total | 12.00 | 109.00 | 111.00 | 43.00 | 275.00 | | | | |

Appendix D. Relative abundance, dominance, and frequency of the tree species identified and assessed in ENFR in 2008 and 2021.

| Species | 2008 | | | | | 2021 | | | | |
|---|---|---|---|---|---|---|---|---|---|---|
| | No. of samples | No. of individual tree | Relative Abundance | Relative Dominance | Relative Frequency | No. of samples | No. of individual tree | Relative Abundance | Relative Dominance | Relative Frequency |
| *Acacia seyal* | 173 | 10745 | 63.28 | 47.91 | 14.58 | 66 | 525 | 35.05 | 22.46 | 14.48 |
| *Acacia seyal var. fistulal* | 162 | 635 | 3.74 | 2.72 | 13.66 | 0 | 0 | 0.00 | 0.00 | 0.00 |
| *Acacia polycantha* | 49 | 304 | 1.79 | 4.39 | 4.13 | 0 | 0 | 0.00 | 0.00 | 0.00 |
| *Acacia Senegal* | 92 | 971 | 5.72 | 6.32 | 7.76 | 22 | 58 | 3.87 | 6.42 | 4.83 |
| *Dichrostachys cinerea* | 40 | 1013 | 5.97 | 5.31 | 3.37 | 0 | 0 | 0.00 | 0.00 | 0.00 |
| *Balanities aegyptiaca* | 89 | 406 | 2.39 | 0.13 | 7.50 | 49 | 160 | 10.68 | 31.72 | 10.75 |

| | | | | | | | | | | |
|---|---|---|---|---|---|---|---|---|---|---|
| *Acacia mellifera* | 8 | 17 | 0.10 | 0.16 | 0.67 | 11 | 38 | 2.54 | 2.14 | 2.41 |
| *Acacia nubica* | 2 | 3 | 0.02 | 0.01 | 0.17 | 46 | 201 | 13.42 | 1.81 | 10.09 |
| *Sterculia setigera* | 156 | 1117 | 6.58 | 23.45 | 13.15 | 73 | 188 | 12.55 | 16.31 | 16.02 |
| *Anogeissus leiocarpus* | 41 | 120 | 0.71 | 1.44 | 3.46 | 22 | 38 | 2.54 | 2.03 | 4.83 |
| *Terminalia laxiflora* | 35 | 102 | 0.60 | 1.51 | 2.95 | 16 | 25 | 1.67 | 0.11 | 3.51 |
| *Terminalia brownii* | 27 | 69 | 0.41 | 1.70 | 2.28 | 13 | 21 | 1.40 | 1.46 | 2.85 |
| *Combretum hartmannianum* | 91 | 648 | 3.82 | 1.07 | 7.67 | 34 | 48 | 3.20 | 0.11 | 7.46 |
| *Combretum aculeatum* | 15 | 87 | 0.51 | 0.04 | 1.26 | 0 | 0 | 0.00 | 0.00 | 0.00 |
| *Combretum molle* | 26 | 93 | 0.55 | 0.02 | 2.19 | 0 | 0 | 0.00 | 0.00 | 0.00 |
| *Combretum glutinosum* | 17 | 63 | 0.37 | 0.08 | 1.43 | 9 | 16 | 1.07 | 2.31 | 1.97 |
| *Lannea fruticosa* | 41 | 105 | 0.62 | 0.42 | 3.46 | 30 | 42 | 2.80 | 0.90 | 6.58 |
| *Sclerocarya birrea* | 11 | 26 | 0.15 | 0.45 | 0.93 | 9 | 21 | 1.40 | 3.42 | 1.97 |
| *Ziziphus spina-christi* | 20 | 242 | 1.43 | 0.21 | 1.69 | 20 | 57 | 3.81 | 3.09 | 4.39 |
| *Ziziphus abyssinica* | 18 | 63 | 0.37 | 0.14 | 1.52 | 16 | 24 | 1.60 | 0.51 | 3.51 |
| *Stereospermum kunthianum* | 14 | 55 | 0.32 | 1.08 | 1.18 | 10 | 16 | 1.07 | 2.31 | 2.19 |
| *Lonchocarpus laxiflorus* | 9 | 14 | 0.08 | 0.02 | 0.76 | 4 | 4 | 0.27 | 0.11 | 0.88 |
| *Dalbergia melanoxylon* | 12 | 25 | 0.15 | 0.33 | 1.01 | 5 | 6 | 0.40 | 1.81 | 1.10 |
| *Grewia tenax* | 5 | 8 | 0.05 | 0.01 | 0.42 | 1 | 10 | 0.67 | 0.96 | 0.66 |
| *Grewia flavescens* | 6 | 10 | 0.06 | 0.01 | 0.51 | 0 | 0 | 0.00 | 0.00 | 0.00 |
| *Xeromphis nilotica* | 2 | 2 | 0.01 | 0.04 | 0.17 | 0 | 0 | 0.00 | 0.00 | 0.00 |
| *Ochna afzelii* | 3 | 6 | 0.04 | 0.14 | 0.25 | 0 | 0 | 0.00 | 0.00 | 0.00 |
| *Maerua angolensis* | 3 | 3 | 0.02 | 0.10 | 0.25 | 0 | 0 | 0.00 | 0.00 | 0.00 |
| *Cassia arereh* | 1 | 1 | 0.01 | 0.02 | 0.08 | 0 | 0 | 0.00 | 0.00 | 0.00 |
| *Strychons innocua* | 4 | 5 | 0.03 | 0.06 | 0.34 | 0 | 0 | 0.00 | 0.00 | 0.00 |
| *Tamarindus indica* | 1 | 1 | 0.01 | 0.05 | 0.08 | 0 | 0 | 0.00 | 0.00 | 0.00 |
| *Piliostigma reticulatum* | 1 | 1 | 0.01 | 0.02 | 0.08 | 0 | 0 | 0.00 | 0.00 | 0.00 |
| *Capparis decidua* | 7 | 13 | 0.08 | 0.21 | 0.59 | 0 | 0 | 0.00 | 0.00 | 0.00 |
| *Adansonia digitata* | 3 | 3 | 0.02 | 0.39 | 0.25 | 0 | 0 | 0.00 | 0.00 | 0.00 |
| *Boswellia papyrifera* | 3 | 3 | 0.02 | 0.05 | 0.25 | 0 | 0 | 0.00 | 0.00 | 0.00 |